

**PERFORMANCE OF POLLUTED COMPOSITE  
INSULATORS FOR THE CONVERSION OF  
SELECTED UK TOWER LINES TO HVDC  
OPERATION UNDER SEVERE  
POLLUTION CONDITIONS**

A thesis submitted to Cardiff University

under the Marie Curie programme

in candidature for the degree of

Doctor of Philosophy

By

DAVIDE PINZAN

School of Engineering

Cardiff University

February 2021

*Alla mia famiglia.*



# Acknowledgments

This work would not have been possible without the expertise, the support and the availability of many people to whom I am grateful for the scientific contribution that has been published and for the skills I have acquired during this Marie Curie PhD journey.

I would like to thank the members of the following organisations: the Cardiff University Advanced High Voltage Engineering Research Centre (AHIVE), the EU funded InnoDC project, the National Grid Innovation team, the High Voltage Laboratory of the University of Porto and the UHVDC Laboratory of China Electric Power Research Institute (CEPRI) in Beijing.

In particular, I want to thank my supervisors: Professor Manu A. Haddad<sup>1</sup> for his professionalism and leadership, Doctor Mohammed El Amine Slama<sup>1</sup> for his expertise and rigour, Doctor Maurizio Albano<sup>1</sup> for his laboratory skills and availability and Professor Jun Liang<sup>1</sup> for his project management skills.

I need to thank the following project members: Professor Emeritus Ronald T. Waters<sup>1</sup> for his research passion, wisdom and belief in me, Professor Helder Leite<sup>2</sup> for his support and research focus, Engineer Fabio Branco<sup>2</sup> for his work and help and Doctor Xinzhe Yu<sup>3</sup> for his availability and expertise.

This research was funded by the European Union's Horizon 2020 research & innovation programme under the Marie Skłodowska-Curie grant agreement no. 765585.

1. Cardiff University, 2. University of Porto, 3. China Electric Power Research Institute (CEPRI).



# Summary

HVDC systems are increasingly being integrated in electric power systems and one of the main challenges to address relates to outdoor insulation. This thesis provides five main contributions with focus on composite insulators. First, an extensive literature review examines the state of the art of relevant research topics: the need of corona rings in HVDC systems; the influence of non-soluble deposit type on the hydrophobicity recovery; the effect of non-uniform hydrophobicity on flashover voltage; DC pollution severities; optimal creepage design at different severities; and the influence of wind speed on pollution accumulation. Secondly, the HVDC analytical and laboratory characterisation of heavily polluted insulators was performed between 121 and 252 kV. The test results confirmed that the insulators oriented horizontally performed better than vertically, which was attributed to the differences in the arc propagation and in the convection heat direction. Thirdly, new laboratory data was obtained for switching impulse (SI) in the range of 168 to 345 kV and for SI superimposed on a direct voltage of 16 kV. As a conclusion, in most conditions, the HVDC pre-energisation has a negative impact on the flashover performance. Then, with the acquired knowledge and using IEC and CIGRE insulation selection and dimensioning recommendations, proposals to convert three existing UK HVAC towers lines to HVDC operation have been designed between 170 and 500 kV, considering heavy and extremely severe pollution. The results show an increase of 1.6 to 2.9 times in power transfer. It was also confirmed that a few nanoamperes leakage current is sufficient to satisfy the electric field distribution requirements without the use of corona rings. Lastly, a laboratory wind tunnel was built to investigate the insulator pollution accumulation, with the option of HVDC energisation. Promising initial test results were obtained, and future work has been suggested.



# Publications

A journal paper on the switching impulse superimposed on direct voltage on a composite insulator has been published with the IEEE Transactions on Power Delivery in 2020. A second paper on HVDC performance of heavily polluted composite outdoor insulators is now (March 2021) under review with the same journal. The method used for the existing overhead line conversion to HVDC has been published in a paper and presented at the International Symposium on High Voltage Engineering (ISH) in 2019, in Budapest, Hungary. However, in this thesis, a more conservative approach is used, to obtain results which can be referenced with a higher degree of confidence. Also, recommendations on finite element simulations for overhead lines are provided in a paper published at the COMSOL Conference in Cambridge in 2019. In addition, initially, the research project objectives were presented at the Manchester University's UHVnet in 2019.

- [1] D. Pinzan, F. Branco, A. M. Haddad, M. E. A. Slama, M. Albano, R. T. Waters, and H. Leite "Performance of Composite Outdoor Insulator under Superimposed Direct and Switching Impulse Voltages," IEEE Transactions on Power Delivery, 2020, doi: 10.1109/TPWRD.2020.3003980.
- [2] D. Pinzan, X. Yu, A. M. Haddad, M. E. A. Slama, M. Albano, and R. T. Waters, "HVDC Flashover of Heavily Polluted Composite Insulators Rated 120 to 250 kV: Laboratory and Analytical Characterization," Submitted to IEEE Transactions on Power Delivery, Jan. 2021.
- [3] D. Pinzan, D. Clark, M. E. A. Slama, and M. A. Haddad, "Voltage Gradient Study of HVDC Overhead Line Suspension Insulation," presented at the COMSOL Conference 2019, Cambridge, UK, Sep. 2019.
- [4] D. Pinzan, M. E. A. Slama, O. Cwikowski, and M. A. Haddad, "Insulation Solutions for HVAC to HVDC Conversion of a High Voltage Transmission Overhead Line: the L7 Tower Case Study," presented at the International Symposium on High Voltage Engineering (ISH), Budapest, Hungary, Sept. 2019.
- [5] D. Pinzan, M. E. A. Slama, M. Albano, R. T. Waters, and A. M. Haddad, "Outdoor Insulation for HVDC Overhead Lines: a Research Project," presented at the Manchester University, UHVnet Conference, Manchester, UK, Jan. 2019.





# Nomenclature

<i>AC</i>	Alternating Current
<i>AD</i>	Arcing (or Axial) Distance in millimetres (mm)
<i>AL</i>	Arcing (or Axial) Length in millimetres (mm)
<i>B, <math>\alpha, \theta</math></i>	parameters dependent on the shed material
<i>C<sub>a</sub></i>	factor for FOV dependence on altitude
<i>CD</i>	Creepage Distance in millimetres (mm)
<i>CL</i>	Creepage Length in millimetres (mm)
<i>C<sub>d</sub></i>	Clearance distance in millimetres (mm)
<i>C<sub>D</sub></i>	factor for the flashover voltage dependence on the average diameter
<i>CF</i>	Creepage Factor
<i>CUR</i>	Contamination Uniformity Ratio between insulator shed bottom and shed top
<i>D<sub>a</sub></i>	Insulator average diameter in millimetres (mm)
<i>DC</i>	Direct Current
<i>ESDD</i>	Equivalent Salt Deposit Density in milligrams per square centimetre (mg/cm <sup>2</sup> )
<i>FEM</i>	Finite Element Method
<i>H</i>	Line altitude above sea level in metres (m)
<i>HC</i>	Hydrophobicity Class
<i>HTM</i>	Hydrophobicity Transfer Material
<i>HV</i>	High Voltage
<i>K<sub>c</sub></i>	factor to account for the type of salt

$K_{CUR}$	CUR factor
$K_D$	factor for flashover voltage dependence on the collected pollution, as a function of the average diameter
$K_N$	factor for the flashover voltage dependence on NSDD
$K_P$	factor for the conversion of $ESDD_{AC}$ to $ESDD_{DC}$
$K_S$	safety factor which accounts for the worse performance of a minority of insulators, in a large group of insulators
$LMW$	Low Molecular Weight
$NSDD$	Non-Soluble Deposit Density in milligrams per square centimetre ( $mg/cm^2$ )
$OHL$	Overhead Line
$P$	Active Power in watts (W)
$PU$	Ratio of a switching surge peak over the operational voltage, also referred to as the SSF
$SDD$	Salt Deposit Density in milligrams per square centimetre ( $mg/cm^2$ )
$SSF$	Switching Surge Factor
$USCD$	Unified Specific Creepage Distance in millimetres per kilovolt (mm/kV)



# Contents

<b>Acknowledgments</b> .....	<b>ii</b>
<b>Summary</b> .....	<b>iv</b>
<b>Publications</b> .....	<b>vi</b>
<b>Nomenclature</b> .....	<b>i</b>
<b>List of figures</b> .....	<b>xii</b>
<b>List of tables</b> .....	<b>xx</b>
<b>Chapter 1. Introduction</b> .....	<b>1</b>
1.1. The relevance of the broad HVDC research .....	1
1.2. The thesis content and contribution.....	1
1.3. Methodology.....	5
1.4. Sources choice .....	6
1.5. The thesis is a deeper dive.....	6
1.6. The implications .....	7
<b>Chapter 2. A review of polluted outdoor insulators</b> .....	<b>9</b>
2.1. An introduction to outdoor insulators.....	9
2.1.1. Outdoor insulation requirements, and costs .....	11
2.2. Insulator nomenclature, classification, performance, and stress.....	11
2.2.1. Insulator nomenclature and functions.....	11
2.2.2. Insulator classification .....	13
2.2.3. Insulator performance .....	14
2.2.4. Insulator electrical stress.....	15
2.3. Shielding electrodes .....	17
2.3.1. Corona ring purposes under AC .....	17
2.3.2. Electric field requirements for composite insulators .....	17
2.3.3. Corona ring need assessment under DC.....	18

2.4. Pollution flashover phenomenon .....	20
2.5. Pollution flashover of hydrophilic and hydrophobic surfaces .....	23
2.5.1. Hydrophilic material modelling .....	23
2.5.2. Hydrophobic material modelling.....	24
2.5.3. Influence of inert material on hydrophobic material .....	24
2.5.4. Influence of U-shaped hydrophilicity on hydrophobic outdoor insulators .....	26
2.6. Climate and environment .....	28
2.6.1. Climate .....	29
2.6.2. Environment .....	31
2.7. ESDD, SDD, NSDD definitions and DC service values.....	32
2.7.1. Definitions and considerations.....	32
2.7.2. Deposit density DC service values.....	33
2.8. HVDC selection and dimensioning .....	34
2.8.1. General aspects .....	35
2.8.2. Specific methodologies for HVDC .....	36
2.8.3. Simplified HVDC dimensioning .....	38
2.8.4. Simplified HVDC dimensioning if pollution and wetting occur at the same time.....	47
2.9. Types of pollution .....	50
2.9.1. Salt solubility .....	53
2.9.2. Type A and Type B pollution .....	54
2.10. Artificial contamination tests .....	54
2.10.1. Artificial contamination tests for hydrophobic materials.....	55
2.11. Pollution accumulation mechanism.....	58
2.11.1. Electric force .....	60
2.11.2. Pollution charge consideration for DC.....	60

2.11.3. Full Lorentz force expression .....	61
2.12. Wetting mechanism .....	61
2.12.1. Rain resistivity .....	64
2.12.2. Tropical precipitation .....	64
2.12.3. Mid-latitude precipitation .....	64
2.12.4. Low precipitation regions .....	64
2.12.5. Fog .....	64
2.12.6. Moisture absorption .....	65
2.12.7. Ice and snow .....	65
2.13. Insulator cleaning based on orientation, diameter, and material .....	66
2.13.1. Orientation .....	66
2.13.2. Average diameter.....	67
2.13.3. Material.....	68
2.13.4. Equilibrium of pollution accumulation .....	69
2.14. Insulator ageing.....	69
2.14.1. Biological growth.....	70
2.15. AC and DC performance-based insulator design.....	71
2.15.1. Insulator design for AC energisation.....	71
2.15.2. Insulator design for DC energisation .....	71
2.15.3. DC design study under light pollution .....	71
2.15.4. DC design study under heavy pollution .....	73
2.15.5. Remarks on DC design with respect to pollution severity.....	76
2.16. Linearity of withstand voltage with arcing distance.....	76
2.16.1. Under AC .....	76
2.16.2. Under DC .....	77
2.17. DC to AC severity ratios in service and in wind tunnel experiments .....	78
2.17.1. DC to AC deposit density ratio $K_p$ in service.....	78

2.17.2. Wind tunnel non-energised salt fog study.....	80
2.17.3. Wind tunnel influence of pollution size under AC and DC .....	81
2.17.4. Wind tunnel pollution size study under increasing direct voltage...82	
2.18. Summary of key points .....	85
<b>Chapter 3. HVDC Flashover of Heavily Polluted Composite Insulators Rated 120 to 250 kV: Laboratory and Analytical Characterization .....</b>	<b>87</b>
3.1. Introduction .....	87
3.2. Background to the Test Programme .....	88
3.2.1. Circuit modelling.....	89
3.2.2. Arc modelling .....	89
3.2.3. Arc propagation.....	89
3.3. Methodology .....	90
3.3.1. Test programme .....	90
3.3.2. Test set up and equipment.....	94
3.3.3. Analog computer circuit simulation .....	94
3.3.4. Finite Element Method (FEM) simulation.....	96
3.4. Main Results and Discussion .....	98
3.4.1. Modified and original electrodes .....	99
3.4.2. Verification of source requirements.....	101
3.4.3. Estimated and measured flashover voltage.....	102
3.4.4. Stages of the flashover phenomenon .....	104
3.4.5. Wet and dry pollution conductivities.....	107
3.4.6. Trunk partial arc phenomenon .....	109
3.4.7. Arc propagation.....	112
3.5. Conclusions .....	113
<b>Chapter 4. Performance of Composite Outdoor Insulator under Superimposed Direct and Switching Impulse Voltages .....</b>	<b>116</b>

4.1. Introduction .....	116
4.2. Background on HVDC insulator flashover under switching impulse superimposed on direct voltage .....	118
4.3. Experimental Setup .....	119
4.4. Methodology.....	124
4.4.1. The Rain Conductivity .....	124
4.4.2. Selection of Direct Voltage Magnitude .....	125
4.4.3. Flashover Voltage Measurement.....	126
4.5.1. EMTP/ATP Simulation .....	127
4.6. Results and Discussion.....	131
4.6.1. Measurement Versus Simulation of Divider Voltage.....	131
4.6.2. Dry and Wet Flashover under Switching Impulse Superimposed on Direct Voltage .....	133
4.6.3. The Influence of Direct Voltage.....	136
4.6.4. Effect of Insulator Orientation on Flashover Voltage.....	137
4.6.5. Time to Flashover.....	140
4.6.6. Flashover voltage in relation to insulator length.....	144
4.7. Conclusions.....	147
<b>Chapter 5. HVDC conversion of UK existing overhead lines for power uprating: 12 proposals for extreme and heavy pollution.....</b>	<b>149</b>
5.1. Introduction .....	149
5.1.1. Magnetic and electric field requirements .....	150
5.1.2. Overview of other constraints.....	150
5.2. Methodology for the conversion .....	151
5.2.1. Insulator selection and dimensioning.....	151
5.2.2. Clearance distances .....	153
5.2.3. AC to DC power ratio.....	153

5.3. Two insulation solutions.....	154
5.4. Method for presentation of results .....	154
5.4.1. Original HVAC tower active powers .....	155
5.5. L6 Results: DC voltages from 380 to 500 kV .....	157
5.6. L2 Results: DC voltages from 310 to 400 kV .....	158
5.7. L7 Results: DC voltages from 170 to 220 kV .....	159
5.8. AC to DC line conversion power ratios: $K_{AC-DC}$ .....	160
5.8.1. Interpretation of tower conversion design results.....	161
5.9. FEM results for electric field requirements (no corona ring) .....	162
5.10. Discussion .....	168
5.10.1. L6 design.....	168
5.10.2. L2 design.....	168
5.10.3. L7 design.....	168
5.10.4. Electric field requirements.....	168
5.11. Conclusions.....	169
<b>Chapter 6. Initial prototype of wind tunnel design and building for DC pollution accumulation .....</b>	<b>171</b>
6.1. Introduction .....	171
6.2. Background and design .....	172
6.3. Design of materials and geometry.....	173
6.4. FEM assessment of two material design options .....	174
6.5. Experiment methodology .....	178
6.6. Pollution accumulation results under DC and non-energised conditions .....	179
6.7. Discussion of results and possible improvements.....	180
6.7.1. Challenges and possible improvements.....	181
6.8. Conclusions and future work .....	182

<b>Chapter 7. Conclusions and future work.....</b>	<b>185</b>
7.1. Future work.....	188
7.2. Comprehensive remarks .....	190
<b>References .....</b>	<b>192</b>
<b>Appendix A .....</b>	<b>210</b>
Current dependent arc resistance model.....	210



# List of figures

Fig. 2.1. Outdoor insulator with indication of its parts and geometrical entities.  
 ..... 12

Fig. 2.2. Insulator classification by application, composition, profile, and material.  
 ..... 13

Fig. 2.3. Scenario 3, as defined in TABLE 2.2. Electric field (kV/m) as a function of the creepage distance (m) in a 9000 (mm) cylindrical insulator with 90 (mm) diameter [8]. ..... 20

Fig. 2.4. Kaolin relationship between contact angle ( $^{\circ}$ ) and hydrophobicity transfer time (h) [28]. ..... 25

Fig. 2.5. Kieselguhr relationship between contact angle ( $^{\circ}$ ) and hydrophobicity transfer time (h), at different particle size [28]. ..... 26

Fig. 2.6 Six insulator conditions with growing hydrophilic fraction  $p$ (%) as a percentage of the arcing distance. (a)  $p=0\%$ , (b)  $p=22.2\%$ , (c)  $p=44.4\%$ , (d)  $p=66.7\%$ , (e)  $p=88.9\%$ , (f)  $p=100\%$  [32]. ..... 27

Fig. 2.7. Specific flashover voltage (kV/m) as a function of hydrophilic fraction  $p$  (%) [32]. ..... 28

Fig. 2.8. Insulation selection and dimensioning: conceptual scheme. .... 35

Fig. 2.9. Flowchart for the determination of  $B$  and  $\alpha$ . .... 37

Fig. 2.10. Simplified dimensioning scheme for HVDC insulators. .... 38

Fig. 2.11. Simplified dimensioning process. Determining the required USCD [4].  
 ..... 39

Fig. 2.12. Profile used for  $USCD_{DC}$  calculation examples. .... 46

Fig. 2.13. Simplified dimensioning if pollution and wetting occur at the same time.  
 ..... 47

Fig. 2.14. AC  $U_{50}/unit$  (kV) as a function of NSDD under two SDD conditions, for the 250S type disc insulator [49]. .... 52

Fig. 2.15. Consolidated data illustrating the effect of the amount of non-soluble materials in the pollution layer on the flashover voltage of the insulator [2], [48], [50]–[52]. ..... 53

Fig. 2.16. Schematic original and improved process of the pollution method for composite insulators [57]. ..... 57

Fig. 2.17. (a) Contact angle relationship with time after pollution (h). (b) Pollution withstand voltage (kV) relationship with time after pollution (h) [57].....	58
Fig. 2.18. ESDD ratio as a function of insulator average diameter. For a), the reference ESDD corresponds to D=115mm, under de-energised condition [87]; for b), the reference is D=200mm, under DC energisation [74].....	67
Fig. 2.19. USCD as a function of the average diameter, under AC [88].....	68
Fig. 2.20. Average contact angle along the core of each insulator in each of the compass directions [90].....	70
Fig. 2.21. Average contact angle on the top surface of the sheds in each of the compass directions [90].....	70
Fig. 2.22. Graphical description of P1, P2, and S, as used in Fig. 2.23 and Fig. 2.25. ....	72
Fig. 2.23. Specific flashover voltage (kV/m) as a function of insulator creepage factor. The labels above the icons show the spacing between two large sheds S, as shown in Fig. 2.22. Post-processed from [88].....	73
Fig. 2.24. Specific flashover voltage (kV/m) as a function of the creepage factor [4].....	74
Fig. 2.25. Specific flashover voltage (kV/m) as a function of CF. The labels above the icons show the spacing S between two large sheds, as shown in Fig. 2.22. Post-processed from [33]. ....	75
Fig. 2.26. Composite insulator linearity of withstand voltage (kV) and effective length (AD) (m), at NSDD=0.1 mg/cm <sup>2</sup> [88]. ....	77
Fig. 2.27. Relationship between ESDD measured on AC energised or non-energised insulators and K <sub>p</sub> [71], [99], [107]–[111]. ....	79
Fig. 2.28. Non-energised salt fog study at various insulator diameters with wind tunnel [112]. ....	80
Fig. 2.29. Pollution size study under AC and DC with wind tunnel [113].....	81
Fig. 2.30. Results of pollution size study under AC and DC with wind tunnel for two different profiles [113]. ....	82
Fig. 2.31. Pollution size study under increasing direct voltage [114]. ....	83
Fig. 2.32. K <sub>p</sub> as a function of wind speed at different mesh sizes. USCD <sub>DC</sub> =21.3 mm/kV [114].....	83

Fig. 2.33.  $K_p$  as a function of wind speed at different mesh sizes.  $USCD_{DC}=33.8$  mm/kV [114] ..... 84

Fig. 2.34.  $K_p$  as a function of wind speed at different mesh sizes.  $USCD_{DC}=67.6$  mm/kV [114] ..... 84

Fig. 3.1. (a) Insulator profile dimensions and radii in mm; (b) model of trunk partial arc on the right in blue; and table of the dimensions and estimated flashover voltage of all tested insulators. V and H stand for vertical and horizontal ..... 92

Fig. 3.2. Polluted specimens left to dry ..... 93

Fig. 3.3. Vertical and horizontal arrangements for DC pollution tests. .... 93

Fig. 3.4. The test equipment for the HVDC test. Pictures are mirrored. .... 94

Fig. 3.5. LTspice equivalent circuit model of the experimental set-up. .... 95

Fig. 3.6. a), b): mesh and its details of the insulator with original electrodes – axisymmetric model. c), d): mesh and its details of the insulator with modified electrodes – three-dimensional model. Metal domains were meshed because the electric current physics has been used ..... 100

Fig. 3.7. (a) Equipotential lines (V) of the original electrodes; (b) equipotential lines of the modified electrodes. On the right, tangent electric field along the creepage path of both electrode types. The results correspond to an energization of 40 kV. .... 101

Fig. 3.8. In green, the simulated clean and dry insulator voltage, when modelled as the capacitance  $C_i$ . In blue, the measured (or simulated because of great agreement with measurement) wet and polluted insulator voltage. In red, the percentage voltage drop, always below the standard-specified 10% limit. .... 102

Fig. 3.9. Estimated and measured flashover voltages (kV) as a function of arcing distance (mm). Abbreviated nomenclature reflects definitions of Fig. 3.1. .... 103

Fig. 3.10. V1 test. Direct voltage (kV), current (mA), and resistance ( $M\Omega$ ) all as a function of time (s). The resistance is shown with a small and a large interval, for ease of visualization ..... 105

Fig. 3.11. V1 test. Test video frames, (i) to (vii). .... 105

Fig. 3.12. Pollution conductivity  $\sigma_p$  (S/m) calculated from each insulator test for an estimated pollution thickness of 0.5 mm. Conductivities relate to the wet

condition at the test start, and to the dry condition just before flashover, both calculated with (3.3). (a) The vertical tests, and (b) the horizontal tests. ....	108
Fig. 3.13. Water vapour moving upwards during HVDC pollution flashover in both vertical, on the left, and horizontal, on the right, orientations.....	108
Fig. 3.14. Thermal images showing advanced stage of dry bands at two different view angles. (a) a clearer view of the sheds, from H3 insulator. (b) a clearer view of the trunks, from H2 insulator. (c) the current density tangent to 270 degrees of the insulator surface.....	109
Fig. 3.15. Tangent electric field $E_t$ (kV/mm) as a function of the creepage distance (mm) in three phases: uniformly wet pollution layer in blue, trunk dry bands in green, and partial arcs in red. On the left the whole creepage path, on the right a detail of a trunk. ....	110
Fig. 3.16. Tangent electric field $E_t$ (kV/mm) as a function of the creepage distance (mm) at same three instants and with same colours of Fig. 3.15. Each chart indicates the insulator name, simulation voltage, time from ramp start, and number of short-circuited trunks.....	111
Fig. 3.17. Arc propagation. Frames of the vertical V1 test, each taken every 5 ms. The recording occurred at 1000fps, 1 frame every 1 ms. The frames show about 3 alternating shed repetitions. ....	112
Fig. 3.18. Frames of the horizontal H1 test, each taken every 10 ms. The recording occurred at 1000fps, 1 frame every 1 ms. The frames show 8 alternating shed repetitions. ....	112
Fig. 4.1. Voltage superimposition waveshapes on HVDC lines. Studies by [136]–[139]. ....	116
Fig. 4.2. Rain pH world map [147], and Japan’s rain conductivity by frequency [148]. ....	118
Fig. 4.3. Laboratory test setup for switching impulse superimposition on direct voltage.....	120
Fig. 4.4. Map view of laboratory setup for voltage superimposition.....	121
Fig. 4.5. Vertical and horizontal arrangement of the insulator.....	122
Fig. 4.6. Tested insulator. All units in millimetres. ....	123
Fig. 4.7. EMTP/ATP circuit model of the experimental set-up. ....	128

Fig. 4.8. Comparison of superimposition test circuits. a) Circuit developed in this work [122], b) Cortina *et al.* [145] and c) Watanabe [146].....130

Fig. 4.9. (a) EMTP/ATP simulation results for the switching impulse superimposed on DC energisation; (b) damped capacitive divider experimental measurement during the superimposition of the switching impulse and DC voltage obtained in the laboratory.....132

Fig. 4.10. On the left y-axis, the flashover voltage as a function of rain conductivity. On the right y-axis, the flashover drop, with respect to the dry condition, as a function of rain conductivity. Each chart includes the dry condition at 0  $\mu\text{S}/\text{cm}$ .....135

Fig. 4.11. The flashover voltage drop due to the DC energisation normalized to 16 kV, which is the applied direct voltage, as a function of rain conductivity. .136

Fig. 4.12. a), b), c): mesh vertical section of vertical insulator model. d), e), f): mesh horizontal section of horizontal insulator model. The metal was not meshed because the electrostatic physics has been used to model the clean and dry insulator.....138

Fig. 4.13. Electric field magnitude along the creepage path of the insulator as a function of axis coordinate, in both orientations, with high voltage electrode at 288.230 kV.....139

Fig. 4.14 Equipotential lines (V) in the vicinity of the ground electrode when the high voltage electrode is at 288 kV. Each section view has been obtained with a cutting plane, which is vertical for (a), and horizontal for (b). .....140

Fig. 4.15. Flashover voltage as a function of the average time to flashover. Each column is characterized at the top by its test condition. Legend of the rain conductivity  $\sigma$  is provided in TABLE 4.3. The bars with vertical lines show the results for the vertical arrangement, likewise, the bars with horizontal lines show the results for the horizontal arrangement. ....141

Fig. 4.16. Cortina *et al.* [145] results on superimposition with zoom on negative direct voltage and negative switching impulse. Post insulator.....144

Fig. 4.17. Watanabe [146] results 1 on superimposition. Post insulator.....145

Fig. 4.18. Watanabe [146] results 2 on superimposition. Cap and pin insulator string.....145

Fig. 4.19. Comparison of (-) SI and (-) SI superimposed on (-) DC performance. Vertical insulator. ....	146
Fig. 4.20. Comparison of (-) SI and (-) SI superimposed on (-) DC performance. Horizontal insulator. ....	146
Fig. 5.1 L6-0.6.....	157
Fig. 5.2 L6-0.2.....	157
Fig. 5.3 L6-0.6-fixed.....	157
Fig. 5.4 L6-0.2 fixed.....	157
Fig. 5.5 L2-0.6.....	158
Fig. 5.6 L2-0.2.....	158
Fig. 5.7 L2-0.6-fixed.....	158
Fig. 5.8 L2-0.2 fixed.....	158
Fig. 5.9 L7-0.6.....	159
Fig. 5.10 L7-0.2.....	159
Fig. 5.11 L7-0.6-fixed.....	159
Fig. 5.12 L7-0.2 fixed.....	159
Fig. 5.13. AC to DC power ratios $K_{AC-DC}$ of a) L6, b) L2, and c) L7 with two different insulation solutions under extreme and heavy pollution severities. ....	161
Fig. 5.14. Maximum electric field on ground fitting (kV/mm) for different tower insulators and different layer conductivities, at a thickness of 0.5 mm. The red dashed line shows the 1.8 kV/mm requirement.....	163
Fig. 5.15. Maximum electric field on HV fitting (kV/mm) for different tower insulators and different layer conductivities, at a thickness of 0.5 mm. The red dashed line shows the 1.8 kV/mm requirement.....	164
Fig. 5.16. Average electric field on insulator surface (or creepage) (kV/mm) for different tower insulators and different layer conductivities, at a thickness of 0.5 mm. The red dashed line shows the 0.42 kV/mm requirement.....	164
Fig. 5.17. Ground triple junction electric field (kV/mm) for different tower insulators and different layer conductivities, at a thickness of 0.5 mm. The red dashed line shows the 0.35 kV/mm requirement. ....	165
Fig. 5.18. HV triple junction electric field (kV/mm) for different tower insulators and different layer conductivities, at a thickness of 0.5 mm. The red dashed line shows the 0.35 kV/mm requirement.....	165

Fig. 5.19. L6 insulator fitting equipotential lines (V), at U=440 kV. ....	166
Fig. 5.20. L2 insulator fitting equipotential lines (V), at U=360 kV. ....	167
Fig. 5.21. L7 insulator fitting equipotential lines (V), at U=210 kV. ....	167
Fig. 6.1. Wind tunnel CAD design. All measurements are in mm. ....	172
Fig. 6.2. Vertical section mesh of three-dimensional model of wind tunnel test facility. Metal parts are meshed because the electric current physics was used. ....	175
Fig. 6.3. Wind tunnel equipotential lines (V) at a layer conductivity of $10^{-9}$ (S/m). ....	176
Fig. 6.4. Wind tunnel equipotential lines (V) at a layer conductivity of $10^{-5}$ (S/m). ....	176
Fig. 6.5. Electric potential (V) and electric field magnitude (kV/mm) along the creepage of the insulator (mm), at a conductivity of $10^{-9}$ S/m. ....	177
Fig. 6.6. Electric potential (V) and electric field magnitude (kV/mm) along the creepage of the insulator (mm), at a conductivity of $10^{-5}$ S/m. ....	177
Fig. 6.7. Built wind tunnel. ....	178
Fig. 6.8. Pictures of insulator after test at maximum wind speed setting. ....	179
Fig. 6.9. NSDD under DC energised and non-energised conditions at three wind speed settings, and calculation of their ratio $K_p$ . $USCD_{DC}=80.5$ mm/kV. ....	180



# List of tables

TABLE 2.1. Electric field requirements for composite insulators.....	18
TABLE 2.2. Scenarios considered in [8] for DC corona ring need assessment....	19
TABLE 2.3. Non-uniform hydrophobicity test specifications of [32].....	27
TABLE 2.4. Environmental classification of pollution and its components. ....	31
TABLE 2.5. ESDD, NSDD, ESDD <sub>eq</sub> DC service values [4]. .....	34
TABLE 2.6. K <sub>p</sub> values as a function of wind speed [4]. .....	40
TABLE 2.7. α values for HTM and non-HTM materials.....	41
TABLE 2.8. Contamination uniformity ratio constant K <sub>s</sub> for different materials. .....	42
TABLE 2.9. Statistical factor values for small and large number of insulators..	43
TABLE 2.10. B and α values for HTM and non-HTM values. ....	44
TABLE 2.11. θ values for HTM and non-HTM materials.....	45
TABLE 2.12. B and α values for compact equation for HTM and non-HTM materials.....	46
TABLE 2.13. USCD dimensioning examples, using severity data from [4]. .....	47
TABLE 2.14. α values for simplified dimensioning when pollution and wetting occur at the same time. ....	49
TABLE 2.15. Active and inert pollution: components and properties [44]. .....	50
TABLE 2.16. AC and DC pollution performance of 250S disc insulator. ....	55
TABLE 2.17. Original and improved process of the pollution method for composite insulators [57]. .....	56
TABLE 2.18. Dominant forces on pollution particle as a function of wind velocity [61]. .....	59
TABLE 2.19. Wetting mechanisms with variation of insulator-ambient temperature difference [2]. .....	63
TABLE 2.20. Test specifications of Matsuoka <i>et al.</i> [88]. .....	72
TABLE 2.21. Test specifications of Zhang <i>et al.</i> [33]. .....	73
TABLE 2.22. K <sub>p</sub> values for different environment types [106]. .....	78
TABLE 2.23. Conservative calculation of significant large DC severities from Fig. 2.27. ....	79
TABLE 3.1. Circuit Parameters and Per Unit Base Values.....	96

TABLE 3.2. Material Properties for FEM Modelling.....	97
TABLE 3.3. Arc Conductivity Formula Parameters.....	98
TABLE 4.1. Test Insulator Dimensions.....	123
TABLE 4.2. Switching Impulse Test Parameters.....	124
TABLE 4.3. Rain Test Data.....	124
TABLE 4.4. Full Description of the Circuit Model.....	128
TABLE 4.5. Legend of symbols for orientation and conductivity.....	142
TABLE 4.6. Time to Flashover Deviation, (+)SI.....	143
TABLE 4.7. Time to Flashover Deviation, (-)SI.....	143
TABLE 4.8. Time to Flashover Deviation, (-)DC and (-)SI.....	143
Table 5.1. L6 proposals for HVDC use.....	157
Table 5.2. L2 proposals for HVDC use.....	158
Table 5.3. L7 proposals for HVDC use.....	159
TABLE 5.4. Material Properties for FEM Modelling.....	162
TABLE 5.5. FEM current results; and FEM electric field results against requirements.....	163
TABLE 6.1. Material Properties for FEM Modelling.....	174

*List of tables*

# Chapter 1. Introduction

High Voltage Direct Current (HVDC) systems are increasingly being adopted in electric power systems around the world for different purposes. These include the long distance transmission of bulk power and the integration of renewable resources like solar radiation and wind energy. HVDC systems are also used to increase the power transfer of transmission lines needed for the electrification of transport and heating to reduce carbon emissions. This thesis contributes to a key aspect of this HVDC revolution, by investigating outdoor insulators for use on new DC lines and on existing lines converted to DC.

## 1.1. The relevance of the broad HVDC research

Due to the lack of extensive service experience and the continuing innovation in HVDC technology, some parts of the industry are reticent to widely adopt HVDC projects even when costs are lower compared to those of High Voltage Alternating Current (HVAC) systems. The reticence that sometimes occurs is due to the long successful track record of HVAC systems over the past century, and the hazards of integrating new HVDC technology in the electric power system, which is critical for human life as we know it. For this reason, HVDC research, in general, is necessary to minimise the risks of adoption, by understanding its core issues, then by defining relevant questions, and ultimately by delivering meaningful conclusions. This thesis focuses on the performance of composite outdoor insulators and their performance under direct voltage under various conditions.

## 1.2. The thesis content and contribution

Generally, overhead lines constitute the majority of electric power transmission systems. Their most critical aspect is the performance of outdoor insulation. Thus, a review on the subject is provided in Chapter 2, which presents the literature knowledge common to both HVAC and HVDC outdoor insulators, and

more specifically, an understanding of why pollution performance is particularly critical under HVDC.

The work presented in this thesis has allowed to achieve the following contributions, which are focused on three research areas.

Firstly, in Chapter 3, the thesis presents the HVDC performance of outdoor insulation under an extremely polluted condition, which causes a great decrease in performance compared to the clean condition. The experimental aspect of this research is the result of a collaboration which occurred during a secondment at the UHVDC pollution test laboratory of China Electric Power Research Institute, in Beijing, China. Also, in Chapter 4, a study is presented on the effects of superimposing a switching impulse on direct voltage, with respect to switching impulse only, as this similarly occurs in operation on the healthy pole of a bipolar scheme, when the other pole experiences a fault to ground. This aspect of the research was enhanced through a collaboration started with a secondment at the High Voltage laboratory of the University of Porto, Portugal. Both Chapter 3 and Chapter 4 investigate the performance difference between the vertical and the horizontal orientations. This is done to understand in detail the advantages of a vertical insulator, such as suspension or post insulators, with respect to a horizontal insulator, such as tension or cross arm insulators, under the same conditions.

Secondly, in Chapter 5, an explorative and conservative investigation on the conversion of existing HVAC overhead lines to HVDC is presented. Based on the knowledge provided by existing literature and Chapter 3, four preliminary designs for each of three existing UK transmission towers are provided for extreme and heavy pollution degrees. Two of these three towers are currently used on 85% of the UK transmission overhead lines. High pollution values are assumed because of the electrostatic attraction of the pollution towards the charged insulators. The UK wind speeds are quite large, which would suggest a corresponding similar level of pollution deposition between AC and DC insulators. However, low wind speed areas may exist along the lines and cause local large pollution accumulation. That is why extreme and heavy contamination

levels are considered. The HVDC conversion proposals would transmit from 1.6 to 2.9 times the original HVAC power, with different degrees of risk involved.

Thirdly, in Chapter 6, a wind tunnel for pollution accumulation on an insulator is designed, modelled, built, and used for tests which provided the following: the NSDDs of a composite insulator at three different wind speeds in the non-energised and energised conditions; and the ratios  $K_p$  between  $NSDD_{DC}$  and  $NSDD_{non-energised}$  at the same three different wind speeds.

Thus, in summary, the objectives of the thesis are to first gather further new information on the most critical component of an overhead line, namely its outdoor insulation system, by means of laboratory testing, as well as reviewing literature in detail; later, part of this knowledge is applied to provide insulation solutions for the conversion of existing lines to HVDC. A wind tunnel experimental investigation is also performed to investigate the influence of direct voltage on the insulator pollution accumulation, with respect to the non-energised case.

The following list summarises what was planned and achieved during the PhD, which is provided in the thesis:

- A recent literature review of composite outdoor insulators on:
  - 1) Assessment of corona ring need for outdoor insulators under direct voltage;
  - 2) Performance characteristic in relation to the hydrophilic portion of composite insulator, in proximity of the insulator ends;
  - 3) Best performing insulator designs for both light and heavy pollution severity in laboratory conditions;
  - 4) Positive relationship between inert material pore size and hydrophobicity recovery speed;
  - 5) Wind tunnel pollution accumulation ratios (of DC over AC or non-energised conditions) at various wind speeds and voltage gradients.
- Analytical and laboratory characterisation of heavily polluted insulators under direct voltage:

- 1) Electrode shape effect on tangent electric field was shown to be negligible using FEM modelling. In fact, at the triple junction, the tangent electric field is at most 6.3 times larger when the electrode is modified. However, the notable difference is present only on less than 55 mm of creepage distance in the proximity of the triple junction. Elsewhere, along the insulator, the difference factor is reduced from 6.3 to 0.03;
  - 2) Good comparison of estimated flashover voltages with measurements was achieved in the range between 96 and 252 kV;
  - 3) Development of proposal for the orientation factor  $K_0$  for a more specific and accurate calculation of the  $USCD_{DC}$ . At present,  $K_0$  is set as 1 for the vertical orientation, and it is found as 0.896 for the horizontal. However, future work is suggested to extend the applicability of this factor to other profiles and pollution conditions;
  - 4) Clarification of the superior horizontal performance explained with arc propagation direction and convection heat direction.
- Direct voltage and switching impulse superimposition under dry and rain conditions.
    - 1) Better understanding of the superior horizontal performance under clean conditions due to the electrode configuration. A FEM model, run at 288 kV, found an electric field of 10.7 kV/mm at the triple junction of the ground electrode when the insulator is vertical, against 8.5 kV/mm for the horizontal;
    - 2) The superior horizontal performance under rain conditions was attributed to the droplet path which is favourable with the voltage gradient when the insulator is vertical, and the larger amount of deposited rain on the shed tops when the insulator is vertical. This allowed withstand voltages of the horizontal insulator about 40% larger than the vertical;
    - 3) Performance loss saturation under large rain conductivity conditions;
    - 4) Quantification of the direct voltage pre-energisation effect on the switching impulse withstand voltage, which was in the range of half the applied direct voltage of 16 kV in the dry condition.

- HVDC conversion of UK existing HVAC overhead lines:
  - 1) Systematic gathering of a comprehensive methodology for the conversion from multiple brochures, reports and papers;
  - 2) Quantification of the power uprating factor, given by the conservative design of the tower insulation solutions for direct voltage application. The factor was found to vary from 1.6 to 2.9, depending on tower type and pollution severity;
  - 3) Benefit quantification given by the use of inclined insulators to fix the position of the poles in space, which ranges from 0% to 13.6% and is more beneficial as the pollution severity decreases;
  - 4) Non-necessity of corona rings for leakage current values in the range of a few nA, which are commonly exceeded in operation.
- Initial prototype of wind tunnel for pollution accumulation under direct voltage:
  - 1) Novel introduction of an insulating enclosure to reduce the electric field stress at the insulator ends or to modify it at will from outside the enclosure;
  - 2) Confirmation and quantification of larger NSDD due to the direct voltage energisation, which causes 1.2 to 1.3 times the NSDD without direct voltage, at a  $USCD_{DC}$  of 80.5 mm/kV. And positive correlation between NSDD and tunnel wind speed for both non-energised and energised cases;
  - 3) Design improvement proposals for the reduction of the contamination injection rate and the increment of the air flow uniformity across the tunnel section.

### 1.3. Methodology

Depending on the thesis contribution type, different and complementary ways of achieving the results have been employed. For the experimental part of the thesis, standards have been followed, where available, to execute the test programmes. To obtain additional insights of the studied phenomena, circuit and finite element method numerical simulations have been implemented. These

were performed using EMTP/ATP, LTspice, COMSOL Multiphysics®, and AutoCAD. Particularly, the CEPRI and University of Porto laboratory equivalent circuits have been calculated for the first time and are provided here. Also, the tools allowed to simulate and explain the transient of the switching impulse superimposition on direct voltage. They have also allowed to confirm why during an HVDC pollution flashover event the trunks are bridged with arcs before the sheds are and why a better performance is shown when the insulator is horizontally oriented, as recorded with the voltage and current measurements, thermal images, normal and fast camera videos.

On the other hand, the line conversion proposals are based on the estimated performance of the considered insulator profile, which is one of the two investigated in the first part of the thesis, under extreme and heavy pollution degrees. This is done by calculating the insulator performance, as explained in section 2.8.3, further explained in IEC 60815-4 and CIGRE TB 518. Although these are authoritative sources, suggestions on future work are made for specific dimensioning factors. The proposals are also based on the conservative assumption of a large overvoltage factor, which determines the air clearances needed to avoid breakdown during a voltage transient.

## **1.4. Sources choice**

The main sources laying the foundations of the thesis contribution are technical brochures from CIGRE, BS EN (from IEC) high voltage standards, and an Electric Power Research Institute (EPRI) report. Specific journal papers have been selected and discussed to compare the results with existing literature.

## **1.5. The thesis is a deeper dive**

Compared to the published papers, this thesis provides more extensive information on the used High Voltage test equipment, and on the test circuit and specimen comparisons with other relevant research. It also provides additional charts, pictures, and details which can be of interest.

Although the thesis is presented as a coherent single story, the chapters are written in a way that, for the most part, they could be read individually. However, reading the full thesis will provide a broader understanding of the topic at the insulator level, and at the overhead line level.

## **1.6. The implications**

The thesis provides new and detailed justifications on why horizontally oriented insulators perform better than when vertically oriented. Also, it provides proposals for converting existing overhead lines to HVDC for power uprating which is expected to be valuable due to the upcoming electrification of transport and household heating.



# Chapter 2. A review of polluted outdoor insulators

## 2.1. An introduction to outdoor insulators

Outdoor insulators are widely used on transmission networks because an overhead line is generally inexpensive compared to an underground cable line. High Voltage Direct Current (HVDC) overhead lines are used to transfer bulk power in Brazil, Russia, Canada and China. For example, they constitute the backbone of China's long-distance electric power transmission. These lines allow to transmit large amounts of power from the remote north-western and western regions of the country to the eastern and south-eastern centres of consumption [1].

The critical part of an overhead line is attributed to outdoor insulators, which insulate and mechanically support the high voltage conductors from the electrical ground. The electrical ground is constituted by the metallic parts of the tower. The main hazard to the proper functioning of outdoor insulators is the deposition of pollution and water on their surfaces [2], which can drastically affect the insulator electrical performance. With the exception of metallic and inert pollution, dry pollution alone is not conductive. However, the dissolution of pollution salts in water causes the formation of an electrolyte which easily conducts electricity on the surface of the insulator. That is when the discharge activity begins.

The pollution severity on an insulator surface is a function of:

- a) the insulator type,
- b) the type of voltage or electrical application,
- c) the nominal voltage of the line,
- d) the climate and
- e) the environment.

- a) The insulator type is defined by its geometry and materials. Various recommendations are given on the geometry characteristics of insulators, to maximise their performance under specific conditions. The materials used for their production react differently with pollution. Of particular interest is silicone rubber which can transfer its hydrophobic property to the deposited pollution, preventing water from depositing on the insulator surface and forming the conductive layer.
- b) The type of voltage, or electrical application, depends on whether the insulator is energised with High Voltage Direct Current (HVDC) or High Voltage Alternating Current (HVAC). It has been observed [2] that DC insulation causes the pollution to be electrostatically attracted to the insulator because of its electrostatic field effect on the airborne particles. This field causes a constant potential distribution in time, which causes the attraction. Whereas in the AC case, the insulators are less covered in pollution because the voltage periodically reverses in time, which does not cause a continuous pull of the pollution.
- c) In the DC case, as the nominal voltage of the line increases, the pollution attraction and deposition increase.
- d) The climate is defined by several physical quantities, such as:
  - d1) temperature,
  - d2) pressure,
  - d3) humidity,
  - d4) rain and its different forms,
  - d5) snow,
  - d6) ice,
  - d7) wind and
  - d8) sun radiation.

All these can vary with time. These parameters influence the pollution chemical composition and behaviour, as well as the dissolution phenomenon and consequential discharge steps.

- e) The environment is defined by specific human production activity or natural surroundings, which mainly determine the chemical composition of the pollution.

Further, in Sections 2.2.2, 2.5, 2.6 and 2.15 of the thesis, these aspects will be analysed in detail.

### **2.1.1. Outdoor insulation requirements, and costs**

One of the main requirements of the insulator is to be able to withstand not only nominal voltage, but overvoltages too in wet-polluted conditions. Other requirements are mechanical support of the conductors, slow ageing, etc.

To determine the insulator performance, a test method is carried out. When several test methods are used in parallel and compared, the best study results are achieved. As an example, a standard method for DC pollution testing on composite insulators is not yet publicly available, so there exist different methods used by different laboratories, which can provide multiple insights.

The costs associated with optimally designing an insulator, are the costs of production and testing the equipment, as well as the labour cost. The cost of an insulation system can be minimised, balancing the trade-off with critical factors, such as power outage costs, ageing costs, etc.

## **2.2. Insulator nomenclature, classification, performance, and stress**

### **2.2.1. Insulator nomenclature and functions**

It is important to clarify the nomenclature used in this thesis, with regards to the insulator parts and geometrical entities. Different types of insulators exist, as shown in section 2.2.2. However, the contribution of this thesis focuses on composite outdoor insulators, as shown in Fig. 2.1. Therefore, the following

description is based on composite insulators, but it applies to the other insulator types too.

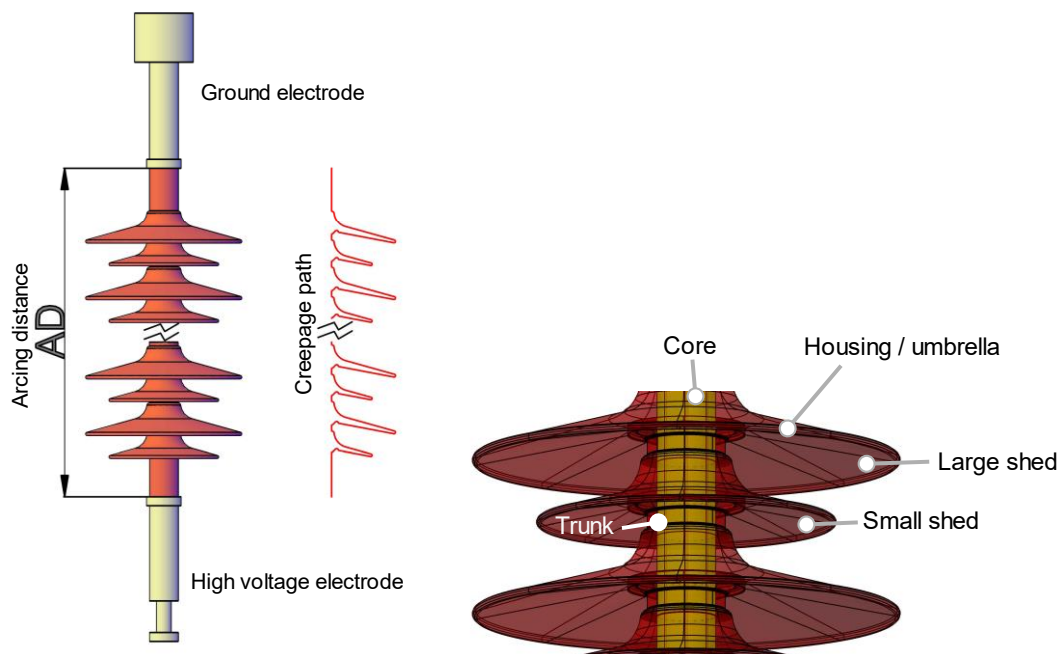


Fig. 2.1. Outdoor insulator with indication of its parts and geometrical entities.

With regards to the insulator parts, it is worth distinguishing its conductive metallic parts, consisting of metal electrodes, and the insulating parts, by the insulator housing and core. The electrodes are standardised by the insulator fittings standard [3] and are different in shape depending on the application. For a composite insulator, the jacket/outer housing material is usually made of silicone rubber or a polymer-based material, and the core is made of fibre glass.

With regards to the geometry, an outdoor insulator does not have the shape of a simple cylinder, but it repetitively goes outwards and inwards giving shape to the so defined sheds and trunks. This is done to lengthen the path that connects the two electrodes, allowing a better performance. When the sheds repeat along the insulator axial length with a small and a large diameter, the profile is called Alternating Long-Short (ALS) profile.

Two critical distances are often reported in the literature, and they are the Arcing Distance (AD) and the Creepage Distance (CD). The arcing distance is the shortest distance between the two electrodes. The creepage distance is the length of the creepage path, which is the shortest path between the electrodes along the insulator surface. The CD is usually 2.5 to 4.5 times the AD. This ratio is defined as the Creepage Factor (CF), which is the ratio between CD and AD.

These definitions reflect those of the most recent technical brochure from CIGRE with regards to HVDC insulator selection and dimensioning [4]. However, it is worth noting that other documents may refer to lengths, rather than distances

### 2.2.2. Insulator classification

Insulators can be classified by the following characteristics, which are also shown in Fig. 2.2:

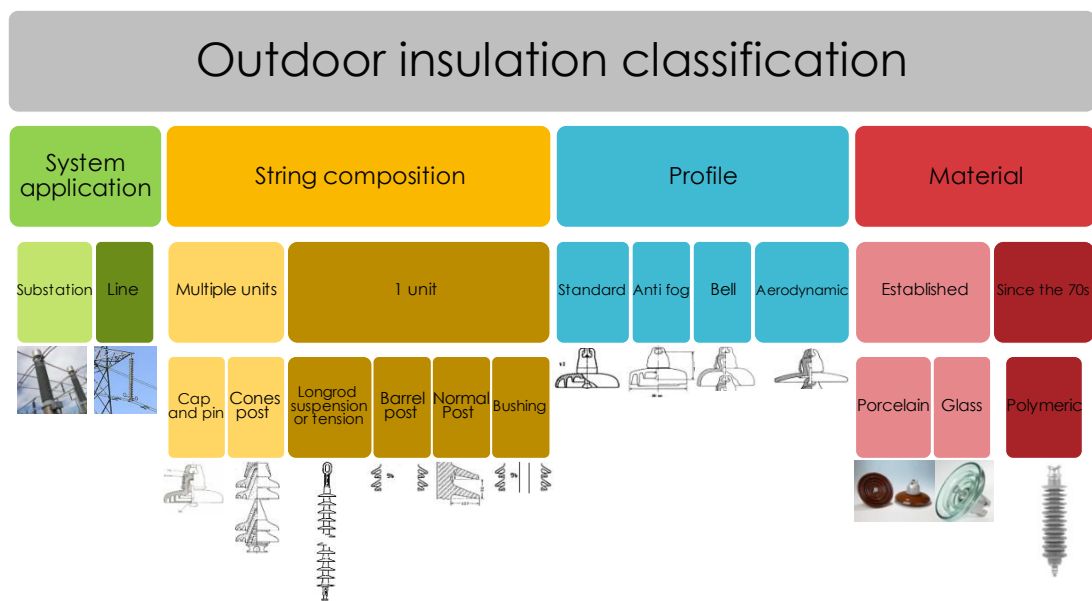


Fig. 2.2. Insulator classification by application, composition, profile, and material.

With regards to material,

- a) Porcelain and glass are well-established materials. They are used to build reliable insulators. For HVDC application: composition, purity,

homogeneity, and resistivity need to be taken care of to avoid spontaneous failure [5].

b) Polymers represent a competitive solution since the 70s, but the variety of polymeric materials imposes great attention on the choice of its composition. To obtain different polymers, the following procedures can be used:

- b1) gravity pouring,
- b2) extrusion and
- b3) high pressure/temperature injection.

And the following parameters can be varied:

- b4) amount of filler and
- b5) type of catalyst.

The final product will be greatly affected by these variables.

### **2.2.3. Insulator performance**

The insulator performance is determined by how large a voltage it is able to withstand in wet-polluted conditions and overvoltage conditions without flashover occurring across its terminal electrodes. The performance is a function of these global parameters:

- a) axial stress,
- b) surface stress,
- c) pollution deposit equilibrium.

These variables change depending on:

- d) design (geometry) of insulator and tower,
- e) material of insulator and tower,
- f) energisation waveform,
- g) climate and

h) environment.

$$Performance = f(\text{axial stress, surface stress, ...}) \quad (2.1)$$

Where

$$Axial\ stress = \frac{U_{50}(kV)}{AL(mm)} \quad (2.2)$$

$$Surface\ stress = \frac{U_{50}(kV)}{CL(mm)} \quad (2.3)$$

Where,  $U_{50}$  is the voltage across the specimen, usually the phase voltage. 50 indicates the percentage of cases in which that voltage statistically causes flashover when it is applied. In AC, it is the RMS value and in DC it is the direct voltage value. If axial and surface stresses are large and the risk of failure is low, the performance is good. In fact, it means that, for each unit length, the insulator is able to withstand a large voltage.

It is very important to understand that axial stress and surface stress are global parameters that are only partially able to tell the performance of the insulator because they differ depending on design, material, and energisation type.

In fact, one particular design can have the same creepage length of another design, but their surface stresses may be very different. Moreover, in some cases, some insulators perform better than others even if they are shorter in creepage length.

#### 2.2.4. Insulator electrical stress

The insulator *electrical stress* is another useful insulator parameter, particularly in the design process. IEC 815 [6], and CIGRE TB 158 [2] define the insulator electrical stress as a function of:

- a) the specific creepage length and
- b) the specific axial length

$$\text{Electrical stress} = f(SCL, SAL) \quad (2.4)$$

When each one is divided by the line to line voltage or phase voltage, the specific length is obtained, i.e.:

For IEC 815:

$$SCL = \frac{CL \text{ (mm)}}{U \text{ (kV)}} \quad (2.5)$$

where U is the line to line voltage.

For CIGRE 158:

$$SCL = \frac{CL \text{ (mm)}}{\text{actual voltage } E \text{ (kV)}} \quad (2.6)$$

where E is the phase voltage. This is also indicated as the Unified Specific Creepage Distance (mm/kV) by CIGRE TB 518 [4].

Note that the actual voltage could be the line to line voltage if the insulator is placed between two conductors.

For IEC 815:

$$SAL = \frac{AL \text{ (mm)}}{U \text{ (kV)}} \quad (2.7)$$

where U is the line to line voltage

For CIGRE 158:

$$SAL = \frac{AL \text{ (mm)}}{\text{actual voltage } E \text{ (kV)}} \quad (2.8)$$

where E is the phase voltage.

Again, note that the actual voltage could be the line to line voltage if the insulator is placed between two phase conductors in the case of an HVAC line, or the pole to pole voltage in the case of an HVDC line.

## 2.3. Shielding electrodes

In high voltage engineering, sharp-edged geometries generally exhibit a large electric field. To reduce the field intensity, shielding electrodes can be used in the shape of a sphere or a toroid [7].

### 2.3.1. Corona ring purposes under AC

One largely used shielding electrode shape for outdoor insulators is the toroid, also commonly referred to as *corona ring*. The purposes of corona ring use on AC outdoor insulators are found in [8] and are listed as follows:

- a) to eliminate corona from insulator fittings: *corona shielding function*,
- b) to grade the voltage potential along the string in order to limit the radio interference from insulators, and for composite insulators to reduce ageing phenomena: *grading function*, and
- c) to limit the effect of power arcs: *protective function*.

### 2.3.2. Electric field requirements for composite insulators

An INMR article provides the electric field requirements used in many practical applications for composite insulators [9], based on a recent study [10] which collects the results of EPRI (USA) and STRI (Sweden) research groups. The requirements are presented in TABLE 2.1.

TABLE 2.1. Electric field requirements for composite insulators.

Location		Threshold
Grading ring and end fitting [9]	<	1.8 (kV/mm)
Average along surface [9]	<	0.42 (kV/mm)
More than 10 mm of CD [10]	<	0.42 (kV/mm)
Triple junction [9], [10]	<	0.35 (kV/mm)

### 2.3.3. Corona ring need assessment under DC

As seen in [9], [10], it is common practice to design and install corona rings under AC energisation. However, there is a difference between AC and DC which depends on how an outdoor insulator can be modelled. As it will be seen in section 3.3.3, an outdoor insulator can be modelled as the parallel of a capacitance and a resistance. These represent respectively the capacitance of the air, the silicone rubber and the fibre glass, and the resistance of the pollution layer, which is the smallest and thus dominant for current conduction with respect to the other material resistances. In DC, after the short transient for charging the capacitance, the behaviour of the insulator is resistive and therefore dominated by the pollution layer. In fact, when modelling an insulator with a Finite Element Method (FEM) under DC, it is critical to consider an electric current model which accounts for Ohm's law, rather than an electrostatic model, which does not.

Pigini *et al.* [8] investigate the voltage distribution and electric field along the surface of a cylindrical insulator to be used in DC with  $CD=AD=9000$  mm and a diameter of 90 mm. Three scenarios are considered depending on leakage current determined by the surface conductivity, as summarised in TABLE 2.2. The pollution thickness is about 1 mm.

When an insulator is new and cleaned with ultrasounds, it can conduct a current of a few nA [8]. Thus, scenario A in TABLE 2.2 is doubtfully possible and it is used only to show that at 1 pA the behaviour is like in AC. Scenario B is possible only when the insulator is new and cleaned with ultrasound. Therefore, it is not the case of outdoor insulators. In fact, a weathered insulator which is then cleaned

(for conservative purposes) conducts currents of 0.5-2  $\mu\text{A}$  [8]. Thus, only scenario C is plausible in the outdoors, only after the insulator has been cleaned by rain. Scenario C is the only one where a corona ring would not be needed, as Fig. 2.3 shows.

TABLE 2.2. Scenarios considered in [8] for DC corona ring need assessment.

Scenario	Conductivity (S/m)	Current	Corona ring useful under DC
A	$10^{-13}$	1 (pA)	Yes
B	$10^{-10}$	1 (nA)	Yes
C	$10^{-17}$	0.02 ( $\mu\text{A}$ )	No

Clearly, the same would apply for larger leakage currents. The paper [8] conclusion is, therefore, that there is no need for corona rings on HVDC outdoor insulators, other than maybe small and specific ones to eliminate corona from the insulator fittings. The latter possibility is excluded in the cases studied in this thesis in Chapter 5.

It is worth mentioning that some papers [11]–[15] investigate the use of corona rings for DC insulators, disregarding the role the conductive layer has on the electric field distribution of an outdoor insulator.

As a conclusion for DC corona rings use, the thesis' author believes it is more meaningful to determine, in an electric currents model, the current above which a DC insulator does not need corona rings to satisfy the requirements of TABLE 2.1. This model-derived current will then have to be compared with current measurements of weathered insulators which have been cleaned, for conservative purposes. However, the current measurement should be found considerably greater than the model-derived current [8].

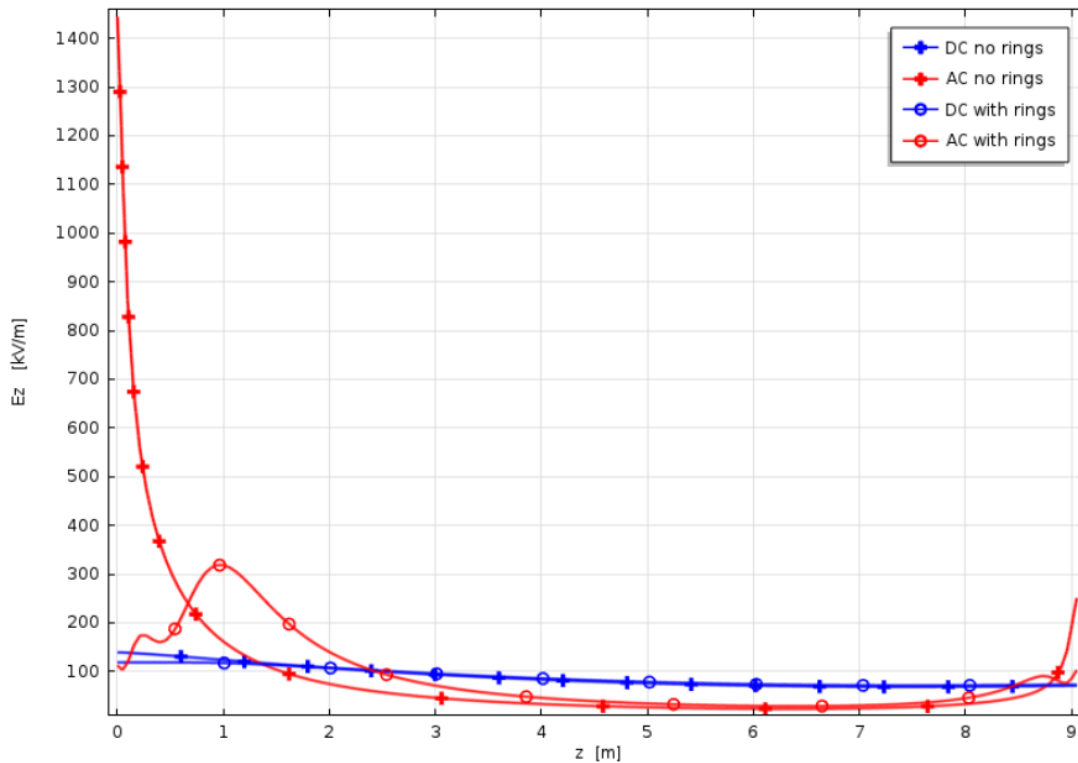


Fig. 2.3. Scenario 3, as defined in TABLE 2.2. Electric field (kV/m) as a function of the creepage distance (m) in a 9000 (mm) cylindrical insulator with 90 (mm) diameter [8].

## 2.4. Pollution flashover phenomenon

The pollution flashover phenomenon consists of the following six main stages, as presented in an Electra publication [16] and further explained in detail in this thesis:

- i) First, *dry pollution deposits* on the surface of the insulator. If the insulator is made of silicone rubber, the hydrophobic property is transferred to the pollution, as it becomes impregnated with low molecular weight silicone migrating from the bulk silicone material. At this stage, the superficial pollution layer is considerably non-conductive.
- ii) The *wetting* of pollution happens because of:
  - a) Humidity deposition, when the percentage of air humidity is sufficiently high with respect to the ambient temperature,

- b) Humidity condensation, which is typical at sunrise when the insulator is colder than the surrounding air,
- c) Rain, drizzle, mist (and other forms of these), and
- d) Snow and ice melting, which is particularly conductive.

At this stage, the pollution dissolves in the water. The result is an electrolyte which is conductive.

Note that the first two steps may occur simultaneously, when the pollution in the form of a salt is already dissolved in water, e.g. polluted water.

Moreover, the pollution may be metallic, in the case of an industrial environment; this kind of pollution does not necessitate water content to be conductive, but its degree of conductivity depends on the type of constituent metals, and its superficial density and distribution on the insulator.

- iii) The presence of conductive paths allows a current to flow between the two extremities of the insulator. Typically, one fitting is at the phase or pole potential, and the other fitting is at the ground potential. Other insulator ends' potential situations may exist, such as phase to phase in AC or pole to pole in DC. In literature, this current is called *leakage current* because it causes loss of active power. In fact, a portion of the current leaks along the line.
- iv) As the leakage current flows, the temperature on the surface rises due to Joule effect, and the liquid component of the superficial layer starts to evaporate. Some areas, typically on the trunks, dry faster than others due to a higher local current density, thus, the current avoids these non-conductive high-resistivity areas flowing around them. The superficial current density increases at the borders of the dry areas, causing more water to evaporate and the dry area to extend in the direction perpendicular to the main leakage current flow direction, in an

axisymmetric way. The evaporation continues around a portion of the insulator until a *dry band* is formed.

- v) At this point, the current is not flowing because of the dry band resistance. However, the voltage normally applied to the insulator extremities is now applied almost fully to the two borders of the dry band. If the voltage is large enough, an arc ignites in air, bridging the dry band. This occurs because the air breakdown voltage of the air gap across the dry band is lower than the dry band breakdown voltage. The phenomenon is defined as *dry band arcing*.
- a) Under DC, the arc does not extinguish and keeps expanding because the voltage is unipolar and sustains the process. Thus, the arc has the time to keep expanding upwards because of its high temperature with respect to the surrounding ambient.
- b) Under AC, the voltage periodically reverses. Therefore, the arc is intermittent. In fact, it extinguishes each time the voltage across the dry band crosses zero, and it reignites when the voltage overcomes the breakdown voltage of the air gap across the dry band.

The result is that, in DC, the dry band arcing expands upwards, possibly reaching other surfaces, e.g., it can possibly short-circuit a larger part of the insulator.

In AC, the dry band arcing remains closer to the surface because the arc does not have sufficient time to expand upwards. It should be possible to show experimentally that a very low voltage frequency would cause the arc to notably rise in the air, as opposed to an arc closer to the insulator surface, when the voltage frequency is higher.

- vi) More dry bands can be formed as well as other dry band arcs, until the insulator is spanned completely from one electrode to the other. The final arc, which connects the two insulator extremities is called *flashover*.

Porcelain and glass are hydrophilic materials, so a continuous water layer can easily form on their surface, whereas silicone rubber is hydrophobic, so the water stays in the form of droplets. However, the pollution flashover phenomenon follows the same main stages for both material types. Chapter 3 will focus on the HVDC pollution flashover phenomenon of insulators with a hydrophobic housing material.

## 2.5. Pollution flashover of hydrophilic and hydrophobic surfaces

As a general definition, a hydrophobic material is a material which tends to repel water molecules, whereas a hydrophilic material does not.

### 2.5.1. Hydrophilic material modelling

In general, the mathematical modelling of the pollution flashover provides a higher degree of knowledge and understanding [17]. *In the DC case*, two main approaches are used to do so:

- a) The determination of the minimum voltage needed to sustain a dry band arc of a given length, in series with the corresponding pollution surface resistance. This voltage is called *critical voltage* ' $U_c$ ' [18],
- b) The consideration that the dry band arc will continue to elongate as long as the arc voltage is lower than the pollution voltage [19].

Many parameters are considered for the mathematical modelling, such as:

- a) Surface resistance [20],
- b) Insulator geometry [20] and [21],
- c) Arc current concentration [22] and [23],
- d) Arc electrode voltage drop [22],
- e) Temperature [23], and
- f) Multiple parallel arcing [24].

In this thesis, the main focus will be on the performance of insulators, rather than the mathematical modelling. However, wet and dry surface resistances are studied in section 3.4.5, with the quantification of the pollution conductivity 24 hours after the housing material has lost its hydrophobicity.

### **2.5.2. Hydrophobic material modelling**

The performance of wet-polluted insulators is generally greater in the case of hydrophobic material, with respect to hydrophilic [25], [26]. In fact, a hydrophobic surface allows water to deposit in the form of droplets because of the electrical repulsion between the surface particles and the water molecules. Thus, a continuous water layer is not likely to form, and the conductive paths are drastically reduced.

However, a variety of phenomena decrease hydrophobicity [2]:

- a) *Heavy wetting,*
- b) *Blown sand, sand blasting,*
- c) *Corona discharges,*
- d) *Spark discharges, and*
- e) *Solar radiation.*

These adverse factors compromise the efficacy of the hydrophobicity on the flashover performance.

At the moment, there is no hydrophobic surface pollution flashover model, but qualitative concepts are arising [27].

A hydrophobic material has the property of transferring its hydrophobicity to the layer of pollution that lays on its surface. This occurs thanks to low molecular weight (LMW) silicone migrating from the bulk of the housing material to the surface, by filling the pores in the contamination layer.

### **2.5.3. Influence of inert material on hydrophobic material**

Yu *et al.* [28] investigated the influence of artificial non-soluble contamination on the hydrophobicity transfer property of room temperature vulcanised silicone rubber. The study considered Kaolin, Kieselguhr, and silicone dioxide as non-

soluble materials. To quantify the hydrophobicity transfer property, the contact angle of a liquid drop on the insulating surface was measured as specified in IEC 62073 [29]. The results in Fig. 2.4 show that Kaolin greatly affects the hydrophobicity transfer speed (transfer time) and hydrophobicity property (angle), as the transfer speed is very slow and the contact angle reaches about  $65^\circ$  after 7 days. This is due to the Kaolin layered structure which has few and small pores to allow LMW silicone to migrate to the pollution layer.

Instead, with Kieselguhr, good hydrophobicity is quickly recovered, after a transient of only 12 hours at a large contact angle of about  $125^\circ$ , as shown in Fig. 2.5.

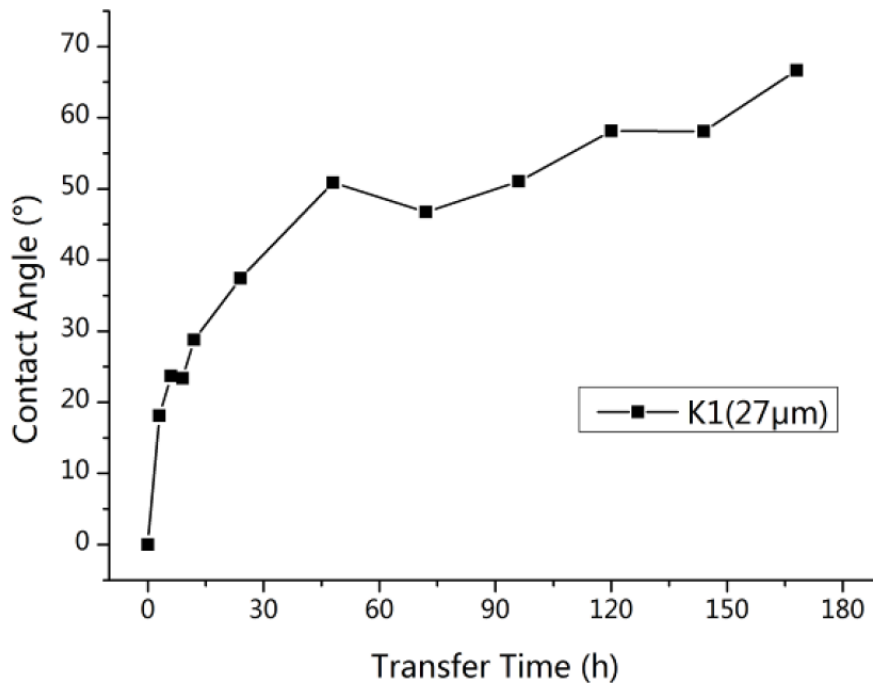


Fig. 2.4. Kaolin relationship between contact angle ( $^\circ$ ) and hydrophobicity transfer time (h) [28].

Similarly to Kieselguhr, the paper [28] also investigates silicone dioxide at various particle size, showing a similar behaviour to Fig. 2.5, with slower transfer speeds in the nanometre particle size range.

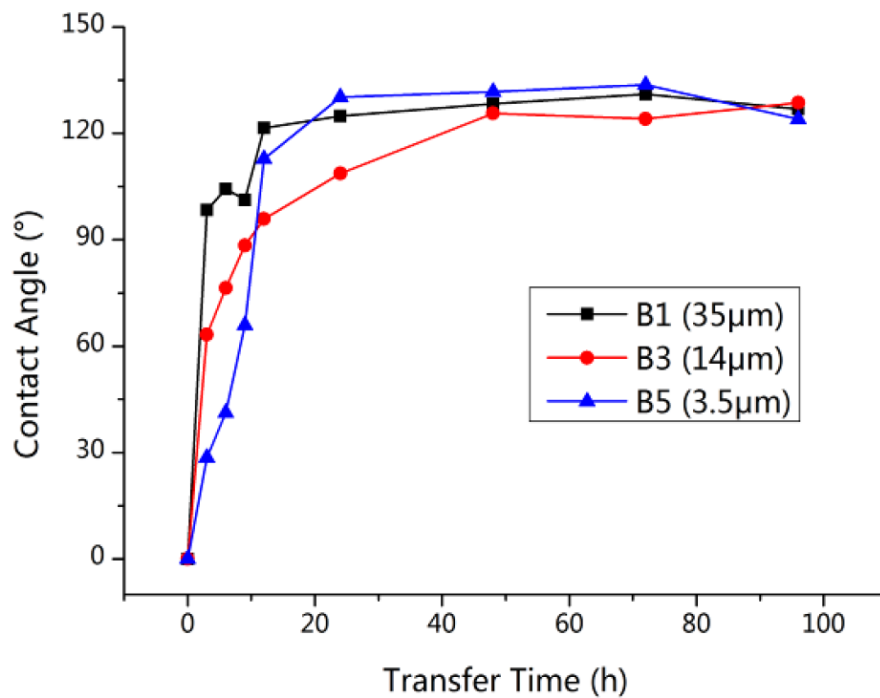


Fig. 2.5. Kieselguhr relationship between contact angle (°) and hydrophobicity transfer time (h), at different particle size [28].

In addition, as the particle size decreases, the pore size decreases too [28]. It can be further observed that there is a positive relationship between pore size and transfer speed, because LMW silicone migrates more easily through larger pores [28].

#### 2.5.4. Influence of U-shaped hydrophilicity on hydrophobic outdoor insulators

It has been observed that the level of hydrophobicity on insulators in operation is lower towards the ground and high voltage electrodes, or that the hydrophilicity is U-shaped along the arcing distance [30], [31]. This is due to a higher electric field towards the electrodes and therefore a higher discharge activity which compromises the hydrophobicity of the material.

Yu *et al.* [32] investigated the non-uniformity of hydrophobicity along the insulator length. 6 different conditions were considered from fully hydrophobic

to fully hydrophilic, by varying the amount of hydrophilic arcing length from each electrode towards the middle of the insulator, as Fig. 2.6 shows.

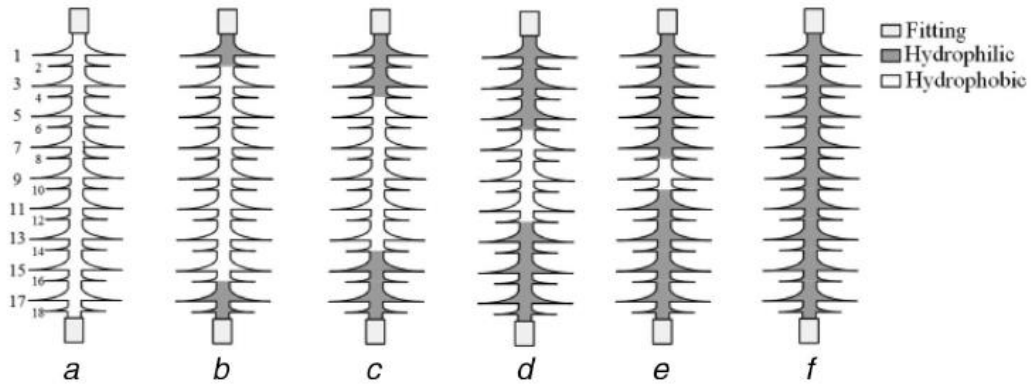


Fig. 2.6 Six insulator conditions with growing hydrophilic fraction  $p(\%)$  as a percentage of the arcing distance. (a)  $p=0\%$ , (b)  $p=22.2\%$ , (c)  $p=44.4\%$ , (d)  $p=66.7\%$ , (e)  $p=88.9\%$ , (f)  $p=100\%$  [32].

The test specifications are listed in TABLE 2.3.

TABLE 2.3. Non-uniform hydrophobicity test specifications of [32].

Location	HC	Inert material	Drying time	NSDD (mg/cm <sup>2</sup> )	SDD (mg/cm <sup>2</sup> )
Ends	6-7	Kaolin	24 h	1	0.1
Middle	2-3	Kieselguhr			

The results are shown in Fig. 2.7.

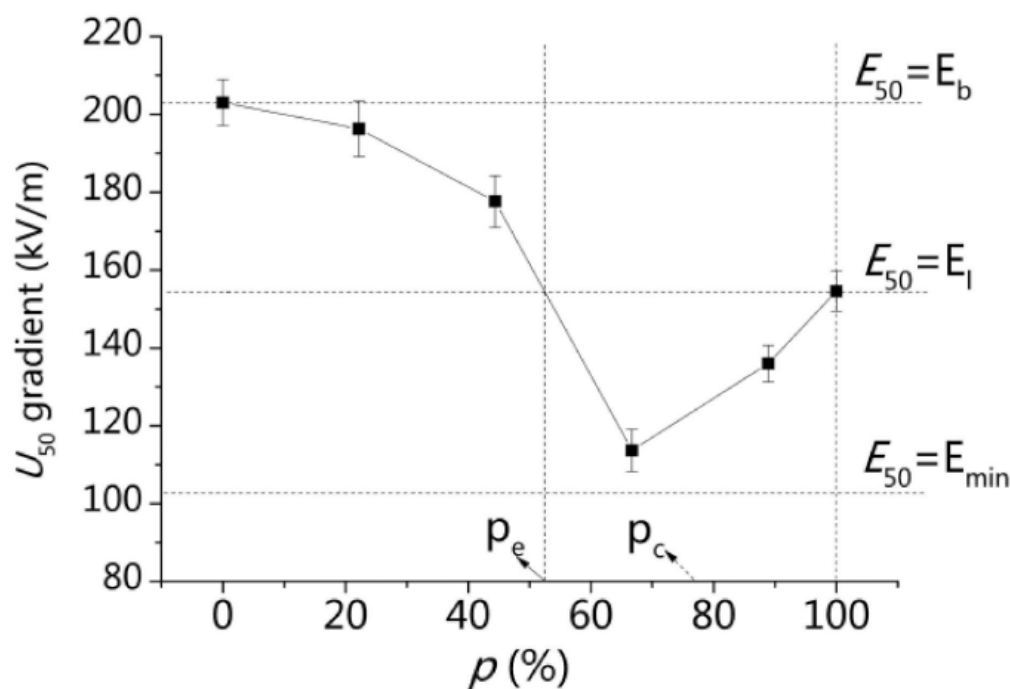


Fig. 2.7. Specific flashover voltage (kV/m) as a function of hydrophilic fraction  $p$  (%) [32].

It is remarkable that the lowest performance is caused by a loss of hydrophobicity on 66.7 % of the arcing distance, rather than a loss of hydrophobicity along the entirety of the insulator, which is the most investigated condition in literature. Moreover, as introduced in the section, the U-shape of hydrophilicity is expected and observed on composite insulators in operation [30], [31]. This fact makes the results of this paper quite meaningful from the point of view of standardisation. However, an insight on what the more probable  $p$  (%) in the field is would validate the significance of Fig. 2.7 results.

## 2.6. Climate and environment

When selecting and dimensioning the insulators for an electric power system, it is critical to know what types of climate and environment the system is subjected to. As the electrical system is possibly spread over a large region, considering only one combination of climate and environment may lead to an unsuccessful insulation coordination.

### 2.6.1. Climate

The climate is a combination of different atmospheric variables:

- a) Temperature;
- b) Pressure: in the case of low pressure (at high altitude), the flashover voltage is lower, as in [33] reviewed in section 2.15.4;
- c) Wind, whose speed, in the DC case, determines whether the electrostatic force is dominant on the pollution particles or not, as it will be seen in section 2.17.3;
- d) Sun radiation, which has an effect on the different circumferential ageing of the insulator;
- e) Humidity, which increases the chances of the insulator surface to be wet and thus conductive if salts are present;
- f) Precipitation such as rain and snow, and the formation of ice, which, once melted, is very high in conductivity and increases the flashover risk.

It would be appropriate to ideally consider a record of 30 years of atmospheric variables because the insulation system should be chosen to last for the whole lines lifetime, which is approximately 50 years.

There are seven distinguished climates around the world, and it is useful to be able to categorise the ones in which the line is or will be built to assess any hazard more widely:

- a) Tropical,
- b) Dry,
- c) Warm temperate,
- d) Cold:
  - d1) Cool temperate oceanic and
  - d2) Cold continental,
- e) Sub-Arctic or Tundra,
- f) Arctic or Ice cap,

g) High mountain and Plateau.

This research project tends to focus on the *cool temperate oceanic* climate, typical of the United Kingdom as a whole, which is characterised by:

- a) rain presence in every month,
- b) stable cool temperatures, with rare extremes,
- c) other atmospheric variables such as sun radiation, wind, humidity, and pressure need to be assessed specifically.

Within the UK, there are differences in climate. The most important is probably the fact that South England rain precipitation is less than average within the UK, and Scotland has a particularly long and cold winter, and short and cool summers. For this reason, the Scottish climate is defined as *subpolar oceanic*, meaning it is halfway between Tundra and cool temperate oceanic.

With regards to the InnoDC Project locations, which this individual project is part of, the climate types are listed below. In particular, Porto and Beijing have been the secondment locations during the course of this PhD.

- a) Denmark: cool temperate;
- b) Belgium: temperate maritime climate (in between the warm temperate and cool temperate oceanic);
- c) Portugal (Porto): warm temperate oceanic. Note that proximity to the ocean and altitude affects the climate definition. Tests in Porto, presented in Chapter 4, were performed during the winter;
- d) Spain (Barcelona): warm temperate Mediterranean;
- e) China (Beijing): Very hot and humid in the summer, and cold and dry in the winter. Tests in Chapter 3 were performed in Beijing during the summer. It would not have been possible to repeat the experiments in the winter and obtain the same results, because of the pollution drying difference at different humidity levels and very different temperatures. In the summer, the temperature is about 30 degrees and, in the winter, it is

below zero, so pollution testing would be very difficult to perform in the winter as freezing of the pollution would be likely while drying.

### 2.6.2. Environment

Environment is a different concept from climate because it outlines the natural and human characteristics of an area. The environment can influence the climate and vice versa. The scope of defining different environments is to categorise their different types of pollution, in terms of chemical constituents and amount of inert component. A pollution is inert when it does not directly affect the performance of an insulator [2]. Still, as it has been shown in section 2.5.3, it can have an effect on it, as it affects the hydrophobicity property. The most common environments for outdoor insulation are shown in TABLE 2.4:

No studies were found on the agricultural sources of flashover, thus, there is a need to investigate them to determine whether they are inert or active pollutants.

Bird streamers can induce flashover because they create a favourable path for current to flow between two conductors at different potential or a conductor and the ground potential of the pole/tower [2].

TABLE 2.4. Environmental classification of pollution and its components.

Type	Active component	Inert component
Marine	NaCl mostly	Small
Industrial	-Dissolved acids -Slow dissolving salts -metals	Large
Desert	-Sand based -NaCl in high amounts [34]	Large
Agricultural	-Bird streamers -ploughing gases -crop spraying	

A mix of the aforementioned environments is possible, and it is expected to have specific percentages of each pollution type. The interaction of diverse chemical components may lead to different dissolution times and temperature changes, with respect to the behaviour of each chemical. Some chemical reactions require thermal energy and others deliver thermal energy. Time and temperature are important to determine the risk (likelihood) of flashover. Therefore, particular focus is needed on the reactions which do not require large energy absorption to occur.

Again, it is critical to predict the evolution of the system environments because the insulation selection and dimensioning needs to be appropriate for the lifetime of the system.

## 2.7. ESDD, SDD, NSDD definitions and DC service values

### 2.7.1. Definitions and considerations

The pollution severity on the surface of the insulator is expressed with the *Equivalent Salt Deposit Density (ESDD)*. To measure it, the solution is removed from the insulator surface and its conductivity is measured, then the *equivalent salt density* having the same conductivity is calculated. This equivalent salt density, expressed in mg of NaCl per each  $\text{cm}^2$  ( $\text{mg}/\text{cm}^2$ ), is the ESDD of the original pollution layer on the surface of the insulator [35].

It is very important to consider that, for Hydrophobicity Transfer Materials (HTMs), like silicone rubber, the measurement of ESDD can be carried out, but it does not lead to comparable results with other ESDD values. In fact, the pollution lying on the HTM surface is impregnated with low molecular weight silicone [2]. Therefore, when an insulator is wetted, only a portion of pollution dissolves in water. Whereas when making the ESDD measurement, the pollution which would not dissolve in the solution is taken into account. Therefore, for HTM insulators, surface conductance measurement may be more applicable. In fact, ESDD

measurements would give larger values than what is the actual contribution of the conductive layer on the insulator.

*Salt Deposit Density (SDD)* is used when the pollution is directly NaCl, so there is no need to calculate an equivalence to NaCl. It is defined [36] as the amount of sodium chloride in an artificial deposit on a given surface of the insulator (metal parts and assembling materials are not to be included in this surface) divided by the area of this surface. Similarly, to the ESDD, SDD is expressed in (mg/cm<sup>2</sup>).

A consideration needs to be made: the ESDD is a useful and practical tool, which enables an easy comparison between the layer conductivities. However, a comparison is relevant when the atmospheric variables make the conductive layers behave in a similar way. The behaviour is characterised by the rate of evaporation, the solubility change with temperature, the ability to absorb water or pollution particles at the same speed and with the same thermal energy balance. This allows to understand that the atmospheric variables are not likely to stay or change in time in a way which allows the different pollutants to behave in the same way. For this reason, it is important to take note of all the variables defining a specific case, and to understand what variables affect the insulation performance more significantly than others.

The *Non Soluble Deposit Density (NSDD)* is defined [36] as the amount of non-soluble residue removed from a given surface of the insulator, divided by the area of this surface, in (mg/cm<sup>2</sup>) [35].

### **2.7.2. Deposit density DC service values**

TABLE 2.5 provides DC service values of ESDD, NSDD, and ESDD<sub>eq</sub>. The latter can be calculated with (2.9), when both ESDD and NSDD are known. The calculation is done to take into account the partially active role of the inert component under DC energisation, as explained in section 2.9. The values refer to composite insulators. K<sub>s</sub> is a statistical factor equal to 1.4, introduced for conservative reasons. The formula's factors are further explained in section "A.2. Corrections for the pollution severity estimation" of section 2.8.3.

$$ESDD_{eq} = ESDD \cdot \left( \frac{NSDD}{0.1} \right)^{\frac{0.106}{0.25}} \cdot K_S \quad (2.9)$$

TABLE 2.5. ESDD, NSDD, ESDD<sub>eq</sub> DC service values [4].

Country	Station	ESDD mg/cm <sup>2</sup>	NSDD mg/cm <sup>2</sup>	ESDD <sub>eq</sub> mg/cm <sup>2</sup>	Reference
China	800 kV	0.05	0.3	0.112	[37]
China	800 kV	0.08	0.48	0.218	[37]
China	800 kV	0.15	0.9	0.533	[37]
USA	Pacific Inertie	0.026	0.3	0.058	[38]
South Africa	Cahora Bassa	0.03	0.15	0.05	[38]
New Zealand	Transpower			0.01	[39]
New Zealand	Transpower	0.15		0.15	[39]
USA	LADWP	0.04	0.2	0.075	[39]

It can be observed that China NSDD values are generally higher than in other areas, due to desert environment. ESDD values are not larger than 0.15 mg/cm<sup>2</sup>, NSDD values are not larger than 0.9 mg/cm<sup>2</sup>, and ESDD<sub>eq</sub> values are not larger than 0.533 mg/cm<sup>2</sup>.

## 2.8. HVDC selection and dimensioning

The main goal of this section is to review the dimensioning methodology for outdoor insulators in polluted conditions under direct voltage and utilise it for the HVDC line conversion proposals. The methodology is well explained in CIGRE TB 518 and BS EN 60815-4 [4], [40], which are authoritative sources. Nonetheless, some recommendations of future work are done on specific dimensioning factors. At the end of the section, calculations of USCD<sub>DC</sub> are provided for different severities, considering the same insulator profile used for tests in Chapter 3.

### 2.8.1. General aspects

The selection and dimensioning of an insulator have the main goal of maximising the performance of the insulation system over a period of half a century from its installation, and it is dependent on at least five parameters, as shown in Fig. 2.8.

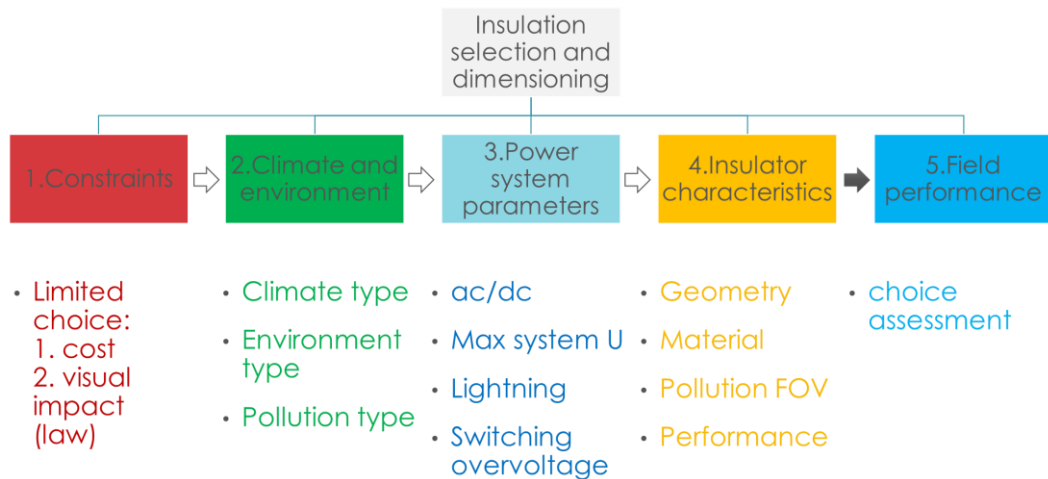


Fig. 2.8. Insulation selection and dimensioning: conceptual scheme.

$$Ins. \text{ selection and dimensioning} = f(P1, P2, \dots, P6) \quad (2.10)$$

The parameters are described in [41] are as follows:

P1 *Constraints* such as:

- a) Limited insulator choice because of technical requirements,
- b) Cost, caused by project budget limit,
- c) Visual impact to be minimised in compliance with the law and for a more nature-based landscape.

P2 *Environment*, which is function of human and nature instances, and *climate*, which is function of atmospheric variables. The *application* depends on the pollution and determines the radial dimension and the orientation of the insulator.

P3 *Power System parameters*:

- a) *AC/DC energisations, maximum system voltage, lightning, switching, temporary overvoltages,*
- b) *the system's sensitivity to outages, which is high if the system is poor in resilience.*

P4 *Characteristics of existing* insulators developed by manufacturers.

P5 *Field performance monitoring* is critical. In fact, it represents a very precious source of data because it can be used to assess the appropriateness of the insulator choice in the short, medium, and long term in a specific spatial and temporal set range of selection and dimensioning parameters.

Secondly, it is critical to assess the parameters which affect the insulation performance the most, such as ESDD and NSDD, but also design parameters such as average diameter, creepage factor, as discussed in Chapter 2. It is critical to do so because the meaningful combinations of these parameters are many.

### **2.8.2. Specific methodologies for HVDC**

#### **HVDC OUTDOOR INSULATION DIMENSIONING**

The critical factor which determines the dimensioning method of outdoor insulation under HVDC stress is the pollution accumulation phenomenon.

With regards to *profile selection*, only typical shapes and general recommendations are provided in CIGRE TB 518 [4]. In fact, field testing is the most reliable source of information to determine an optimised profile specific to environment and climate.

From testing experience [4], it has been found that there is an exponential dependence between the Unified Specific Creepage Distance (mm/kV) (USCD), defined as the Creepage Distance in mm divided by the maximum operating voltage in kV, and the pollution severity  $\gamma$  (mg/cm<sup>2</sup>) expressed as Equivalent Salt Deposit Density (ESDD) or Non-Soluble Deposit Density (NSDD). The proposed relationship is:

$$USCD = B \cdot \gamma^\alpha \quad (2.11)$$

Where  $B$  and  $\alpha$  are experimentally determined constants, specific to each insulator type. Tests are carried out on insulators with Axial Distance (AD) of at least 1.5 (m). In fact, a shorter distance would not give transferrable results to longer distances being the end fitting high field too dominant. The results are sometimes scaled up for longer arcing distances.

The flowchart of Fig. 2.9 schematically describes the process to calculate  $B$  and  $\alpha$ .

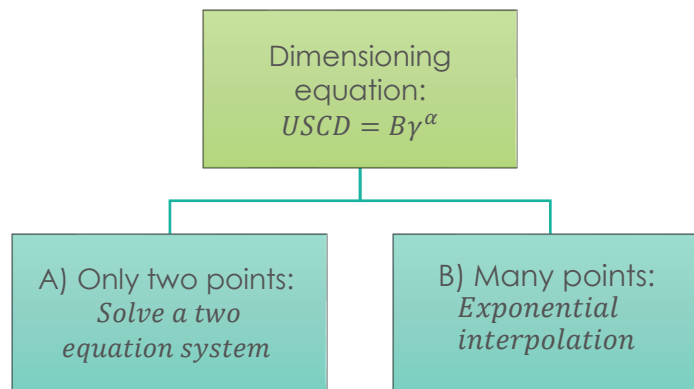


Fig. 2.9. Flowchart for the determination of  $B$  and  $\alpha$ .

- i. Mathematically,  $B$  and  $\alpha$  could be determined for one insulator with two tests only. In fact, applying two different pollution severities  $\gamma_{1,2}$  would result in two different maximum operating voltages and so two different  $USCD_{1,2}$ . But  $B$  and  $\alpha$  would be the same. Therefore, from the system of equations:

$$\begin{cases} USCD_1 = B\gamma_1^\alpha \\ USCD_2 = B\gamma_2^\alpha \end{cases} \quad (2.12)$$

$$\quad (2.13)$$

$B$  and  $\alpha$  can be determined with two sets of equation systems, which have been mathematically calculated as follows.

$$1. \begin{cases} \alpha = \frac{\ln\left(\frac{USCD_2}{USCD_1}\right)}{\ln\left(\frac{\gamma_2}{\gamma_1}\right)} & \text{"=" needs verification,} & (2.14) \\ B = \frac{USCD_1}{\gamma_1^\alpha} = \frac{USCD_2}{\gamma_2^\alpha} & & (2.15) \end{cases}$$

Or

$$2. \begin{cases} B = e^{\left(\frac{\ln USCD_2 \cdot \ln \gamma_1 - \ln USCD_1 \cdot \ln \gamma_2}{\ln \gamma_1 - \ln \gamma_2}\right)} & \text{"=" needs verification.} & (2.16) \\ \alpha = \frac{\ln\left(\frac{USCD_1}{B}\right)}{\ln \gamma_1} = \frac{\ln\left(\frac{USCD_2}{B}\right)}{\ln \gamma_2} & & (2.17) \end{cases}$$

- ii. It may be more reliable to carry out many tests for the determination of B and  $\alpha$  of a specific insulator. Each test "t" output is a point with the coordinates  $(SDD_t, USCD_t)$ . The "T" points can be exponentially interpolated in order to obtain B and  $\alpha$ .

Following the determination of B and  $\alpha$ , the dimensioning of an HVDC insulator with the same profile can be made for a specific voltage and field pollution severity.

### 2.8.3. Simplified HVDC dimensioning

A simplified dimensioning is also available from [4], as presented in Fig. 2.10.

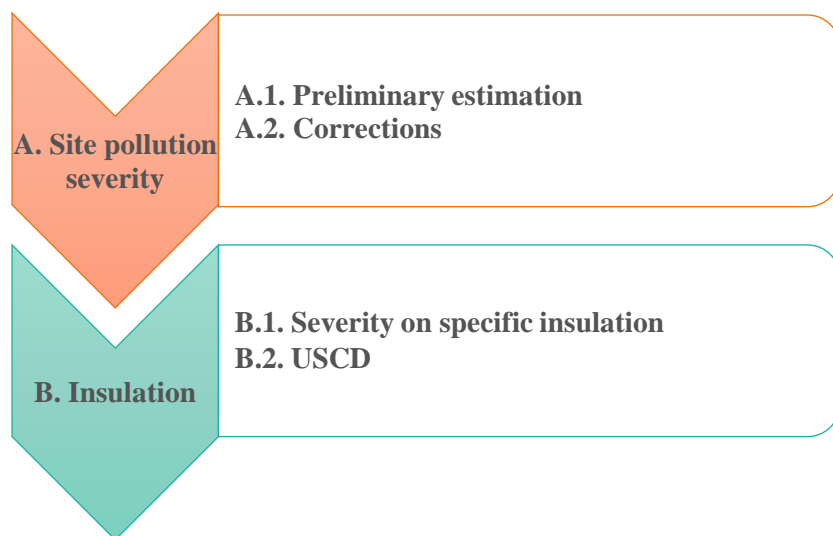


Fig. 2.10. Simplified dimensioning scheme for HVDC insulators.

First, the preliminary estimation of the site pollution severity is made, and then corrections are applied. Secondly, the USCD is determined for a specific insulator profile, as shown in Fig. 2.11 from [4].

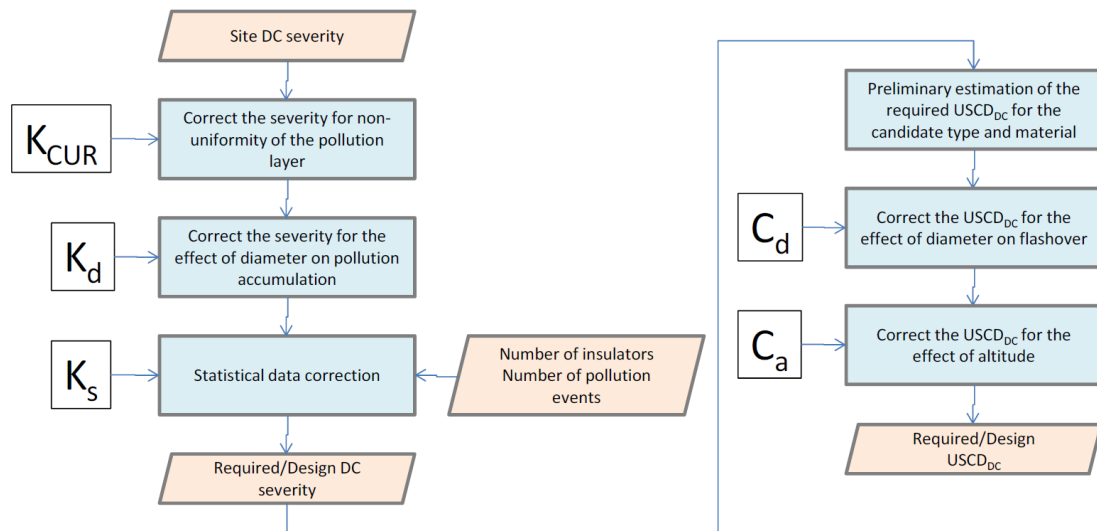


Fig. 2.11. Simplified dimensioning process. Determining the required USCD [4].

### ***A.1. Preliminary estimation of site pollution severity***

To have a first estimation of the site pollution severity, the following methods are presented. Their order reflects a descending confidence of accuracy.

- i. Field measurement of dc energised outdoor insulation on the same site of future installation:
  - a) ESDD measurement,
  - b) NSDD measurement,
  - c) Non-uniformity of pollution accumulation:
    - c1) Top to bottom or bottom to top (CUR), and
    - c2) axial.
- ii. Site severity estimation from scientific literature, such as that reviewed in TABLE 2.5 and Fig. 2.27, or world laboratory sources.

- iii. Field measurement of ac energised outdoor insulation at the same site of future installation
- iv. Estimation based on environment classification and conversion from ac to dc.

Points iii and iv require the application of the conversion factor  $K_P$  which is applied as shown in the following equations.

$$ESDD_{dc} = K_P \cdot ESDD_{ac} \quad (2.18)$$

$$NSDD_{dc} = K_P \cdot NSDD_{ac} \quad (2.19)$$

However, a cautious approach should be taken, when using this factor, as it may not represent the entirety of insulator pollution accumulations along a line, as seen in Fig. 2.27. Here, it is assumed that some small areas along the line may be considerably less windy than average, causing  $K_P$  to be locally very large. The risk of this hazard should be estimated carefully, by studying available wind maps and historical data. TABLE 2.6 shows the values that might be assumed for  $K_P$ , where  $t(\max_p)-t(\min_p)$  is the time difference between the largest and the smallest pollution severities on the insulation system.

TABLE 2.6.  $K_P$  values as a function of wind speed [4].

Pollution type	Environment	Wind speed (m/s)	$t(\max_p)-t(\min_p)$	$K_P$ typical	$K_P$ range
B	/	>6	Short time (order of a day)	1.1	1 - 1.2
A or B	Coastal or human	3 - 6	Times of the order of a month	1.6	1.3 - 1.9
A	Human	1.5 - 3	1-2 year(s)	2.5	2 - 3
Extended dry periods				>2.5	

Notes:

- $K_p$  decreases from the given typical value if frequent natural cleaning occurs.
- $K_p=1$  when the pollution severity is measured on DC energised insulators.

## A.2. Corrections for the pollution severity estimation

### i. Correction for type of salt

Lab tests are mostly performed with NaCl, but field pollution may contain different solubility pollution type, e.g. CaSO<sub>4</sub>. However, at the present time  $K_C=1$  for all salt types. Future work is recommended to have a more specific representation of the effect of different types of salt on  $USCD_{DC}$ .

### ii. Correction for NSDD, applicable when $NSDD > 0.02$

As it will be later discussed in section 2.9, NSDD refers to an inert material which is, in fact, not inert in DC. A correction for the value of SDD to be used in the laboratory test can be made, as NaCl is used in the lab with the idea that it can substitute inert material effect on the flashover phenomenon. This assumption should be investigated, as this procedure is based on  $NSDD=0.1$  (mg/cm<sup>2</sup>). The factor  $K_N$  is introduced and calculated with (2.20).

$$K_N = \left( \frac{NSDD}{NSDD_0 = 0.1 \text{ or } 1} \right)^{\frac{0.106}{\alpha}} \quad (2.20)$$

Where  $\alpha$  values for HTM and non-HTM insulators are given in TABLE 2.7.

TABLE 2.7.  $\alpha$  values for HTM and non-HTM materials.

	HTM	Non-HTM
$\alpha$	0.25	0.33

**B.1. Severity adjustment for specific insulation**

**i. Non-uniformity ratio correction**

A non-uniformity ratio correction factor  $K_{CUR}$  is introduced to consider the pollution non-uniform deposition of pollution in the field. The Contamination Uniformity Ratio (CUR) is defined and calculated as the ESDD level on the bottom surface of the insulator divided by that of the top surface. The  $K_{CUR}$  depends on the umbrella material, as summarised in TABLE 2.8.

TABLE 2.8. Contamination uniformity ratio constant  $K_s$  for different materials.

	Non-HTM		HTM
	Ceramic disc type	HTM coated	
$K_{CUR}$	$\frac{1.59}{1+0.59\left(\frac{1}{CUR}\right)} \left[1 - 0.4 \log_{10} \left(\frac{1}{CUR}\right)\right]^{-\frac{1}{\alpha}}$	Not available	1

At present, the contamination uniformity ratio factor  $K_{CUR}$  is not available for HTM coated insulators, thus, future investigations would be beneficial to make the methodology more comprehensive.

**ii. Diameter - pollution deposition**

The average diameter of an insulator can be calculated as in [42]. As the average diameter increases, the collected pollution decreases. (2.21) is used for average diameters larger than 250 mm.

$$K_D = \left(\frac{D}{250}\right)^{-0.32} \tag{2.21}$$

Alternatively, a Japanese proposal [43] with a reference diameter of 115 mm can be used, and it is shown as follows:

$$K_D = \left(\frac{D}{115}\right)^\eta \quad (2.22)$$

Where D is expressed in mm. The exponent  $\eta$  can be equal to -0.55, based on Japanese data from a coastal site with rapid pollution accumulation [43], or it can be equal to -0.22, based on a proposal from the same paper [43].

If  $D < 300$  (mm), the effect may be smaller than that described by the mathematical relationship.

If  $D > 500$  (mm), there may be a saturation of accumulated pollution on the surface of the insulator.

However, it is clear that the pollution accumulation will also depend on the insulator orientation. Thus, it could be worth carrying out investigations on the applicability of  $K_D$  to horizontal arrangements.

**iii. Statistical factor for the consideration of many insulators**

To reduce the risk of flashover,  $K_s$  is introduced. It depends on the number of considered insulators, and it allows to over-dimension the insulator, in a way that the worst performing insulators on the line will still be able to withstand the most critical electrical, climatic, and environmental conditions.

TABLE 2.9 gives values of the statistical factor  $K_s$ .

TABLE 2.9. Statistical factor values for small and large number of insulators.

	$N \leq 100$	$N > 100$
$K_s$	1	1.4

**iv.  $SDD_{dc}$**

The  $SDD_{dc}$  severity for laboratory testing can then be determined with (2.23).

$$SDD_{dc} = K_P K_C K_N K_{CUR} K_D K_S E SDD_{meas} \quad (2.23)$$

**B.2. USCD calculation**

**i. Basic**

The basic USCD for DC energisation can be calculated with (2.24) similar to the one discussed in section 2.8.2:

$$USCD_{dc \text{ basic}} = B \cdot SDD_{dc}^\alpha \quad (2.24)$$

Where  $\alpha$  and B values for HTM and non-HTM insulators are given in TABLE 2.10.

TABLE 2.10. B and  $\alpha$  values for HTM and non-HTM values.

	HTM	Non-HTM
B	65	110
$\alpha$	0.25	0.33

**ii. Diameter – flashover voltage correction**

As previously reviewed in sections 2.15.3 and 2.15.4, the increase in creepage length increases the performance up to a certain threshold after which the performance decreases again. When the average diameter is greater than 250 (mm), (2.25) is used.

$$C_D = \left(\frac{D}{250}\right)^\theta \quad (2.25)$$

$\theta$  values for HTM and non-HTM insulators are given in TABLE 2.11.

TABLE 2.11.  $\theta$  values for HTM and non-HTM materials.

	HTM	Non-HTM
$\theta$	0.17	0.30

### iii. Air density factor

As altitude increases, air density decreases and flashover voltage decreases, as described by (2.26).

$$C_a = e^{0.35\left(\frac{H}{8150}\right)} \quad (2.26)$$

IEC defines H as the altitude above sea level. However, it is standard industry practice to offset the sea level to 1000 m, so that the altitude effect is taken into account from that height, as it were 0 m.

### iv. Final expression of USCD

USCD can be calculated with the following compact (2.27) which has been derived in this thesis as follows, by combining the described equations above.

$$USCD_{dc} = C_D C_a B (K_P K_C K_N K_{CUR} K_D K_S ESDD_{meas})^\alpha \quad (2.27)$$

Where  $\alpha$  and B values are given in TABLE 2.12.

TABLE 2.12. B and  $\alpha$  values for compact equation for HTM and non-HTM materials.

	HTM	Non-HTM
B	65	110
$\alpha$	0.25	0.33

It is clear from (2.27) that a small  $\alpha$  (HTM insulators) reduces the expression in the parentheses. However, a small  $\alpha$  also increases  $K_N$ . With regards to the factor B, a small B (HTM insulators) reduces the USCD needed. An example in Section 5.2.1 clarifies the difference in USCD results, based on the insulator material.

***USCD<sub>DC</sub> dimensioning examples***

Making use of the profile later investigated in Chapter 3, USCD calculations are made for different DC pollution severities already presented in TABLE 2.5.

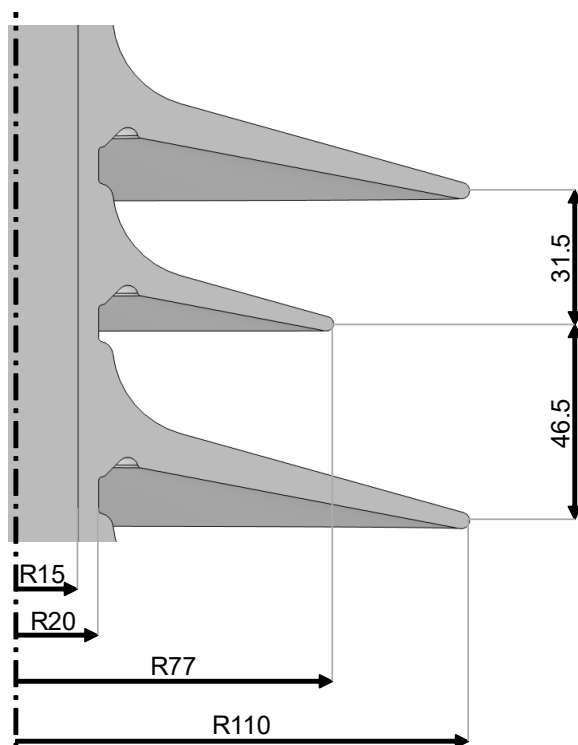


Fig. 2.12. Profile used for USCD<sub>DC</sub> calculation examples.

TABLE 2.13. USCD dimensioning examples, using severity data from [4].

Country	Station	ESDD <sub>DC</sub> mg/cm <sup>2</sup>	NSDD <sub>DC</sub> mg/cm <sup>2</sup>	USCD <sub>DC</sub> (mm/kV)
China	800 kV	0.05	0.3	37.9
China	800 kV	0.08	0.48	44.8
China	800 kV	0.15	0.9	56.0
USA	Pacific Inertie	0.026	0.3	32.2
South Africa	Cahora Bassa	0.03	0.15	31.0
USA	LADWP	0.04	0.2	34.3

#### 2.8.4. Simplified HVDC dimensioning if pollution and wetting occur at the same time

If pollution and wetting occur at the same time, a different simplified dimensioning approach is available [4], as shown in Fig. 2.13. First the Site Equivalent Salinity (SES) is determined. Then, the salinity is corrected for the diameter effect on flashover voltage with  $K_D$  and for the statistical factor  $K_s$ .



Fig. 2.13. Simplified dimensioning if pollution and wetting occur at the same time.

### **A. Determination of Site Equivalent Salinity**

The Site Equivalent Salinity SES (kg/m<sup>3</sup>) is the salinity degree of the Salt-Fog test which causes a laboratory test leakage current equal to the peak of the field leakage current under wet-polluted conditions [4].

#### **B.1. Salinity adjustment for specific insulation**

Once the SES is determined, the diameter effect on pollution accumulation and the statistical correction are applied, with  $K_D$  and  $K_S$  defined as seen above. The equivalent salinity ES is obtained with (2.28) [4].

$$ES = K_D K_S SES \quad (2.28)$$

#### **B.2. USCD calculation**

The USCD can be finally calculated with (2.29)

$$USCD_{dc\ basic} = 15 \cdot ES^\alpha \quad (2.29)$$

This is then corrected for diameter influence on flashover voltage, and air density, as previously explained in the simplified dimensioning of section “B.1. Severity adjustment for specific insulation”, as (2.30) shows:

---



---


$$USCD_{dc} = C_D C_\alpha 15 (K_D K_S SES)^\alpha \quad (2.30)$$


---



---

Where  $\alpha$  values for HTM and non-HTM insulators are given in TABLE 2.14.

TABLE 2.14.  $\alpha$  values for simplified dimensioning when pollution and wetting occur at the same time.

	HTM	Non-HTM
$\alpha$	0.25	0.33

## 2.9. Types of pollution

TABLE 2.15 presents a pollution classification based on type, which can be active or inert [44].

TABLE 2.15. Active and inert pollution: components and properties [44].

Active pollution	<p>Conductive without water:</p> <ol style="list-style-type: none"> <li>1. Metallic deposit close to mining industry: drastic performance drop. <i>Magnetite, pyrite.</i></li> <li>2. Bird streamer: very high salt content [45]–[47].</li> </ol>
	<p>Conductive when dissolved:</p> <ol style="list-style-type: none"> <li>1. Gas in solution: hard to detect because measurement provokes evaporation [44]. <i>SO<sub>2</sub>, H<sub>2</sub>S, NH<sub>3</sub>.</i> When the rain droplets fall from the clouds towards ground, gases like SO<sub>2</sub> can be collected, especially in industrial areas. The rain becomes acid, and when it deposits on the surface of the insulator, it causes a higher surface conductivity with respect to a surface conductivity given by non-contaminated rain.</li> <li>2. Ionic salts: <i>NaCl, Na<sub>2</sub>CO<sub>3</sub>, MgCl<sub>2</sub>, CaSO<sub>4</sub> (gypsum).</i></li> <li>3. Fly ash, cement.</li> </ol>
Inert pollution <i>Tonoko</i> <i>Kaolin</i> <i>Kieselguhr</i>	<ol style="list-style-type: none"> <li>1. In AC, it has small and indirect influence on the withstand voltage. It retains water, which allows more active pollutant to be dissolved. The impact of the water depends on the quantity of active pollution and its solubility.</li> <li>2. In DC: <ol style="list-style-type: none"> <li>a. the withstand voltage is dependent on the inert pollution, under the same ESDD conditions.</li> <li>b. the hydrophobicity of polymeric insulators is affected by the inert pollution. Whereas, as anticipated, a portion of dry active pollution becomes hydrophobic, when deposited on the hydrophobic surface.</li> </ol> </li> </ol>

This indicates that pollution is mostly inert under AC, in terms of withstand voltage, and it is non-inert under DC. Furthermore, under DC, the inert pollution affects the hydrophobicity of the HT material.

With regards to the influence of inert material type, IEC 60507 [36] recommends 40g of inert material per 1 litre of water for all inert material test methods, even if insulator geometry can influence NSDD (mg of inert material/cm<sup>2</sup>). Two different inert materials behave differently with regards to NSDD and the concentration of non-soluble contaminants per litre. Two common inert materials are Kaolin and Tonoko. First, they both have a non-linear behaviour, more similarly, it is a quadratic relationship. As the concentration per litre increases, the NSDD increases almost quadratically. Moreover, Tonoko increase is higher than Kaolin's. It means that the concentration of inert material per surface unit increases faster than its concentration per liquid unit [48].

As the amount of inert pollution deposition increases on the insulator surface, the amount of water retained increases, so the amount of active pollution dissolved is higher. As a consequence of inert material deposition, the withstand voltage is likely to drop (not as much as for the active pollution). This mechanism has been experimentally proven with measurements of the AC withstand flashover voltage [49], as shown in Fig. 2.14.

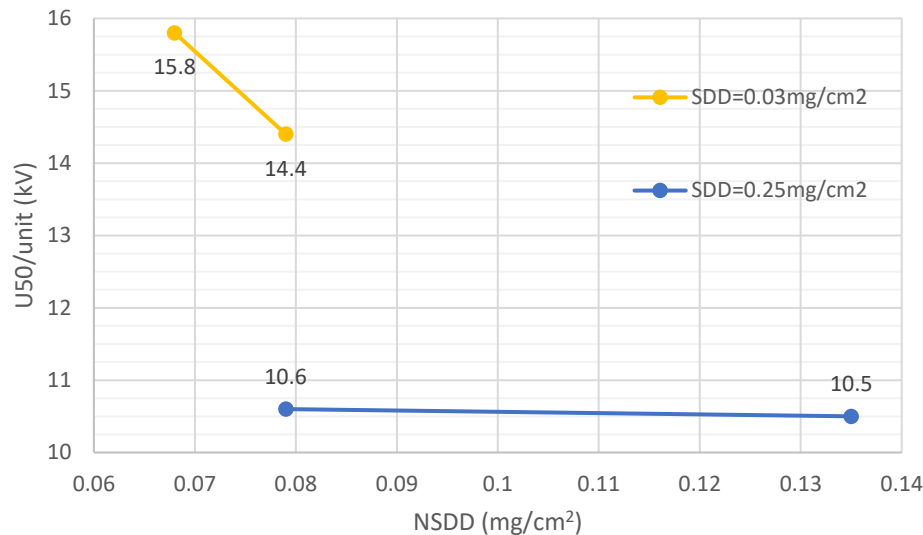


Fig. 2.14. AC  $U_{50}$ /unit (kV) as a function of NSDD under two SDD conditions, for the 250S type disc insulator [49].

Fig. 2.15 shows a review of results from [4] of the sources [2], [48], [50]–[52] with respect to the influence of non-soluble contamination on the withstand voltage.

The results of Fig. 2.15 are considered in section “A.2. Corrections for the pollution severity estimation” with regards to the selection and dimensioning of DC outdoor insulators. A correction factor  $K_N$  to account for the influence of the non-soluble material on the insulator performance will be introduced.

In addition to the water retention by the non-soluble material, a second factor affects the performance of HTM insulators. When pollution deposits on silicone rubber, low molecular weight silicone emerges on the surface from the bulk. These molecules of silicone combine with pollution [28]. As a result, the hydrophobicity transfers to pollution and the insulator recovers its hydrophobicity. This process takes time, which increases with pollution severity.

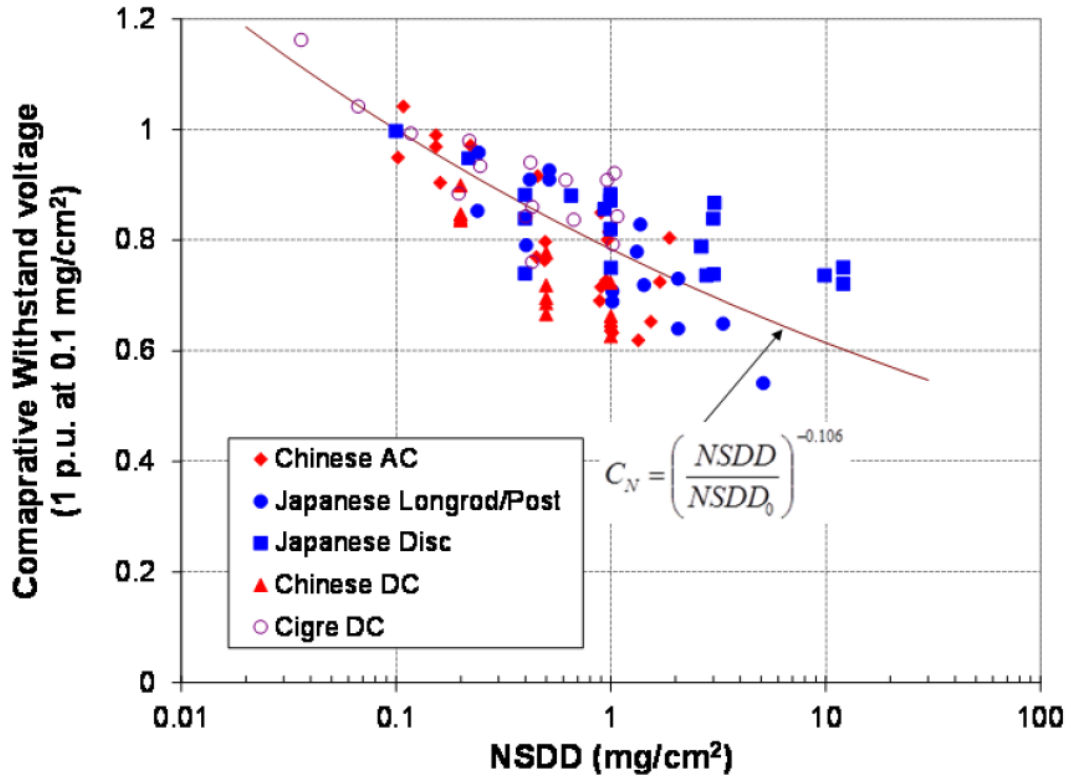


Fig. 2.15. Consolidated data illustrating the effect of the amount of non-soluble materials in the pollution layer on the flashover voltage of the insulator [2], [48], [50]–[52].

Thus, when tests are performed, part of the hydrophobicity is lost if tests are performed shortly after the non-soluble contamination. Details of the transfer time can be observed in Fig. 2.4 and Fig. 2.5, which have previously been discussed.

### 2.9.1. Salt solubility

In AC, there is almost no dependence of salt solubility on pollution flashover voltage under the same ESDD condition [53]. Moreover, as the ESDD increases, the withstand voltage decreases, as expected. Whereas in DC, the withstand voltage is very different for the same ESDD condition [48], [54].

The dissolution process of salts needs to take into account the temperature variation caused by increased current flow because temperature influences conductivity [55].

### 2.9.2. Type A and Type B pollution

A classification of pollution is made, based on its composition[56]:

- a) *Type A* pollution is both soluble and non-soluble, respectively measurable with ESDD and NSDD.
- b) *Type B* pollution is already in the form of electrolyte. One example would be sea spray.

## 2.10. Artificial contamination tests

*Artificial contamination tests* are carried out to determine the voltage which causes flashover 50% of the times it is applied, often referred as  $U_{50}$  or 50% FOV.

The variables of the tests are:

- a) salt/non-soluble material ratio,
- b) the SDD which is investigated from very low values of  $0.01 \text{ mg/cm}^2$  to large values such as  $0.6 \text{ mg/cm}^2$ ,
- c) the NSDD which is generally constant at  $0.1 \text{ mg/cm}^2$  or similar values [57], with the exception of Chinese tests which may use  $1 \text{ mg/cm}^2$ , like at China EPRI UHVDC pollution laboratory, or similar values due to the larger NSDDs found in China's service, as shown in TABLE 2.5 [4],
- d) Specimen insulator (e.g. 250S, 320DC, which are disc type insulators, and other types),
- e) Test voltage, whether AC, DC, SI, LI, ramps, or particular superimpositions.

The results for a 250S disc insulator [48] are shown in TABLE 2.16:

Overall, many variables are considered, so the complexity of the problem is very high. However, it is clear that the wetting of the pollution deposition is the main cause of fault related to outdoor insulation (overvoltages neglected). Therefore, efforts to find performant solutions need to be addressed to avoid pollution and water deposits on insulation surfaces.

TABLE 2.16. AC and DC pollution performance of 250S disc insulator.

	AC	DC	
Flashover voltage	Higher	Lower 2.4% Tonoko	Lower 13.5 % Kaolin
Max leakage current	Higher	Lower 8% Tonoko	Lower 6%

To avoid pollution under DC, the following factors need consideration:

- a) DC energisation causes pollution attraction, especially to high electric field surface regions,
- b) Direction of the pollution brought by wind,
- c) Lastly, rain direction, as its effect may be negative if light enough not to clean the insulator and initiate the flashover phenomenon or it may be positive if heavy enough to allow the cleaning of the insulator.

### 2.10.1. Artificial contamination tests for hydrophobic materials

No standard test is yet available for hydrophobic insulators under contaminated conditions. In the standard BS EN 62217 [58], it is mentioned that the applicability of standard pollution tests specified in IEC 60507 and 61245 [36], [59] has not yet been proven on composite insulators and still requiring study by CIGRE. "The results of such pollution tests performed on insulators made of polymeric materials do not correlate with experience obtained from service".

This may be due to the non-uniform distribution of hydrophobicity in service insulators, as seen in section 2.5.4, and the influence of non-soluble material on the hydrophobicity transfer speed, as seen in section 2.5.3. Hydrophobicity class at the moment of test and hydrophobicity uniformity should, therefore, be addressed in the upcoming standard for composite insulator pollution testing.

Nonetheless, research on the test has been done, in particular, to realise a uniform pollution layer which is challenging due to the hydrophobicity. Naito *et al.* [57] propose an improved process to obtain a more uniform pollution layer, as shown in TABLE 2.17 and Fig. 2.16.

TABLE 2.17. Original and improved process of the pollution method for composite insulators [57].

Testing phase		Duration	Description
A Pre-treatment / pre- conditioning	A1	5 min	Pre-contamination original or improved*
	A2	30 min	Drying
	A3	5 min	Washing with running tap water
	B	5 min	Dipping in the pollution slurry
	C	Variable	Drying (variable or 30 min)
	D	60 min	Clean fog test procedure
	E	5 min	Washing

\*Original: spraying minute water droplets (may be non-uniform on trunk and shed bottoms) and then uniformly sprinkling of Tonoko powder. Improved: spraying of Tonoko slurry.

To compromise the hydrophobicity, rather than spraying water droplets and sprinkling Tonoko powder, a Tonoko slurry is sprayed on the surface of the insulator. Then, drying and washing are done. Finally, a pollution slurry is applied and drying occurs until the desired level of hydrophobicity is recovered. At this stage, a fog test can be performed.

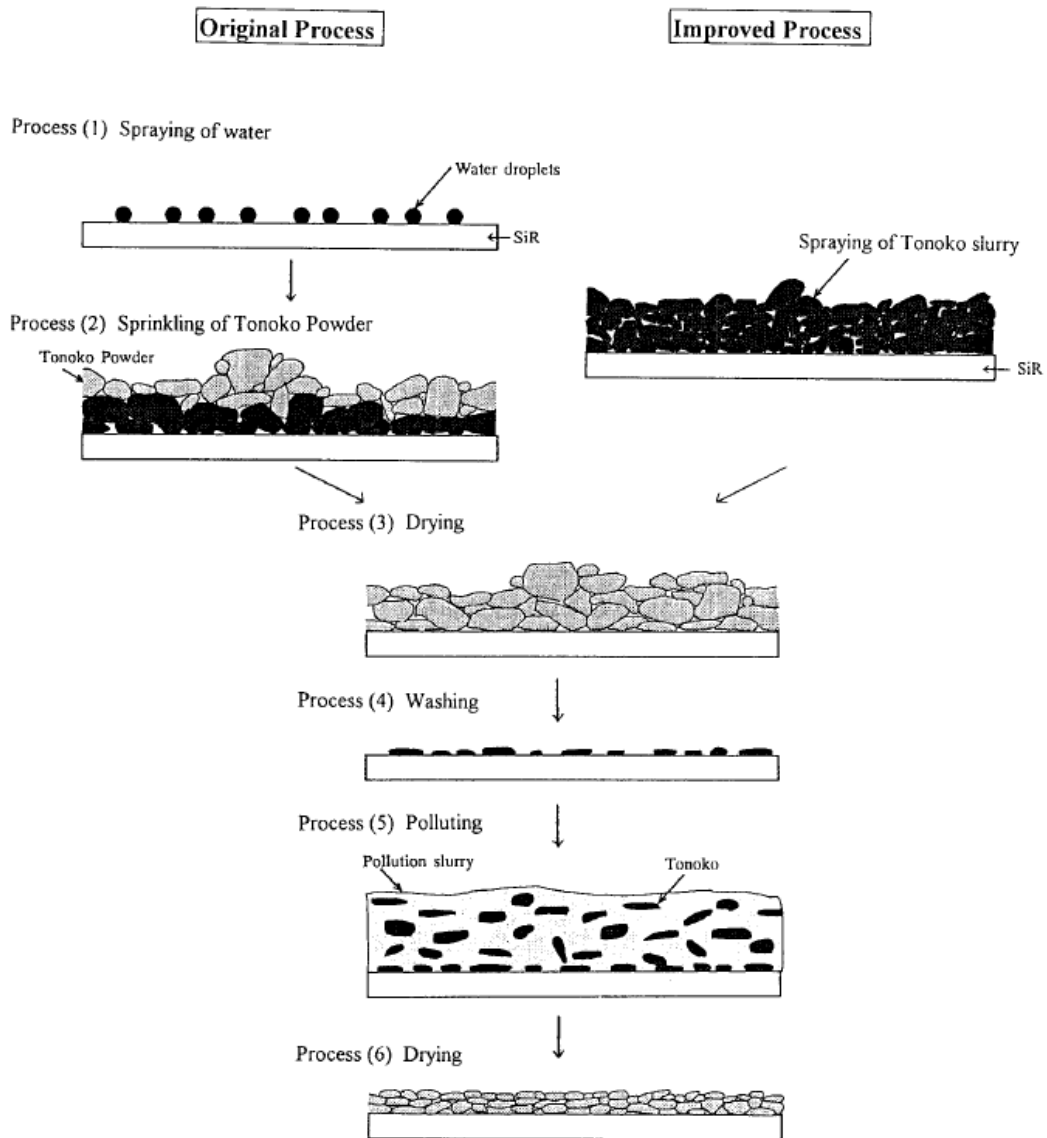


Fig. 7 Schematic process of the new pollution method for hydrophobic composite insulators

Fig. 2.16. Schematic original and improved process of the pollution method for composite insulators [57].

The authors of [57] also investigated the performance of a composite insulator with different hydrophobicity classes, depending on the drying time C of TABLE 2.17. The results are shown in Fig. 2.17.

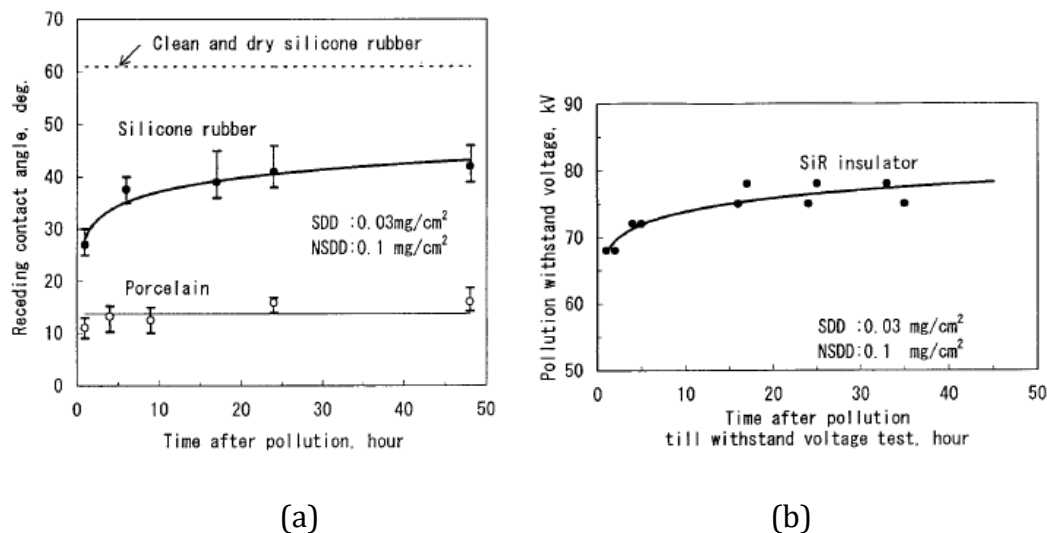


Fig. 2.17. (a) Contact angle relationship with time after pollution (h). (b) Pollution withstand voltage (kV) relationship with time after pollution (h) [57].

As expected, a positive correlation between hydrophobicity class, indicated by the contact angle, and withstand voltage exists.

## 2.11. Pollution accumulation mechanism

Some pollution is being deposited on the surface of the insulator, some is being carried away or falls from the insulator. The nett of the two gives the pollution amount that is being accumulated or reduced.

The physical forces which determine the resulting force exerted on a pollution particle are considered in [60]–[63] and are:

- a) Wind force,
- b) Gravitational force, and
- c) Electric force, which has two components:
  - c1) The electrostatic component, only present in DC energisation, and
  - c2) Dielectrophoretic attraction of neutral particles., which is negligible compared to the other forces.

Thus, the resulting force can be expressed with (2.31):

$$\mathbf{F}_p = \mathbf{F}_w + \mathbf{F}_g + \mathbf{F}_E \quad (2.31)$$

This equation is in fact a system of three equations, each referring to one of the x, y, and z axes, which fully describe the position of the particle in space.

As the wind velocity  $v_w$  (m/s) varies, the dominant forces exerted on the pollution particle vary, in a way described by TABLE 2.18.

TABLE 2.18. Dominant forces on pollution particle as a function of wind velocity [61]

If the wind velocity is:	Then, the dominant forces are:	
	AC	DC
$v_w < 2$ (m/s)	Gravitational	Electrostatic, gravitational
$2$ (m/s) $< v_w < 3$ (m/s)	Gravitational and wind	All three forces
$v_w > 3$ (m/s)	Wind	Wind, appreciable electrostatic

In a marine environment, the Salt Deposit Density SDD is generally proportional to wind velocity. It means that as the wind increases, the nett SDD remaining on the insulator surface is larger [64]. The ESDD is larger for insulators close to the coast [65]. The precise amount depends on topography and climate. A consequence is that the highest salt pollution deposits should be found on windy coasts.

With respect to axisymmetry of the pollution deposition, the wind side of an insulator, which is the one exposed to wind, is cleaner than the lee side, which is the opposite side to where the wind leaves pollution on the insulator [66], [67]. In general, the non-uniform pollution deposition or non-uniform wetting reduces withstand voltage by about 70% [68], [69].

For windy and polluted regions, like a desert environment, flat aerodynamic profiles of the sheds are more preferable than fog profiles. In fact, even if aerodynamic profiles are shorter in creepage length, they allow the wind to clean their surface more easily than when having under-shed ribs [60].

### 2.11.1. Electric force

In AC, the electric force is constantly alternating in time, as the electric field reverses. Therefore, there is not an electrostatic attraction of pollution, but there exists a dielectrophoretic attraction for neutral particles. However, as anticipated, the dielectrophoretic force is negligible with respect to wind and gravitational forces. However, if a neutral particle has a dimension which is large enough, dielectrophoretic attraction towards the insulator happens as well.

In DC, there exists an electrostatic force because the electric field is unidirectional [70], [71].  $E$  is also almost constant in time, depending on how small the ripple of the DC voltage is. Thus, charged pollution particles are attracted to high electric field regions, as described by the following vectorial (2.32).

$$F = qE \quad (2.32)$$

Where the electric field vector  $E$  is large in magnitude, the charged pollution is attracted with greater force. The electric field  $E$  is not easy to calculate analytically in the case of an outdoor insulator because it depends on the insulator shape. The shape is very different from simple geometries like cylinders, but some behaviours usually recur, regardless of the specific insulator profile, e.g., usually, the high electric field region, which corresponds to the high electric force region, is situated around the insulator electrodes and in proximity of sharp corners and needles.

### 2.11.2. Pollution charge consideration for DC

Pollution particles can be electrically charged before approaching the insulator, for example, they can be charged in the air due to the friction caused by wind. Pollution particles can also be neutral in charge. These particles can be polarised when they approach the electrically charged insulator. In fact, the electrons do

not leave their nucleus, but still an atom polarisation takes place, because the electrons spend more time on one side of the atom [72]. The negative cloud of electrons is distorted because of the interaction with the electrostatic field of the insulator.

It has been observed that DC polarity has very little influence on the amount of deposition [4], [73], [74]. However, as a fundamental requirement, it would be desirable to avoid pollution deposit in the first place, by means of an effective design.

### 2.11.3. Full Lorentz force expression

It may also be useful to consider the full Lorentz force expression with (2.33):

$$\mathbf{F} = q\mathbf{E} + q\mathbf{v} \times \mathbf{B} \quad (2.33)$$

which includes the contribution of the vectorial product of the particle velocity  $\mathbf{v}$  and the induction field  $\mathbf{B}$ . There are two components of the induction field that need consideration. One is related to the current flowing through the line conductor, below the insulator (in the case of suspension insulators) or above the insulator (in the case of substation post insulators), and the other component is related to the leakage current, which is substantially smaller than the line current. The  $\mathbf{B}$  related component of the force seems negligible with respect to the electric field force, and it is not reported by CIGRE TB 158 [2].

## 2.12. Wetting mechanism

The mechanisms of insulator wetting are the following:

- a) Condensation [75], [76],
- b) Precipitation [77],
- c) Hygroscopic behaviour [55], [75], [78], and
- d) Molecular diffusion.

- a) Condensation usually occurs during the early hours of the morning, when the insulator is still cold, and the air starts getting hotter because of solar irradiation. Condensation can only happen when the insulator temperature is lower than the air temperature. The larger the temperature difference is, the larger will be the wetting rate due to condensation.

More specifically, condensation happens when the insulator temperature falls below the dew-point temperature, which depends on pressure. The higher the density, the lower the dew-point temperature because of the proximity of particles. Condensation is heavier on the top of the insulator in the early morning because, during the night, this part radiates more heat towards the atmosphere than the rest of the insulator. Condensation usually occurs in the morning following a clear still night [79], [80].

- b) Precipitation is later discussed in detail.

- c) The hygroscopic behaviour is defined by:

c1) how the surface reacts with water (liquid and gas more generally).

If the water is absorbed in the insulating material or adsorbed (just adheres to the surface), and

c2) the chemical composition variation of the liquid/gas, and the surface particles after the reaction takes place.

- d) molecular diffusion is the diffusion in space of gas and liquid particles due to their stochastic thermal movement.

In the case of no rain: if the insulator temperature is higher than air, then the wetting is due to hygroscopic and molecular diffusion, whereas if the air is hotter than the surface, like in the early morning, then the wetting is due to hygroscopic and molecular diffusion and condensation [2].

Moreover, as the temperature difference between the insulator surface and the air increases, the wetting becomes scarcer because of evaporation.

TABLE 2.19 summarises the discussed wetting mechanisms:

TABLE 2.19. Wetting mechanisms with variation of insulator-ambient temperature difference [2].

Temperature relationship	Wetting mechanism	Wetting amount
$T_i < T_a$	<ol style="list-style-type: none"> <li>1. hygroscopic diffusion</li> <li>2. molecular diffusion</li> <li>3. condensation</li> </ol>	If $T_a - T_i \gg 0$ , then high wetting
$T_i > T_a$	<ol style="list-style-type: none"> <li>1. hygroscopic diffusion</li> <li>2. molecular diffusion</li> <li>3. condensation not possible</li> </ol>	If $T_i - T_a \gg 0$ , then low wetting

Where  $T_i$  is the insulator temperature and  $T_a$  is the ambient temperature.

With regards to precipitation, it is worth referencing the two main precipitation types [77]:

- a) cumulus are very tall and usually standalone clouds characterised by short and intense rain precipitations.
- b) stratus instead are thin clouds that uniformly cover the sky. The rain of stratus is usually long in duration, and the rate is small.

Depending on the precipitation state, density, shape, and dimension, it is possible to elaborate a classification. It is worth noting that when rain droplets are fine with a diameter smaller than 0.5 mm, the type of precipitation is defined as *drizzle*. In the UK, this kind of precipitation is frequent [81].

### **2.12.1. Rain resistivity**

It is important to note that rain resistivity can greatly affect the withstand voltage of an insulator when the rain resistivity is smaller than 14 (kΩcm) [82]. The smaller the rain resistivity, the larger the withstand voltage drop of the insulator.

In Japan for example, the resistivity is frequently between 5 and 30 (kΩcm), so having a resistivity smaller than 14 (kΩcm) is a frequent event. If the rain resistivity is as small as 2 to 4 (kΩcm), the AC withstand voltage can be reduced by half [82].

This thesis studies the effect of rain resistivity under SI, and SI superimposed on DC in Chapter 4.

### **2.12.2. Tropical precipitation**

The tropical precipitation type is intense, short-lived, and usually supplied by cumulus clouds. Based on China Electric Power Research Institute field experience, learnt while working on the contents of Chapter 3, this can lead to a fast insulator flashover, but it is positive as it naturally cleans the insulator.

### **2.12.3. Mid-latitude precipitation**

In this case, the rain is gentle, and it spreads over a broad area.

### **2.12.4. Low precipitation regions**

There are low precipitation regions because of the lack of mechanism to saturate the air and thus create the cloud. However, over the oceans and the majority of desert environment, moisture is present, and it deposits on insulators. Sometimes, high precipitation areas become low precipitation areas for several years. In recent years, this is the case for the Brazilian lines in the Amazon area, as reported by Edson Guedes da Costa at the International Symposium on High Voltage Engineering (ISH) 2019 in Hungary, Budapest [83].

### **2.12.5. Fog**

Fog will occur when atmosphere cooling happens and its temperature is low enough to bring to condensation the air humidity [77]. The amount of cooling necessary for fog to occur depends on the air humidity percentage, air pressure, and air temperature.

Natural fog density is in the range  $0.01 \text{ g/m}^3 < \delta_{\text{fog}} < 1 \text{ g/m}^3$  [2]. However, 90% of fog density  $\delta_{90\% \text{ fog}}$  corresponds to 0.5 g of water per  $\text{m}^3$  ( $\text{g/m}^3$ ), which means that simulating a higher fog density for insulator fog test methods does not represent the majority of fog cases.

### 2.12.6. Moisture absorption

When an aqueous solution is present on the surface of the insulator, unfortunately, moisture absorption always happens. It occurs because the vapour pressure of the atmosphere is higher than the aqueous solution vapour pressure.

It is worth noting that a drastic withstand voltage drop occurs when the relative humidity of the ambient is higher than 75% [84]. This means that very humid areas heavily compromise the performance of outdoor insulation.

### 2.12.7. Ice and snow

Ice and snow affect the mechanical requirements of the system. In fact, their presence along the conductors can be significant in terms of conductor distance to ground and distance between conductors. They also greatly influence the electrical strength of outdoor insulation.

Ice is classified by density, appearance, shape, and conductivity. One very critical factor to consider is the conductivity of melting ice water, which is generally ten times the conductivity of freezing water, as (2.34) summarises.

$$\sigma_{\text{melting ice water}} \cong 10 \sigma_{\text{freezing water}} \quad (2.34)$$

As a consequence, melting ice substantially increases the likelihood of flashover, being the surface resistance significantly decreased.

When the insulator is relatively warm and the ambient temperature is below zero, ice melts and the resulting water droplets may freeze again before falling from the insulator shed. In this case, icicles are formed, and they can bridge string insulators (multiple units, such as cap and pin insulators) or insulator sheds (single unit, such as composite insulators). In this case, flashover risk can be

minimised by installing sufficiently inclined insulators or strings. In the case of inclined parallel insulators, icicles can bridge two strings if one string is positioned below the other.

Ice flashover mechanism is now better understood and, in general, this is how it works: flashover occurs when ice melts. As anticipated, the water dripping from ice has a very high conductivity, especially close to the sea, so high voltage is applied elsewhere in the dry zones. The arcing process begins, and it can lead to flashover if the voltage applied to the dry bands is large enough to provoke the breakdown of air in the vicinity of each dry band. Insulator flashover under icing conditions is explained in greater detail by Farzaneh in [85].

One of the conclusions [2] is that vertical mounting shall be avoided in locations prone to night icing and day melting.

## **2.13. Insulator cleaning based on orientation, diameter, and material**

Different insulator profiles catch pollution in different ways and amounts. Their shape suitability to natural cleaning varies [67]. For example, the aerodynamic profile has a short creepage length per unit axial length (i.e. a relatively small creepage factor), but it is highly cleanable by wind, as opposed to convoluted shed designs. Other than shape, the factors playing a role in the amount of deposited pollution are orientation, average diameter, and material.

### **2.13.1. Orientation**

Orientation is critical in the case of:

- a) well-defined polluting sources,
- b) rapid pollution accumulation, and
- c) scarce natural cleaning.

Available literature shows that the inclined insulators (tension insulators) accumulate less pollution than the vertical insulators (suspension insulators),

and horizontal strings catch even less pollution [86]. Moreover, the rain generally cleans the insulator more efficiently, when inclined [4].

This thesis provides insights on the laboratory performance of composite insulators with respect to orientation. Chapter 3 investigates the vertical and horizontal HVDC performance of composite insulators of various lengths under the same pollution severity, showing a better performance in the horizontal case. Chapter 4 investigates the vertical and horizontal orientations, under dry and rain conditions, under SI and SI superimposed on DC. The results show a better performance of the horizontal insulator in both dry and rain conditions, respectively for reasons related to the electrode configuration and the rain droplets direction.

### 2.13.2. Average diameter

There is a relationship between ESDD and the average diameter of insulators. Insulators with a large diameter catch less pollution per  $\text{cm}^2$  compared with small diameter ones [74], [87], even though this is not what one would expect. The results are shown in Fig. 2.18.

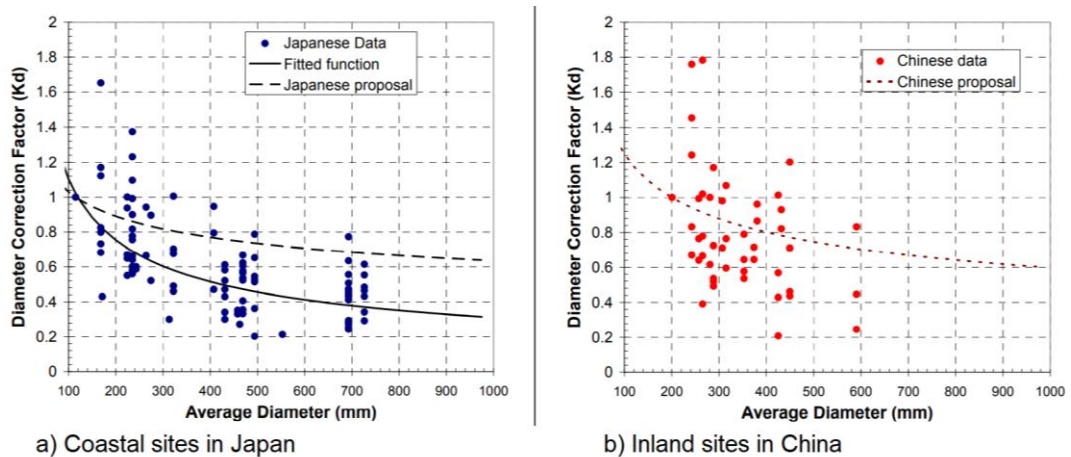


Fig. 2.18. ESDD ratio as a function of insulator average diameter. For a), the reference ESDD corresponds to  $D=115\text{mm}$ , under de-energised condition [87]; for b), the reference is  $D=200\text{mm}$ , under DC energisation [74].

However, an increase in average diameter can lead to lower flashover voltages. In fact, Fig. 2.19 shows that under AC, a larger USCD is needed as the diameter increases. It also shows that polymeric insulators require less specific creepage distance with respect to porcelain ones, due to their superior performance given by the hydrophobicity property.

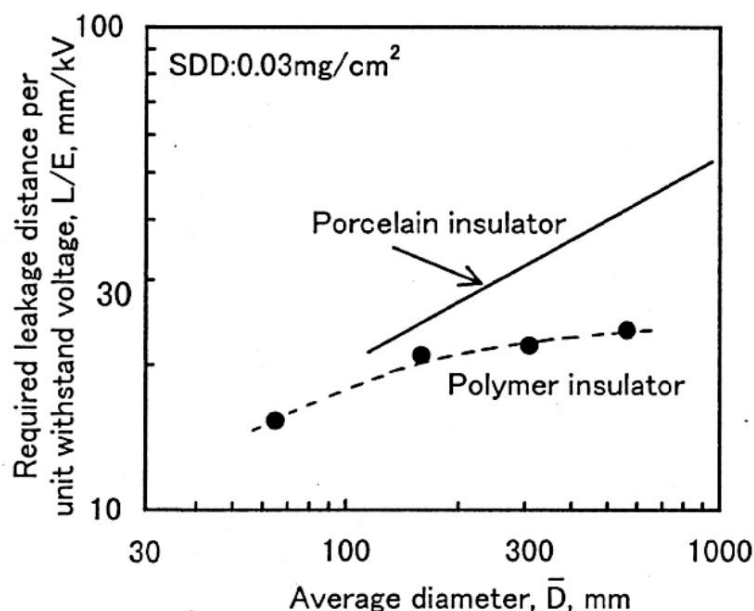


Fig. 2.19. USCD as a function of the average diameter, under AC [88].

The influences of the average diameter on pollution accumulation and on flashover voltage are taken into account in section 2.8.3, respectively with the factors  $K_D$  and  $C_D$ .

### 2.13.3. Material

In the majority of cases, silicone rubber insulators get dirtier than those made of porcelain [66], [89]. However, silicone rubber transfers the hydrophobicity property to the deposited pollution, which then becomes hydrophobic, and prevents water deposition and hence initiation of a pollution flashover event. Therefore, depending on the hydrophobicity class on the insulator, part of the deposited pollution does not directly account for the flashover performance.

#### **2.13.4. Equilibrium of pollution accumulation**

When the insulator is first put in service, it is clean. With service time, pollution accumulates on the insulator, but wind and precipitation clean it outdoors. This process continues increasing the pollution severity up to an equilibrium average. Usually, the equilibrium of pollution deposit is reached in a few years with an exponential convergence. One measured example for the equilibrium convergence of ceramic insulator pollution deposit is 2-3 years [60].

### **2.14. Insulator ageing**

Many factors are associated with the ageing of insulators. These factors are heavy wetting, blown sand, corona, spark discharges, solar radiation and biological growth.

The ageing effects are not uniform on the insulator. On composite insulators, the non-uniformity was found both axially and circumferentially by Rowland *et al.* [90]. In fact, with regards to the axial non-uniformity, the water droplet contact angles were found high at the insulator ends and low towards the middle part of the insulator. The use of corona rings may explain the reason for this distribution, because they locally reduce the electrical stress and decelerate the ageing process due to corona. With regards to the circumferential non-uniformity, the north side contact angles were found higher than on the south side, which is especially true on the shed top surfaces. The reduced hydrophobicity on the south side highlights the importance of solar radiation on the ageing process. These results are shown in Fig. 2.20 and Fig. 2.21.

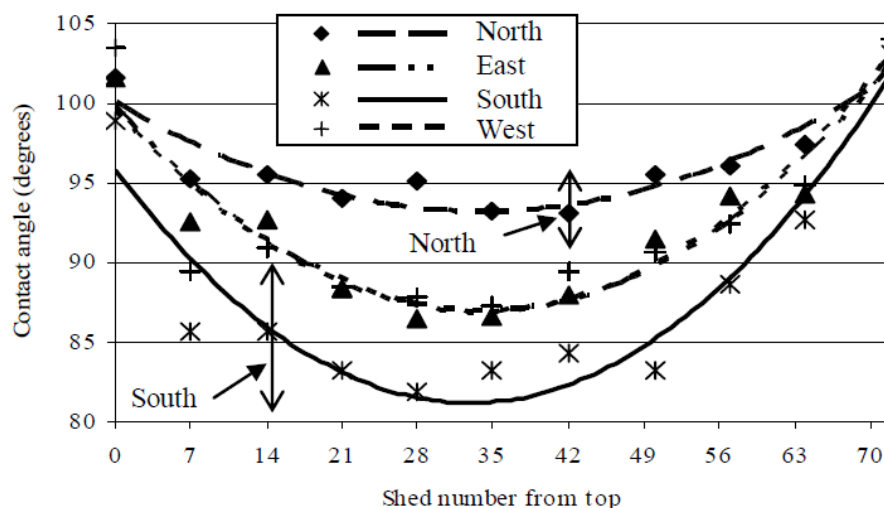


Fig. 2.20. Average contact angle along the core of each insulator in each of the compass directions [90].

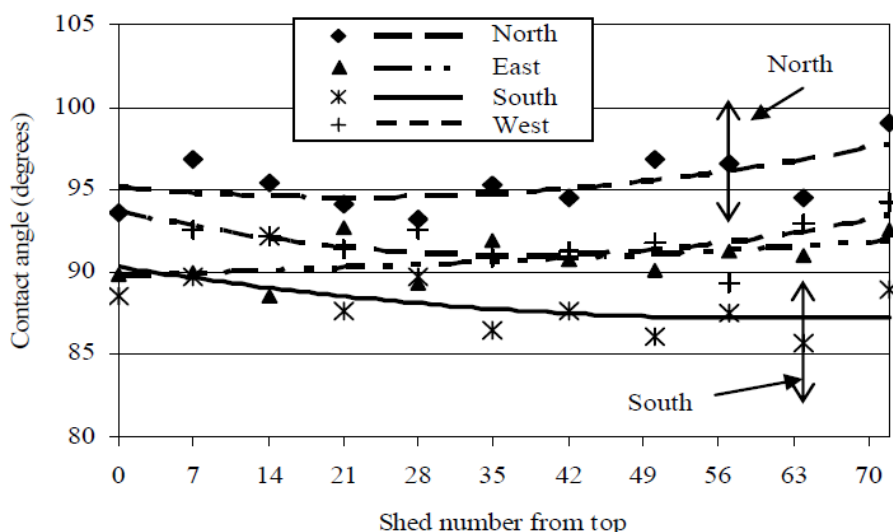


Fig. 2.21. Average contact angle on the top surface of the sheds in each of the compass directions [90].

### 2.14.1. Biological growth

With regards to biological growth effects on composite insulators, Gubanski *et al.* [91] found that wet flashover levels reduce by approximately 30%. However, they concluded that the impact of biological growth on the electrical performance is rather low.

In a more recent work from Shang [92], it was observed that the hydrophobicity is lost where biological growth covers the composite insulator surface, and it was

verified that biological growth causes an increase in leakage current, with respect to the hydrophobic condition.

## 2.15. AC and DC performance-based insulator design

### 2.15.1. Insulator design for AC energisation

For AC energisation, evidence-based conclusions are reviewed as follows.

For a standard profile, only a large increase in creepage length can increase contamination performance [60], [93]. However, it is clear that there exists a threshold creepage factor above which the performance starts decreasing again.

For the antifog profile, attention should be paid to under ribs bridging arcing [93]. Therefore, the proper dimensioning of the ribs is critical. In general, alternating rib lengths increase the withstand voltage performance.

### 2.15.2. Insulator design for DC energisation

Two research projects [94], [95] demonstrated that increasing the creepage factor does not necessarily increase the performance of an insulator under the Solid-Layer test method for porcelain post insulators. In fact, as seen in CIGRE TB 518 [4], there are some recommended limits in the creepage factor, depending on the application type. In the case of porcelain insulators, CF should not exceed 4 to 4.4. In the case of composite line insulators which are investigated in this thesis, the creepage factor should not exceed 4.3, according to [4].

The laboratory performance of line composite insulators with focus on the profile design parameters has been studied by Matsuoka *et al.* [88] under light pollution, and by Zhang *et al.* [33] under heavy pollution. Alternating large-small (ALS) shed profile will be reviewed as opposed to profiles with constant shed diameter, due to the known better performance of alternating profiles, with respect to non-alternating ones [88].

### 2.15.3. DC design study under light pollution

Matsuoka *et al.* [88] have investigated the role of the creepage factor on the flashover voltage per metre of AD under the conditions shown in TABLE 2.20.

TABLE 2.20. Test specifications of Matsuoka *et al.* [88].

NSDD (mg/cm <sup>2</sup> )	SDD (mg/cm <sup>2</sup> )	HC (1-7)
0.1	0.03	7

The NSDD is not explicitly specified in [88]. However, the paper references Naito, Matsuoka, *et al.* [57] which specifies their practice with NSDD=0.1 mg/cm<sup>2</sup>.

The results have been post-processed in this thesis and shown in Fig. 2.23. P1 and P2 indicate the distances in mm between the trunk and the large shed extremity (large shed overhang), and between the trunk and the small shed extremity (small shed overhang), respectively. The graphical description of P1, P2, and S is provided in Fig. 2.22.

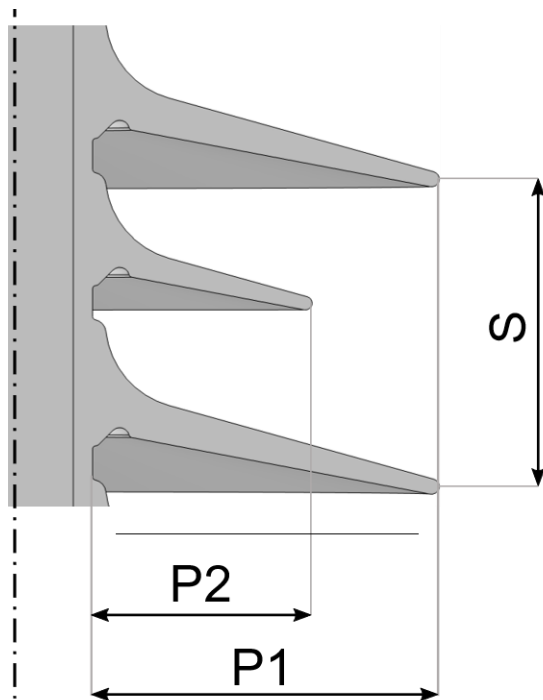


Fig. 2.22. Graphical description of P1, P2, and S, as used in Fig. 2.23 and Fig. 2.25.

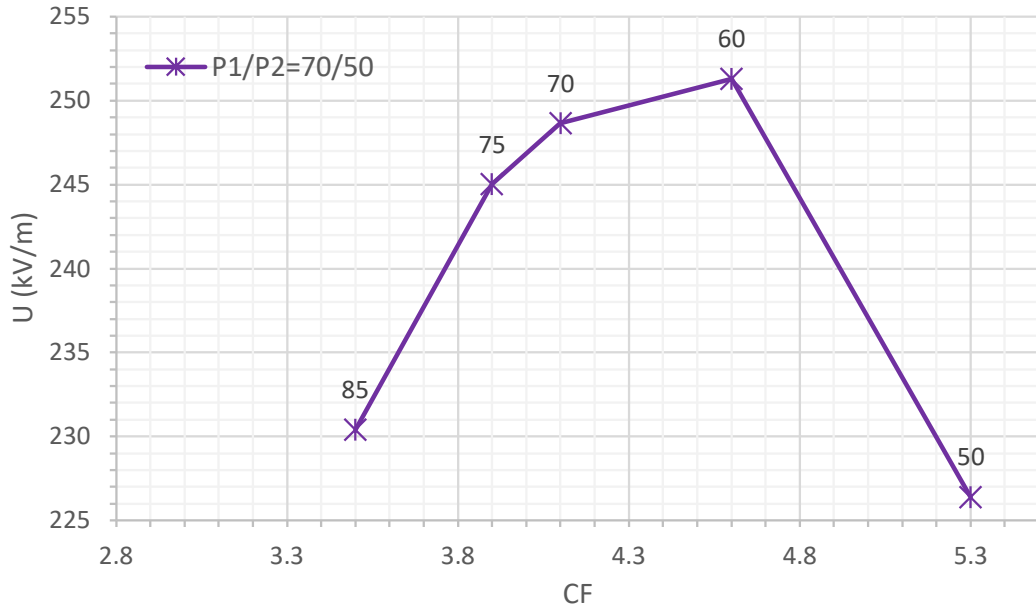


Fig. 2.23. Specific flashover voltage (kV/m) as a function of insulator creepage factor. The labels above the icons show the spacing between two large sheds  $S$ , as shown in Fig. 2.22. Post-processed from [88].

It can be observed that the best performing design has a spacing  $S$  between two large shed tips of 60 mm, with a  $CF=4.6$ , which is larger than the 4.3 recommendation limit from [4].

#### 2.15.4. DC design study under heavy pollution

Zhang *et al.* [33] have investigated the role of the profile at an altitude of 1970 m above sea level, at a pressure of 80% the one found at sea level. Still, the result trends should be applicable to lower altitudes.

The test specifications of [33] are reported in TABLE 2.21.

TABLE 2.21. Test specifications of Zhang *et al.* [33].

NSDD ( $\text{mg}/\text{cm}^2$ )	SDD ( $\text{mg}/\text{cm}^2$ )	HC (1-7)
0.6	0.1	7

CIGRE TB 518 [4] reviews [33] with the U – CF chart reported in Fig. 2.24.

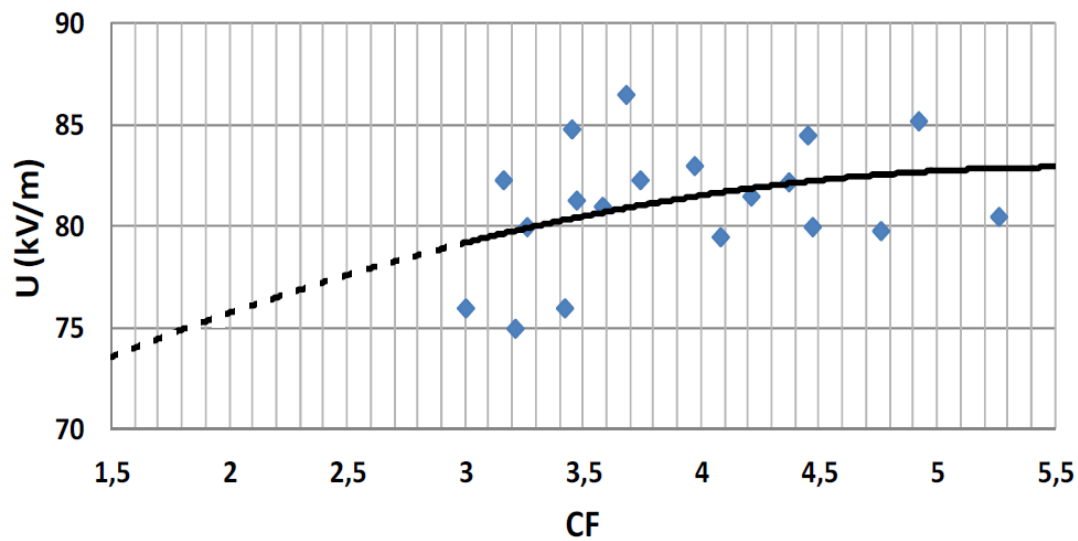


Fig. 2.24. Specific flashover voltage (kV/m) as a function of the creepage factor [4].

However, Fig. 2.24 does not differentiate between the four different shed profiles investigated by [33]. Moreover, the trend line may induce to think that an increase in CF leads to a performance increase, which is not the case. In this PhD work, the paper data [33] has been post-processed in the same manner as used in Fig. 2.23 for ease of comparison purposes. The post-processing results are shown in Fig. 2.25. The graphical description of P1, P2, and S is provided in Fig. 2.22.

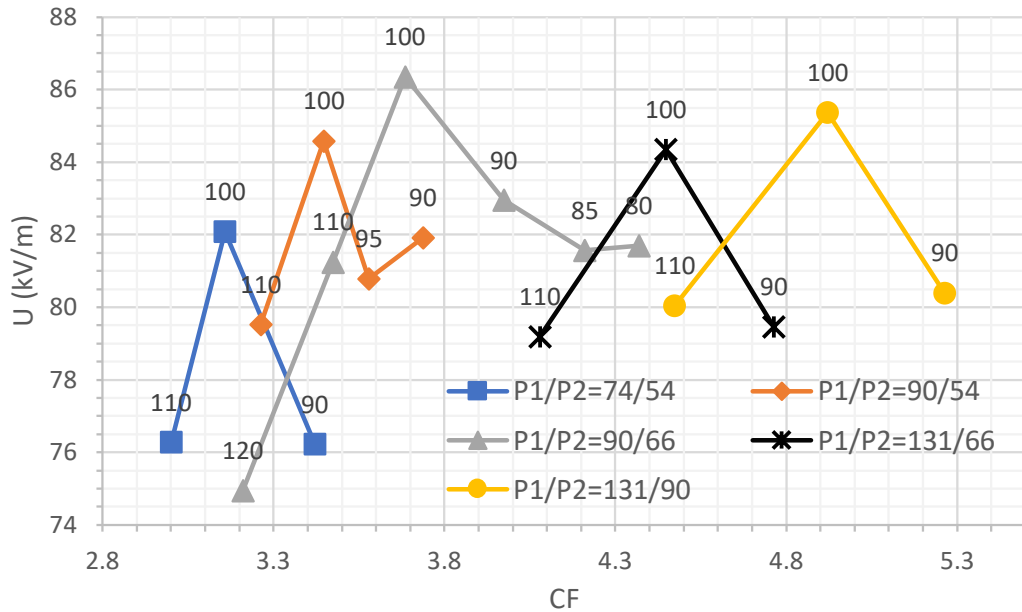


Fig. 2.25. Specific flashover voltage (kV/m) as a function of CF. The labels above the icons show the spacing  $S$  between two large sheds, as shown in Fig. 2.22. Post-processed from [33].

The following observations can be made regarding the reviewed heavy pollution study.

- The first observation is that when the spacing between two large sheds (or two small sheds), defined in the paper as  $S$  (mm) repeat unit distance, is 100 mm, the performance of each design is maximum.
- The specific flashover voltage peaks in the same way for each of the five investigated profiles, with respect to the spacing  $S$ . This observation suggests that a different P1/P2 ratio, not included in the reviewed study [33], would exhibit a similar trend with respect to  $S$ , at the same pollution level.
- Secondly, by comparing the five designs at  $S=100$  mm, P1/P2=90/66 performs best, and its CF is 3.68.
- It is worth noting that, at  $S=100$  mm, the specific flashover voltage of the P1/P2=131/66 design is lower than the adjacent designs P1/P2=90/66 and P1/P2=131/90. Same observations can be made when  $S=90$  mm and  $S=110$  mm. Thus, it could be worth questioning the results of the

P1/P2=131/66 design as they do not reflect the reasonably expectable trend which would cause its performance to be higher than what is shown. Equally, it could be worth questioning the results of the P1/P2=131/90 design which could be lower than shown, if P1/P2=131/66 are correct.

- e) To check the results of the questioned designs, it is critical to accurately keep the same hydrophobicity class for each tested insulator, which is specified in [33] to be HC7.

### **2.15.5. Remarks on DC design with respect to pollution severity**

Having analysed the designs under light and heavy pollution, a comparison can now be made between the two severities. In [88], the authors investigated only one P1/P2=70/50 ratio. The most similar ratio from [33] is P1/P2=74/54. Thus, these two will be compared.

Under light pollution, the best performing design has a large to large shed spacing of  $S=60$  mm at  $CF=4.6$ . Whereas, under heavy pollution, the best performance is exhibited by  $S=100$  mm at  $CF=3.16$ . From this observation, it can be concluded that as the pollution severity increases, the large to large shed spacing  $S$  should increase.

It is also worth noting that the best performing  $CF$  under light pollution is 4.6 and, under heavy pollution, is 3.7. Thus, as the pollution severity increases, the best  $CF$  decreases. However, as previously observed, a verification of the results of P1/P2=131/66 and P1/P2=131/90 with respect to hydrophobicity class could be made.

## **2.16. Linearity of withstand voltage with arcing distance**

### **2.16.1. Under AC**

The relationship of insulator withstand voltage performance with string length is non-linear. In fact, linearity exists up to the EHV range, i.e. 275-500 kV [93], [96], [97]. A coefficient is used to define the non-linearity of UHV, with voltage levels above 500 kV. The coefficient is defined as the string coefficient  $\lambda$ . Its

value varies depending on the severity of pollution ESDD to which the insulator is exposed.

**2.16.2. Under DC**

In non-HTM insulators, non-linearity has sometimes been found for DC, when  $SDD < 0.05 \text{ mg/cm}^2$ . Evidence of this can be found in the study conducted on cap and pin insulators [98] and station post insulators [95]. Also for HTM insulators, non-linearity has been observed at  $SDD = 0.03 \text{ mg/cm}^2$ , and linearity has been observed at heavy pollution levels of  $0.5 \text{ mg/cm}^2$  [88].

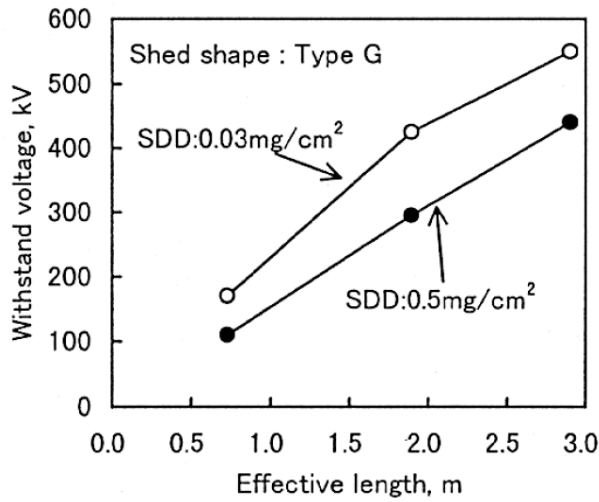


Fig. 4 Linearity between WSV and effective length

Fig. 2.26. Composite insulator linearity of withstand voltage (kV) and effective length (AD) (m), at NSDD=0.1 mg/cm² [88].

Thus, when extrapolating laboratory results to UHV levels, a correction factor of 1.1 for dimensioning may be considered if the pollution severity of the application site has low pollution levels.

## 2.17. DC to AC severity ratios in service and in wind tunnel experiments

### 2.17.1. DC to AC deposit density ratio $K_p$ in service

There exists an approach for estimating the pollution contamination level of DC energised insulators with respect to those energised with AC. The approach is based on the site severity correction factor  $K_p$  [35], [64], [99]–[105].  $K_p$  is the ratio of pollution deposit density (active or inert) under DC over that under AC. Thus, by multiplying the known AC severity by  $K_p$ , it is possible to estimate the DC energised insulator contamination.

Values of  $K_p$ , as given by Wu *et al.* [106], are shown in TABLE 2.22.

TABLE 2.22.  $K_p$  values for different environment types [106].

$K_p$	Environment type
1-1.2	Natural environment, e.g. sea and desert
1.3-1-9	Natural environment and a few km distant industrial source
2-3	Within a few km distant industrial source

Average values of  $K_p$  and its distributions are available in Fig. 2.27 from a more recent review done in [4] of the papers [71], [99], [107]–[111]. The original figure has been edited in this thesis, by including the vertical and horizontal gridlines, which enable a more accurate reading of the results.

Three observations are made with regards to Fig. 2.27:

- a)  $K_p$  decreases as the ESDD increases,

- b) The largest  $K_p$  distributions can be seen for low values of ESDD, namely below  $0.02 \text{ mg/cm}^2$ , and
- c) Four significant large DC severities are calculated conservatively in TABLE 2.23, which shows the maximum  $\text{ESDD}_{\text{DC}}$  to be  $0.32 \text{ mg/cm}^2$ .

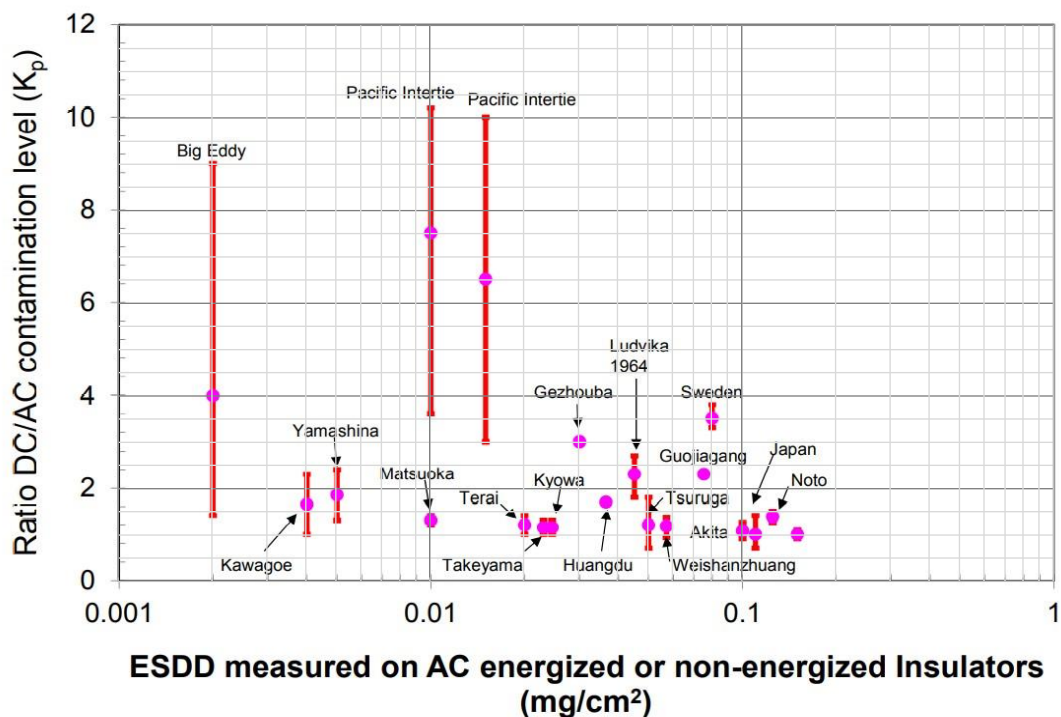


Fig. 2.27. Relationship between ESDD measured on AC energised or non-energised insulators and  $K_p$  [71], [99], [107]–[111].

TABLE 2.23. Conservative calculation of significant large DC severities from Fig. 2.27.

Location	$\text{ESDD}_{\text{AC or non-energised}}$ ( $\text{mg/cm}^2$ )	Largest $K_p$ (conservative)	$\text{ESDD}_{\text{DC}} = \text{ESDD}_{\text{AC}} \cdot K_p$ ( $\text{mg/cm}^2$ )
Sweden	0.08	4	0.32
Noto (Japan)	0.15	1.5	0.225
Pacific Inertie 1 (western USA)	0.015	10	0.15
Pacific Inertie 2 (western USA)	0.01	10.5	0.105

In Chapter 5, two deposit density assumptions are made for the conversion of UK existing lines to HVDC. The first is  $ESDD_{DC}=NSDD_{DC}=0.6 \text{ mg/cm}^2$  and the second is  $ESDD_{DC}=NSDD_{DC}=0.2 \text{ mg/cm}^2$ . As far as seen in Fig. 2.27 and TABLE 2.23, the first assumption is considerably conservative and, therefore, safe to consider in absence of  $ESDD_{AC}$  and  $NSDD_{AC}$  data, and the second assumption is still mostly conservative but it is exceeded by the Sweden and Noto (Japan) cases, as shown in Fig. 2.27.

Three wind tunnel studies, [112], [113], and [114], on the pollution accumulation behaviour at different wind speeds and energisations are found and reviewed as follows.

### 2.17.2. Wind tunnel non-energised salt fog study

Matsumoto *et al.* [112] investigated the SDD for various cylindrical insulator diameters. A wind tunnel with a relaxation chamber at the end has been used to contaminate the insulators with salt fog.

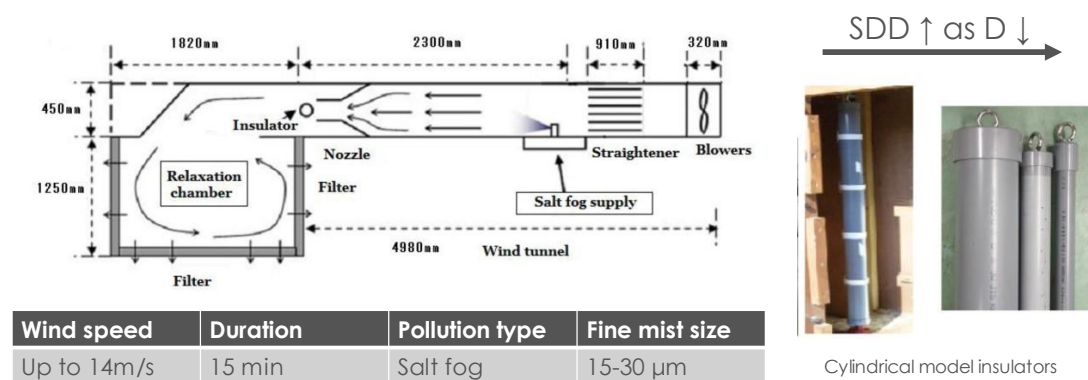
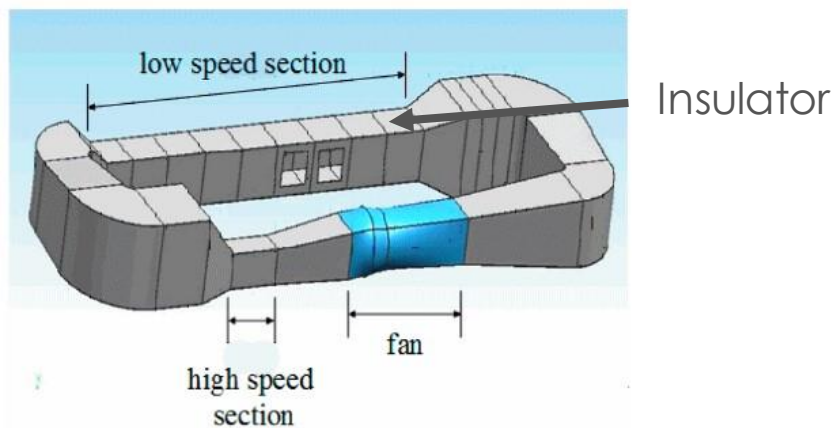


Fig. 2.28. Non-energised salt fog study at various insulator diameters with wind tunnel [112].

The study [112] confirms the findings of [87] discussed in section 2.13.2. The deposit density increases as the insulator diameter decreases.

### 2.17.3. Wind tunnel influence of pollution size under AC and DC

This study [113] intended to obtain the contamination ratios between DC energisation and AC energisation, previously defined as  $K_p$ . This has been done at various contaminant dimensions, as indicated in Fig. 2.29.



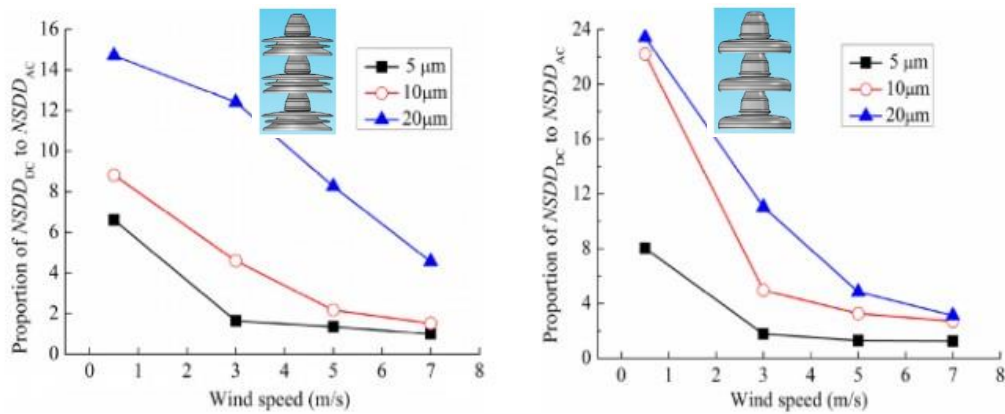
Wind speed	Duration	Pollution type	Pollution size
0.5-7 m/s	Up to 15 h	Sand	2.32 $\mu\text{m}$
		Diatomite	50 $\mu\text{m}$
		NaCl	100 $\mu\text{m}$

Fig. 2.29. Pollution size study under AC and DC with wind tunnel [113].

Two insulator profiles have been tested. A three skirt profile and a bell profile with a CD of 545 and 340 mm, respectively, per insulator. 7 insulators have been used to form a string and have been energised at 90 kV.

The results shown in Fig. 2.30 clearly indicate that at large wind speeds, the contaminations under AC and DC are relatively similar, as the wind force dominates the other forces, as seen in section 2.11. At low wind speeds, however, the contamination degree under DC is much larger than under AC because the dominant force is the electrical force. The results also show that this difference is accentuated for small pollution particles. In the controlled wind tunnel experiment,  $K_p$  values are found as high as 24, which is much larger than the largest observed in service in Fig. 2.27, namely 10.5. Thus, it could be assumed

that the wind tunnel experiment can therefore conservatively and safely provide  $K_p$  values which should not occur in service.



a)  $USCD_{DC}=42.4$  mm/kV

b)  $USCD_{DC}=26.4$  mm/kV

Fig. 2.30. Results of pollution size study under AC and DC with wind tunnel for two different profiles [113].

#### 2.17.4. Wind tunnel pollution size study under increasing direct voltage

As Fig. 2.31 summarises, Qiao *et al.* [114] investigated the pollution accumulation under various direct voltage levels.

The results show a visible difference in pollution accumulation distribution on the insulator surface. As the direct voltage increases, the deposition distribution is more uniform as expected because the electric force gains importance over the wind component. At low energisation values instead, the pollution is distributed depending on the aerodynamic behaviour of the insulator, which well resembles the AC behaviour.

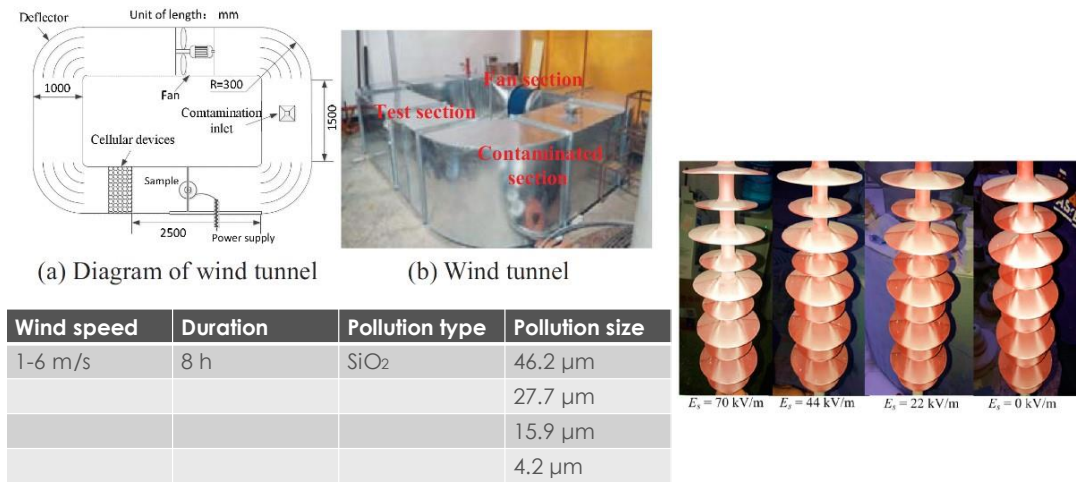


Fig. 2.31. Pollution size study under increasing direct voltage [114].

The  $K_p$  results have been post-processed in the following figures for decreasing DC voltage levels, namely 70 kV/m, 44 kV/m, and 22 kV/m. The insulator has an AD of 500 mm and an approximate CD of 1488 mm.

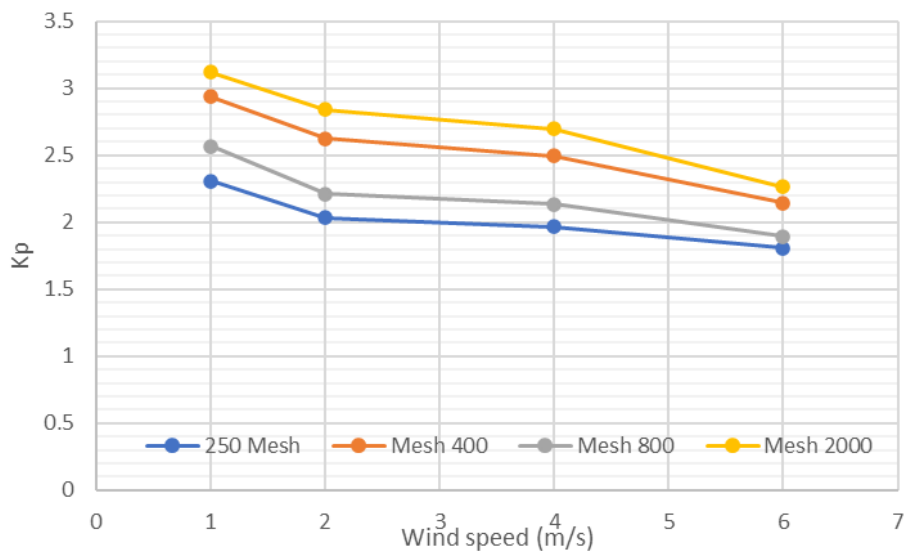


Fig. 2.32.  $K_p$  as a function of wind speed at different mesh sizes.  $USCD_{DC}=21.3$  mm/kV [114].

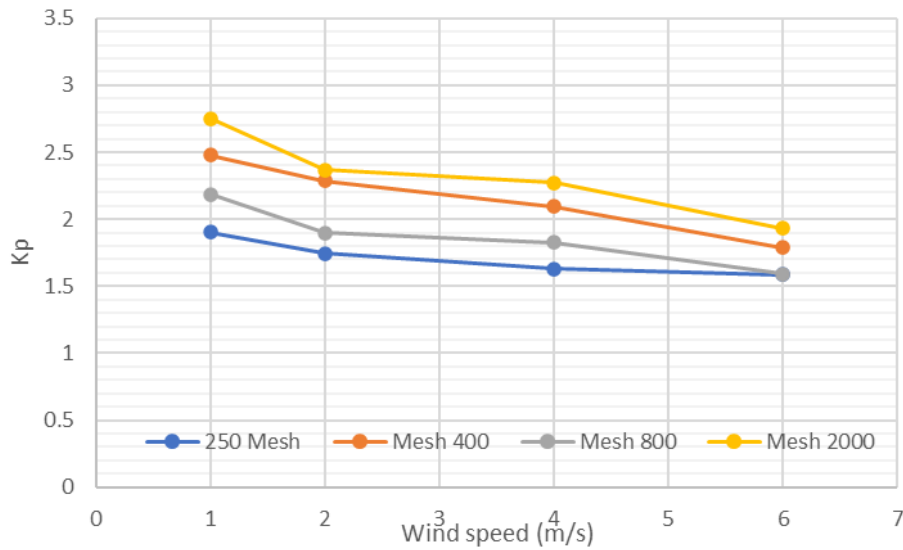


Fig. 2.33.  $K_p$  as a function of wind speed at different mesh sizes.  $USCD_{DC}=33.8$  mm/kV [114].

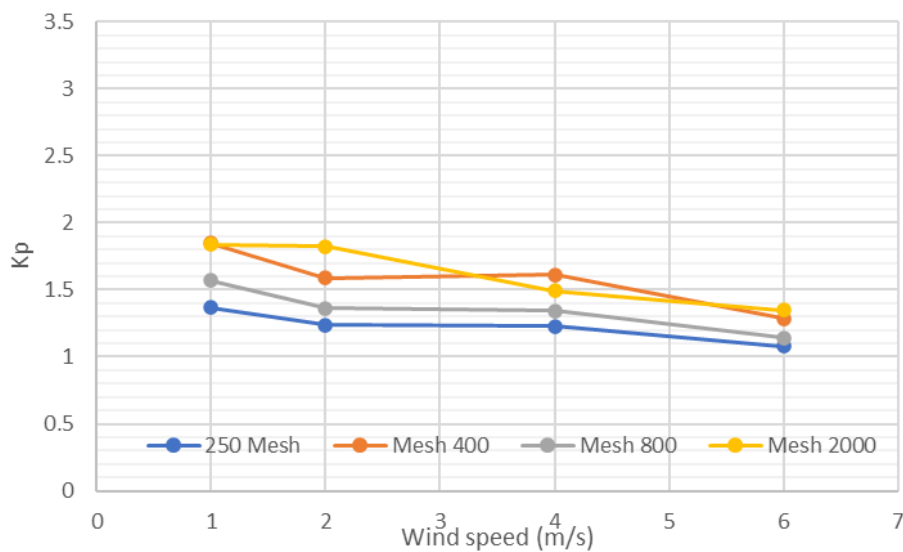


Fig. 2.34.  $K_p$  as a function of wind speed at different mesh sizes.  $USCD_{DC}=67.6$  mm/kV [114].

As expected,  $K_p$  increases as the wind speed decreases, and the influence of DC on accumulation is stronger for particle with a larger mesh size, which means smaller particles. Furthermore, a larger  $USCD$  corresponds to a lower DC influence on accumulation, as the electric field is smaller.

## 2.18. Summary of key points

- The non-necessity of corona rings under DC polluted condition has been reviewed [8]. This is due to the domination of the conductive layer on the voltage distribution along the insulator, which occurs above a threshold current, specific to the insulator design. This current is generally exceeded in service.
- The influence of non-soluble deposit on the hydrophobicity is reviewed [28] and a positive correlation is found between the non-soluble material pore size and the transfer recovery speed. In fact, the LMW silicone migrates more easily to the surface when pores are large. Kaolin is found to have slow transfer speeds with respect to Kieselguhr.
- The non-uniformity of hydrophobicity and, in particular, the U-shape of HTM insulator service hydrophilicity is reviewed [32]. It is found that a partial loss of 66.7 % of hydrophobicity (on the insulator ends) causes a loss of DC performance greater than the fully hydrophilic case.
- DC severities are reviewed and it is found that ESDD values are not larger than  $0.32 \text{ mg/cm}^2$  [71], [99], [107]–[111], NSDD values are not larger than  $0.9 \text{ mg/cm}^2$  [4], and  $\text{ESDD}_{\text{eq}}$  values are not larger than  $0.533 \text{ mg/cm}^2$  [4].
- As expected, the hydrophobicity recovery positively affects the pollution flashover performance [57].
- Under light pollution [88], namely  $\text{NSDD}=0.1 \text{ mg/cm}^2$  and  $\text{SDD}=0.03 \text{ mg/cm}^2$ , the best performing creepage factor is 4.6. Under heavy pollution [33], namely  $\text{NSDD}=0.6 \text{ mg/cm}^2$  and  $\text{SDD}=0.1 \text{ mg/cm}^2$ , the best performing CF is 3.68.
- In service,  $K_p$  values decrease as the ESDD decreases [71], [99], [107]–[111]. The largest distributions are seen for low ESDD values, below  $0.02 \text{ mg/cm}^2$  [71], [99], [107]–[111]. In wind tunnel experiments, it is clear that as the wind speed increases,  $K_p$  decreases, due to the domination of the wind force over the electric force. It is also clear that there is a negative correlation between  $\text{USCD}_{\text{DC}}$  and  $K_p$  [113], [114].



# Chapter 3. HVDC Flashover of Heavily Polluted Composite Insulators Rated 120 to 250 kV: Laboratory and Analytical Characterization

## 3.1. Introduction

To ensure reliable transmission of the bulk power, the high direct voltage line needs an effective outdoor insulation system, and composite insulators are extensively used for this purpose. Field evidence recorded by China Electric Power Research Institute (CEPRI) suggests that wet contamination is the main cause of insulation failure. Thus, the insulator pollution performance is a critical factor in ensuring a reliable power transmission, highlighting the research need in this area.

For line energisation, or after a fault clearance, the overhead line is energized with a direct voltage ramp, up to its rated voltage. This chapter presents the experimental test results of such energisation with focus on the dynamic mechanism of the insulator fault resistance. This has been done also to provide power electronics control researchers and engineers further knowledge on the fault resistance before the instant of flashover. In fact, it is common practice to assume an instantaneous change in resistance to simulate a fault, e.g. 200  $\Omega$  for overhead lines [115], and 7  $\Omega$  for cables [116]. This chapter provides an insight into the overhead line pole to ground fault case.

Different insulator lengths and orientations were investigated, and estimated and measured flashover voltages are provided.

Also, an in-depth analysis of the partial arc phenomenon on the trunks is performed, using Finite Element Method simulations, voltage and current measurements, thermal images and video recordings.

An accurate equivalent circuit of Beijing CEPRI's laboratory is developed and analysed. Moreover, the arc propagation is investigated using the extensive experimental data.

The laboratory test results indicate that a better performance is obtained with the horizontal orientation of the insulators, which is attributed to the differences in the arc propagation and in the convection heat direction.

This work will be of interest primarily to outdoor insulator technical experts and Standard Tests developers, HVDC protection engineers and scientists and, secondarily, to Transmission System Operators (TSOs). This chapter is the result of a collaboration between Cardiff University and Beijing's CEPRI, as part of the EU funded InnoDC Project.

## **3.2. Background to the Test Programme**

A laboratory test programme was undertaken to investigate the performance of composite outdoor insulators under a heavy degree of pollution. This choice was made to investigate the insulator performance under severe conditions, which would be more useful for industrial applications. Four artificially polluted composite insulators of increasing arcing distance have been stressed with an HVDC ramp of negative polarity, while oriented vertically. Similarly, the same insulators have been tested horizontally. However, a portion of the two longest insulators has been short-circuited, only when horizontal, to achieve flashover. Voltage and current readings were recorded as well as infrared images and visible light videos. The visible light videos were recorded at normal and high speeds: 50 and 1000 fps respectively.

The insulators have been energized with an HVDC ramp to achieve the flashover of each insulator and to do so in a relatively short time. This was done to study the performance of the insulators under a voltage ramp, which occurs in the field, after a fault is cleared. The ramp energization led to two advantages:

- a) First, the ramp allowed to achieve flashover in less than 1 minute. The short voltage and current recordings of the phenomena could be then used for the proposed computer modelling. In fact, excessively long

recordings (up to 1 hour for standard testing) may lead to the non-practical feasibility of reproducing the experiment with a computer simulation.

- b) Secondly, in each test, the ramp guaranteed flashover occurrence, which was then used as a synchronizing event of the electrical recordings with the video recordings.

### **3.2.1. Circuit modelling**

Computer simulations of HVDC pollution flashovers have been undertaken to study the interaction with the voltage source in a testing environment. The voltage drop of a three-phase voltage doubler rectifier circuit has been investigated at increasing leakage current in [117]. Also, Rizk et al. [118] studied the pollution flashover in a similar way to the present study. Moreover, the source used in [118] was a voltage doubler circuit, similar to the one used in this chapter.

### **3.2.2. Arc modelling**

Extensive modelling has been performed for insulator pollution discharges, as reviewed and investigated by Slama et al. [119]. Pioneered by Obenaus [18], the model has been expanded by the contributions of many authors. Ayrton [120] characterized the electrical discharge with the longitudinal voltage gradient expression, which has been further characterized by others, as reviewed in [119]. Moreover, these studies [119] focused on calculating the critical stage of arc length, current and applied voltage which, by definition, precedes an inevitable flashover. In this chapter, the critical physical quantities could not be determined, because an HVDC ramp forces the flashover to occur, which does not provide information on the critical stage at which flashover is inevitable.

### **3.2.3. Arc propagation**

As mentioned in [4], some studies have documented aspects of the difference between AC and DC arc propagation on polluted outdoor insulators. This chapter explores the previous observations regarding direct voltage and provides further details on the DC arc propagation physical mechanism under the described conditions.

### 3.3. Methodology

The investigation is carried out with the following methodology: a test programme, an analog LTspice computer circuit simulation and a Finite Element Method (FEM) simulation.

#### 3.3.1. Test programme

Standard test methods are not yet available for Hydrophobicity Transfer Material (HTM) insulators under HVDC energization. Standardization exists for HTM insulators under HVAC [121], and non-HTM insulators under HVDC [59]. For this reason, the practice established at CEPRI has been used, and it is described below.

The artificial pollution has been obtained mostly with Kaolin and some Kieselguhr for the inert component and NaCl for the active component. For each test, the non-soluble deposit density (NSDD) and solid deposit density (SDD) are chosen as NSDD=SDD=0.6 mg/cm<sup>2</sup>, which corresponds to a heavy degree of pollution. The pollution slurry has been brushed onto the insulator surfaces and left to dry for 24 hours, obtaining a hydrophobicity class of 6 (HC6). Then, each insulator has been uniformly wet with fog for 20 minutes, the fog was then extracted from the chamber to allow clear filming, and the ramp was started until flashover.

To estimate the flashover voltage prior to the test, the same equation applied in [122], and further explained in [4] and Section 2.8.3, has been used.

$$\begin{aligned}
 U &= \frac{CD}{K_0 \cdot B \cdot C_d \cdot C_a \cdot \left[ ESDD_{dc} \cdot K_C \cdot \left( \frac{NSDD_{dc}}{NSDD_0} \right)^{\frac{0.106}{\alpha}} \cdot K_{CUR} \cdot \left( \frac{D_a}{D_0} \right)^{-\rho} \cdot K_S \right]^\alpha} \text{ (kV)} = \\
 &= \frac{CD}{K_0 \cdot 65 \cdot 1 \cdot 1 \cdot \left[ 0.6 \cdot 1 \cdot \left( \frac{0.6}{1} \right)^{\frac{0.106}{0.25}} \cdot 1 \cdot \left( \frac{97.6}{115} \right)^{-0.21} \cdot 1 \right]^{0.25}} \text{ (kV)}
 \end{aligned} \tag{3.1}$$

Where

- i. It is convenient to know CD is the creepage distance in mm.

- ii. The calculation of the average diameter  $D_a$  of the insulator is needed to calculate the direct voltage, and is in this case 97.6 mm, which is less than 250 mm. For this reason,  $C_d=1$ .
- iii. Due to the small number of insulators considered, the statistical factor  $K_s$  is 1.
- iv. There are options for the values of  $NSDD_0$ ,  $D_0$ , and  $\rho$ , the choice of which can be found later in section 3.4.3.
- v.  $K_0$  is a proposed orientation correction factor, later discussed in section 3.4.3, which can initially be assumed as 1.
- vi. For brevity, the explanation of the other parameters is not included, and can be found in [4].

that  $D_a$  can be calculated with IEC 60815-2 [42] formula, which can be expressed as a function of the insulator surface  $S_{ins}$  ( $mm^2$ ) and the creepage distance  $CD$  (mm), as follows:

$$D_a = \frac{\int_0^{CD} D(x)dx}{CD} \equiv \frac{S_{ins}}{\pi CD} \quad (\text{mm}) \quad (3.2)$$

The insulator profile used for the tests is shown in Fig. 3.1.

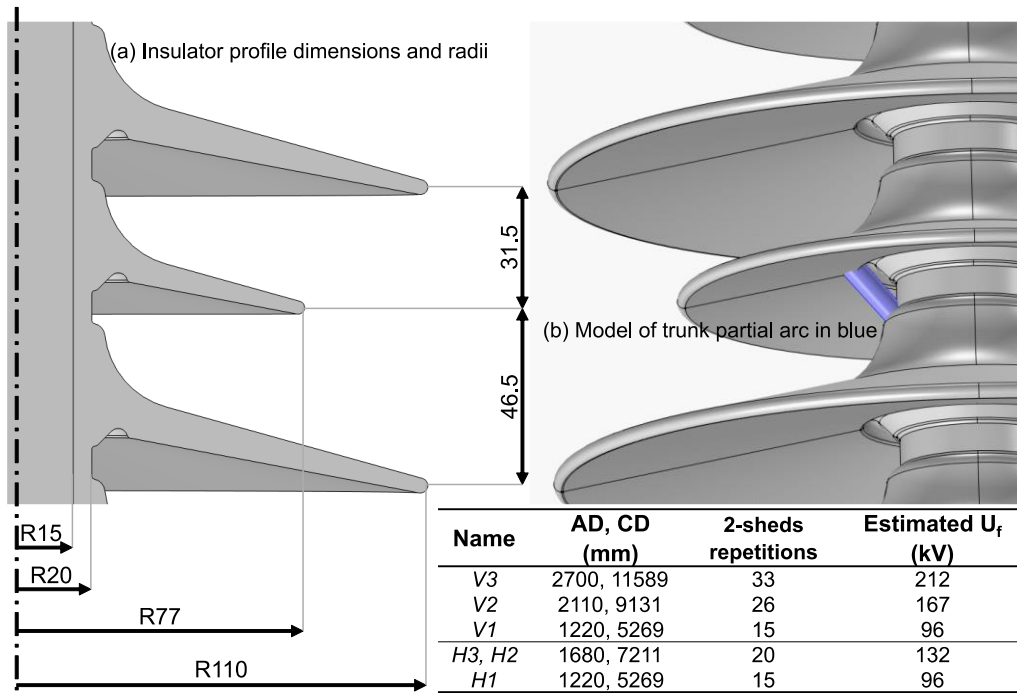
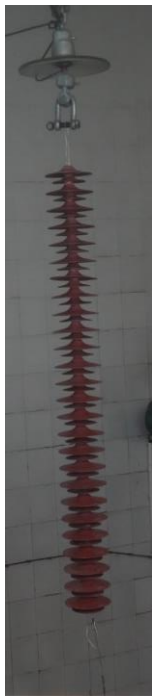


Fig. 3.1. (a) Insulator profile dimensions and radii in mm; (b) model of trunk partial arc on the right in blue; and table of the dimensions and estimated flashover voltage of all tested insulators. V and H stand for vertical and horizontal.

The polluted specimens left to dry are shown in Fig. 3.2, and the vertical and horizontal test arrangements are shown in Fig. 3.3.



Fig. 3.2. Polluted specimens left to dry.



a) V2 with modified electrodes



b) H1 with original electrodes

Fig. 3.3. Vertical and horizontal arrangements for DC pollution tests.

According to IEC 60060-1 [29], the source should supply a voltage with a rate of rise of 2% of the final voltage per second. The supply used in the test programme can deliver a constant rate of rise of about 5 kV/s, which ideally followed the standard, when the final voltage was 250 kV. Furthermore, it is specified by the same standard [29], that a voltage drop of less than 10% needs to be achieved during non-disruptive discharges of pollution tests. This requirement was also met and verified.

### 3.3.2. Test set up and equipment

The test equipment is shown in Fig. 3.4. To allow an easier visualisation and comparison with the equivalent circuit model of Fig. 3.5, the pictures of Fig. 3.4 have been mirrored.

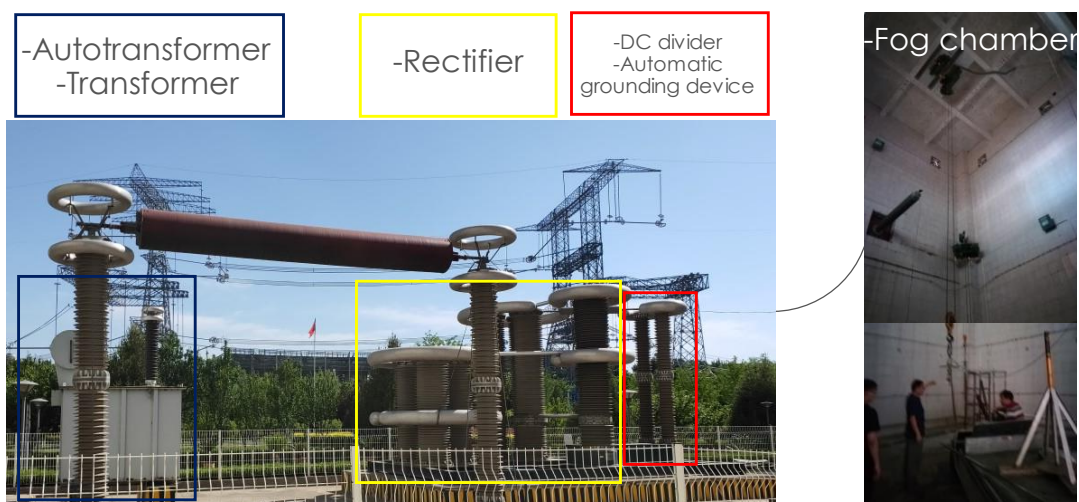


Fig. 3.4. The test equipment for the HVDC test. Pictures are mirrored.

### 3.3.3. Analog computer circuit simulation

An LTspice circuit simulation has been carried out to model the flashover phenomenon. Fig. 3.5 and TABLE 3.1 show the circuit, its parameters, and the per unit method base values.

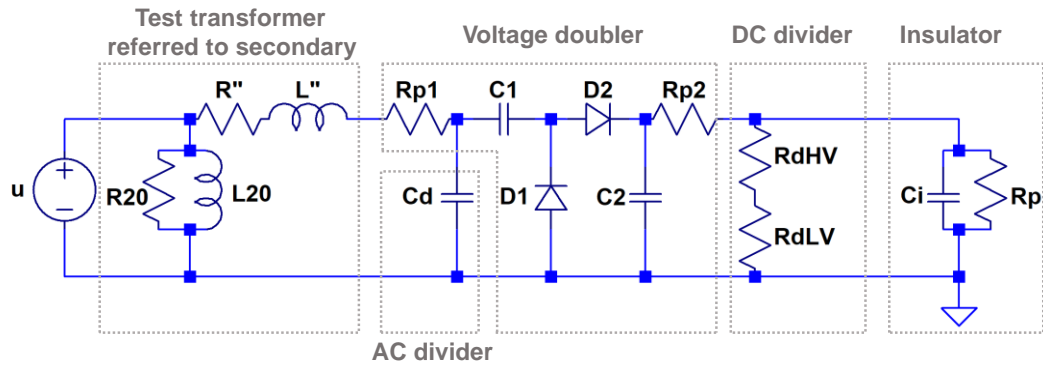


Fig. 3.5. LTspice equivalent circuit model of the experimental set-up.

The circuit parameters have been determined as follows. The transformer equivalent circuit, referred to the secondary side, has been calculated as explained in [123]. The AC divider, the voltage doubler, and the DC divider parameters were available on spreadsheets and equipment plates. The insulator model has been realized with a parallel branch of a capacitance  $C_i$  and a resistance  $R_p$ .  $C_i$  represents the air, silicone rubber, and fibre glass capacitances.  $R_p$  represents the pollution resistance, which is the smallest among the resistances of the other physical media and is, therefore, the most critical for circuit modelling.  $C_i$  has been calculated with a FEM, and the pollution resistance has been evaluated as the ratio of voltage and current recordings. Before being used for the resistance calculation, the current high frequency component has been filtered through a  $250 \mu\text{F}$  capacitance. This was done to allow a clearer visualization of the resistance at large values, by filtering out relatively fast current oscillations close to 0 A.

The per unit method [124] was used to minimize computational time. In this case, the method has been proven necessary to run simulations in a convenient time.

TABLE 3.1. Circuit Parameters and Per Unit Base Values.

Symbol	Description	Magnitude
$u$	Autotransformer voltage ramp	$5.5/\sqrt{2}$ kV/s
$R_{20}$	Iron core losses resistance	26.7 M $\Omega$
$L_{20}$	Core magnetization inductance	4.9 kH
$R''$	Winding ohmic losses resistance	67.0 $\Omega$
$L''$	Leakage flux inductance	878.5 mH
$C_d$	AC divider high voltage capacitance	0.5 $\mu$ F
$R_{p1}$	Protective resistor 1	10 k $\Omega$
$C_1$	Voltage doubler capacitor 1	1.1 $\mu$ F
$D_1, D_2$	Diodes 1 and 2	-
$C_2$	Voltage doubler capacitor 2	3.3 $\mu$ F
$R_{p2}$	Protective resistor 2	10 k $\Omega$
$R_{dHV}$	DC divider high voltage resistor	300 M $\Omega$
$R_{dLV}$	DC divider low voltage resistor	10 k $\Omega$
$C_i$	Insulator and air capacitance, from FEM	1 pF
$R_p$	Pollution resistance	Variable $\Omega$
$U_b$	Base voltage, same as transformer HV	200 kV
$S_b$	Base power, same as transformer's	1000 kVA
$Z_b$	Base impedance = $U_b^2 / S_b$	40 k $\Omega$
$I_b$	Base current = $S_b / U_b$	5 A

### 3.3.4. Finite Element Method (FEM) simulation

The FEM simulation has been carried out to analyse three major instants of the flashover phenomenon of every test. For this purpose, COMSOL Multiphysics® was used. The three instants represent the uniformly polluted and wet condition, the trunk dry bands condition and the trunk partial arc condition. The material properties used for the simulations are shown in TABLE 3.2.

TABLE 3.2. Material Properties for FEM Modelling.

Material	Conductivity (S/m)	Relative permittivity (adim)
<i>Air</i>	$1 \cdot 10^{-14}$ [125]	1
<i>Silicone rubber</i>	$1 \cdot 10^{-14}$ [126]	3.5 [126]
<i>Fibre glass</i>	$1 \cdot 10^{-14}$ [127]	3.5
<i>Pollution</i>	(3.3)	80 [128]
<i>Partial arc</i>	2.12 [119], from (3.4)	1

The surface layer of pollution was uniformly wetted at the beginning of the test, and it is assumed to be uniformly dry at the end. In between these two stages, the pollution layer dries first on the trunks and later on the sheds. As observed during the test programme, this is due to the smaller surface available on the trunks, with respect to the sheds. The consequence is a larger current density and heating on the trunks, which causes a faster local evaporation. For FEM modelling, the pollution conductivity has been calculated at two different instants: at the ramp start for the wet pollution, and just before flashover when no arcing was present for the dry pollution. The IEC 60507 standard [36] formula was used, and expressed in S/m:

$$\sigma_p = \frac{I}{U \cdot t} \int_0^L \frac{dx}{\pi D(x)} \equiv \frac{I \cdot CD}{U \cdot \pi D_a \cdot t} \left( \frac{S}{m} \right) \quad (3.3)$$

Where I is the current (A), CD is the creepage distance (m), U the voltage (V),  $D_a$  the average diameter (m) which can be calculated with (3.2), t the pollution thickness (m). In this case, due to the heavy pollution degree, t has been estimated to be 0.5 mm. It is important to note that the estimation accuracy of t is not critical with regards to FEM modelling. In fact, (3.3) binds t and  $\sigma_p$  in a way

that, if a different  $t$  is estimated, the  $\sigma_p$  result is different, but the current flowing through the insulator and the electric field distribution will be the same.

The partial arc regions were assumed to be filled by air and water vapour [119], and their conductivity has been calculated with (3.4):

$$\begin{aligned} \sigma_a &= 10^3 \{ [r_d] [s_d] \}^{-1} = \\ &= 10^3 \left\{ \left[ r_{od} \exp\left(\frac{W_i}{2K_B T_d}\right) \right] \left[ \frac{10^2 i}{1.45} \right] \right\}^{-1} \left(\frac{S}{m}\right) \end{aligned} \quad (3.4)$$

The expression of the discharge resistance per unit length  $r_d$  ( $\Omega/\text{mm}$ ) is explained in detail by Slama et al. [119], and the expression of the discharge section  $s_d$  ( $\text{mm}^2$ ) can be found in [129]. The description and values of the parameters for (3.4) are given in TABLE 3.3.

TABLE 3.3. Arc Conductivity Formula Parameters.

Symbol	Description	Magnitude
$r_{od}$	Pre-exponential constant	0.182 $\Omega/\text{mm}$
$W_i/K_B$	Ionization energy / Boltzmann constant	$3.210 \cdot 10^4$ K/mol
$T_d$	Discharge temperature	2250 K
$i$	Current for FEM simulation	$30 \cdot 10^{-3}$ A

### 3.4. Main Results and Discussion

The following results are presented and discussed. First, the modification of the insulator ends is studied, and the source voltage drop requirement is experimentally verified. Then, the estimated and measured flashover voltages are shown. The voltage, current, and resistance waveshapes of the test are

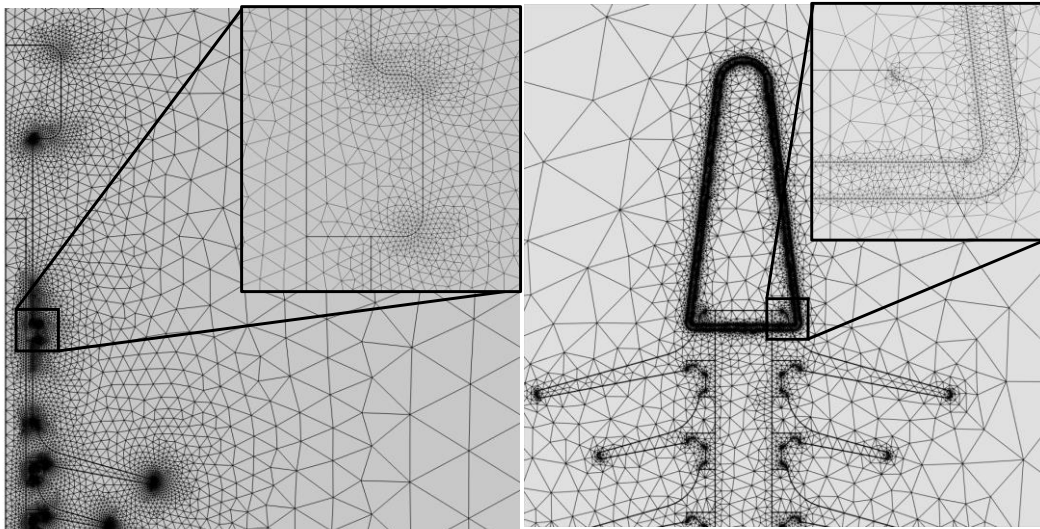
discussed. The wet and dry pollution conductivities calculation follows. Finally, an analysis of the trunk partial arc phenomenon is performed, and details of the arc propagation in both vertical and horizontal orientations are presented.

#### **3.4.1. Modified and original electrodes**

To realize the different specimen lengths, some insulators have been cut in the laboratory. This practice is common at CEPRI for pollution testing, as laboratory evidence suggests the electrode configuration has little to no influence on the phenomenon and the flashover voltage. To verify that the tangent electric field would be similar on the great majority of the insulator surface, regardless of the electrode geometry, a FEM simulation was performed, as shown in Fig. 3.7, and the mesh is shown in Fig. 3.6. The energisation voltage of the simulation corresponds to a stable resistance region, which starts a few seconds after the ramp start.

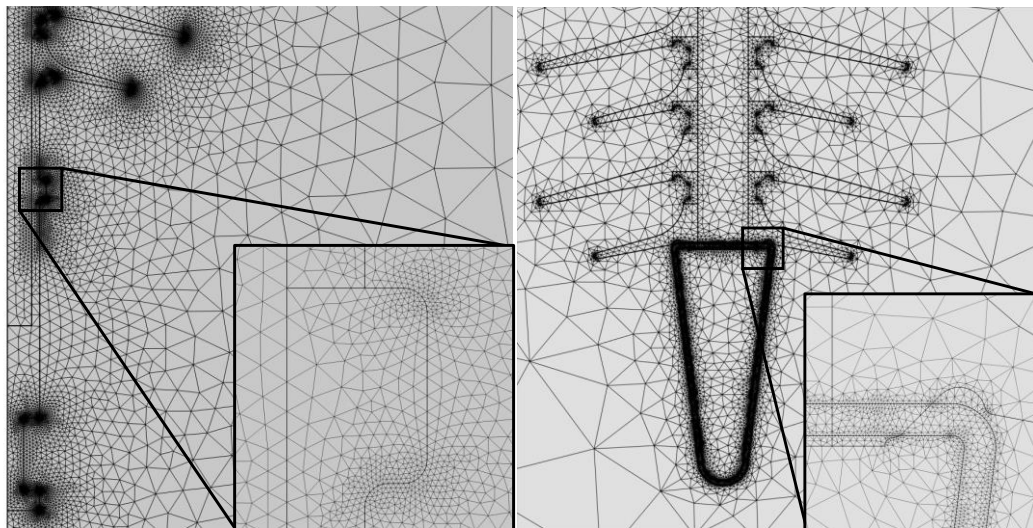
Fig. 3.7 shows that at the triple junction, constituted by metallic electrode, silicone rubber housing, and surrounding air, the tangent electric field is at most 6.3 times larger when the electrode is modified. However, due to the wet pollution on the insulator surface, the notable difference is present only on less than 55 mm of creepage distance in the proximity of the triple junction. Elsewhere, along the insulator, the difference factor is reduced from 6.3 to 0.03.

It should be acknowledged that the modification of the electrodes, performed on some of the insulator ends, may cause moisture ingress in the core-housing interface and a reduction of the flashover voltage, as reviewed in [130]. However, these insulators have been exposed to moisture no longer than the test duration. Moreover, the insulators are conformant with the dye ingress test. The modified electrodes were used for simulations, to consider the worst-case scenario with the higher electric field.



a) Ground, original electrode

c) Ground, modified electrode



b) High Voltage, original electrode

d) High voltage, modified electrode

Fig. 3.6. a), b): mesh and its details of the insulator with original electrodes – axisymmetric model. c), d): mesh and its details of the insulator with modified electrodes – three-dimensional model. Metal domains were meshed because the electric current physics has been used.

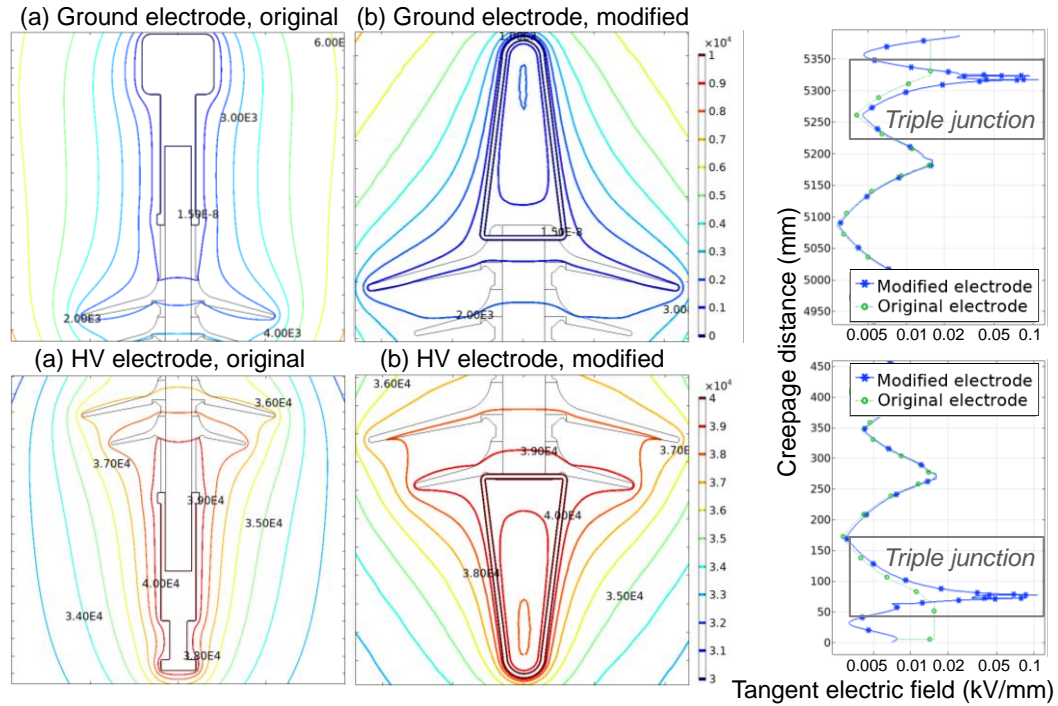


Fig. 3.7. (a) Equipotential lines (V) of the original electrodes; (b) equipotential lines of the modified electrodes. On the right, tangent electric field along the creepage path of both electrode types. The results correspond to an energization of 40 kV.

### 3.4.2. Verification of source requirements

During the experiments, a voltage drop of less than 10% was met and verified, in accordance with [131], as shown in Fig. 3.8.

The green voltage waveshape  $V_s$  refers to the simulated clean and dry insulator voltage, which was obtained by modelling the insulator as an ideal capacitance  $C_i$ . The blue voltage waveshape  $V_m$  is the measured insulator voltage, which showed close agreement with the parallel  $C_i$ - $R_p$  modelling. The red function is the percent voltage drop, calculated as per  $v_d$  equation in Fig. 3.8, which always falls below 10%.

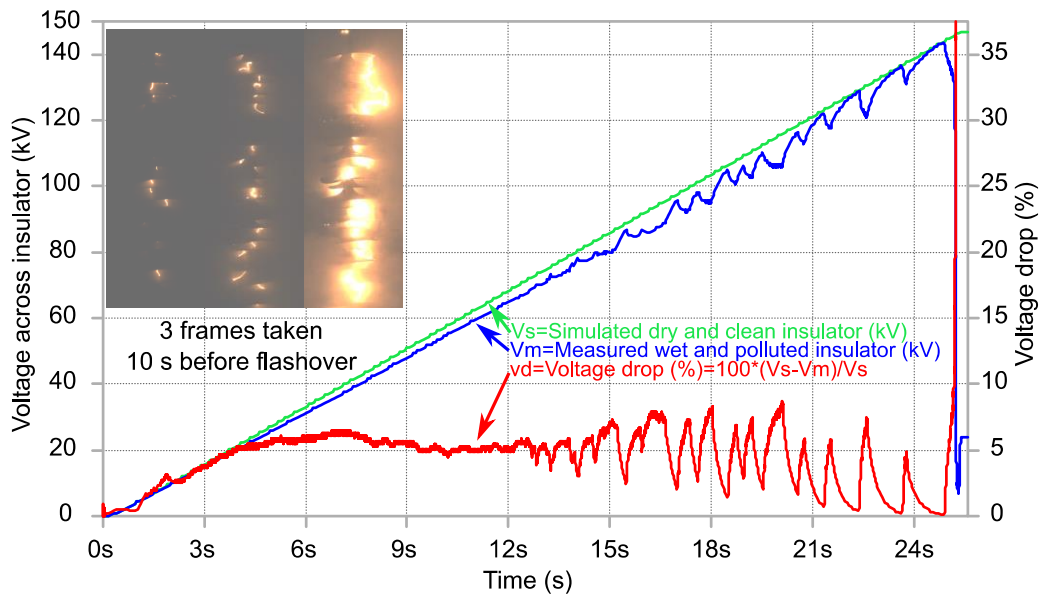


Fig. 3.8. In green, the simulated clean and dry insulator voltage, when modelled as the capacitance  $C_i$ . In blue, the measured (or simulated because of great agreement with measurement) wet and polluted insulator voltage. In red, the percentage voltage drop, always below the standard-specified 10% limit.

### 3.4.3. Estimated and measured flashover voltage

The maximum direct voltage that the source is able to supply is 250 kV. To select the insulator maximum arcing distance that the supply would reliably cause to flashover at the given heavy pollution degree, there was a need to estimate the flashover voltage at varying arcing (or creepage) distances. For this purpose, (3.1) was used. It had been estimated that V3 insulator with an AD of 2700 mm would reach flashover at 212 kV, which would be suitable for the source capability. However, the V3 test exceeded expectations with a flashover voltage of 252 kV, and likewise shorter insulators exceeded the estimations.

Moreover, when the longest insulator with AD=2700 mm was oriented horizontally, it could not reach flashover. Even the insulator with AD=2110 mm could not reach flashover when horizontal, which suggests both their flashover voltages are greater than 250 kV. These preliminary horizontal tests proved the horizontal orientation to perform better than the vertical one, and they justified the decision to short-circuit a portion of these two longer insulators, realizing a shorter AD of 1680 mm, to achieve flashover.

Fig. 3.9 shows the estimated and measured flashover voltages. The flashover voltages were measured once for each insulator. Thus, measurements may slightly vary if tests are repeated.

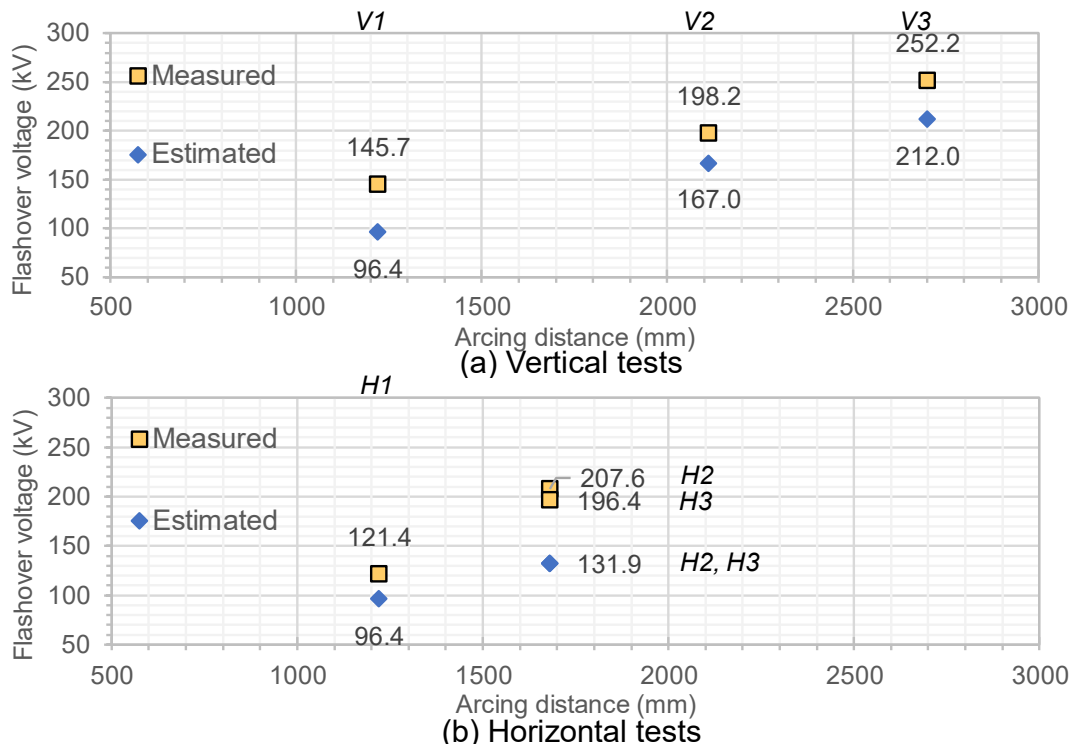


Fig. 3.9. Estimated and measured flashover voltages (kV) as a function of arcing distance (mm). Abbreviated nomenclature reflects definitions of Fig. 3.1.

As anticipated in the Methodology, there are options for the values of  $NSDD_0$ ,  $D_0$ , and  $\rho$  [4] of (3.1) and are discussed below.

Both 0.1 and 1 can be used for  $NSDD_0$ , and a value of 1 has been chosen because it is closer to the test  $NSDD$  ( $0.6 \text{ mg/cm}^2$ ), and the estimation results better reflect the laboratory flashover voltage measurements.

The reference diameter  $D_0$  and the exponent  $\rho$  are coupled, and they take into consideration that as the average diameter  $D_a$  increases, the collected pollution per unit area decreases. CIGRE TB 518 [4] advises  $D_0=250 \text{ mm}$  and  $\rho=0.35$  as they produce the best fit with the analysed service experience data. However, a

Japanese study [43] is also referenced, and it proposes  $D_0=115$  mm and  $\rho=0.21$ . The latter values have been used in this chapter because they produce an estimation which is closer to the measured flashover voltages.

Notably, the measured flashover voltages are larger than the estimated ones, and this could be due to the energization, which is not constant, as it is a ramp. It could also be due to the fog injection termination before the ramp start, done to allow clear camera recordings, which causes the pollution to be non-uniformly wetted while evaporation occurs.

CIGRE TBs [2], [4] review linearity of the flashover voltage with the insulator arcing distance, when  $SDD>0.05$  mg/cm<sup>2</sup> for the low influence of the electrodes as Fig. 3.7 shows. The vertical results of Fig. 3.9 confirm this finding at both SDD and NSDD equal to 0.6 mg/cm<sup>2</sup>.

The better pollution performance under HVDC in the horizontal orientation was previously found in [4], because of the arcs extension away from the insulator surface due to convection. No orientation correction for the estimation of the Unified Specific Creepage Distance USCD (mm/kV) is yet available in [4]. Therefore, the introduction of an orientation correction factor  $K_0$  is proposed. From Fig. 3.9, it is possible to calculate the average Unified Specific Creepage Distance (USCD) for each orientation. For the vertical case, the average USCD is 42.7 mm/kV and, for the horizontal orientation, it is 38.3 mm/kV. Thus,  $K_0$  can be preliminarily chosen as 1 for the vertical orientation, and 0.896 for the horizontal orientation. As proposed,  $K_0$  would be a factor at the denominator of the voltage estimation calculation, as (3.1) shows.

#### **3.4.4. Stages of the flashover phenomenon**

The common stages of a pollution flashover phenomenon are known for hydrophilic surfaces [132], and also for hydrophobic surfaces under a power-frequency ramp voltage [133]–[135], which show a similar behaviour to the present HVDC ramp tests.

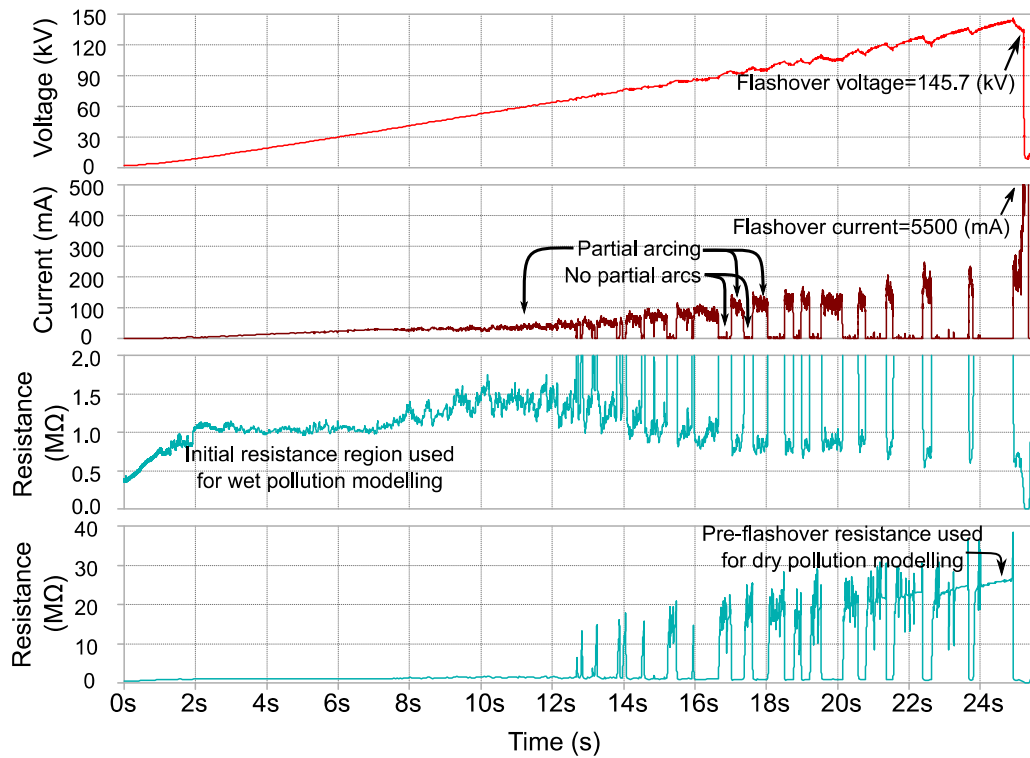


Fig. 3.10. V1 test. Direct voltage (kV), current (mA), and resistance (MΩ) all as a function of time (s). The resistance is shown with a small and a large interval, for ease of visualization.

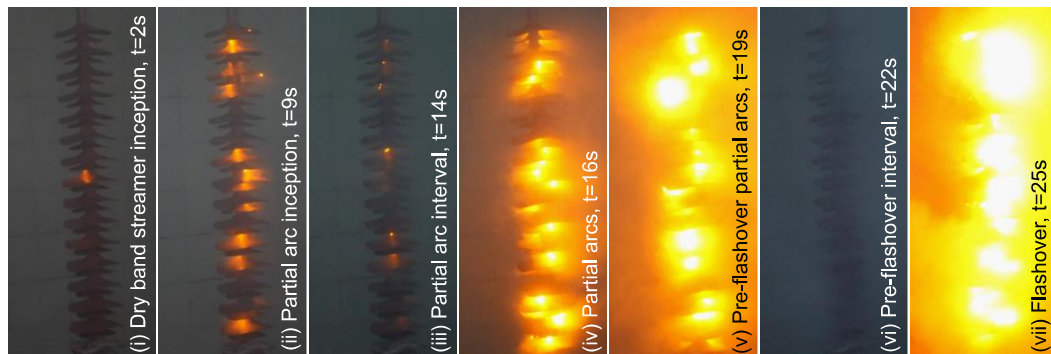


Fig. 3.11. V1 test. Test video frames, (i) to (vii).

Fig. 3.10 shows that the current increased linearly for 2 s to an applied voltage of 10 kV, during which no discharge activity was observed. At this time, the first dry-band streamer discharge was initiated on a trunk section of the insulator, Fig. 3.11 (i). During the period of a further voltage ramp increase to 50 kV at 9 s, the

number of trunks which supported dry band streamer discharges increased (ii) and the overall leakage resistance of the insulator remained approximately constant at 1 M $\Omega$ . From this point on the voltage ramp, the current became intermittent, and partial arcs intermittently spanned increasing numbers of trunks (iii – v). Partial-arc current increased with voltage, current pulse durations statistically decreased, while periods of arc inactivity progressively increased. The video frames confirmed these changes. The period before flashover at 25 s was characterized by a dark period, and flashover occurred when the partial-arc current exceeded 500 mA.

Fig. 3.10 is further discussed as follows. Firstly, the measured *voltage* ramp presents drops when there is partial arc activity on the insulator.

With regards to the *current*, as expected, a clear correspondence between partial arcing and a non-zero current reading can be observed. During the first half of the test, the current increases relatively steadily, in correspondence to a continuous partial arcing on the trunks, and an increasing number of short-circuited trunks. This initial partial arcing is due to water evaporation, which happens on the trunks at a higher rate than on the sheds. Section 3.4.6 later provides details on why this occurs. Approximately from half of the test time, the current becomes intermittent, which is when the arcs start to intermittently span increasing portions of sheds. More specifically, the current pulses duration statistically decreases as time progresses, while periods of arc inactivity progressively increase. This occurs because fog injection is suspended from the start of the test, and as the insulator increasingly dries, partial arcing needs a larger voltage to occur.

From the *resistance* point of view, an almost constant region, or stable region, can be observed in the first half of the test when the partial arc activity is continuous. This suggests that the wet pollution resistance per unit length is the same or very close to the partial arc resistance per unit length. In the second half of the experiment, the resistance intermittently spikes when the partial arc activity is not visible, and the current is close to zero. This is due to the small conductivity of the dry pollution, which has a large influence on the current, when the high conductivity arcs are not present. Moreover, it can be observed that, during the

partial arcing periods, the resistance steadily decreases, as more and more insulator portions are bridged with highly conductive arcs. Also, when partial arcing is not present, the resistance steadily increases due to the water evaporation from the wet pollution layer.

In AC instead [133]–[135], the first trunk dry-band occurs immediately, at 2–3 kV. As a result, the majority of the voltage gradient is transferred to the dry band, where rewetting is prevented by low-current streamer-corona discharges. The increased resistance limits the leakage current to a few mA. As the voltage increases, further dry bands are formed on other trunks, maintaining the low current regime. Eventually, the voltage becomes large enough to launch partial arcs which bridge the dry bands. Finally, flashover occurs at a peak current exceeding 500 mA.

In conclusion, the AC and DC flashover phases appear very similar, with the difference of current intermittency during the second half of the present DC tests.

#### **3.4.5. Wet and dry pollution conductivities**

Thanks to (3.3), it is possible to calculate the wet and dry pollution conductivities  $\sigma_{pw}$  and  $\sigma_{pd}$ , respectively, shown in Fig. 3.12. Their accuracy has been verified with a FEM model, which well reflected the laboratory measurement. E.g., the V1 FEM simulation current is 21 mA for the wet condition at 30 kV, and 45  $\mu$ A for the dry condition, at 140 kV.

Firstly, no dependence of the pollution conductivity  $\sigma_p$  on arcing distance is notable. Secondly, while the  $\sigma_{pw}$  are relatively similar to each other, the horizontal  $\sigma_{pd}$  are one order of magnitude larger than the vertical  $\sigma_{pd}$ . This suggests that as the test progresses, in the horizontal case, the water content is larger, and the evaporation rate is smaller. In fact, the hot air, vapour, and plasma move upwards in both orientations, and thus heating the insulator by convection when vertically oriented, allowing more evaporation. This heat transfer by convection does not happen as much on the horizontal insulator because the heat is dispersed in the upper air, as recorded and shown in Fig. 3.12. This is the first identified reason for the better performance of the horizontal orientation.

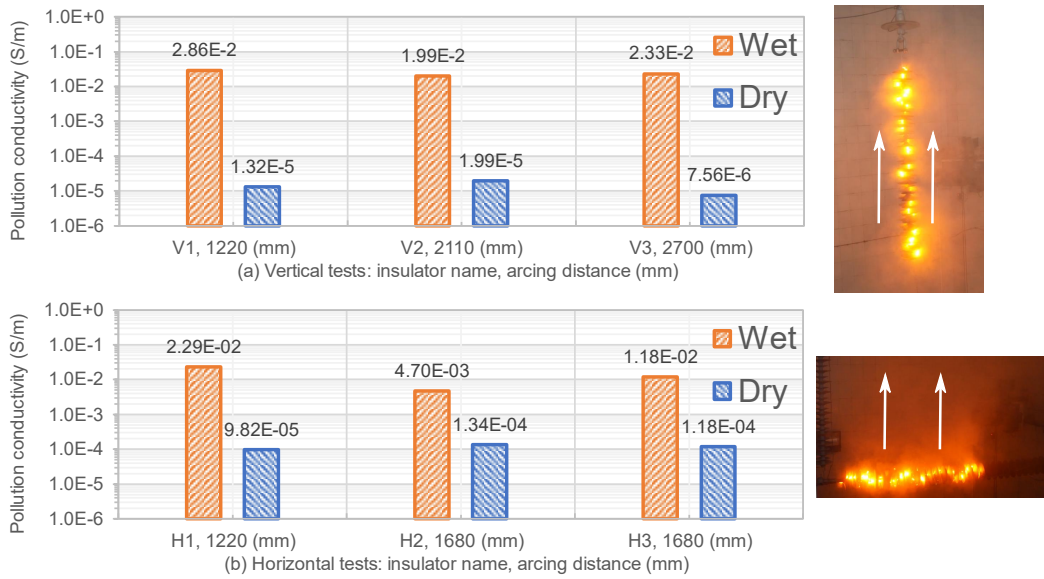


Fig. 3.12. Pollution conductivity  $\sigma_p$  (S/m) calculated from each insulator test for an estimated pollution thickness of 0.5 mm. Conductivities relate to the wet condition at the test start, and to the dry condition just before flashover, both calculated with (3.3). (a) The vertical tests, and (b) the horizontal tests.



Fig. 3.13. Water vapour moving upwards during HVDC pollution flashover in both vertical, on the left, and horizontal, on the right, orientations.

It is worth noting that the conductivities are given for the purpose of direct application in new models. However, these  $\sigma_p$  are inversely proportional to the pollution thickness  $t$ , which is estimated at 0.5 mm. A different estimation of  $t$  could be made, e.g. 0.1 mm, and it would change the values of  $\sigma_p$  according to (3.3). In both cases, the conductance of the pollution layer will be the same and the current flowing through the pollution layer will be the same.

### 3.4.6. Trunk partial arc phenomenon

As anticipated in Section 3.4.4, from the voltage ramp start, a leakage current flows on the wet pollution layer of the insulator. This current is equal at every position along the creepage path, due to the high conductivity of the wet pollution, with respect to the surrounding silicone rubber and air. The pollution layer thickness  $t$  is approximately the same along the profile, and the pollution section ( $\pi \cdot D(x) \cdot t$ ) is proportional to the diameter  $D(x)$ , which varies along the creepage path coordinate  $x$ , and is smaller on the trunks and larger on the sheds. The result is a higher current density  $J$  (A/m<sup>2</sup>), where  $D(x)$  is small, which is on the trunks. The laboratory infrared pictures and the FEM simulation confirm this as clearly indicated in Fig. 3.14.

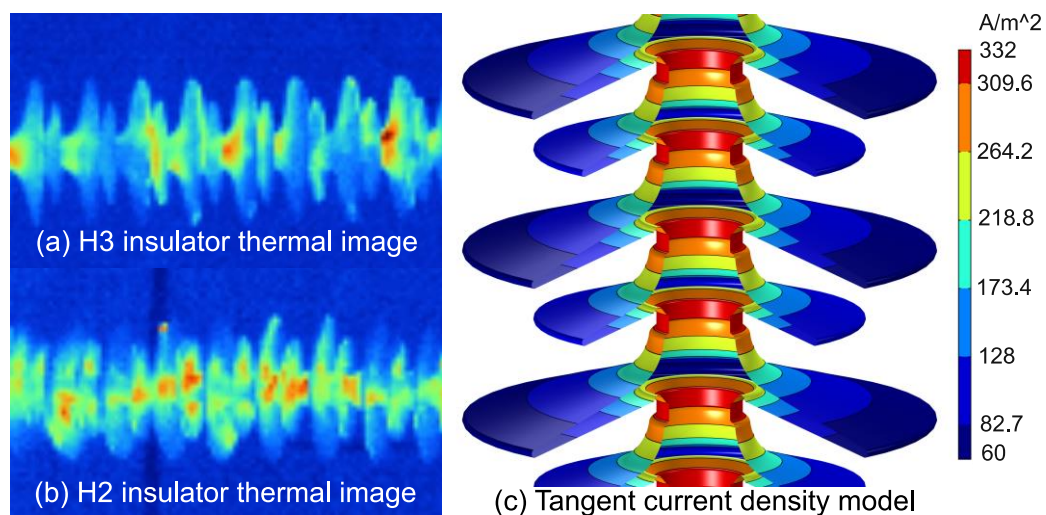


Fig. 3.14. Thermal images showing advanced stage of dry bands at two different view angles. (a) a clearer view of the sheds, from H3 insulator. (b) a clearer view of the trunks, from H2 insulator. (c) the current density tangent to 270 degrees of the insulator surface.

As a consequence, the evaporation is faster on the trunks than on the sheds. Dry bands are formed on the trunks, and almost all the voltage is applied on their extremities due to the high dry pollution resistance. As the voltage ramps up, the air breakdown occurs, bridging the dry band.

The electric field tangent to the insulator creepage path drives the current through the pollution layer. Fig. 3.15 shows the tangential electric field  $E_t$  (kV/mm) in three different phases: when the pollution layer is wet, when it is dry on the trunks, and when partial arcs bridge the air alongside the trunk dry bands. The partial arc locations have been modelled according to the video recordings, and the electrode high voltage has been selected according to the voltage measurement in the stable resistance region discussed in section 3.4.4. This was done to allow a better arc geometry modelling and an acceptable comparison of the results, which is when the arcs still have not expanded away from the trunks, and their shape can be assumed as cylindrical.

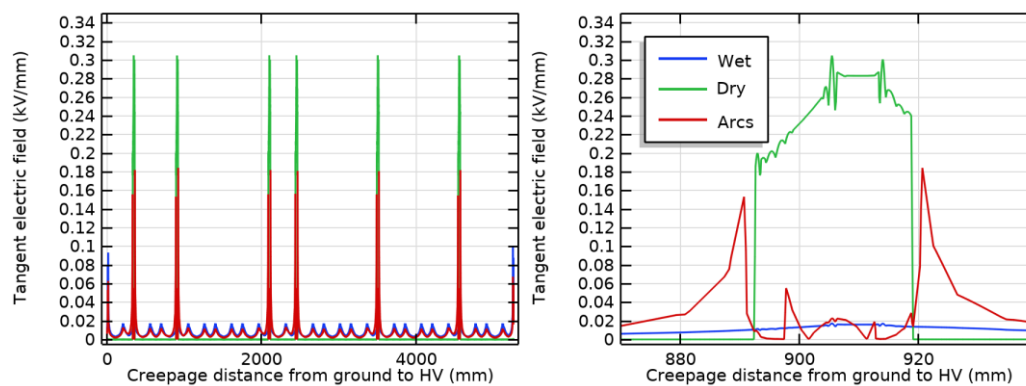


Fig. 3.15. Tangent electric field  $E_t$  (kV/mm) as a function of the creepage distance (mm) in three phases: uniformly wet pollution layer in blue, trunk dry bands in green, and partial arcs in red. On the left the whole creepage path, on the right a detail of a trunk.

When the pollution is wet,  $E_t$  is relatively uniform along the profile, with slight increases on the wet trunks. Then, when dry bands are formed on the trunks,  $E_t$  substantially increases on the dry pollution and decreases on the wet pollution.

Finally, when a partial arc is formed,  $E_t$  is relatively large on the arc extremities because that is where the current is being driven, and it is small in the middle.

The wet, dry, and arced conditions of the trunk slightly differ, depending on the test. Details are shown in Fig. 3.16. Similarly to Fig. 3.15, the voltage selected for each simulation corresponds to an instant of the stable resistance region, in which the arcs propagate with no interruptions.

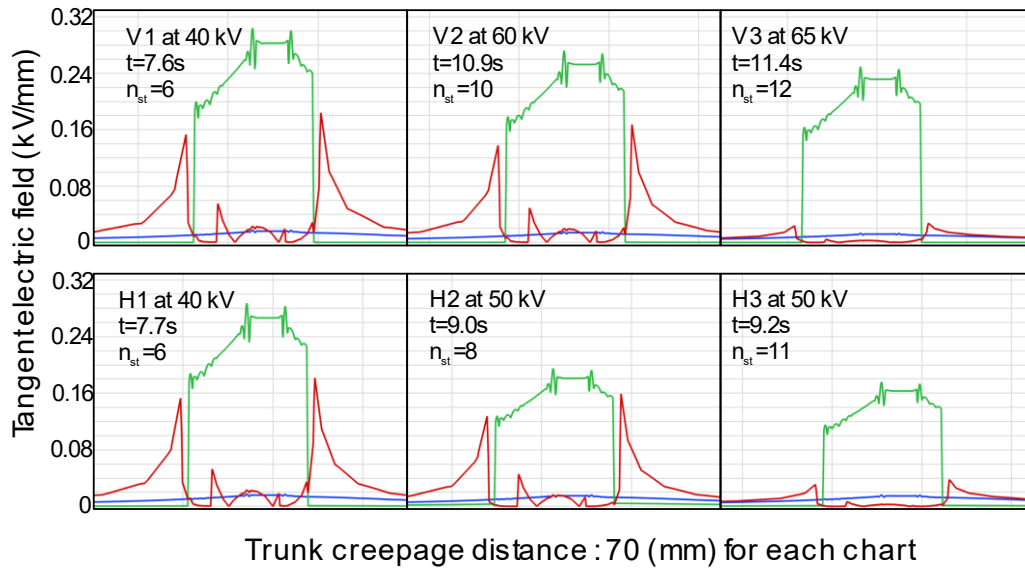


Fig. 3.16. Tangent electric field  $E_t$  (kV/mm) as a function of the creepage distance (mm) at same three instants and with same colours of Fig. 3.15. Each chart indicates the insulator name, simulation voltage, time from ramp start, and number of short-circuited trunks.

The individual results of Fig. 3.16 show the same trends identified in the Fig. 3.15 result.

Due to the relatively high dry pollution conductivities, H1, H2, and H3 exhibit a smaller  $E_t$  in the dry band simulation in green, than V1, V2, and V3, respectively.

Also, as the number of dry bands increases,  $E_t$  decreases on the individual dry bands, driving less current and thus slowing down the flashover phenomenon.

Finally, as the number of partial arcs increases,  $E_t$  decreases with respect to the dry band condition, with relatively high peaks on the arc extremities.

### 3.4.7. Arc propagation

With regards to arc propagation, the video recordings show that partial arcs are located on paths which most often do not follow the insulator profile, confirming observations under DC reviewed in [4]. However, Fig. 3.17 and Fig. 3.18 can reveal further information on the arc propagation under DC.

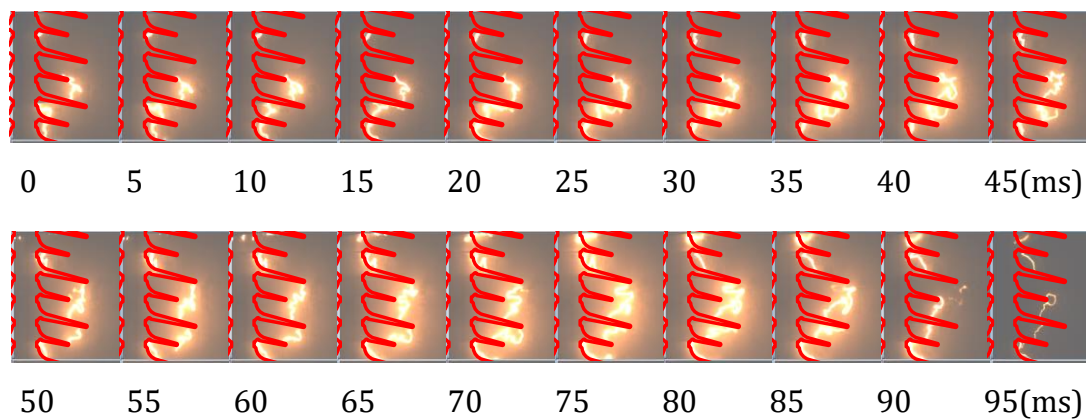


Fig. 3.17. Arc propagation. Frames of the vertical V1 test, each taken every 5 ms. The recording occurred at 1000fps, 1 frame every 1 ms. The frames show about 3 alternating shed repetitions.

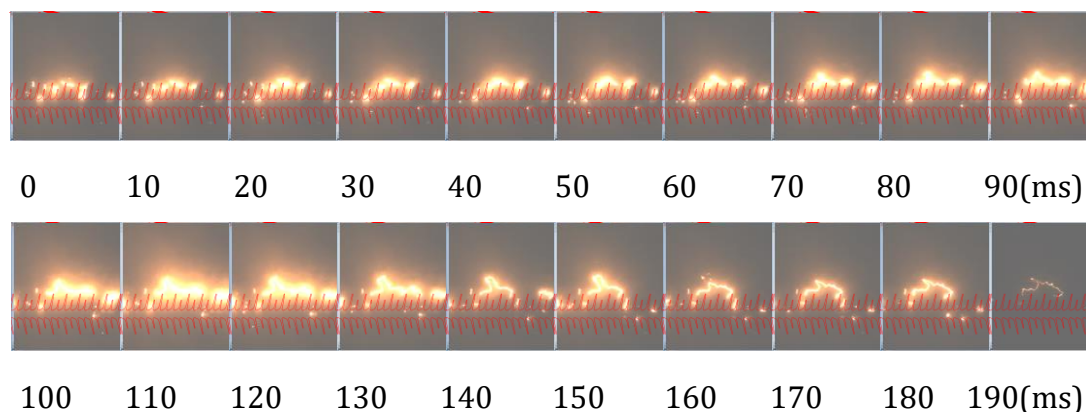


Fig. 3.18. Frames of the horizontal H1 test, each taken every 10 ms. The recording occurred at 1000fps, 1 frame every 1 ms. The frames show 8 alternating shed repetitions.

In both orientations, the partial arcs move upwards in time by heat convection, because of their high temperature. The difference is that, in the horizontal orientation, the arc expands upwards and tends to extinguish more easily. This is the second identified reason for the better performance of the horizontal orientation. Also, as Fig. 3.17 shows, in the vertical orientation, the arc moves upwards and it quickly connects two shed tips, which helps accelerate the flashover phenomenon.

### 3.5. Conclusions

The results confirm that for HVDC insulators performance under heavy pollution conditions, the electrode influence on the electric field tangent to the insulator creepage path is negligible.

It is also established that the insulators in the horizontal orientation perform better than when in vertical configuration. This was attributed to two reasons:

- a) Firstly, in the horizontal case, the convection heat is dispersed in upper air and not on the insulator, which results in lower insulator temperature, slower evaporation, and larger dry pollution conductivities. The consequence is a decelerated formation of dry bands, and ultimately a decelerated flashover phenomenon.
- b) Secondly, the horizontal arcs expand upwards, and tend to extinguish more easily. Thus, for the calculation of the USCD, the introduction of an orientation correction factor  $K_0$  is proposed. From the findings of this work,  $K_0$  is proposed as 1 for the vertical orientation, and 0.896 for the horizontal. However, more test conditions, such as different pollution severities and different insulator profiles, need to be investigated to accurately determine this factor for a vast range of applications.

It is also concluded that, with respect to the sheds, the first dry bands appear on the trunks because their pollution layer section is smaller, and the current density is larger which causes more local evaporation.

The electric field tangent to the insulator surface drives the current through the pollution layer. This field is small and uniform when the insulator is wet, it later

becomes substantially larger on the dry bands. Finally, when arcs are formed, the field decreases with relatively high peaks at the arc extremities where most of the current is being driven into.

With regards to the arc propagation, the partial arc moves upwards in both orientations. The consequence is that in the vertical orientation, the arc tends to connect portions of the insulator more quickly, whereas in the horizontal orientation the arc tends to extinguish more easily.



# Chapter 4. Performance of Composite Outdoor Insulator under Superimposed Direct and Switching Impulse Voltages

## 4.1. Introduction

The development and implementation of HVDC technology, done to integrate renewable resources, increase power transfer, and allow flexible grid operation, bring new research challenges that need to be investigated. One of these challenges is to determine how outdoor insulators perform under various stress conditions. For example, when a pole to ground fault occurs on bipolar DC lines, the healthy pole is stressed by a slow transient overvoltage superimposed on the system DC voltage [136]–[139], as shown in Fig. 4.1. The same happens for the neutral conductor [140]. These superimposed overvoltages are similar to a Switching Impulse (SI) [140].

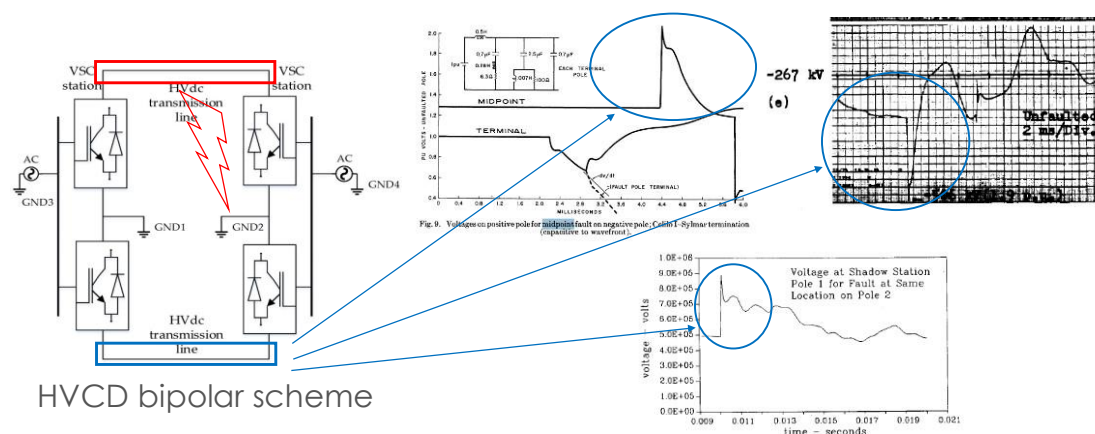


Fig. 4.1. Voltage superimposition waveshapes on HVDC lines. Studies by [136]–[139].

This chapter aims at contributing to the understanding of the new problem by bringing new experimental data of tests operated on a composite insulator. These tests have been performed with positive and negative SI voltage, and negative SI voltage superimposed on negative direct voltage. The reason for the use of negative only direct voltage is due to the laboratory capabilities. The voltage level for the negative direct voltage is 16 kV, and the voltage range for the SI varies from about 168 kV to about 345 kV.

These tests were performed for both vertical and horizontal arrangements, and in dry and rain conditions too. Four different rain conductivities have been used in the test programme because these insulators can be exposed to different acid conductive rain types, typical of industrialized environments.

A comparison between the two tests (negative SI and negative superimposition) has been conducted to quantify the degradation of performance due to DC energisation when switching impulse is superimposed and explore whether an indicative [141], [142] switching surge factor (SSF) of 1.5 can be safely withstood. SSF is defined as the ratio between the maximum switching surge voltage and maximum operating pole to ground voltage of the power system [143].

An analysis of the time to flashover with respect to the flashover voltage has also been performed to determine the possible relationship with the superimposition test. This analysis of the time to flashover is essential to HVDC systems control engineers to accurately simulate the instant of fault caused by switching surges.

It was possible to conclude that, in most cases, the direct voltage pre-energisation has a negative impact on the flashover performance. The increase in rain conductivity leads to lower flashover values, and the horizontal orientation outperforms the vertical configuration. Under these test conditions, the flashover voltages were all larger than a typical DC operational switching surge. Thus, in the case of pole to ground fault, the healthy pole failure risk appears to be small. However, further research is needed on higher voltages and polluted conditions.

This work will be of interest primarily to outdoor insulator technical experts and Standard Tests developers, HVDC protection engineers and scientists and, secondarily, to Transmission System Operators (TSOs).

## 4.2. Background on HVDC insulator flashover under switching impulse superimposed on direct voltage

A number of papers have been published on the characterization of outdoor insulation under HVDC, as reviewed in [2], [4], and under lightning impulse superimposed on direct voltage [144]. However, to the author's knowledge, only Cortina's paper [145] and Watanabe's paper [146] describe the superimposition energisation, which is carried out in this work. Cortina *et al.* [145] used a fixed amount of Salt Deposit Density (SDD), using rain on substation post insulators, glass cap-and-pin and composite long rod suspension insulators. Watanabe [146] investigated non-composite insulators under the dry condition only.

Despite the consistent deployment of DC outdoor insulation in industrial environments characterized by acid conductive precipitation [2], such as eastern North America, Europe and eastern China [147], the dependence of flashover on rain conductivity has not been adequately studied under SI, and SI superimposed on direct voltage. This chapter investigates this aspect through the measurement of flashover performance of composite insulators when rain is applied at different conductivities. The conductivities have been chosen from a critical range of the conductivities investigated by Fujimura *et al.* [148], as shown in Fig. 4.2. For comparison purposes, the dry condition has been investigated too.

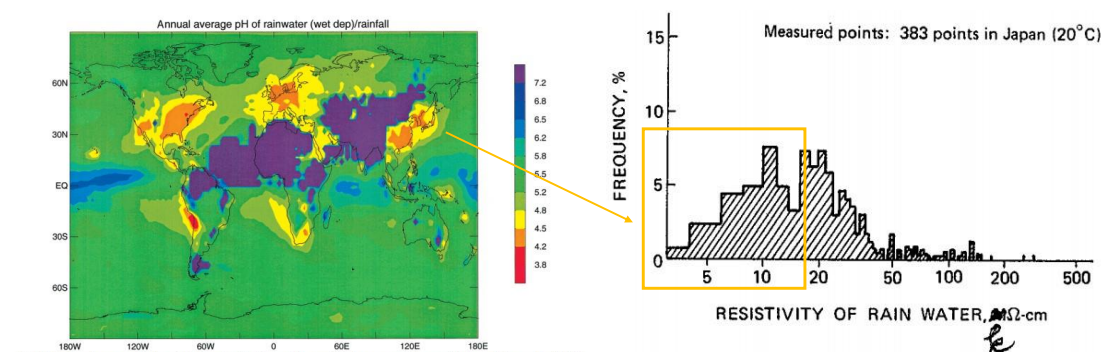


Fig. 4.2. Rain pH world map [147], and Japan's rain conductivity by frequency [148].

This voltage superimposition may cause an arc alongside the insulator, which should be avoided by the DC insulation coordination [8]. The flashover may occur in the case of substation vertical post insulators, overhead line horizontal tension, post, and cross-arm insulators. It may also occur alongside suspension line insulators if they are sufficiently short.

It is worth noting that Liao *et al.* [149] show results regarding the SI superimposition on DC voltage, but they consider the electric arc to occur across a uniform air medium (clear, open-air), not alongside the insulator. This assumption is valid for traditional high voltage towers equipped with suspension insulation. However, as stated in the examples above, there are cases where this hypothesis is not valid anymore.

### 4.3. Experimental Setup

The laboratory layout (Fig. 4.3), components and test specifications are described in this section. Two laboratory test arrangements were used in this programme, depending on the presence of the DC power supply (Fig. 4.4). For both arrangements, the rain tank and the rain nozzles have been employed at different water conductivities. In addition, the dry condition has been investigated.

Fig. 4.5 shows the vertical and horizontal test configurations of the test insulators as used in this work. The vertical arrangement was achieved by hanging the insulator from the metallic structure with a thick copper strip conductor. The horizontal arrangement was achieved fixing the insulator to the side of the metallic structure. The shortest distance between the high voltage energized rod and ground is set to be across the insulator, not across any other air gap. This is done to reproduce the electrical behaviour of line tension, post and cross-arm insulators, and substation post insulators. The tested composite insulator is described in Fig. 4.6 and TABLE 4.1.

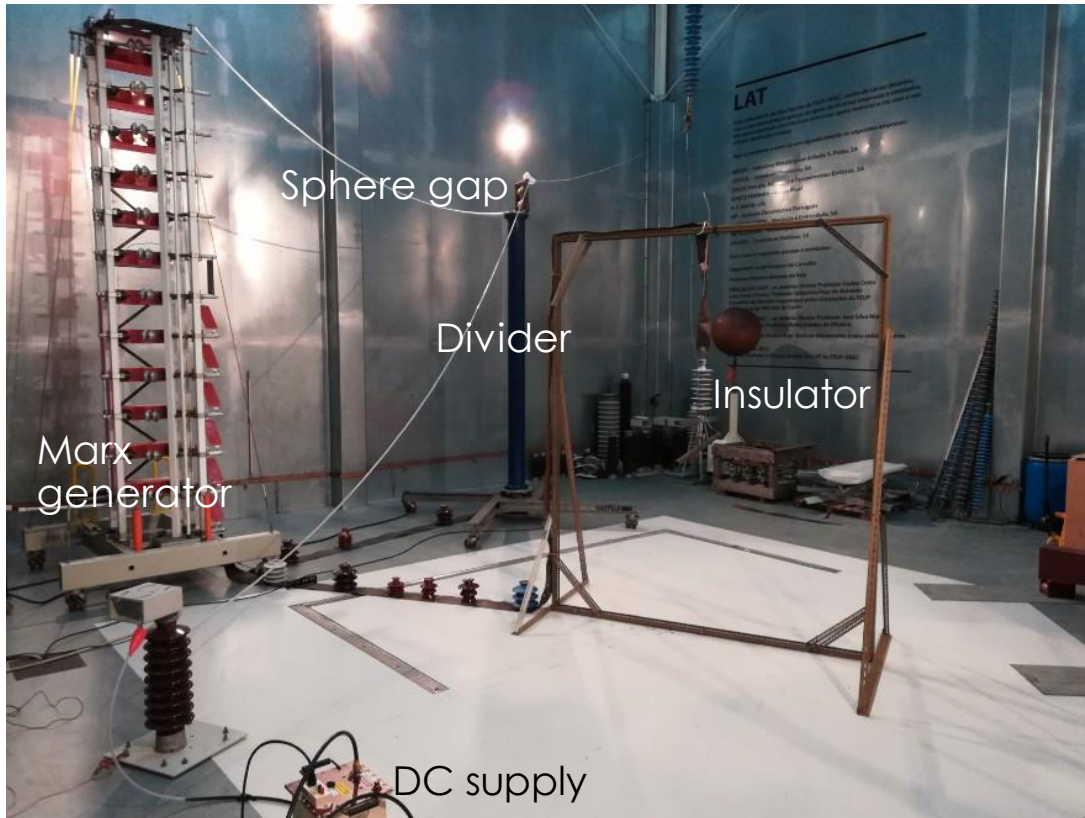


Fig. 4.3. Laboratory test setup for switching impulse superimposition on direct voltage.

To supply the high voltage waveshapes, the following equipment has been used: a Phenix 120 kV DC Hipot test set and 6 stages of a 12-stage Haefely SGS impulse voltage generator. To protect the DC source from the switching impulse, a 120M $\Omega$  water resistor has been used. This resistor is made of a polyvinyl chloride (PVC) tube filled with distilled water. This allowed the DC source to stay part of the circuit during the switching impulse. To isolate the voltage divider from the DC source, a sphere gap was employed, with spheres of 125 mm diameter and separated by a gap of 25 mm.

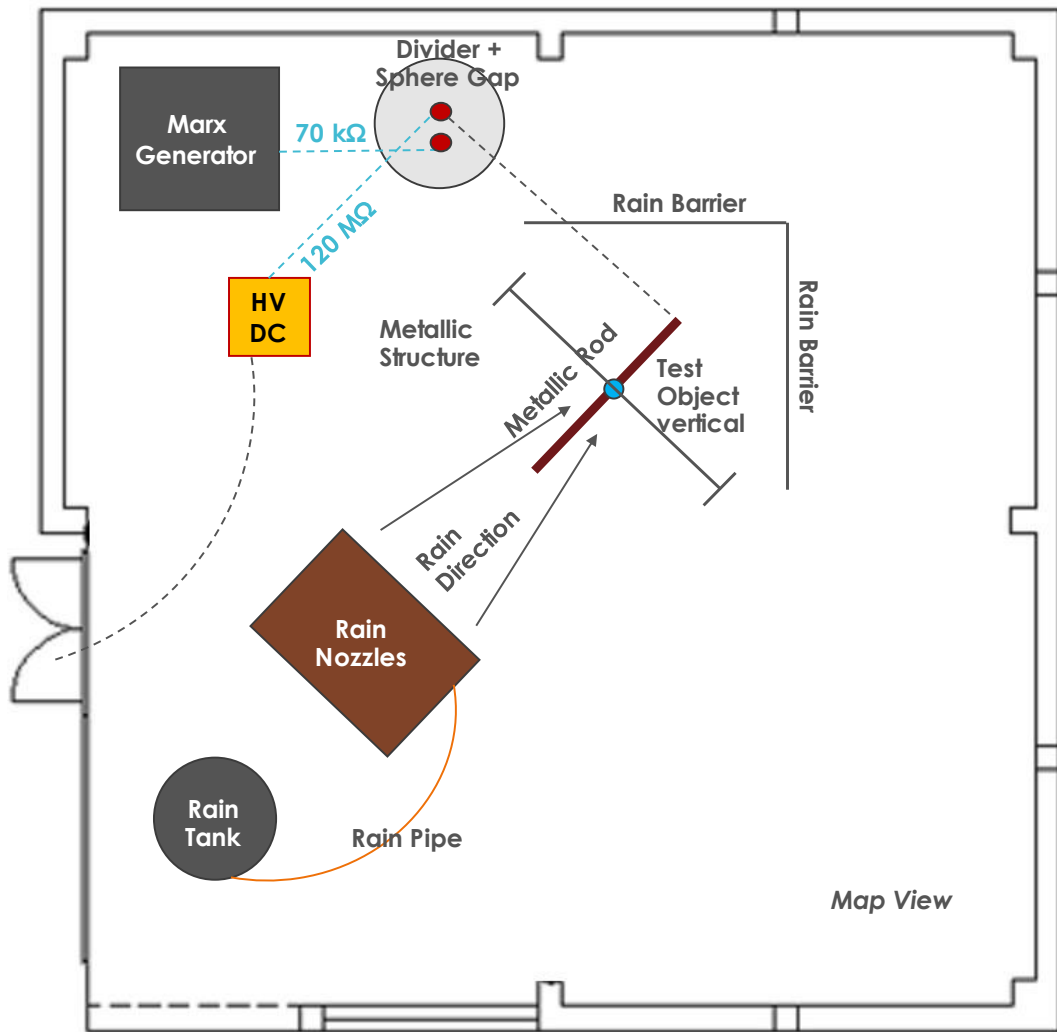
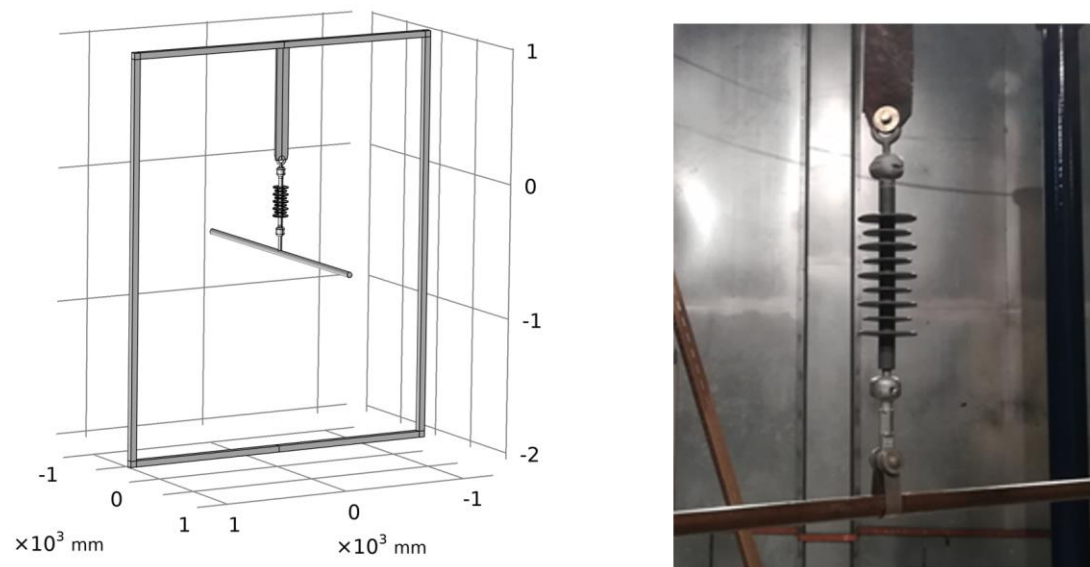
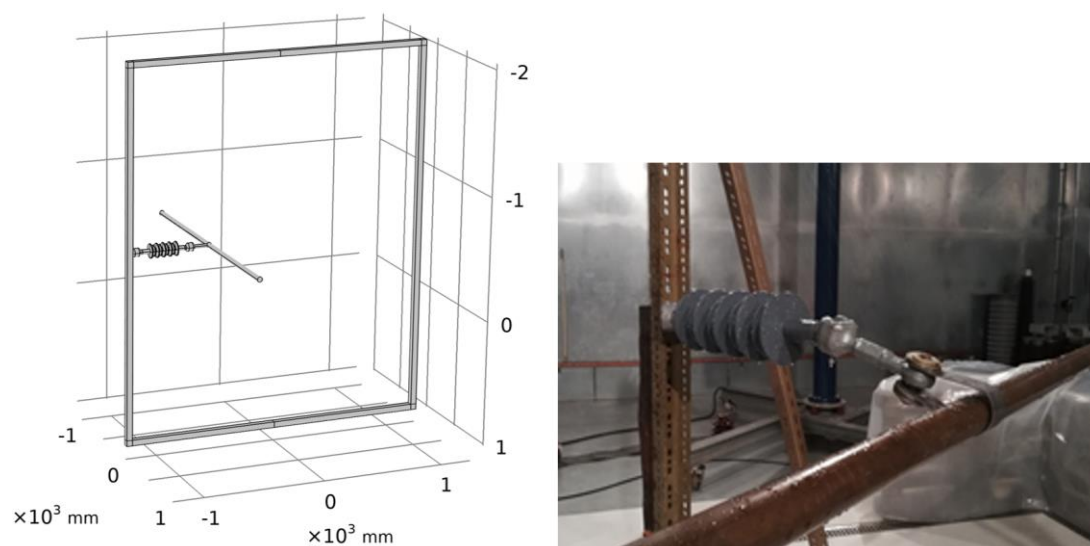


Fig. 4.4. Map view of laboratory setup for voltage superimposition.

The various tests carried out in this work are presented in TABLE 4.2, and TABLE 4.3, which show the requirements set by BS EN 60060-1:2010 Standard [150]. As can be seen in TABLE 4.2 and TABLE 4.3, the interval ranges and values applied in our tests are more demanding than required, whenever possible.



(a) Vertical test configuration



(b) Horizontal test configuration

Fig. 4.5. Vertical and horizontal arrangement of the insulator.

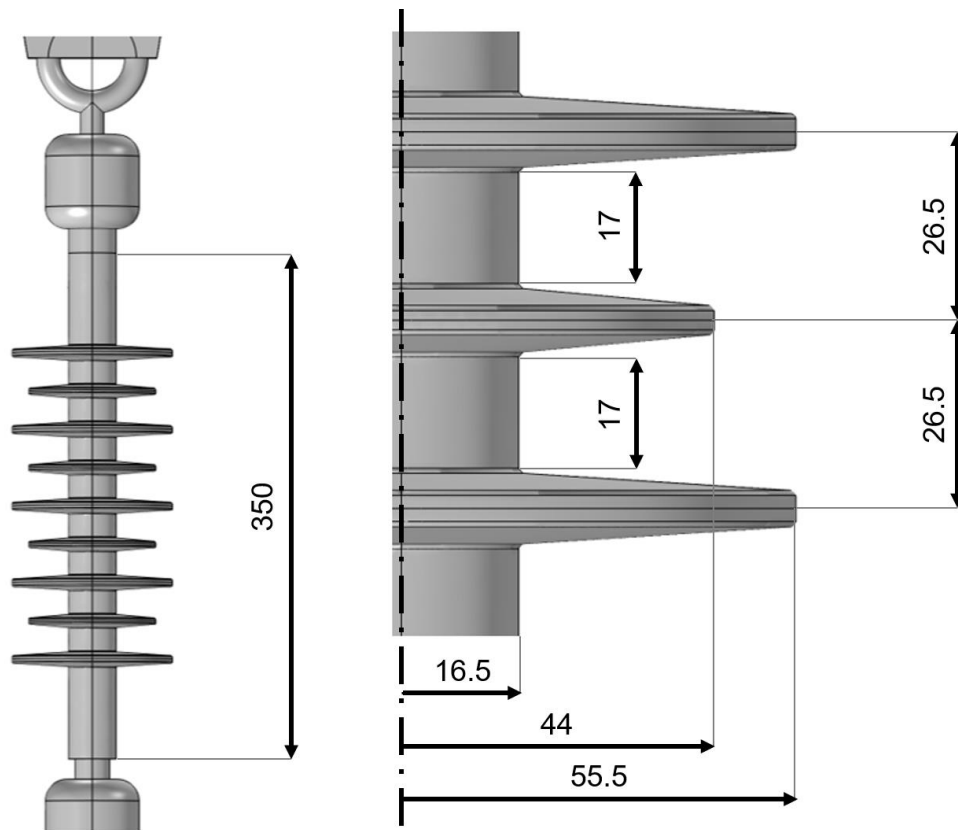


Fig. 4.6. Tested insulator. All units in millimetres.

TABLE 4.1. Test Insulator Dimensions.

$AD$ (mm)	$CD$ (mm)	$CF$	Material of	
			Core	Umbrella
350	1047	3.0	Fibre glass	SiR <sup>a</sup> and EPDM <sup>a</sup> mix

Where  $AD$  is the arcing distance,  $CD$  is the creepage distance,  $CF$  is the creepage factor, <sup>a</sup>SiR is Silicone Rubber, EPDM is Ethylene Propylene Diene Monomer.

TABLE 4.2. Switching Impulse Test Parameters.

$t_p$ ( $\mu$ s)	$t_h$ ( $\mu$ s)	$\Delta U\%$	Impulses per group
Standard 250 $\pm$ 50	Standard 2500 $\pm$ 1500	Standard 1.5% - 3%	20
Applied 250 $\pm$ 10	Applied 2500 $\pm$ 50	Applied 2 %	

TABLE 4.3. Rain Test Data.

Rain rate (mm/min)	Application time (min)	Standard conductivity ( $\mu$ S/cm)	Applied Conductivities		
			( $\mu$ S/cm)	(k $\Omega$ ·cm)	
Vertical	$\geq 15$	100 $\pm$ 15	$\sigma_1$	96.2	10.4
1.5 $\pm$ 0.5			$\sigma_2$	160.8	6.2
Horizontal			$\sigma_3$	354	2.8
1.5 $\pm$ 0.5			$\sigma_4$	527	1.9

For both configurations, the rain orientation was kept constant in front of the grounded metallic structure, at about 45° with respect to the floor.

## 4.4. Methodology

### 4.4.1. The Rain Conductivity

As shown in TABLE 4.3, a conductivity of 96.2  $\mu$ S/cm has been applied as recommended by the standard [150]. However, many conductivities have been used to study the insulation performance in conductive rain conditions. One of the main molecules present in acid rain is sulphur dioxide [151]. However, using it to vary the test rain conductivity would affect the reliability of the test results because it would evaporate during the test [152]. Therefore, to reproduce

different conductivities, the following technique has been used: different combinations of distilled water, aquifer water, and NaCl have been employed.

The first conductivity has been obtained by using distilled water only; the second has been obtained by mixing distilled and tap water; the third is the laboratory aquifer water conductivity; and the fourth is the aquifer water conductivity when NaCl is dissolved in it. The quantities of the components have been adjusted in a way to obtain a uniform set of conductivities that would evenly describe the relationship between the flashover voltage and the conductivity of the wetting solution.

The choice of the conductivity interval has been inspired by a previous study [82], which investigated the AC flashover performance reduction due to an increase in rain conductivity. The study [82] had shown that, with respect to 71  $\mu\text{S}/\text{cm}$  (14  $\text{k}\Omega\cdot\text{cm}$ ), a significant decrease in flashover performance would appear when the solution conductivity is greater than 100  $\mu\text{S}/\text{cm}$  (below 10  $\text{k}\Omega\cdot\text{cm}$ ) and would be drastically reduced by 50% at 500  $\mu\text{S}/\text{cm}$  (2  $\text{k}\Omega\cdot\text{cm}$ ).

#### 4.4.2. Selection of Direct Voltage Magnitude

The direct voltage magnitude has been selected for the insulator under the hypothesis of high NSDD and ESDD on the field, both of 0.6  $\text{mg}/\text{cm}^2$ . From a previous paper [153] and Section 2.8.3, it is possible to derive (4.1) for the direct voltage calculation. The calculated direct voltage is a function of the insulator material, geometry and hypothetical installation environment:

$$U = \frac{CD}{B \cdot C_D \cdot C_a \cdot \left[ ESDD_{dc} \cdot K_C \cdot \left( \frac{NSDD_{dc}}{0.1} \right)^{\frac{0.106}{\alpha}} \cdot K_{CUR} \cdot K_D \cdot K_S \right]^\alpha} = 16 \text{ (kV)} \quad (4.1)$$

To calculate the direct voltage value, the calculation of the average diameter of the insulator [42] is needed and gives in this case 60.7 mm. For brevity, the explanation of all remaining parameters is not included and can be found in [153].

### 4.4.3. Flashover Voltage Measurement

The applied direct voltage and current were measured at the source, by the Phenix supply. To measure the voltage impulse, the Haefely damped capacitive impulse divider has been used. To measure both DC and switching impulse components, a mixed divider would be the best option. However, the damped capacitive impulse divider has proven to be sufficient to accurately measure the impulse transient, which was causing the flashovers. A detailed explanation is provided here.

Immediately before the impulse trigger, the voltage across the test object is equal to the direct voltage applied by the DC source minus a small voltage drop (3% of 16 kV) along the portion of the circuit that connects the DC source to the insulator. At this instant, the voltage divider measures 0V. After the trigger event, the sphere gap charges up to -70 kV in about 38  $\mu$ s and it breaks down at that voltage. Following the instant of sphere gap breakdown, the divider measures precisely the voltage across the insulator. Therefore, the voltage peak of a withstand case and the flashover voltage measured by the divider did not need to be added to the DC component value.

To verify that the peak of the voltage superimposition lies in an expected interval, a gap can be used at the specimen location, and multiple tests are performed. As the voltage superimposition remains the same for each test, the initially large gap distance is reduced. The interval in which the voltage peak lies is determined by two subsequent tests of opposite result, namely withstand and breakdown.

### 4.5. $U_{50}$ and $\sigma_{tf}$ % Calculation

According to [150], to calculate  $U_{50}$ , which is the prospective voltage value that has a 50% probability of producing a disruptive discharge on the test object, the up and down method has been followed for each case. All flashover or withstand voltages have been corrected according to the ambient pressure, humidity, and temperature. The  $U_{50}$  value has then been computed as shown in (4.2):

$$U_{50} = \frac{\sum_{i=1}^n U_i}{n} \quad (4.2)$$

where  $U_i$  is the flashover voltage or withstand peak voltage of each impulse and  $n$  is the number of impulses per case. In this work,  $n$  was 20 for every case.

The percent time to flashover standard deviation  $\sigma_{tf}\%$  has also been calculated, with respect to the switching impulse peak time, as shown in (4.3).

$$\sigma_{tf}\% = \frac{\sqrt{\frac{\sum_{j=1}^m [t_{f,j}(\mu s) - \bar{t}_f(\mu s)]^2}{m-1}}}{250(\mu s)} \cdot 100 \quad (4.3)$$

Where  $m$ , 10 statistically, is the number of flashovers per test case,  $t_{f,j}$  is the time to flashover of each impulse, and  $\bar{t}_f$  is the average time to flashover per test case.

#### 4.5.1. EMTP/ATP Simulation

An Electromagnetic Transient Program, EMTP/ATP, simulation has been carried out to analyse the transient characterized by the sphere gap breakdown and determine the voltage applied to the insulator. The calculation of the sphere gap and the insulator capacitances was performed in COMSOL Multiphysics®. This can be done by using a capacitance global probe, or a charge probe when the energised electrode is set at 1 V. The second method works based on the known relationship between charge  $Q$ , and capacitance  $C$  and voltage  $V$ ,  $Q=CV$ . It is good to use both methods to double check the results. The simulation circuit is shown in Fig. 4.7. TABLE 4.4 summarizes the parameters used for the circuit model.

Many current-variable resistance arc models are available in the literature [154]–[161]. As recommended in [162], the Toepler law [160] has been adopted, as (4.4) shows in TABLE 4.4.

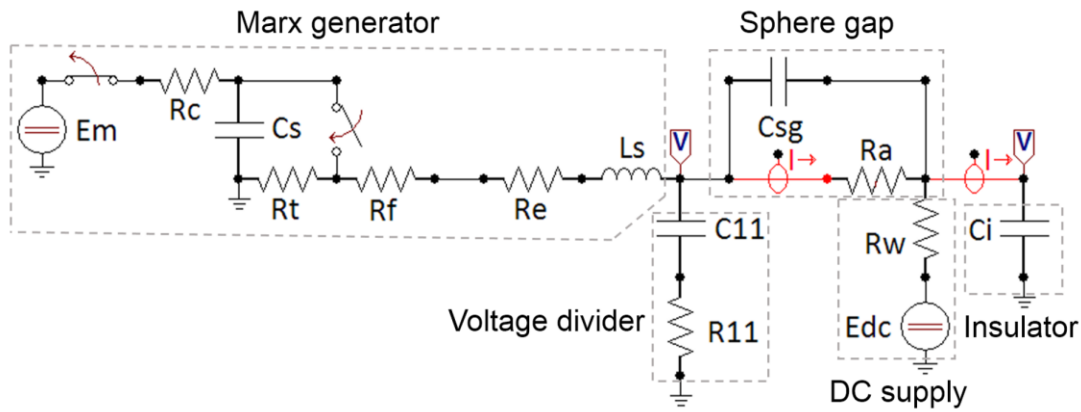


Fig. 4.7. EMTP/ATP circuit model of the experimental set-up.

TABLE 4.4. Full Description of the Circuit Model.

Elements	Description	Magnitude
$E_m$	Marx generator voltage	Variable V
$R_c$	Resistor for capacitor charging	8400·6 $\Omega$
$C_s$	Stage capacitor	0.6/6 $\mu\text{F}$
$R_t$	Impulse tail resistor	8400·6 $\Omega$
$R_f$	Impulse front resistor	20·6 $\Omega$
$R_e$	External water resistor	50 k $\Omega$
$L_s$	Inductance due to how stage is configured	2.5·6 $\mu\text{H}$
$C_{11}$	Voltage divider high voltage capacitor	1200 pF
$R_{11}$	Voltage divider high voltage resistor	100 $\Omega$
$C_{sg}$	Sphere gap capacitance - FEM calculated	0.325 pF
$R_a$	Current dependent arc resistance, by Toepler	(4.4)
$k_t$	Toepler formula constant	$0.5 \cdot 10^{-4}$ V·s/cm
$d$	Gap between spheres	2.5 cm
$R_w$	Protective water resistor, for DC supply	120 M $\Omega$
$E_{dc}$	Direct voltage	16 kV
$C_i$	Insulator capacitance - FEM calculated	0.877 pF

The resistance  $R(i(t))$  is expressed as

$$R(i(t)) = \frac{k_t \cdot d}{\int_0^t i(t) dt} (\Omega) \quad (4.4)$$

Fig. 4.8 provides a comparison between the circuit developed in this work and other two circuits from Cortina *et al.* [145], and Watanabe [146].

The three circuits have the same structure, composed of a Marx generator highlighted in orange, a sphere gap in black, an HVDC supply in green, and the test object in red.

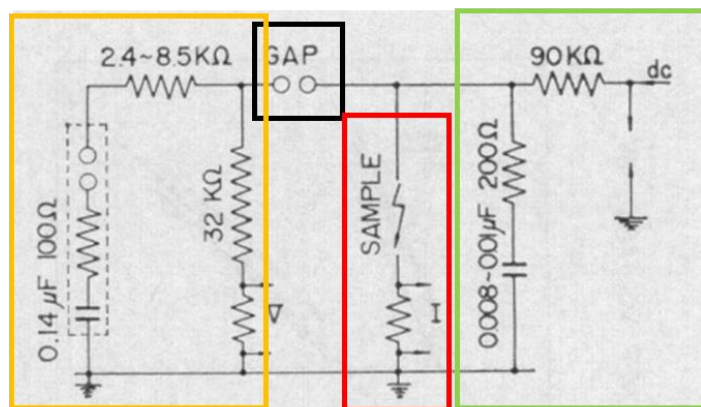
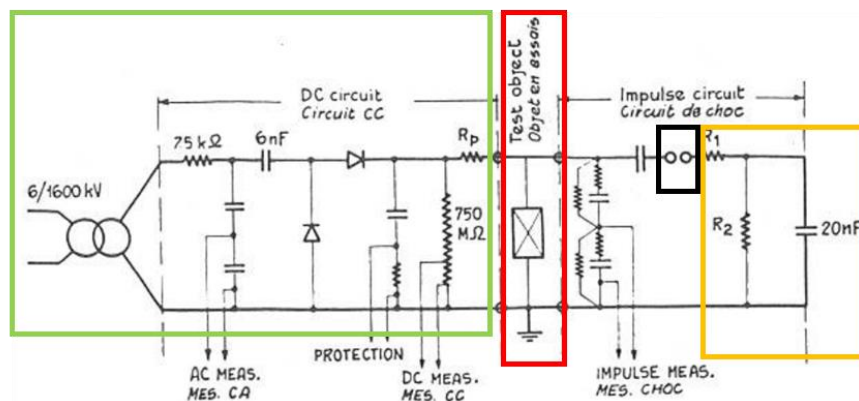
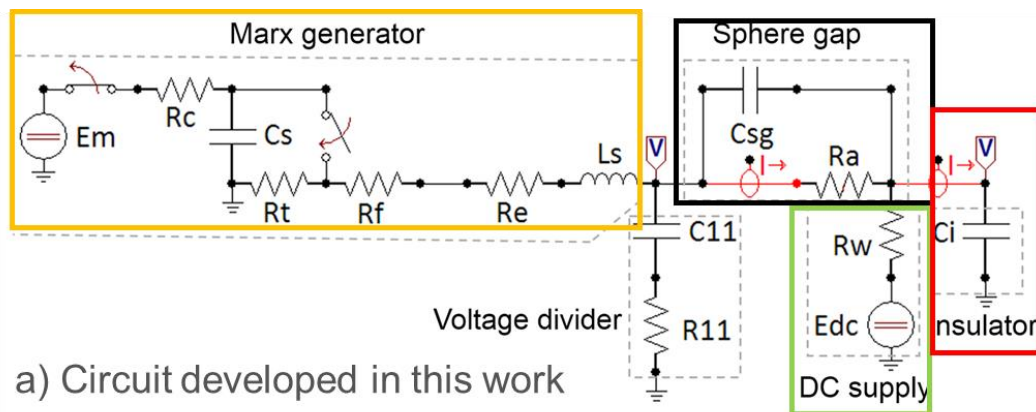


Fig. 4.8. Comparison of superimposition test circuits. a) Circuit developed in this work [122], b) Cortina *et al.* [145] and c) Watanabe [146].

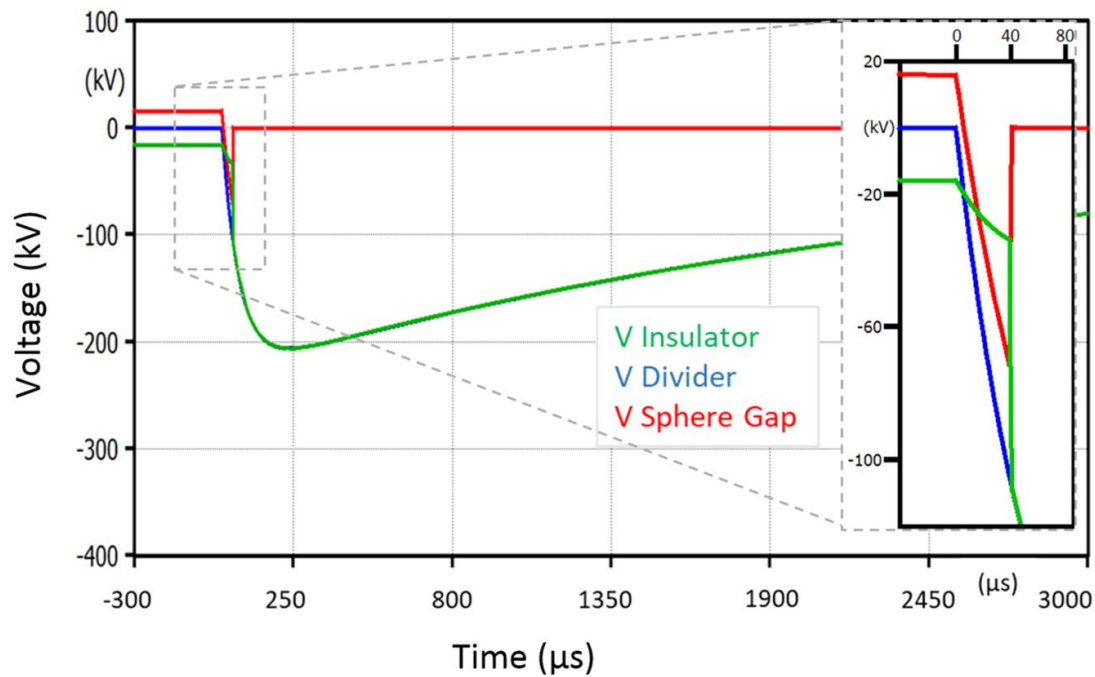
## 4.6. Results and Discussion

### 4.6.1. Measurement Versus Simulation of Divider Voltage

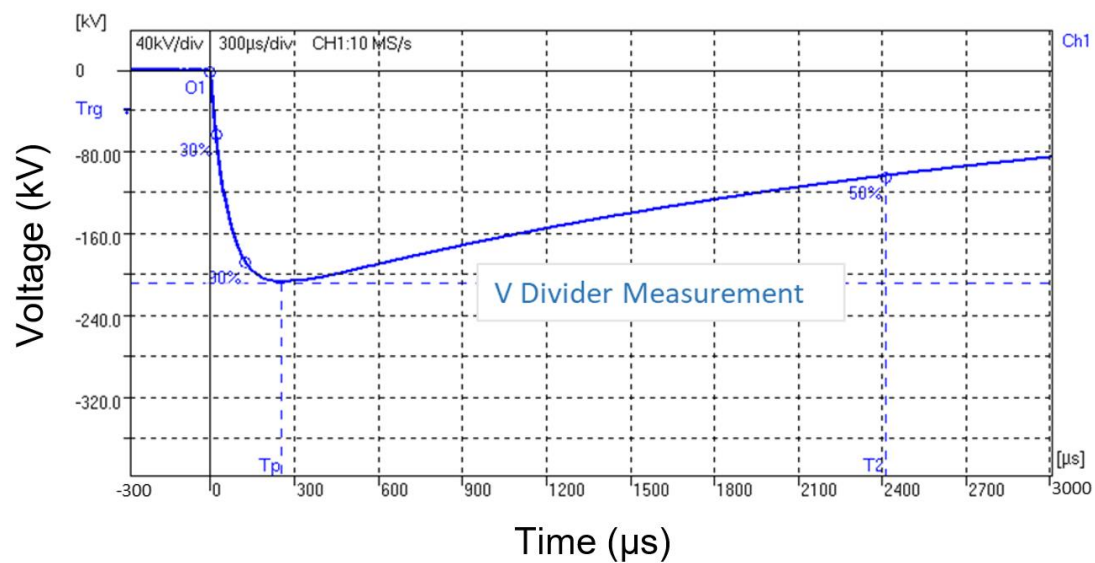
The EMTP/ATP simulation results show the applied voltage on the insulator in Fig. 4.9 (a) which allowed to observe the difference compared with the damped capacitive divider measurement shown in Fig. 4.9 (b).

The divider-measured voltage and the insulator actual voltage differ by the sphere gap voltage. As Fig. 4.9 shows, the sphere gap is DC charged positively, despite the negative DC voltage. When the impulse generator is triggered, the sphere gap behaves first as a capacitance charging negatively and, when it breaks down at -70 kV [163], it follows the Toepler law [160] as a variable resistance arc, in parallel with the gas stray capacitance. Therefore, the voltage applied across the insulator differs from the Marx generator switching impulse. In fact, at first, the insulator is charged more slowly than it should because the sphere gap is also being charged negatively by the impulse. Then, when the sphere gap voltage collapses, a relatively high capacitive current is applied to the insulator. This current is high relatively with the time window considered in Fig. 4.9 (a), and it causes a higher risk of puncture, compared to the risk of a slower switching impulse front.

The laboratory measurement agrees well with the simulation and confirms that the damped capacitive divider can measure a fast impulse voltage but cannot measure the DC component just before the start of the impulse. Thus, the flashover and withstand voltages detected by the divider did not need to be added to the DC component.



(a) EMTP/ATP simulation results



(b) Voltage divider measurement

Fig. 4.9. (a) EMTP/ATP simulation results for the switching impulse superimposed on DC energisation; (b) damped capacitive divider experimental measurement during the superimposition of the switching impulse and DC voltage obtained in the laboratory.

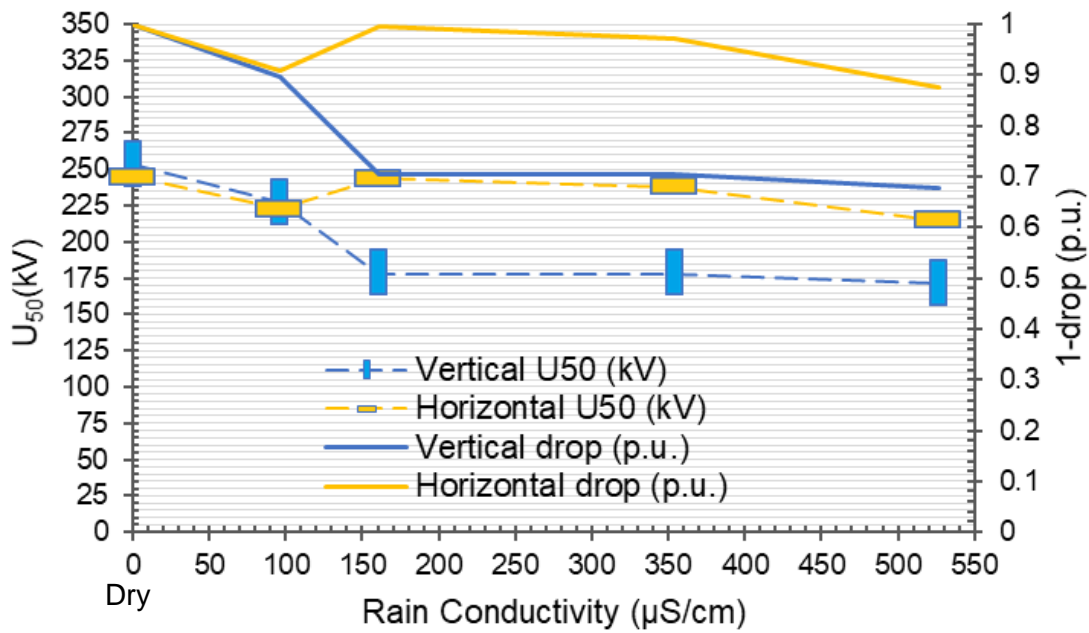
#### 4.6.2. Dry and Wet Flashover under Switching Impulse Superimposed on Direct Voltage

In this work, the test programme examined the performance of the outdoor insulator under different energisations, orientations and rain conductivities. Three groups of results are presented: (a) positive switching impulse, (b) negative switching impulse and (c) negative switching impulse superimposed on negative DC energisation. In addition to the wet tests, the dry condition has been included in the charts at 0  $\mu\text{S}/\text{cm}$ . To visualize the results from the point of view of the  $U_{50}$  drop with respect to the dry case, (4.5) has been used.

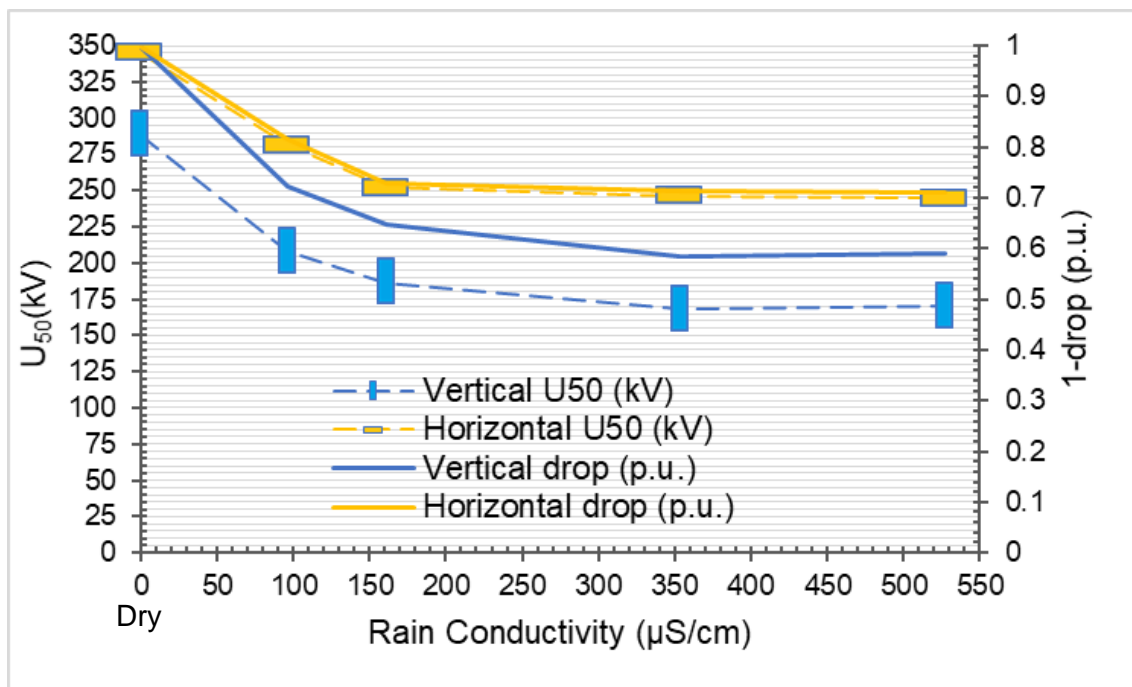
$$1 - drop = 1 - \frac{U_{50,dry} - U_{50,wet,i}}{U_{50,dry}} \text{ (p. u. )} \quad (4.5)$$

Fig. 4.10 (a), (b), and (c) show a decrease of performance when the rain is applied and when the conductivity is increased. This is true in every case with only one evident exception which is the positive horizontal flashover under the 96.2  $\mu\text{S}/\text{cm}$  rain. The test has been repeated to confirm this was not due to bad measurements. These results confirm the expected behaviour of decreased performance when the insulators surface is wet and becomes more conductive, facilitating the discharge inception and propagation until flashover.

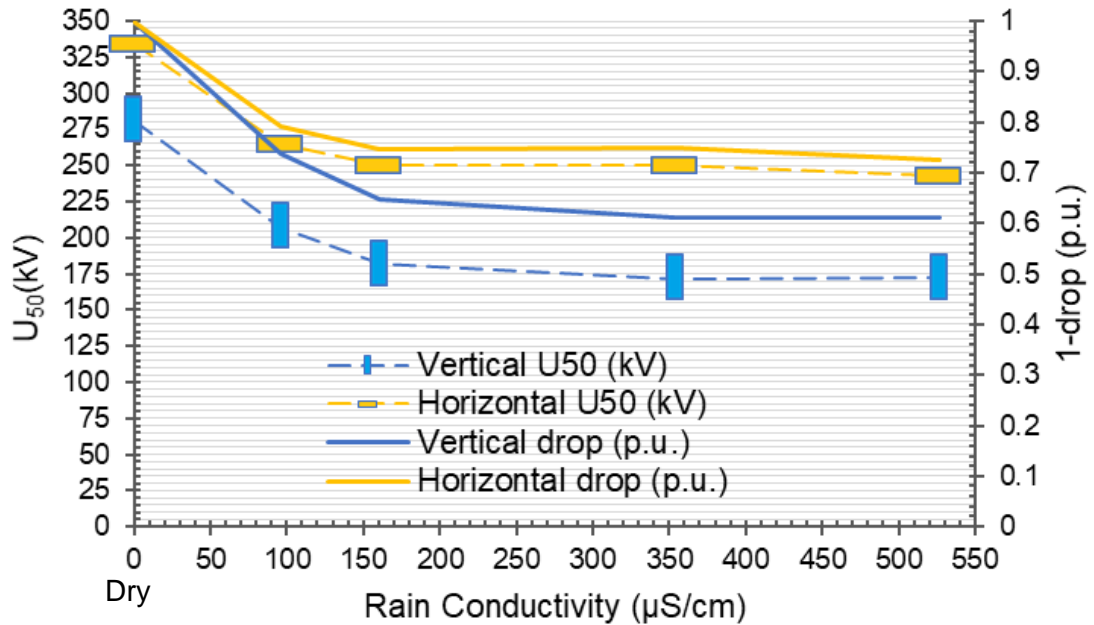
The insulator performance drops the most between the dry and the 96.2  $\mu\text{S}/\text{cm}$  rain conditions, when stressed with both the negative impulse with and without negative superimposed direct voltage. As can be seen in Fig. 4.10, beyond a rain conductivity of 160.8  $\mu\text{S}/\text{cm}$ , very little decrease of the flashover is measured. The positive SI flashover of the vertical orientation chart shows the largest drop in breakdown voltage between the lowest rain conductivity and the next conductivity. Whereas, for the horizontal case, the positive impulse chart shows a variable behaviour.



(a) Positive SI



(b) Negative SI



(c) Negative DC and negative SI

Fig. 4.10. On the left y-axis, the flashover voltage as a function of rain conductivity. On the right y-axis, the flashover drop, with respect to the dry condition, as a function of rain conductivity. Each chart includes the dry condition at 0  $\mu\text{S}/\text{cm}$ .

The minimum and thus most critical switching surge factor that the insulator is able to withstand is  $172 \text{ kV} / 16 \text{ kV} = 10.8$ , which is much larger than 1.5 [141]. Cortina *et al.* [145] have shown a minimum of  $1500 \text{ kV} / 300 \text{ kV} = 6$ . It follows that, in the absence of pollution accumulation, the arc span of the healthy pole insulators is not likely during the transient overvoltage due to pole to ground fault of a bipolar circuit, but the risk is higher [145] with increasing DC system voltage.

Fig. 4.10 (a) and (b) show that the positive SI is more severe in the dry case. However, the same does not occur for the wet conditions. In some cases, the negative SI has proven to be more severe than the positive polarity, and, in other cases, the difference is not evident. Thus, at these voltage levels, both positive and negative superimpositions need to be investigated. This chapter contributes to

the understanding of the phenomenon by investigating in detail the negative, as shown in Fig. 4.10 (c).

### 4.6.3. The Influence of Direct Voltage

To clarify the influence of the DC energisation application before the SI on the flashover voltage, the chart of Fig. 4.11 gives the percentage of the flashover voltage drop due to the DC energisation with respect to the DC voltage.

Compared with negative SI, the application of the negative DC pre-energisation causes the largest performance drop in the dry and in the horizontal lowest rain conductivity cases; particularly, the largest difference is found for the horizontal wet condition. In most cases, the direct voltage negatively affects the flashover performance, but with an unclear profile. Moreover, it needs to be noted that the DC is only 6.8% of the average impulse. A higher DC energisation may have caused a larger degradation of performance.

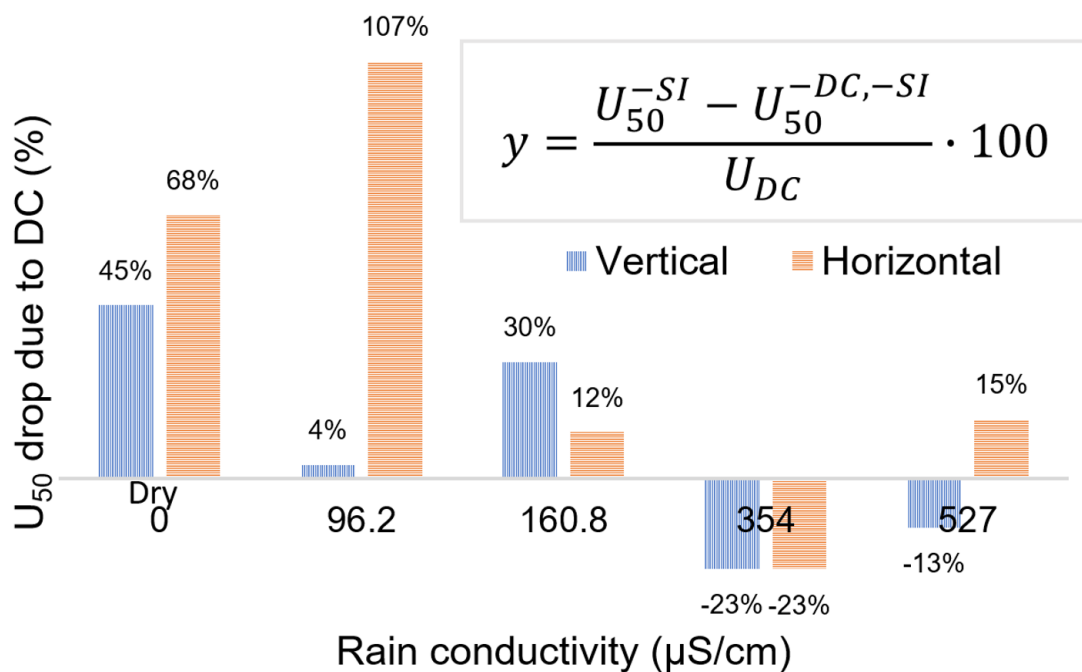


Fig. 4.11. The flashover voltage drop due to the DC energisation normalized to 16 kV, which is the applied direct voltage, as a function of rain conductivity.

#### **4.6.4. Effect of Insulator Orientation on Flashover Voltage**

The insulator shows a notably better performance when tested horizontally, except for the first two cases of positive switching impulse. The trend is attributed to the larger horizontal surface area and thus larger amount of deposited rain when the insulator is vertically oriented. Furthermore, because the elongation of water droplets during their free fall is oriented vertically, the creation of an arc path in the vertical orientation is facilitated. However, it was not obvious that the vertical arrangement would perform worse also in the dry case. A FEM model has been developed, whose mesh can be seen in Fig. 4.12. The calculation of the electric field magnitude along the creepage path of the two arrangements has been carried out, as shown in Fig. 4.13.

As can be seen, Fig. 4.13 indicates the maximum electric field magnitude is located on the edge of the ground electrode for both orientations. In the vertical orientation, the maximum value is larger than that of the horizontal arrangement because the ground electrodes are different.

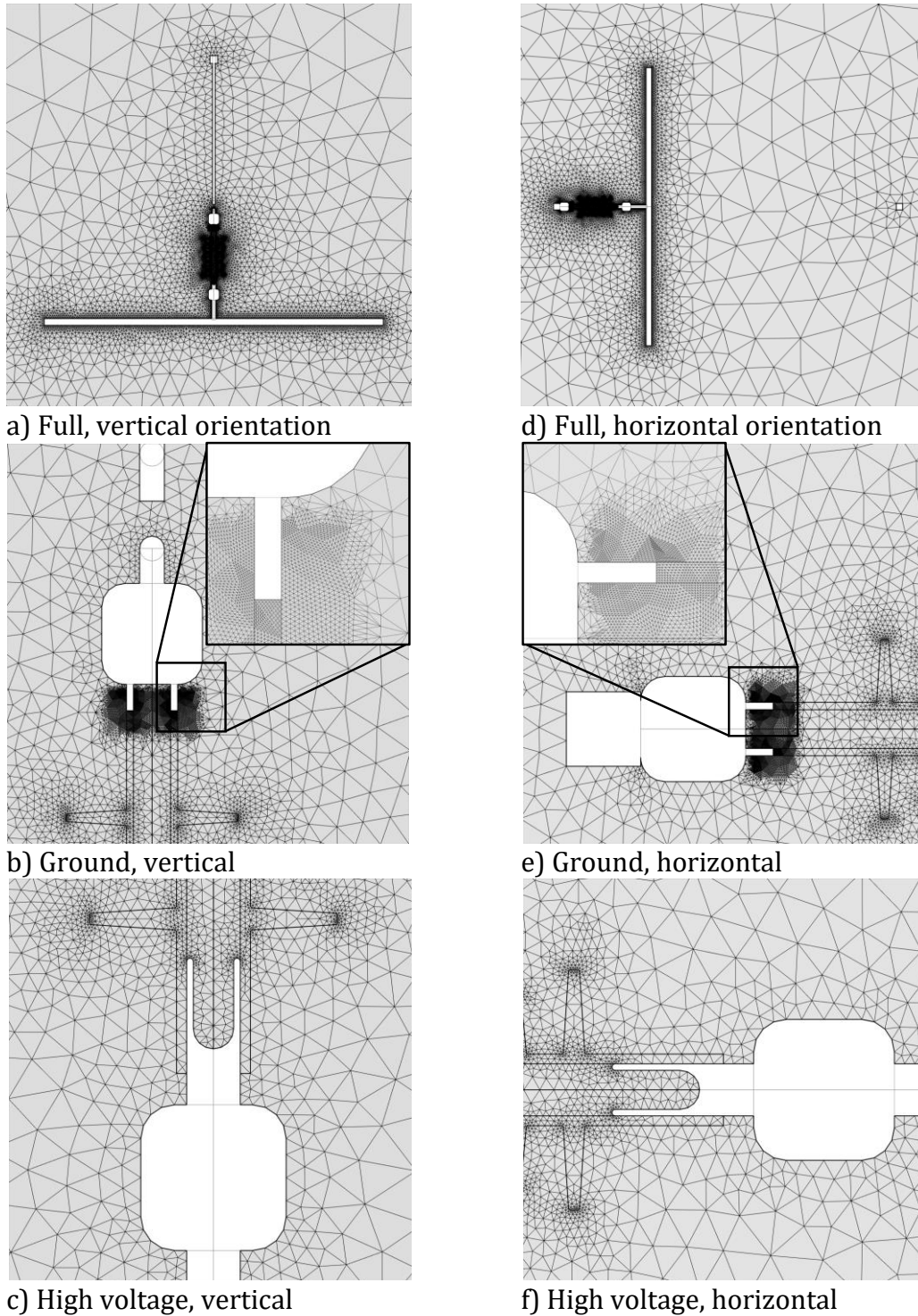


Fig. 4.12. a), b), c): mesh vertical section of vertical insulator model. d), e), f): mesh horizontal section of horizontal insulator model. The metal was not meshed because the electrostatic physics has been used to model the clean and dry insulator.

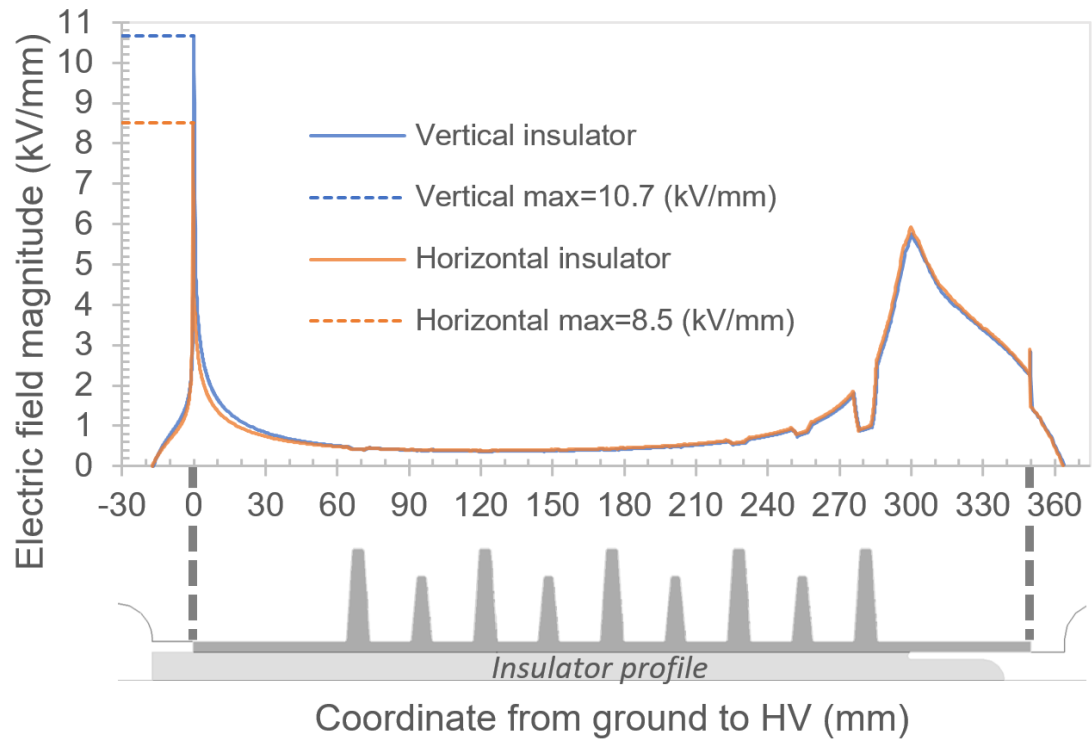
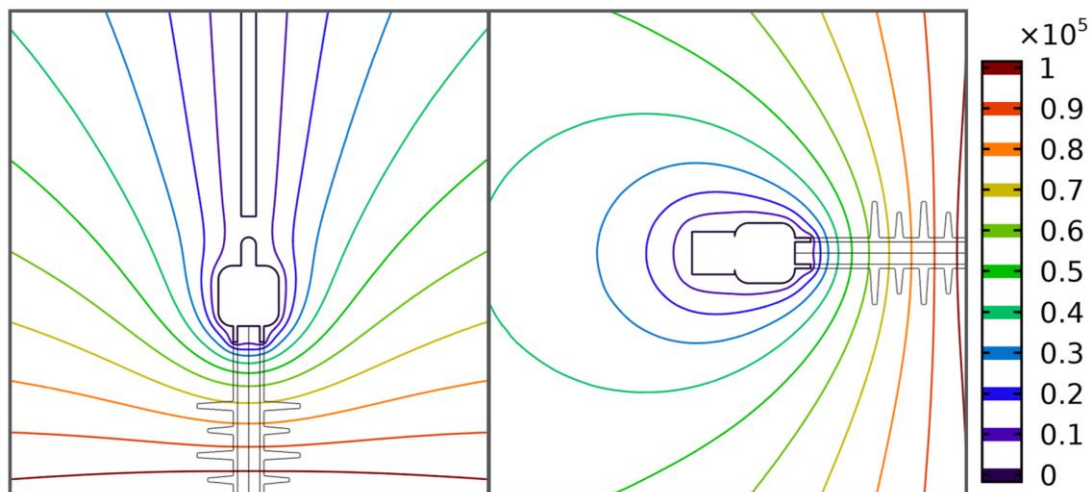


Fig. 4.13. Electric field magnitude along the creepage path of the insulator as a function of axis coordinate, in both orientations, with high voltage electrode at 288.230 kV.

In the vertical case, the copper strip conductor causes the equipotential lines to squeeze in the vicinity of the ground electrode, as shown in Fig. 4.14.

If the ground electrodes were the same, the flashover voltage would be expected to be the same in the dry case. However, as can be seen in Fig. 4.10, regardless of the electrode configuration, compared to the dry case, the wet vertical cases drop more than the horizontal cases.

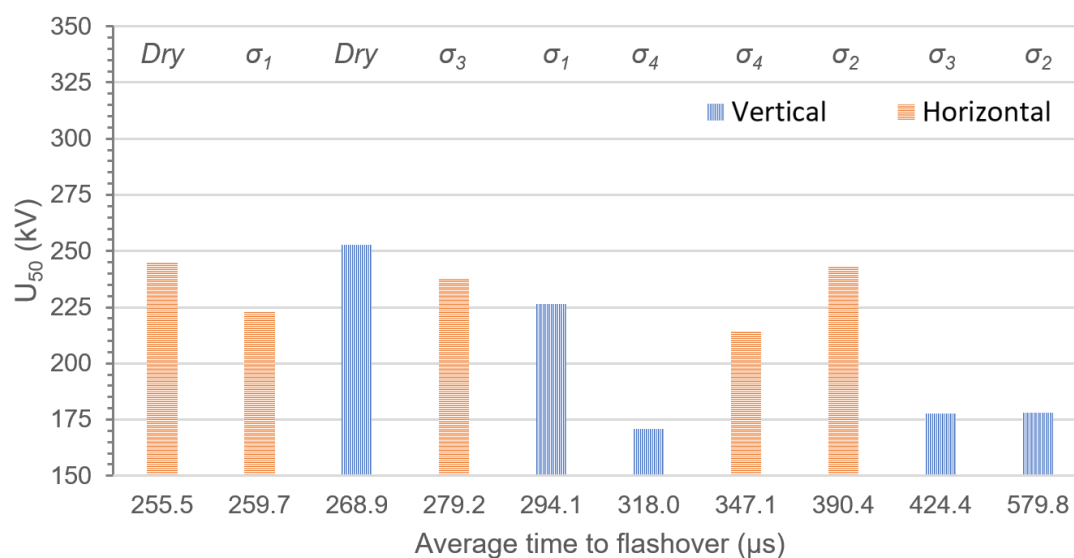


(a) Vertical arrangement. (b) Horizontal arrangement.

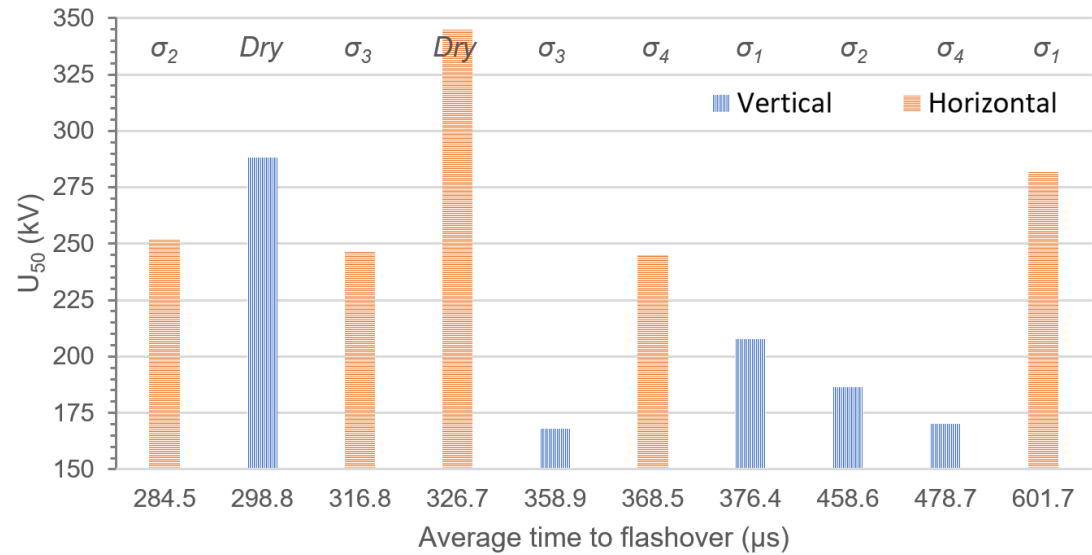
Fig. 4.14 Equipotential lines (V) in the vicinity of the ground electrode when the high voltage electrode is at 288 kV. Each section view has been obtained with a cutting plane, which is vertical for (a), and horizontal for (b).

#### 4.6.5. Time to Flashover

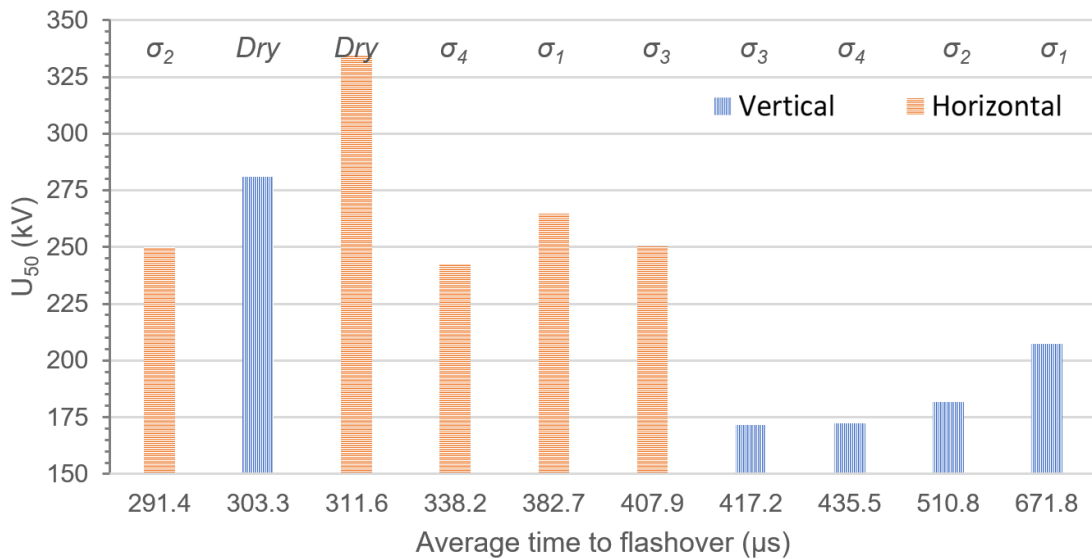
For the purpose of advancing protection control and power system fault simulations, Fig. 4.15 illustrates the time to flashover dependence on flashover voltage.



(a) Positive SI



(b) Negative SI



(c) Negative DC and negative SI

Fig. 4.15. Flashover voltage as a function of the average time to flashover. Each column is characterized at the top by its test condition. Legend of the rain conductivity  $\sigma$  is provided in TABLE 4.3. The bars with vertical lines show the results for the vertical arrangement, likewise, the bars with horizontal lines show the results for the horizontal arrangement.

The results show a trend of decreasing time to flashover with increasing flashover voltage, as expected. Therefore, the vertical orientation takes longer to

full breakdown. Moreover, the average of the insulator time to flashover increases in the presented order: positive impulse, negative impulse, negative impulse superimposed on negative DC. These results demonstrate that the protection and control are required to be faster when the impulse front voltage rate of change in time is large.

Also, if wet, the insulator takes more time to flashover. However, the DC energisation does not seem to cause any noticeable effect on the time to flashover.

TABLE 4.6, TABLE 4.7, and TABLE 4.8 show the percent standard deviation of each time to flashover as defined in (4.3), as well as the correspondent time to flashover  $t_f$  and flashover voltage  $U_{50}$ . No specific pattern has been identified.

The symbols used in the tables are explained in TABLE 4.5.

TABLE 4.5. Legend of symbols for orientation and conductivity.

Symbol	Orientation	Conductivity $\mu\text{S/cm}$
	Vertical	Dry
	Vertical	96.2
	Vertical	160.8
	Vertical	354
	Vertical	527
	Horizontal	Dry
	Horizontal	96.2
	Horizontal	160.8
	Horizontal	354
	Horizontal	527

By observing the average time to flashover of Fig. 4.15 and each associated standard deviation in TABLE 4.6, TABLE 4.7, and TABLE 4.8, it is possible to conclude that the vast majority of the individual times to flashover is greater than the SI peak time, namely 250  $\mu\text{s}$ .

TABLE 4.6. Time to Flashover Deviation, (+)SI.

Vertical				Horizontal			
Rain Conductivity ( $\mu\text{S}/\text{cm}$ )	$U_{50}$ kV	$t_f$ $\mu\text{s}$	$\sigma_{tf}$ %	$U_{50}$ kV	$t_f$ $\mu\text{s}$	$\sigma_{tf}$ %	
Dry	252.8	268.9	19%	244.9	255.5	35%	
96.2	226.6	294.1	18%	222.7	259.7	35%	
160.8	177.9	579.8	119%	243.5	390.4	264%	
354	177.8	424.4	56%	238.0	279.2	22%	
527	171.0	318.0	32%	214.6	347.1	47%	

TABLE 4.7. Time to Flashover Deviation, (-)SI.

Vertical				Horizontal			
Rain Conductivity ( $\mu\text{S}/\text{cm}$ )	$U_{50}$ kV	$t_f$ $\mu\text{s}$	$\sigma_{tf}$ %	$U_{50}$ kV	$t_f$ $\mu\text{s}$	$\sigma_{tf}$ %	
Dry	288.2	298.8	43%	345.1	326.7	26%	
96.2	207.8	376.4	37%	281.7	601.7	84%	
160.8	186.5	458.6	53%	251.9	284.5	22%	
354	168.1	358.9	38%	246.4	316.8	24%	
527	170.2	478.7	59%	244.9	368.5	35%	

TABLE 4.8. Time to Flashover Deviation, (-)DC and (-)SI.

Vertical				Horizontal			
Rain Conductivity ( $\mu\text{S}/\text{cm}$ )	$U_{50}$ kV	$t_f$ $\mu\text{s}$	$\sigma_{tf}$ %	$U_{50}$ kV	$t_f$ $\mu\text{s}$	$\sigma_{tf}$ %	
Dry	281.1	303.3	34%	334.3	311.6	33%	
96.2	207.3	671.8	236%	264.6	382.7	17%	
160.8	181.7	510.8	37%	249.9	291.4	18%	
354	171.8	417.2	62%	250.1	407.9	79%	
527	172.2	435.5	61%	242.4	338.2	42%	

#### 4.6.6. Flashover voltage in relation to insulator length

Evidence from other research shows similar trends at higher voltages for longer insulators. Specifically, under the dry condition [145], [146], the flashover voltage of the negative superimposition is smaller, and thus more severe, than the flashover voltage of the negative SI alone. Similarly, from the data provided by [145], the same trend can be identified for the wet condition.

The comparison of the available data provided by [145], [146], and the results obtained in this work as presented in this chapter should be treated with caution. In fact, the studies are performed on insulators of different profiles, materials, and electrode configurations. Moreover, in these studies, the direct voltage of each insulator length has not been selected with the same method. Results of [145], [146] are reproduced in Fig. 4.16, Fig. 4.17, and Fig. 4.18 for completeness.

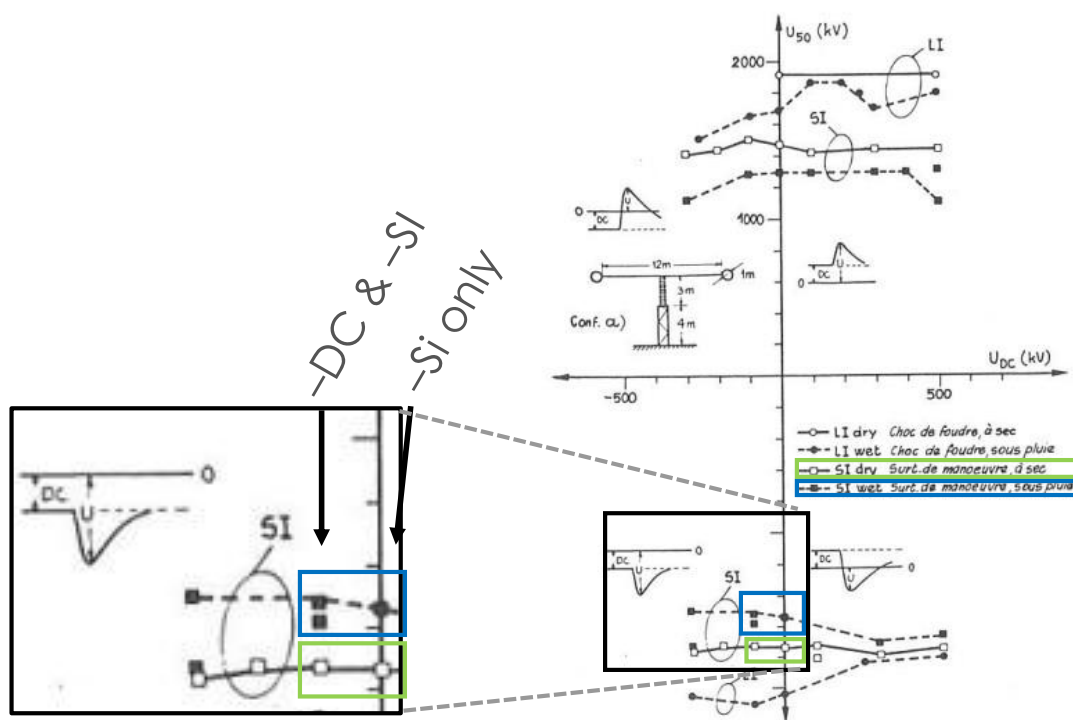


Fig. 4.16. Cortina *et al.* [145] results on superimposition with zoom on negative direct voltage and negative switching impulse. Post insulator.

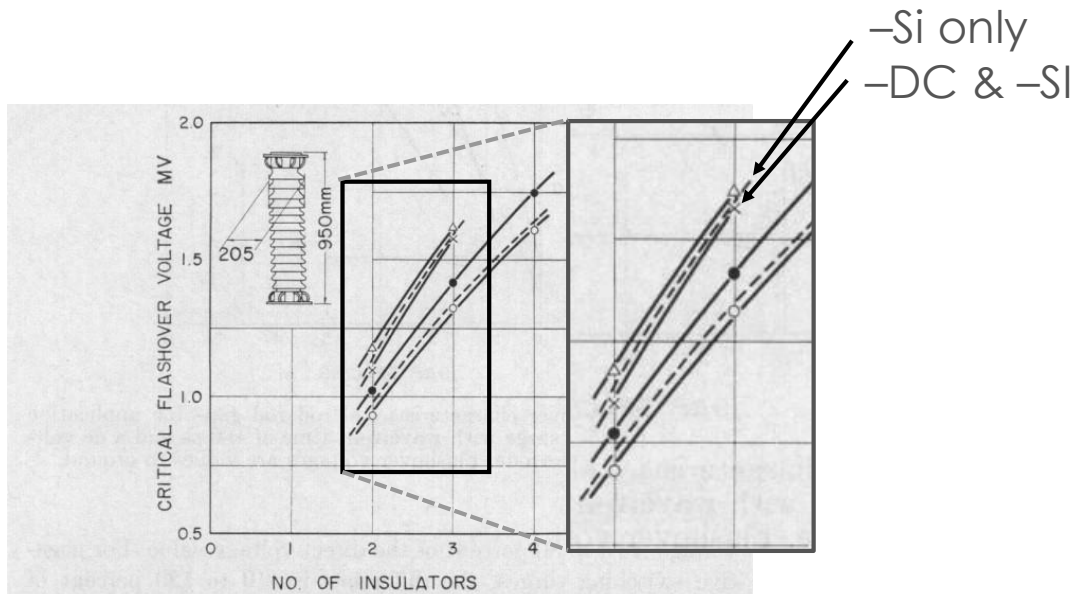


Fig. 13. Flashover characteristics of 205- by 950-mm cylindrical-post insulator stacks for application of a switching surge with wavefront time of  $180 \mu\text{s}$  and a dc voltage to the same electrode.

Fig. 4.17. Watanabe [146] results 1 on superimposition. Post insulator.

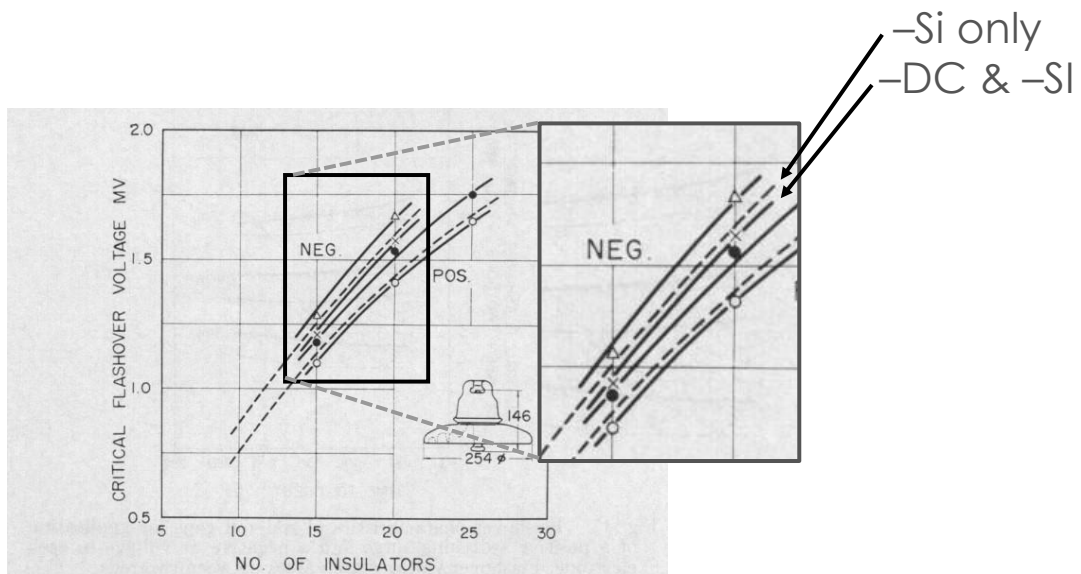


Fig. 11. Flashover characteristics of 254- by 146-mm suspension insulator strings for application of a switching surge with wavefront time of  $180 \mu\text{s}$  and a dc voltage to the same electrode.

Fig. 4.18. Watanabe [146] results 2 on superimposition. Cap and pin insulator string.

The results provided by the referenced literature show a similar trend to the results obtained in this work. Fig. 4.19 and Fig. 4.20 focus on the three cases

which have been affected the most by direct voltage presence. These cases are the dry horizontal, the dry vertical, and the 96.2  $\mu\text{S}/\text{cm}$  rain horizontal cases.

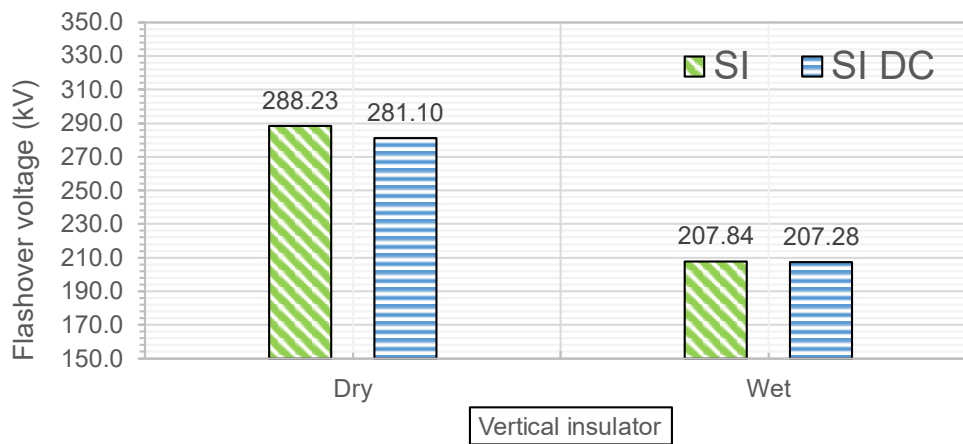


Fig. 4.19. Comparison of (-) SI and (-) SI superimposed on (-) DC performance. Vertical insulator.

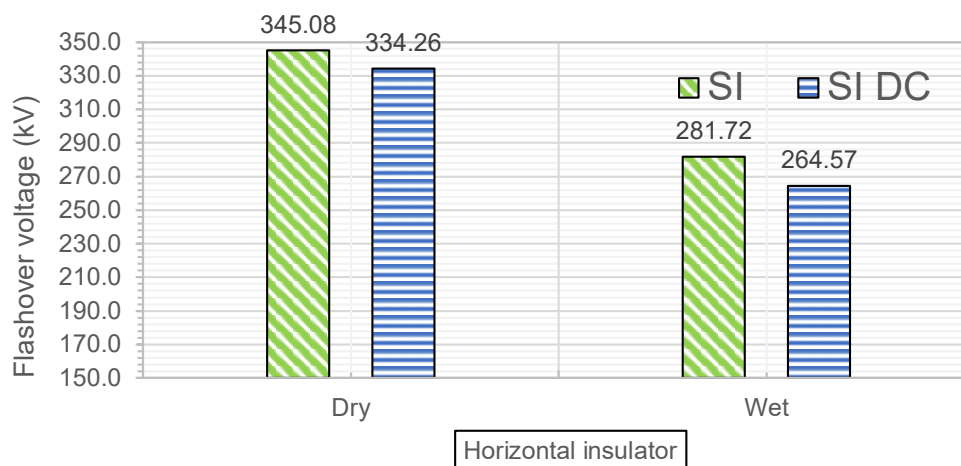


Fig. 4.20. Comparison of (-) SI and (-) SI superimposed on (-) DC performance. Horizontal insulator.

Fig. 4.19, and Fig. 4.20 indicate a decrease in performance when the switching impulse is superimposed on direct voltage, compared to the application of switching impulse only.

## 4.7. Conclusions

New test data has been obtained for insulators tested under different configurations and with different surface conditions.

This chapter has quantified experimentally the difference between the superimposition of a negative SI on a negative DC energisation and a negative SI. Furthermore, it has assessed how rain and its conductivity value reduce the flashover performance of an outdoor composite insulator.

In most cases, the application of a negative SI superimposed on a negative direct voltage has been proven to affect the performance of the insulator more severely compared with the same negative SI on its own. In particular, the three cases which have been affected the most by direct voltage presence are the dry horizontal, the dry vertical, and the  $96.2 \mu\text{S}/\text{cm}$  rain horizontal cases.

However, the test object has always withstood switching impulses with peak values much greater than 1.5 times the applied direct voltage. Thus, at the studied voltage levels and in the absence of accumulated pollution, it is suggested that this type of flashover is not likely to happen in operation. To verify the same conclusion for pollution application and the positive superimposition, further investigations are needed. It is stressed here as a caveat that 16 kV is not the voltage level usually selected for OHL bulk transmission, which is usually in the range of hundreds of kV. However, examples of OHL transmission of tens of MWs at about 30 kV exist, such as the ANGLE DC project [164].

In almost all cases, the horizontal orientation has proven to perform better than the vertical. Also, when wet, the horizontally oriented insulator has shown a performance drop ratio smaller than in the vertical configuration, with respect to the dry case.

It has been confirmed that the time to flashover shortens with increasing flashover voltage, but negligible role seems to be played by the direct voltage pre-energisation.



# Chapter 5. HVDC conversion of UK existing overhead lines for power uprating: 12 proposals for extreme and heavy pollution

## 5.1. Introduction

The electrification of transportation and household heating requires the increase in electric power generation, which is growingly provided by renewable resources, and the development and innovation of the onshore transmission system in order to safely and reliably transmit increased power flows from the bulk generation to the consumption areas.

Converting existing overhead lines to HVDC is one way to uprate the onshore power transmission system. In the UK, assessment and planning of the HVDC bulk generation of offshore wind power are ongoing. This chapter suggests that it could be advantageous to plan the construction locations of HVDC/AC converter stations more inland, rather than on the coast. This would allow to convert existing AC lines to DC, and to directly connect them to the offshore HVDC cabling, without the need for additional converter stations.

This chapter puts forward proposals to uprate the power transfer capability of three existing UK electricity towers by determining the safe maximum direct voltage they can transmit with newly dimensioned insulators. The three transmission towers considered are the L6 tower, the L2 tower, and the L7 tower. The first two towers make up 85% of the UK transmission overhead line system.

It is known from CIGRE TB 583 [140], that HVDC outdoor insulation coordination is mainly done with respect to the pollution accumulation, and secondarily, clearance distances are calculated based on the expected HVDC system overvoltages.

The conversion is done for two different pollution scenarios. The first is NSDD=ESDD=0.6 mg/cm<sup>2</sup>, the second is NSDD=ESDD=0.2 mg/cm<sup>2</sup>, which are here respectively defined as extreme and heavy pollution degrees. The choice of these values is made to consider critical conditions which are unlikely (extreme pollution) or possible but still unlikely (heavy pollution) to occur in service, as observed in TABLE 2.5 in section 2.7.2 and in TABLE 2.23 in section 2.17.1.

High values are assumed because of the electrostatic attraction of the pollution towards the charged insulators. The UK wind speeds are quite high, which would suggest a similar pollution deposition between AC and DC insulators. However, low wind speed areas may exist along the lines and cause local large DC pollution accumulation relative to AC. That is why extreme and heavy contamination levels are considered.

The power of the converted line would increase by a factor of 1.6 to 2.9, depending on the specific solution. FEM models confirm that corona rings may not be needed at a leakage current level that is likely to be easily exceeded in the field.

#### **5.1.1. Magnetic and electric field requirements**

DC lines magnetic fields are in the order of magnitude of the earth's magnetic field, and restrictions are set at values which are several order of magnitude higher than these [165].

The electric fields and currents caused inside the human body by DC lines electric fields do not cause biological effects, thus, no limits were set by ICNIRP [140].

#### **5.1.2. Overview of other constraints**

This chapter focuses on the outdoor insulation selection and dimensioning under extreme and heavy pollution, and the verification of the electric field limit requirements on the insulators. However, the engineering challenges associated with the conversion of an existing HVAC OHL to HVDC are multiple and the following are not covered in this chapter. These challenges include the assessment of corona on specific and complete ground and high voltage electrodes, the assessment of audible noise and radio interference [140]. At the system level, the challenges to address include substation design, converter

design, insulation coordination, control and protection, grid code reactive power support requirements, grid studies, capital and operating expenditure (CAPEX and OPEX) estimations, environmental impact of larger substation footprint (not needed for Right of Way, which is already in place), land permissions, and community engagement.

## 5.2. Methodology for the conversion

As introduced, the conversion is performed first by selecting and dimensioning the insulators, as explained in Section 2.8.3, based on the assumed pollution level. Secondly, the clearance distances between the high voltage conductors and the live parts of the tower are verified, based on an assumed Switching Surge Factor (SSF). The SSF is the ratio between the maximum system overvoltage and the nominal operational DC system voltage.

The axisymmetric FEM modelling of the most critically energised insulators is done for each tower type. Each case is modelled ideally, with a non-realistic conductivity layer of  $10^{-14}$  S/m, and with a conductivity which is large enough to satisfy the electric field requirements introduced and set in TABLE 2.1 from sources [9], [10]. This is done, as opposed to design corona rings, because of the conclusions achieved by Pignini *et al.* [8] on the non-necessity of DC corona rings due to the conductive layer dominant influence on the voltage distribution. The results of this chapter confirm conclusions by Pignini *et al.* [8] are correct, thus, results are focused on the determination of the minimum current (or conductivity and thickness) which satisfies the electric field requirements .

### 5.2.1. Insulator selection and dimensioning

For the conversion, the selected profile is the composite outdoor insulator profile studied at China Electric Power Research Institute, which is used in the field for Chinese HVDC lines (Fig. 2.12). This insulator is in line with the selection recommendations of CIGRE TB 518 [4], presented in section 2.8.3.

The insulator Arcing Distance (AD) is the ratio of the Creepage Distance (CD) over the Creepage Factor (CF), and CD is the product of the Unified Specific Creepage

Distance (USCD) and the direct voltage U, based on the definitions provided in [4]. Therefore:

$$AD = \frac{CD}{CF} = \frac{USCD \cdot U}{CF} \text{ (mm)} \quad (5.1)$$

Where, for the profile considered, CF=4.3.

The total distance L between the tower cross arm and the conductor is the sum of the insulator arcing distance and the fittings. The fittings considered in this study are fixed and listed as follows. They are taken from BS EN 3288-2 standard [166]. The fittings are a shackle from Fig. 7, a ball ended eye link from Fig. 13, a socket end fitting as per existing insulator, a ball end fitting as per existing insulator, a socket tongue from Fig. 28, and a conductor clamp from Fig. 78, shown in [166]. The fittings amount to a fixed distance F of 854 mm. Thus, L is calculated as follows:

$$L = AD + F = AD + 854 \text{ (mm)} \quad (5.2)$$

It is worth noting that the fitting length may differ, depending on conductor loading and bundling. However, the proposed fittings are considered to compute a preliminary design, which can reveal the power transmission potential of certain insulation solutions. Detailed fitting choices will have to be made, once the most interesting conversion candidates are identified, and finalised designs will have to be amended accordingly.

USCD is calculated as follows, similarly to Chapter 3, as explained in Section 2.8.3 [4]. In contrast to Chapter 3, the statistical factor Ks is herein set as 1.4, to conservatively consider that a minority of line insulators will perform worse than expected.

$$\begin{aligned}
 \text{USCD} &= B \cdot C_d \cdot C_a \cdot \left[ \text{ESDD}_{\text{dc}} \cdot K_C \cdot \left( \frac{\text{NSDD}_{\text{dc}}}{\text{NSDD}_0} \right)^{\frac{0.106}{\alpha}} \cdot K_{\text{CUR}} \cdot \left( \frac{D_a}{D_0} \right)^{-\rho} \cdot K_S \right]^{\alpha} \\
 &= 65 \cdot 1 \cdot 1 \cdot \left[ 0.6 \cdot 1 \cdot \left( \frac{0.6}{1} \right)^{\frac{0.106}{0.25}} \cdot 1 \cdot \left( \frac{97.6}{115} \right)^{-0.21} \cdot 1.4 \right]^{0.25} \quad (\text{mm/kV}) \quad (5.3)
 \end{aligned}$$

The result of (5.3) is 59.5 mm/kV.

If, hypothetically, non-HTM insulators were used, B would be 110 instead of 65, and  $\alpha$  would be 0.33 instead of 0.25, and the final USCD would be 99.5 mm/kV. The much higher USCD would be due in particular to the parameter B.

### 5.2.2. Clearance distances

The overvoltage clearance distance has been calculated with (5.25) developed by EPRI [142], which is more conservative and satisfies the switching impulse air clearances set in [167].

$$C_d = 3.916 \cdot 10^{-2} \cdot (U \cdot \text{PU})^{1.667} \quad (\text{mm}) \quad (5.4)$$

Where PU is the Switching Surge Factor (SSF). The SSF depends on the line characteristics, such as its length. Moreover, the overvoltage amplitude is not the same along the line. The reviews by ORNL [141], EPRI [142], and CIGRE [140] consider SSFs of 1.5, 1.5 and 1.8, respectively. This Chapter conservatively assumes an SSF of 2, as the maximum value found in [168] for a 1500 km line when the fault occurs at the line midpoint.

### 5.2.3. AC to DC power ratio

To compare the converted DC line power with the original AC overhead line power, the AC to DC power ratio  $k_{\text{AC-DC}}$  between the two is computed as in (5.5):

$$k_{\text{AC-DC}} = \frac{P_{\text{DC}}}{P_{\text{AC}}} = \frac{n_c \cdot U_{\text{DC}} \cdot I_{\text{DC}}}{n_c \cdot U_{\text{In}} \cdot I_{\text{RMS}} \cdot \text{PF}} = \frac{U_{\text{DC}}}{U_{\text{In}}} \quad (5.5)$$

Where  $n_c$  is the number of conductors, which is the same for the AC and the converted DC line, assuming the use of the same conductors for the conversion.  $U_{DC}$  is the direct pole to ground voltage,  $I_{DC}$  is the pole current per conductor, which is equal to the rms AC phase current per conductor,  $U_{ln}$  is the line to neutral or phase voltage, and PF is the power factor, which is assumed as 1 for a conservative calculation of  $K_{AC-DC}$ .

The AC power has been conveniently written to allow direct mathematical simplification, but it may equivalently be written in the following more common way:

$2 \cdot \sqrt{3} \cdot U_{ll} \cdot \left(\frac{n_c}{6} \cdot I_{RMS}\right) \cdot PF$ , which is equal to:

$\frac{U_{ll}}{\sqrt{3}} \cdot n_c \cdot I_{RMS} \cdot PF = n_c \cdot U_{ln} \cdot I_{RMS} \cdot PF$ , as written at the denominator of (5.5).

### 5.3. Two insulation solutions

For each of the 3 towers, and for each of the 2 pollution degrees, 2 insulation solutions have been calculated, which makes 4 solutions per tower and a total of 12 different proposals. The 2 insulation solutions are described as follows.

- a) The first one uses a suspension insulator at each tower cross arm. With this arrangement, the wind can move the conductor up to an angle of 30 degrees from the vertical, as explained in [142].
- b) The second is the same as the first, with the addition of inclined suspension insulators to lock the position of the conductor in space, and to allow a larger available clearance to use for a further increase in voltage.

### 5.4. Method for presentation of results

Each of the 12 proposals, shown in Fig. 5.1 to Fig. 5.12, has been drawn in AutoCAD with the following method.

The tower is drawn in red and only half of it is presented, since the other half is symmetrical. It is assumed that on one side of the tower the three poles are all positive and on the other side they are all three negative.

The insulators are drawn in black. For the first insulation solution, namely the suspension insulators, they are oriented in three ways, namely vertically, orthogonally to the closest tower arm, and at 30 degrees from the vertical. The last two orientations refer to windy conditions. For the second solution, the additional insulators which fix the conductor position are dimensioned to connect the conductor to the middle of the tower arm, but a different angle may be chosen.

The clearances are visualised with circumferences. For each tower arm, the smaller and, therefore, more critical clearance is shown. Additionally, the smallest clearance of the whole tower is shown in red, with a dashed line type, to highlight the most critical clearance position. In all cases, the number of conductors per pole is more than one. Thus, the centre of each circumference is the centre of gravity of the conductors of each pole. This represents a small approximation on the verification of clearances, because the small distance between the circumference centre and the closest conductor to the tower ground is not included in the verification. However, the benefit of this small approximation was to investigate a wide range of cases.

The total distance  $L$  between tower cross arm and the conductor, which is the sum of the insulator arcing distance and the fittings, is indicated only once for each drawing. This is done because the other insulators are the same. Also, the most critical clearance dimension is indicated.

Moreover, the main tower dimensions are indicated only once because they do not change.

The figure captions refer to the tower type, the pollution degree they refer to, and the insulation type.

#### **5.4.1. Original HVAC tower active powers**

The ratios between the modified HVDC line and the original HVAC line, as defined in the Methodology 5.2.3, do not need the conductor current for their calculation.

However, the results in section 5.8 provide the original AC active power of each original tower (L6, L2, and L7), to have the reference of the power which corresponds to  $K_{AC-DC}=1$ . For this calculation, a current of 1000 A flowing through each conductor is assumed, but this value could be lower in operation. Based on this assumption, the original AC powers would amount to the following values.

$$\begin{aligned}
 P_{AC,L6} &= 2 \cdot \sqrt{3} \cdot U_{ll} \cdot \left( \frac{n_c}{2 \cdot 3} \cdot I_{RMS} \right) \cdot \cos \phi = \\
 &= 2 \cdot \sqrt{3} \cdot 400e3 \cdot \frac{24}{2 \cdot 3} \cdot 1e3 \cdot \cos 0 = 5.54 \text{ (GW)}
 \end{aligned}
 \tag{5.6}$$

$$\begin{aligned}
 P_{AC,L2} &= 2 \cdot \sqrt{3} \cdot U_{ll} \cdot \frac{n_c}{2 \cdot 3} \cdot I_{RMS} \cdot \cos \phi = \\
 &= 2 \cdot \sqrt{3} \cdot 270e3 \cdot \frac{12}{2 \cdot 3} \cdot 1e3 \cdot \cos 0 = 1.87 \text{ (GW)}
 \end{aligned}
 \tag{5.7}$$

$$\begin{aligned}
 P_{AC,L7} &= 2 \cdot \sqrt{3} \cdot U_{ll} \cdot \frac{n_c}{2 \cdot 3} \cdot I_{RMS} \cdot \cos \phi = \\
 &= 2 \cdot \sqrt{3} \cdot 132e3 \cdot \frac{6}{2 \cdot 3} \cdot 1e3 \cdot \cos 0 = 0.46 \text{ (GW)}
 \end{aligned}
 \tag{5.8}$$

Where the power factor  $\cos \phi$  has been conservatively (for  $K_{AC-DC}$ ) assumed as unity. The expression of the power, as shown in (5.6), (5.7) and (5.8) is the classical expression of the power of a three-phase system, with the exception of the factors shown in bold in (5.6), which are explained as follows. The power is initially multiplied by 2, to account for the 2 three-phase systems existing on each tower. Then, the whole factor  $\left( \frac{n_c}{2 \cdot 3} \cdot I_{RMS} \right)$  is the current of each phase. In fact,  $I_{RMS}$  is the current of a single conductor,  $n_c$  is the total number of conductors, which is divided by the 2 circuits and by the 3 phases to obtain the number of conductors per phase.

## 5.5. L6 Results: DC voltages from 380 to 500 kV

Table 5.1. L6 proposals for HVDC use.

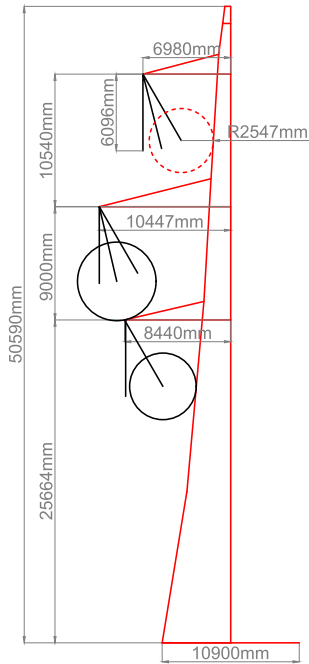


Fig. 5.1 L6-0.6

I)  
 ESDD=NSDD  
 =0.6 mg/cm<sup>2</sup>  
 n<sub>c</sub>=24  
 n<sub>c</sub>/pole=4  
 U<sub>dc</sub>=380 kV  
 USCD=59.3  
 mm/kV  
 AD=5242 mm  
 C<sub>d</sub>>2484 mm  
 K<sub>AC-DC</sub>=1.6

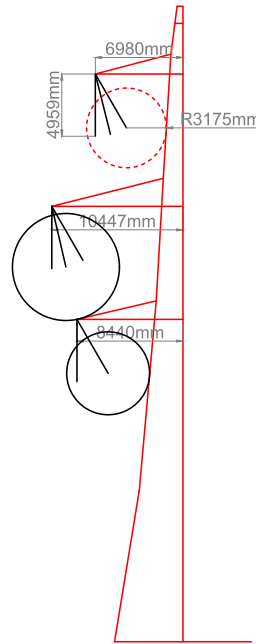


Fig. 5.2 L6-0.2

I)  
 ESDD=NSDD=0.2  
 mg/cm<sup>2</sup>  
 n<sub>c</sub>=24  
 n<sub>c</sub>/pole=4  
 U<sub>dc</sub>=440 kV  
 USCD=40 mm/kV  
 AD=4105 mm  
 C<sub>d</sub>>3172 mm  
 K<sub>AC-DC</sub>=1.9

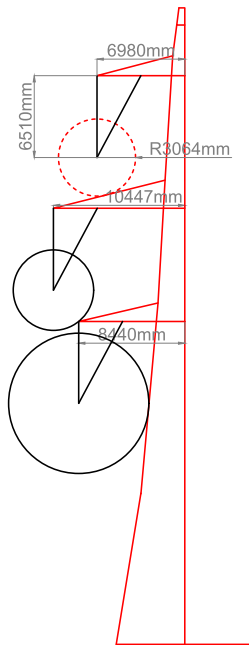


Fig. 5.3 L6-0.6-fixed

II)  
 ESDD=NSDD  
 =0.6 mg/cm<sup>2</sup>  
 n<sub>c</sub>=24  
 n<sub>c</sub>/pole=4  
 U<sub>dc</sub>=410 kV  
 USCD=59.3  
 mm/kV  
 AD=5656 mm  
 C<sub>d</sub>>2819 mm  
 K<sub>AC-DC</sub>=1.8

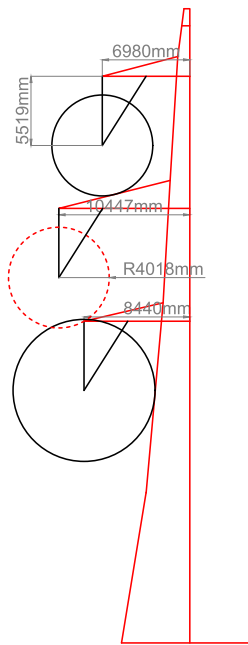


Fig. 5.4 L6-0.2 fixed

II)  
 ESDD=NSDD=0.2  
 mg/cm<sup>2</sup>  
 n<sub>c</sub>=24  
 n<sub>c</sub>/pole=4  
 U<sub>dc</sub>=500 kV  
 USCD=40 mm/kV  
 AD=4665 mm  
 C<sub>d</sub>>3925 mm  
 K<sub>AC-DC</sub>=2.2

## 5.6. L2 Results: DC voltages from 310 to 400 kV

Table 5.2. L2 proposals for HVDC use.

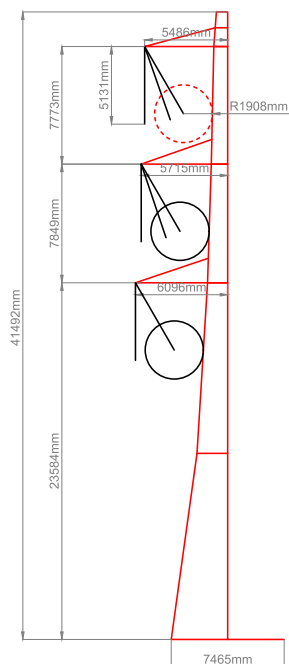


Fig. 5.5 L2-0.6

I)  
 ESDD=NSDD=  
 0.6 mg/cm<sup>2</sup>  
 n<sub>c</sub>=12  
 n<sub>c</sub>/pole=2  
 U<sub>dc</sub>=310 kV  
 USCD=59.3  
 mm/kV  
 AD=4277 mm  
 C<sub>d</sub>>1769 mm  
 K<sub>AC-DC</sub>=2.0

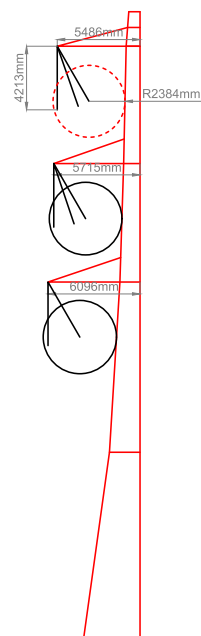


Fig. 5.6 L2-0.2

I)  
 ESDD=NSDD=0.2  
 mg/cm<sup>2</sup>  
 n<sub>c</sub>=12  
 n<sub>c</sub>/pole=2  
 U<sub>dc</sub>=360 kV  
 USCD=40 mm/kV  
 AD=3359 mm  
 C<sub>d</sub>>2270 mm  
 K<sub>AC-DC</sub>=2.3

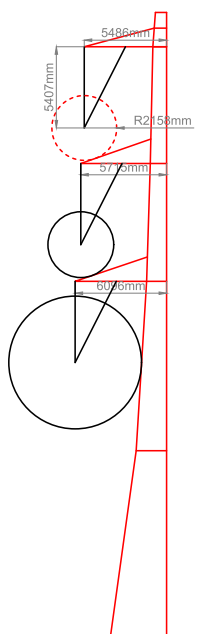


Fig. 5.7 L2-0.6-fixed

II)  
 ESDD=NSDD=  
 0.6 mg/cm<sup>2</sup>  
 n<sub>c</sub>=12  
 n<sub>c</sub>/pole=2  
 U<sub>dc</sub>=330 kV  
 USCD=59.3  
 mm/kV  
 AD=4553 mm  
 C<sub>d</sub>>1963 mm  
 K<sub>AC-DC</sub>=2.1

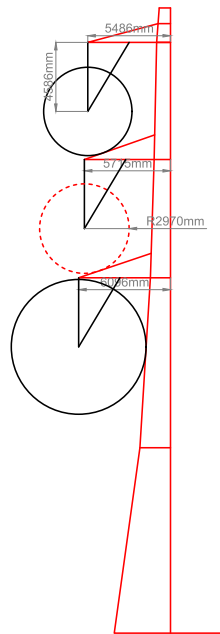
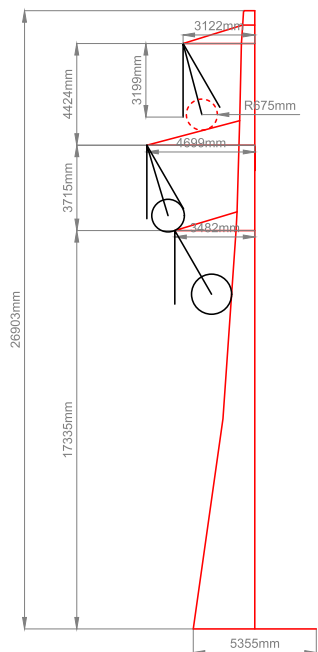
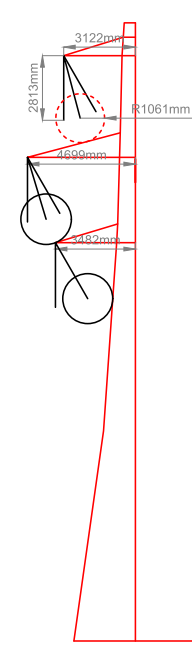
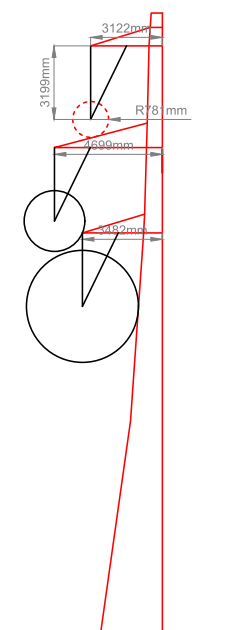
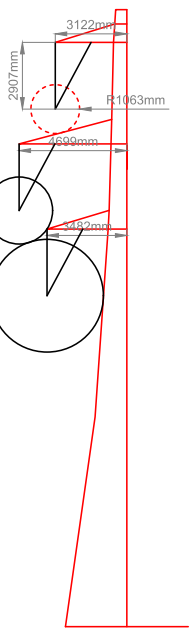


Fig. 5.8 L2-0.2 fixed

II)  
 ESDD=NSDD=0.2  
 mg/cm<sup>2</sup>  
 n<sub>c</sub>=12  
 n<sub>c</sub>/pole=2  
 U<sub>dc</sub>=400 kV  
 USCD=40 mm/kV  
 AD=3732 mm  
 C<sub>d</sub>>2706 mm  
 K<sub>AC-DC</sub>=2.5

## 5.7. L7 Results: DC voltages from 170 to 220 kV

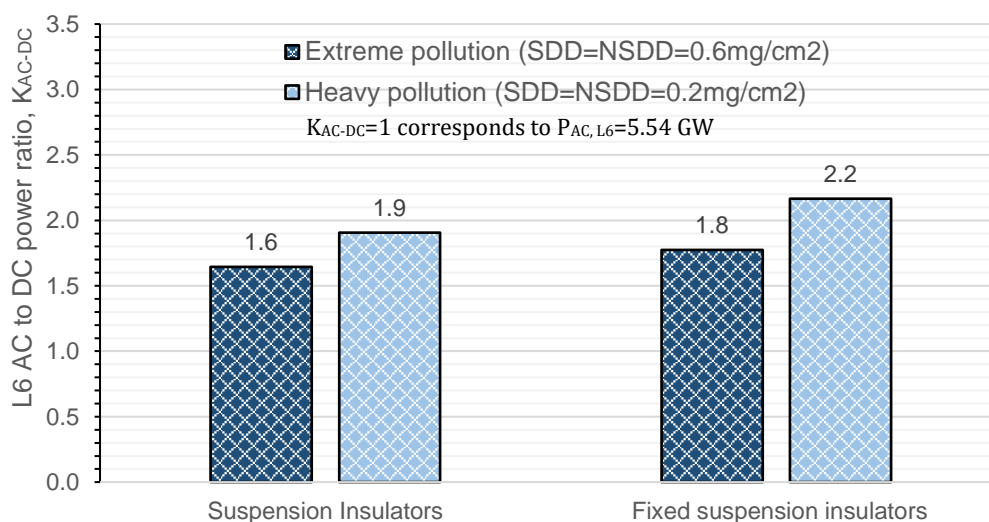
Table 5.3. L7 proposals for HVDC use.

 <p>I)  ESDD=NSDD=  0.6 mg/cm<sup>2</sup>  n<sub>c</sub>=6  n<sub>c</sub>/pole=1  U<sub>dc</sub>=170 kV  USCD=59.3  mm/kV  AD=2345 mm  C<sub>d</sub>&gt;650 mm  K<sub>AC-DC</sub>=2.2</p>	 <p>I)  ESDD=NSDD=0.2  mg/cm<sup>2</sup>  n<sub>c</sub>=6  n<sub>c</sub>/pole=1  U<sub>dc</sub>=210 kV  USCD=40 mm/kV  AD=1959 mm  C<sub>d</sub>&gt;924 mm  K<sub>AC-DC</sub>=2.8</p>
 <p>II)  ESDD=NSDD=  0.6 mg/cm<sup>2</sup>  n<sub>c</sub>=6  n<sub>c</sub>/pole=1  U<sub>dc</sub>=170 kV  USCD=59.3  mm/kV  AD=2345 mm  C<sub>d</sub>&gt;650 mm  K<sub>AC-DC</sub>=2.2</p>	 <p>II)  ESDD=NSDD=0.2  mg/cm<sup>2</sup>  n<sub>c</sub>=6  n<sub>c</sub>/pole=1  U<sub>dc</sub>=220 kV  USCD=40 mm/kV  AD=2053 mm  C<sub>d</sub>&gt;999 mm  K<sub>AC-DC</sub>=2.9</p>
<p>Fig. 5.9 L7-0.6</p>	<p>Fig. 5.10 L7-0.2</p>
<p>Fig. 5.11 L7-0.6-fixed</p>	<p>Fig. 5.12 L7-0.2 fixed</p>

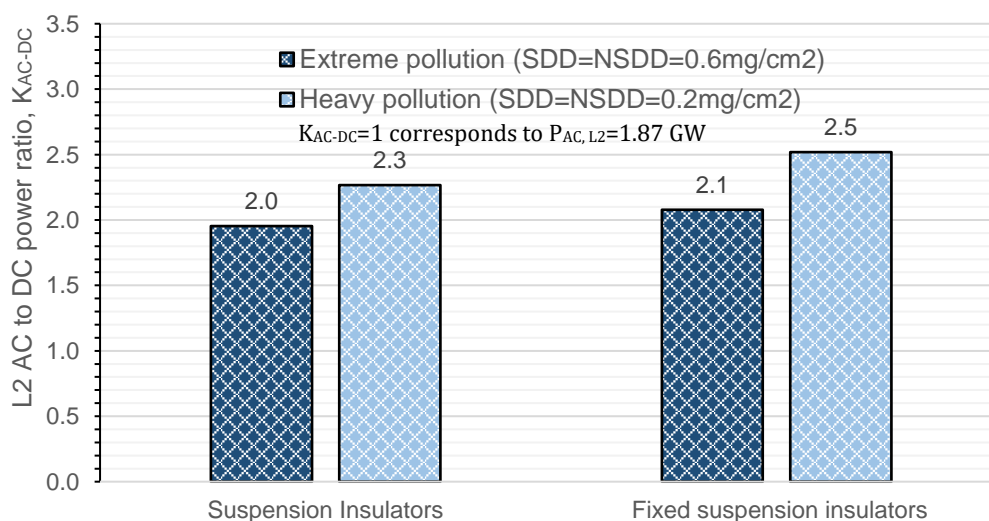
## 5.8. AC to DC line conversion power ratios: $K_{AC-DC}$

By using (5.5), the power ratio between the AC line and the DC line,  $K_{AC-DC}$ , can be calculated. Per each of the three charts shown in Fig. 5.13, the AC power is the same and the DC power varies, depending on the considered insulation solution and pollution severity.

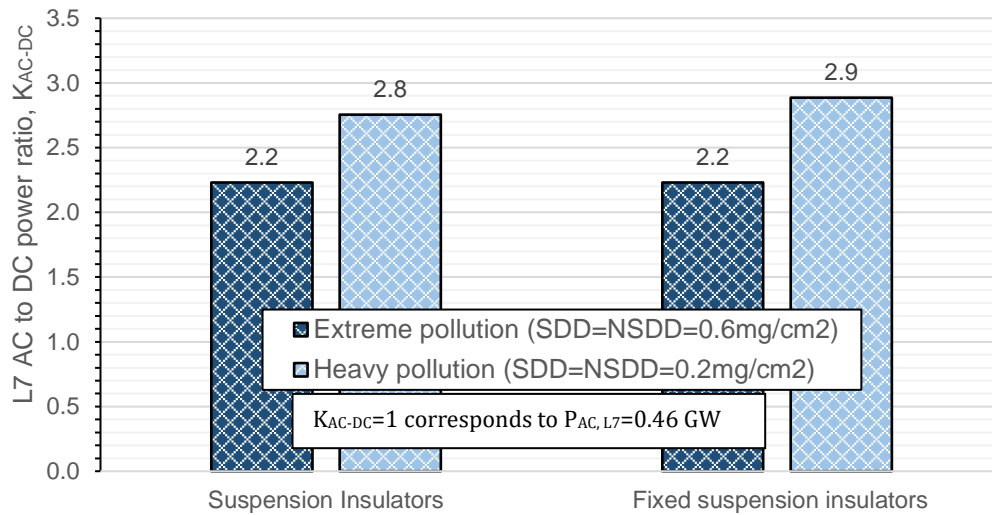
The charts summarise an indicator which contributes to the level of interest a transmission owner may have for a particular solution, as their revenue is proportional to the transmitted power.



a) L6 tower



b) L2 tower



c) L7 tower

Fig. 5.13. AC to DC power ratios  $K_{AC-DC}$  of a) L6, b) L2, and c) L7 with two different insulation solutions under extreme and heavy pollution severities.

### 5.8.1. Interpretation of tower conversion design results

The arcing distance is linear with voltage, and the clearance distance is exponential with voltage. As a consequence, as the voltage level increases from L7, to L2, and ultimately L6, the ratio  $C_d/AD$  increases, which constrains the maximum voltage that can be applied to the DC line. This is reflected in the results shown in Fig. 5.13.

## 5.9. FEM results for electric field requirements (no corona ring)

The cases identified by low creepage and high voltage (or low USCD) are the most critical from the point of view of electrical stress. Thus, the ones with USCD=40 mm/kV have been modelled, as opposed to those with USCD=59.3 mm/kV. All the cases refer to the suspension insulator solution, and axisymmetric models of the dimensioned insulators have been considered. The mesh and details of the models have the same features shown in Fig. 3.6 a) and b). The material properties are shown in TABLE 5.4.

TABLE 5.4. Material Properties for FEM Modelling.

Material	Conductivity (S/m)	Relative permittivity (adim)
<i>Air</i>	$1 \cdot 10^{-14}$ [125]	1
<i>Silicone rubber</i>	$1 \cdot 10^{-14}$ [126]	3.5 [126]
<i>Fibre glass</i>	$1 \cdot 10^{-14}$ [127]	3.5
<i>Pollution (0.5 mm)</i>	$10^{-9, -10, -11, -14}$	80 [128]
<i>Metal</i>	$4 \cdot 10^6$	$\infty$

As discussed in the Methodology of this chapter, focus has been directed towards the determination of the minimum current above which the electric field requirements set in [9], [10] are satisfied, as outlined in the second row of TABLE 5.5. To do so, four layer conductivities have been studied: the ideal non-realistic case of  $10^{-14}$  S/m, and the  $10^{-9, -10, -11}$  S/m range in which the solution is found. The results are shown in TABLE 5.5. A green cell shows the requirement is satisfied, as opposed to a red cell. The results presented in TABLE 5.5 are also shown with column charts to visualise any dependency more easily. Per each chart, a dashed red line shows the electric field threshold requirement.

TABLE 5.5. FEM current results; and FEM electric field results against requirements.

Tower, <i>U</i> (kV)	<i>AD</i> , <i>CD</i> (mm)	$\sigma$ (S/m)	<i>I</i> <sub>DC</sub> (nA)	<i>E</i> <sub>max</sub> <i>ground</i> (kV/mm)	<i>E</i> <sub>max</sub> <i>HV</i> (kV/mm)	<i>E</i> <sub>avg</sub> <i>surface</i> (kV/mm)	<i>Ground</i> <i>tr. junct.</i> (kV/mm)	<i>HV tr.</i> <i>junct.</i> (kV/mm)
				<1.8?	<1.8?	<0.42?	<0.35?	<0.35?
L6, 440	4113, 17685	1E-9	5.52	1.08	1.27	0.13	0.08	0.09
		1E-10	<b>2.20</b>	1.52	1.68	0.10	0.24	0.26
		1E-11	1.47	2.79	3.29	0.06	0.85	0.97
		1E-14	1.18	4.32	5.50	0.05	2.29	2.88
L2, 360	3313, 14246	1E-9	5.38	1.04	1.23	0.13	0.08	0.08
		1E-10	<b>2.04</b>	1.40	1.71	0.10	0.22	0.24
		1E-11	1.31	2.49	2.93	0.06	0.76	0.86
		1E-14	1.04	3.79	4.83	0.05	2.01	2.53
L7, 210	1953, 8398	1E-9	4.75	0.86	1.03	0.13	0.07	0.07
		1E-10	<b>1.52</b>	1.05	1.26	0.11	0.17	0.18
		1E-11	0.91	1.72	2.01	0.06	0.52	0.59
		1E-14	0.69	2.53	3.21	0.04	1.34	1.68

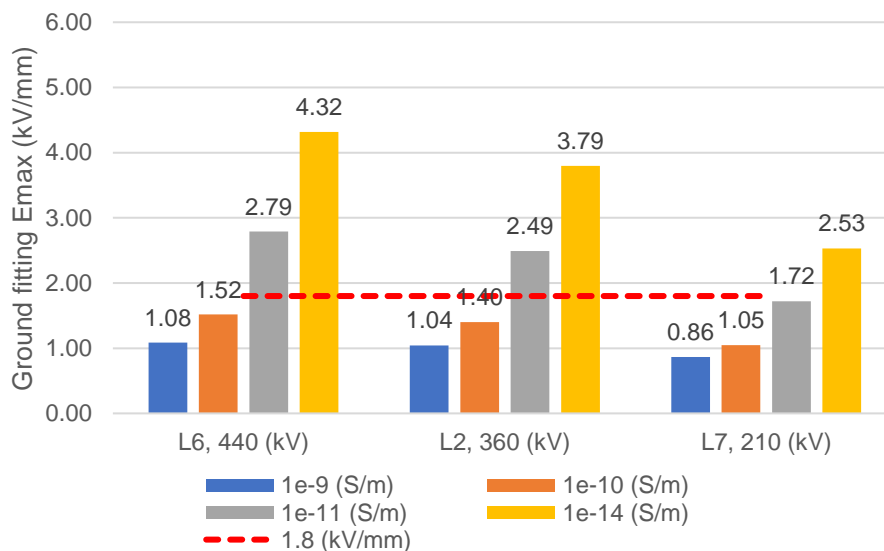


Fig. 5.14. Maximum electric field on ground fitting (kV/mm) for different tower insulators and different layer conductivities, at a thickness of 0.5 mm. The red dashed line shows the 1.8 kV/mm requirement.

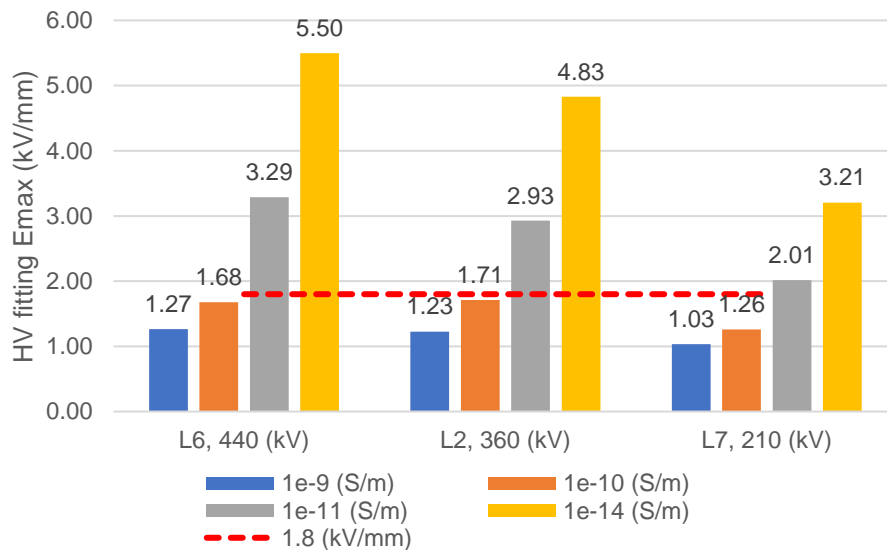


Fig. 5.15. Maximum electric field on HV fitting (kV/mm) for different tower insulators and different layer conductivities, at a thickness of 0.5 mm. The red dashed line shows the 1.8 kV/mm requirement.

The maximum electric field on the ground and HV fittings is below the required value in all cases at a conductivity of  $10^{-10}$  or larger, as shown in Fig. 5.14 and Fig. 5.15.

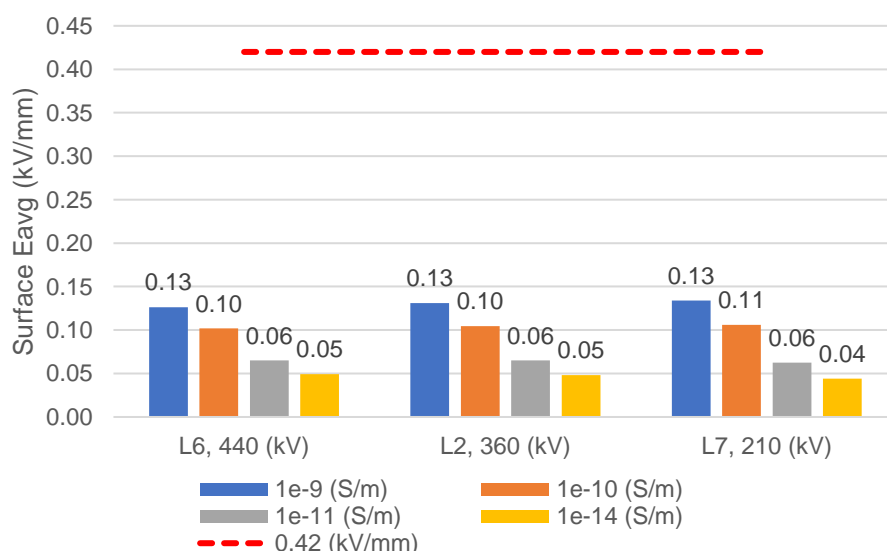


Fig. 5.16. Average electric field on insulator surface (or creepage) (kV/mm) for different tower insulators and different layer conductivities, at a thickness of 0.5 mm. The red dashed line shows the 0.42 kV/mm requirement.

The average electric field is well below the required value for all the studied cases, as shown in Fig. 5.16.

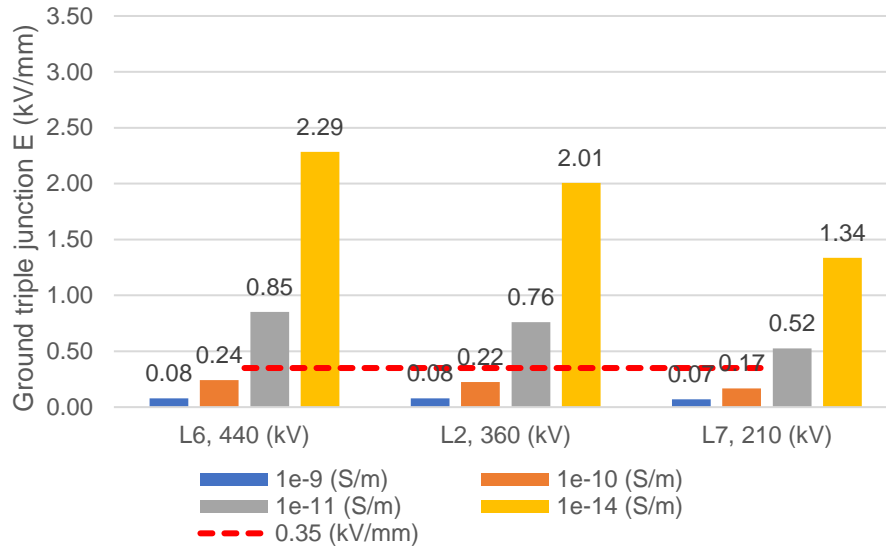


Fig. 5.17. Ground triple junction electric field (kV/mm) for different tower insulators and different layer conductivities, at a thickness of 0.5 mm. The red dashed line shows the 0.35 kV/mm requirement.

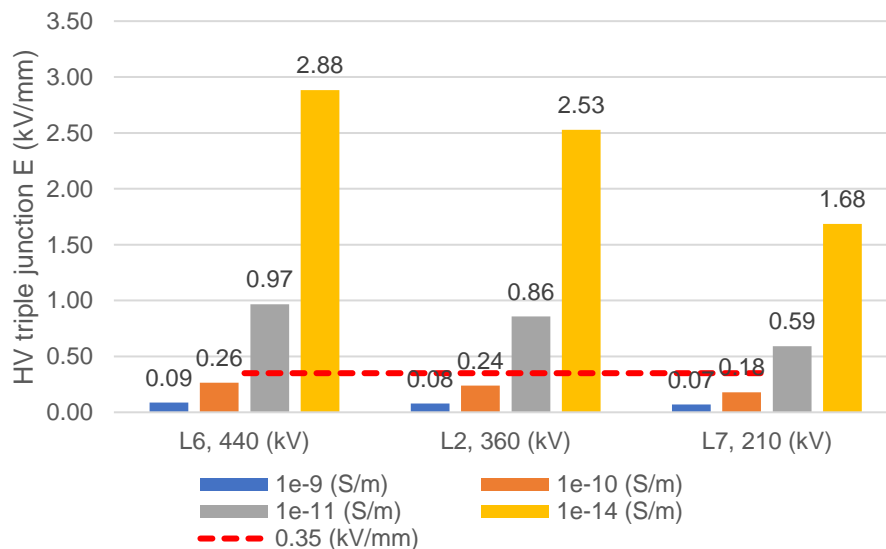
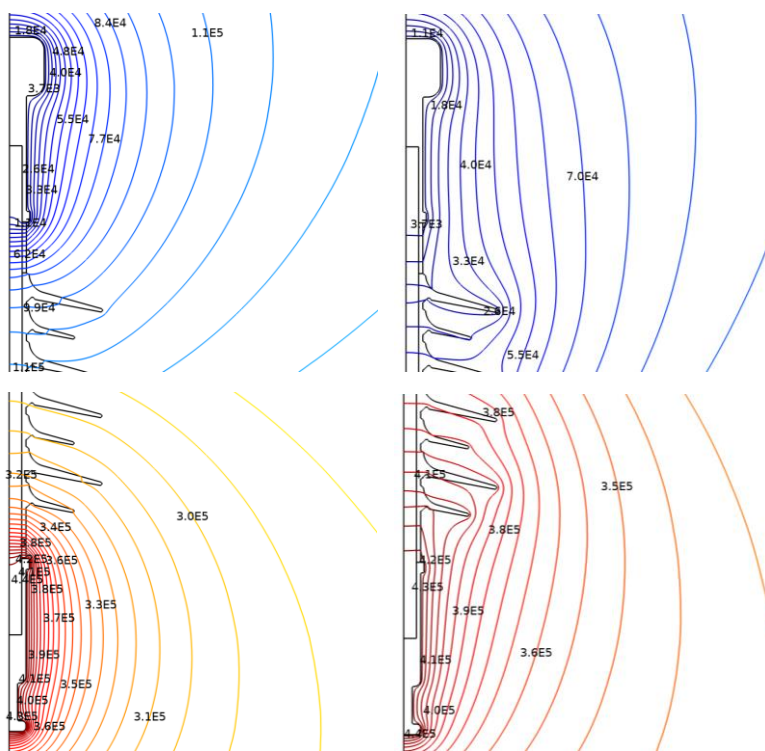


Fig. 5.18. HV triple junction electric field (kV/mm) for different tower insulators and different layer conductivities, at a thickness of 0.5 mm. The red dashed line shows the 0.35 kV/mm requirement.

Fig. 5.17 and Fig. 5.18 show that a conductivity of  $10^{-10}$ , or larger, satisfies the triple junction electric field requirements.

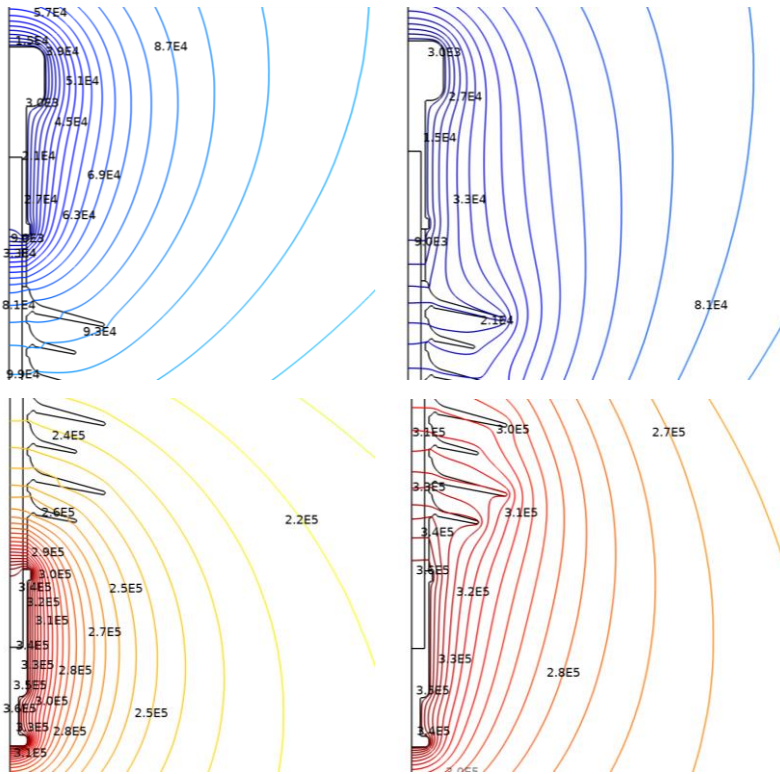
Fig. 5.19, Fig. 5.20 and Fig. 5.21 show the equipotential lines of a) the ideal non-realistic case at  $\sigma=10^{-14}$  S/m, and b) the minimum conductivity, namely  $10^{-10}$  S/m, and current satisfying the electric field requirements.

Fig. 5.19, Fig. 5.20 and Fig. 5.21 are presented to show the effect of the pollution conductivity on the equipotential line distribution in the vicinity of the electrodes, where the electric field is larger. The results show that regardless of the insulator AD, the effect of the conductive pollution on the equipotential lines is evident, with respect to the ideal case, and very similar among the three different insulators.



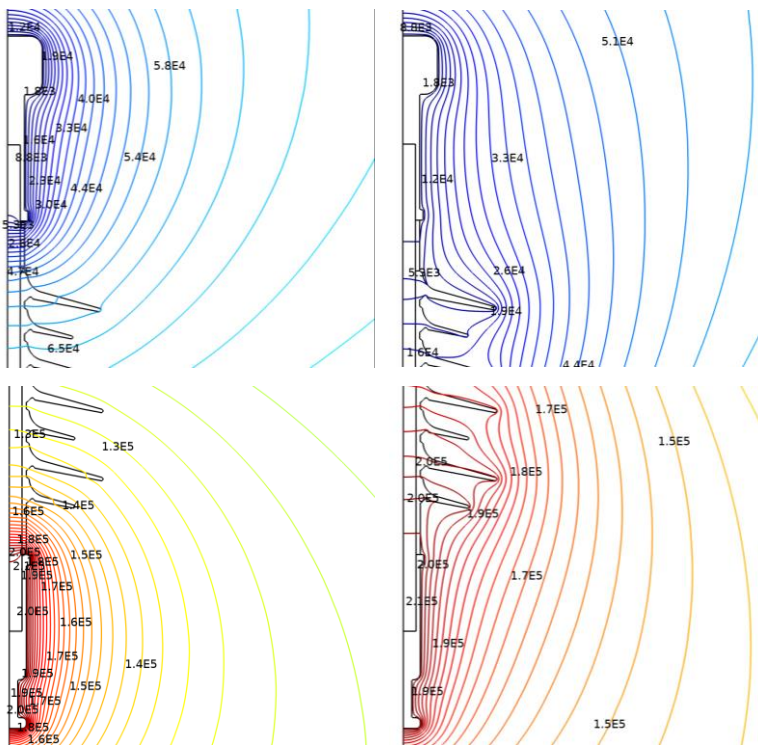
a)  $\sigma=10^{-14}$  S/m,  $i=1.18$  nA      b)  $\sigma=10^{-10}$  S/m,  $i=2.20$  nA

Fig. 5.19. L6 insulator fitting equipotential lines (V), at  $U=440$  kV.



a)  $\sigma=10^{-14}$  S/m,  $i=1.04$  nA      b)  $\sigma=10^{-10}$  S/m,  $i=2.04$  nA

Fig. 5.20. L2 insulator fitting equipotential lines (V), at  $U=360$  kV.



a)  $\sigma=10^{-14}$  S/m,  $i=0.69$  nA      b)  $\sigma=10^{-10}$  S/m,  $i=1.52$  nA

Fig. 5.21. L7 insulator fitting equipotential lines (V), at  $U=210$  kV.

## 5.10. Discussion

The discussion is made in the same order as the results order. A comparison between the two pollution degrees is done for each insulation solution. Also, the comparison of the two insulation solutions with the same pollution degrees is carried out.

### 5.10.1. L6 design

- I) At an ESDD and NSDD of 0.6, the suspension insulator is very long; at 0.2, the insulator is shorter, and the clearance is larger, due to the larger voltage.
- II) Fixing the pole position allows a power increase of  $3/38=7.9\%$  under extreme pollution; under heavy pollution, the power increase is  $6/44=13.6\%$ . Thus, at lower pollution, constraining is more rewarding.

### 5.10.2. L2 design

- II) Constraining the conductor position allows an additional power increase of 6.4% and 11%, respectively for extreme and heavy pollution.

### 5.10.3. L7 design

- II) Fixing the L7 tower poles positions in space does not produce any appreciable voltage gain because the shortest clearance is between the top pole and the middle tower arms, unlike for L6 and L2 where it is between top pole and tower body.

### 5.10.4. Electric field requirements

Fig. 5.14, Fig. 5.15, Fig. 5.16, Fig. 5.17 and Fig. 5.18 show, as expected, that the electric field requirements are not satisfied for the ideal conductivity of  $10^{-14}$  S/m, with the exception of  $E_{avg}$  on the insulator surface. For all cases, the layer thickness is 0.5 mm, and the minimum conductivity which satisfies all the requirements for all the dimensioned insulators is  $10^{-10}$  S/m. For the L6, L2, and L7 insulators, this conductivity corresponds respectively to a current of 2.20, 2.04, and 1.52 nA. As seen in Pignini's paper [8], currents in the range of  $\mu A$  are to be expected in weathered and cleaned insulators. Thus, the non-necessity of corona rings under DC is confirmed in the cases analysed in this chapter, as a small current in the nA range is enough to satisfy the electric field requirements.

## 5.11. Conclusions

All the proposed HVDC conversions would allow a larger power transfer capability with respect to the original HVAC towers, and this is measured by the  $k_{AC-DC}$  ratio. The converted lines would carry 1.6 to 2.9 times the original power.

On average, the line converted with simple suspension insulators would carry 2.1 times the original power. Adding insulators to fix the pole positions in space is slightly beneficial only for the L6 and L2 towers. Also, constraining the pole is more rewarding for the lower pollution severity.

The non-necessity of fitting corona rings under DC in the outdoors is confirmed in the cases analysed in this chapter. In fact, the FEM models have shown that a small current in the nA range is enough to satisfy the electric field requirements, as a current at least in the  $\mu$ A range is to be expected in service.



# Chapter 6. Initial prototype of wind tunnel design and building for DC pollution accumulation

## 6.1. Introduction

The critical dimensioning factor of HVDC outdoor insulation is contamination severity, rather than switching overvoltages which are more critical in HVAC systems [4]. The reason why contamination severities are larger under DC is that the electrostatic field, caused by the energised electrode, exerts a force on charged pollution particles, allowing them to be accumulated at a higher rate than what wind alone would cause.

A thorough investigation on natural contamination is, therefore, essential in determining key aspects of DC outdoor insulation coordination. Thus, the aims of this chapter are:

- a) to provide the Kaolin NSDD on a composite insulator at three different wind speeds in the non-energised and energised conditions, and
- b) to provide the ratios  $K_p$  between  $NSDD_{DC}$  and  $NSDD_{non-energised}$  at the same three different wind speeds.

It is important to highlight that no standardised procedure exists for the construction of a wind tunnel designed for this purpose, and neither for methodologies on how to inject pollution in the tunnel. This premise explains the challenging nature of the investigation, which is nonetheless worth being pursued due to the importance of a better quantification of  $K_p$ . In fact, more information on  $K_p$  would allow to use in-situ HVAC energised insulator pollution severity data with more confidence for the dimensioning of HVDC energised insulators to be installed in the same or a similar location.

## 6.2. Background and design

As reviewed in sections 2.17.2, 2.17.3, and 2.17.4, indoor controlled experiments were performed using wind tunnels [112], [113], and [114].

To verify some of the findings and possibly increase the level of knowledge in the area, an initial prototype of a wind tunnel has been designed, as shown in Fig. 6.1, as a first step to realising a small-scale experiment.

Normally, a wind tunnel section would be constant or slightly different along the circuit. However, for laboratory space constraints, the section reduction has been proposed to allow the tunnel to fit in one of Cardiff University's High Voltage laboratory cages. Originally, it was known that this choice would impact the fluid dynamics, but the project has been undertaken as an initial prototype to make initial experiments and later assess how to improve or re-build the system.

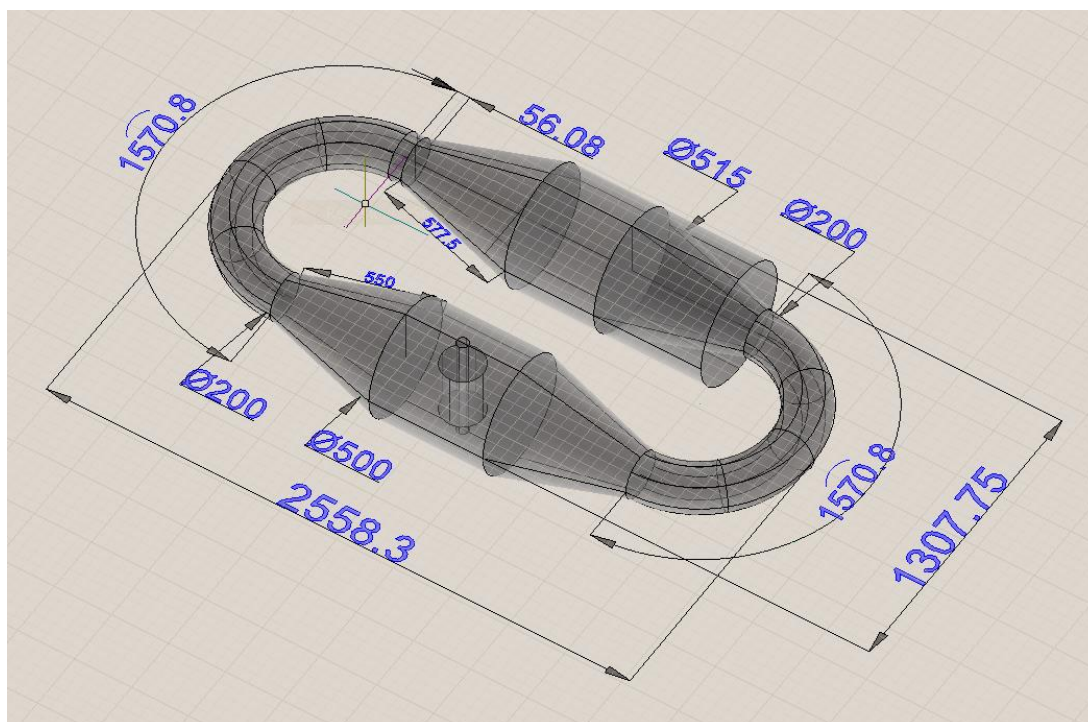


Fig. 6.1. Wind tunnel CAD design. All measurements are in mm.

### **6.3. Design of materials and geometry**

An important novelty of this design is the introduction of an insulating material to realise the enclosure, rather than a grounded metallic material as used in the reviewed studies [112], [113], and [114]. This was done to enable the equipotential lines to expand in the vicinity of the insulator electrodes, rather than to be squeezed in the case of a grounded metallic enclosure, and reproduce a more realistic scenario. This choice also allows the electric field to be modified in space easily, by adding metallic geometries outside the enclosure, to reproduce a desired electric field. It is worth noting that the choice of using an insulating material for the enclosure in the vicinity of a DC electrode causes the enclosure to be electrically charged and accumulate pollution. This would not happen with a grounded metallic enclosure in the vicinity of an insulated DC electrode. This chapter does not provide an investigation on which enclosure insulating material would minimise the pollution accumulation on the enclosure and, thus, the interference with the insulator pollution accumulation. Therefore, it is suggested as future work. The investigation on the material would also have to account for practicality of enclosure construction and wind tunnel assembly.

As introduced, the insulating material was used for the construction of the cylindrical enclosure of the insulator, with a diameter of 500 mm, and for the truncated cones, which reduce the section to a diameter of 200 mm. For these components, a polycarbonate sheet of 3 mm was used, which granted solidity to the enclosure but was thin enough to be bent and create the curved structures. Two flexible ducts, with a diameter of 200 mm, were used to connect the insulator side of the wind tunnel with the wind generator side. These ducts have been covered with aluminium foil and grounded, for safety purposes and because their location is too distant from the high voltage to cause an appreciable influence on the electric field in the vicinity of the insulator.

The other side of the wind tunnel consists of a wind generator, which came with a built-in metallic enclosure, and two metallic truncated cones which were built as a connection to the flexible ducts. These components have also been grounded.

## 6.4. FEM assessment of two material design options

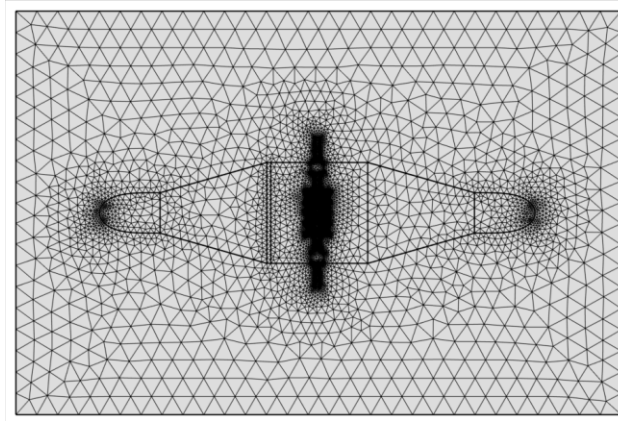
As introduced in the previous section, two options were considered from the electrical point of view. The first, found in literature, consists of a grounded metallic material for the whole enclosure. The second, proposed in this study, consists of an insulating material for the enclosure in the vicinity of the insulator, to allow the equipotential lines to be more relaxed in space and thus the electric field not to be particularly large around the high voltage electrode, which would increase the level of contamination under DC energisation.

The two options have been modelled with a Finite Element Method (FEM), whose mesh is shown in Fig. 6.2. For each option, two layer conductivity scenarios have been considered. Both at a thickness of 0.5 mm, the considered conductivities are  $10^{-9}$  S/m and  $10^{-5}$  S/m, corresponding to a current of 2 nA, which is ideal, and 14  $\mu$ A, which is the order of magnitude expected in non-ideal dry conditions [8]. The insulator, which is shown in Fig. 4.6, and selection of the 16 kV energisation level are the same as in Chapter 4.

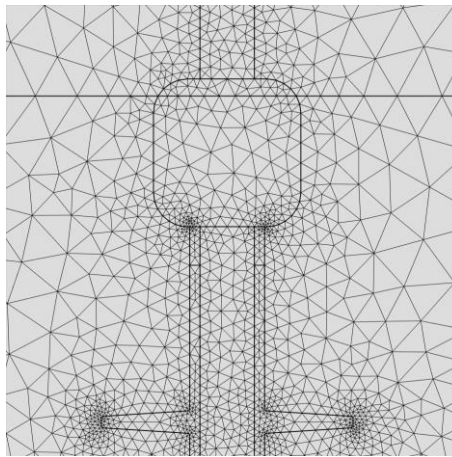
The material properties used for the simulations are shown in TABLE 6.1, and the mesh is shown in Fig. 6.2.

TABLE 6.1. Material Properties for FEM Modelling.

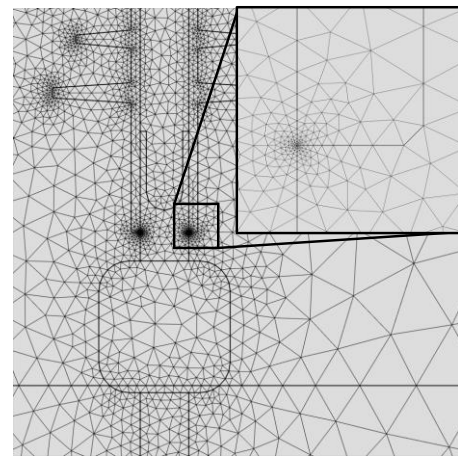
Material	Conductivity (S/m)	Relative permittivity (adim)
<i>Air</i>	$1 \cdot 10^{-14}$ [125]	1
<i>Silicone rubber</i>	$1 \cdot 10^{-14}$ [126]	3 [126]
<i>Fibre glass</i>	$1 \cdot 10^{-14}$ [127]	3
<i>Pollution (0.5mm)</i>	$1 \cdot 10^{-9}$ , $1 \cdot 10^{-5}$	80 [128]
<i>Metal</i>	$3.8 \cdot 10^7$	$\infty$



a) Full geometry



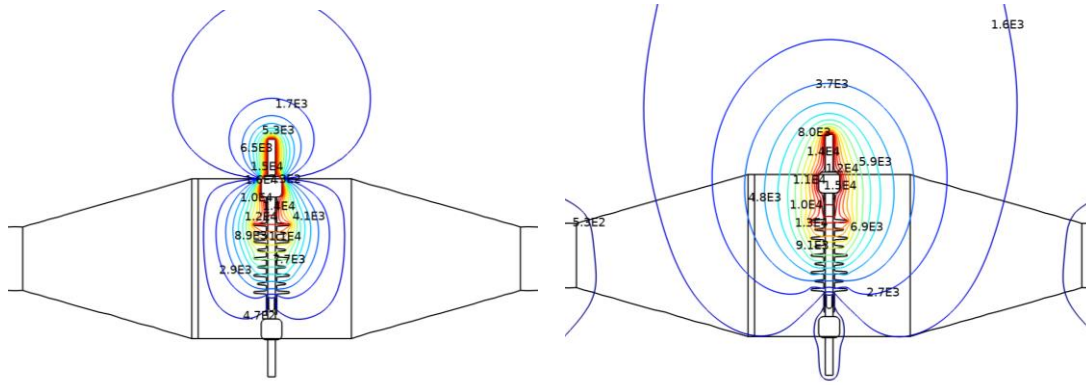
b) High voltage electrode



c) ground electrode

Fig. 6.2. Vertical section mesh of three-dimensional model of wind tunnel test facility. Metal parts are meshed because the electric current physics was used.

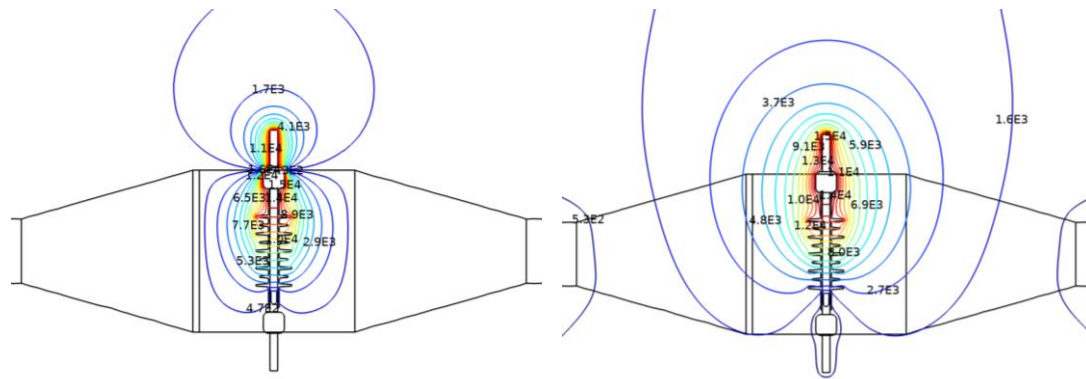
The most evident influence on the equipotential line distribution in Fig. 6.3 and Fig. 6.4 is due to the enclosure material. As expected, the equipotential lines are squeezed in the case of grounded metallic enclosure, as opposed to the expanded equipotentials when the enclosure is made of an insulating material. Little dependency is observable with respect to layer conductivity between Fig. 6.3 and Fig. 6.4. Thus, voltage and electric field charts have been developed to quantify possible differences due to the layer conductivity.



a) Aluminium grounded enclosure

b) Polycarbonate enclosure

Fig. 6.3. Wind tunnel equipotential lines (V) at a layer conductivity of  $10^{-9}$  (S/m).



a) Aluminium grounded enclosure

b) Polycarbonate enclosure

Fig. 6.4. Wind tunnel equipotential lines (V) at a layer conductivity of  $10^{-5}$  (S/m).

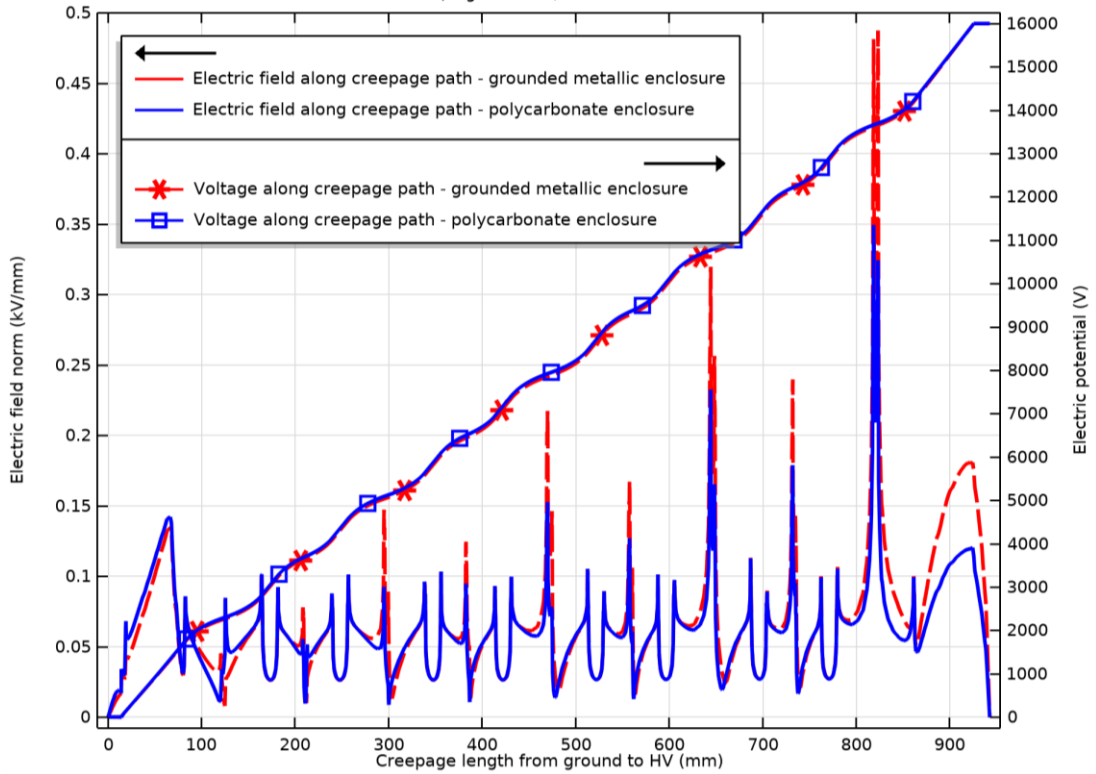


Fig. 6.5. Electric potential (V) and electric field magnitude (kV/mm) along the creepage of the insulator (mm), at a conductivity of  $10^{-9}$  S/m.

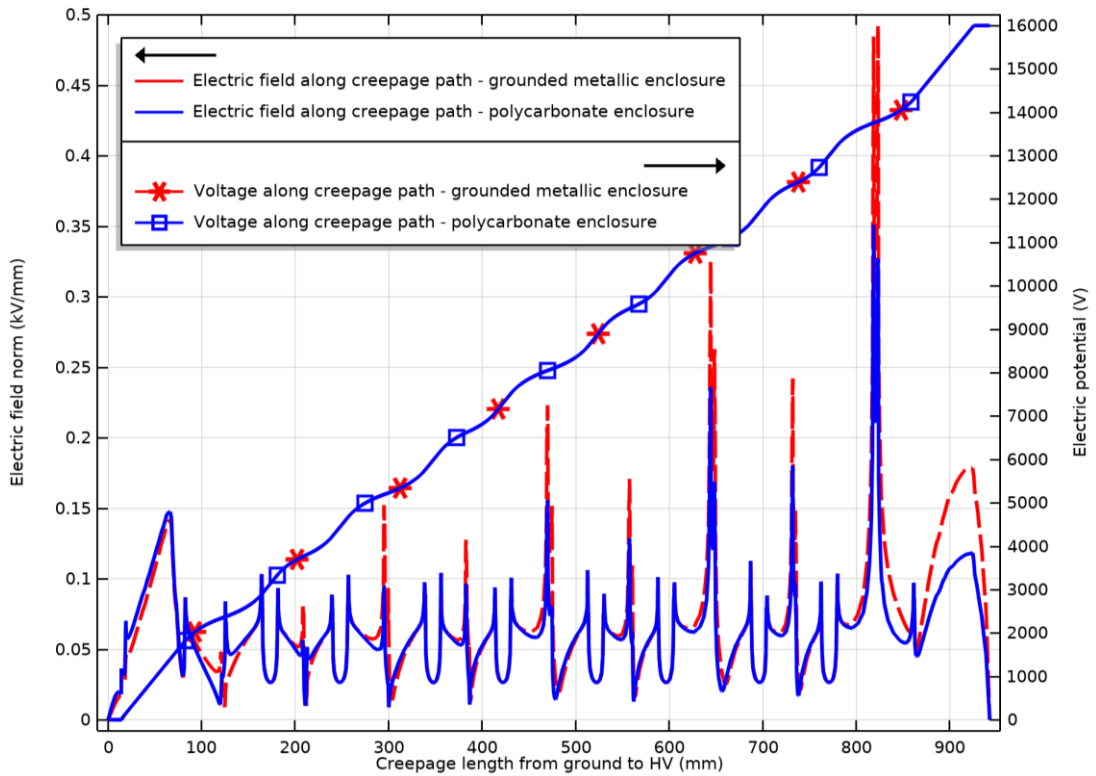


Fig. 6.6. Electric potential (V) and electric field magnitude (kV/mm) along the creepage of the insulator (mm), at a conductivity of  $10^{-5}$  S/m.

As already observed with the equipotential lines in Fig. 6.3 and Fig. 6.4, the electric potential and electric field along the creepage path of Fig. 6.5 and Fig. 6.6 do not vary considerably with the conductivity. An appreciable difference is caused by the realisation of the enclosure with the insulating material. In particular, the electric field magnitude at the high voltage end considerably differs between the two design options.

## 6.5. Experiment methodology

The construction of the wind tunnel with insulating enclosure in the vicinity of the insulator has been realised as in Fig. 6.7.

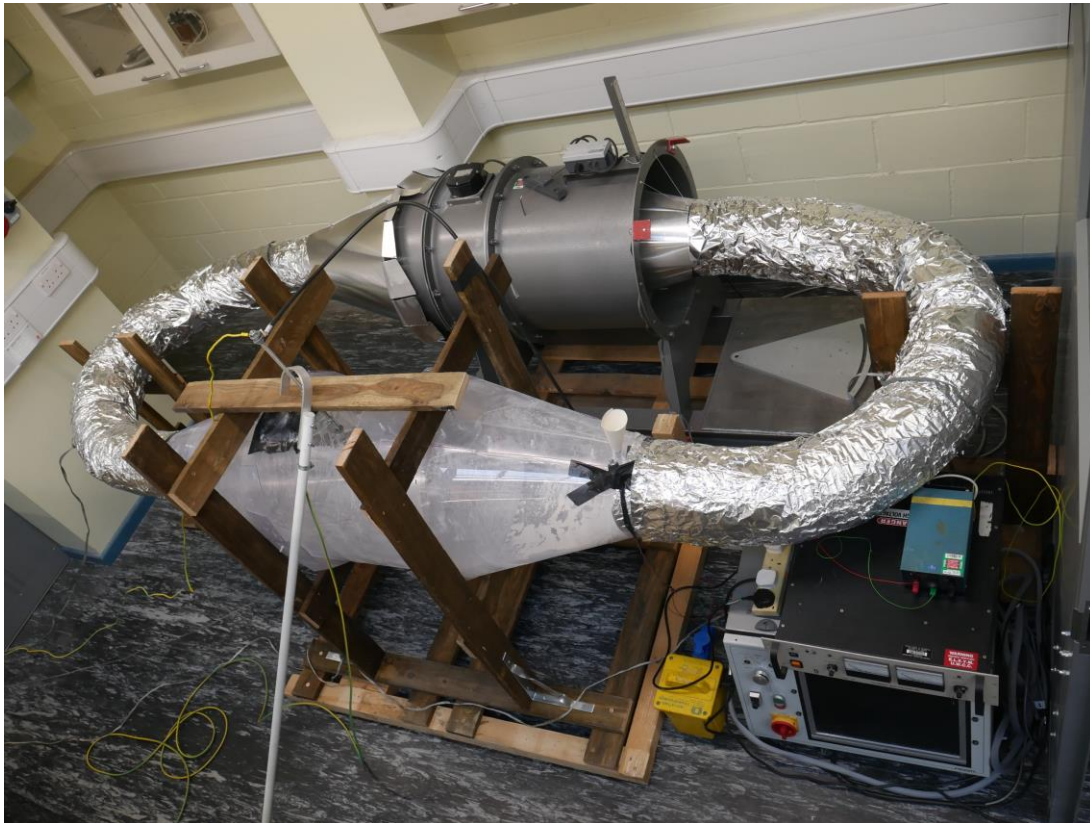


Fig. 6.7. Built wind tunnel.

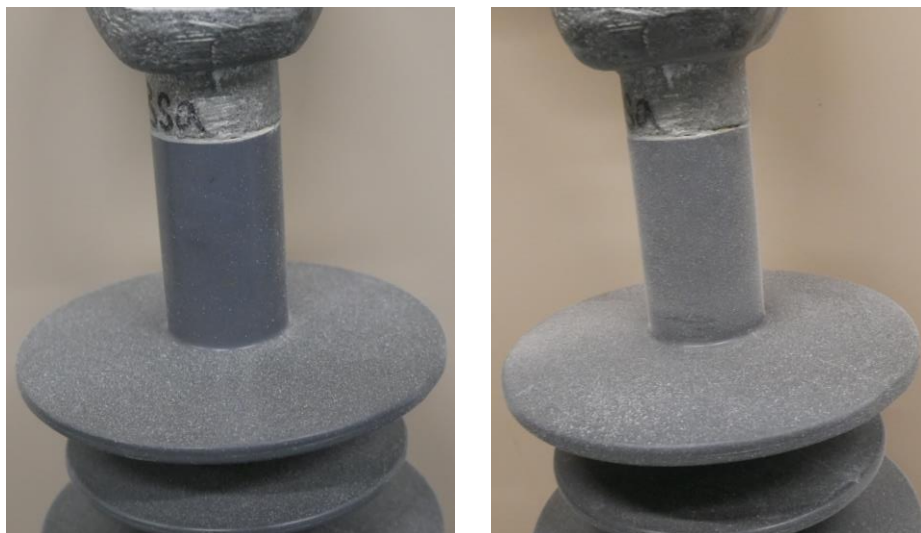
To realise the contamination, Kaolin was injected at a constant pace through a small circular opening on top of the small section end of the air inlet

polycarbonate truncated cone. The injection was due to a constant vibration originated from a small DC motor with a centre of mass dislocated from the shaft axis. A Kaolin quantity of 30 g was injected in the tunnel in each experiment.

The selection of the wind speed range was done to obtain sufficient deposit density to be measured reliably. Thus, the chosen settings were the maximum speed setting and the minimum setting which still allowed a reliably measurable density. An intermediate speed was included to have three different wind speeds. The measurement of the wind profile across the section is important, as it will have an impact on the flow of pollution. However, some challenges were encountered on the measurement of the actual wind speed corresponding to a given setting, and they are addressed in the discussion section.

## 6.6. Pollution accumulation results under DC and non-energised conditions

As expected, the energised insulator visibly collected more pollution than the non-energised one, in particular, close to the high voltage electrode, as shown in Fig. 6.8. The measurement of the NSDD confirms this observation in Fig. 6.9.



a) non-energised insulator

b) DC energised insulator

Fig. 6.8. Pictures of insulator after test at maximum wind speed setting.

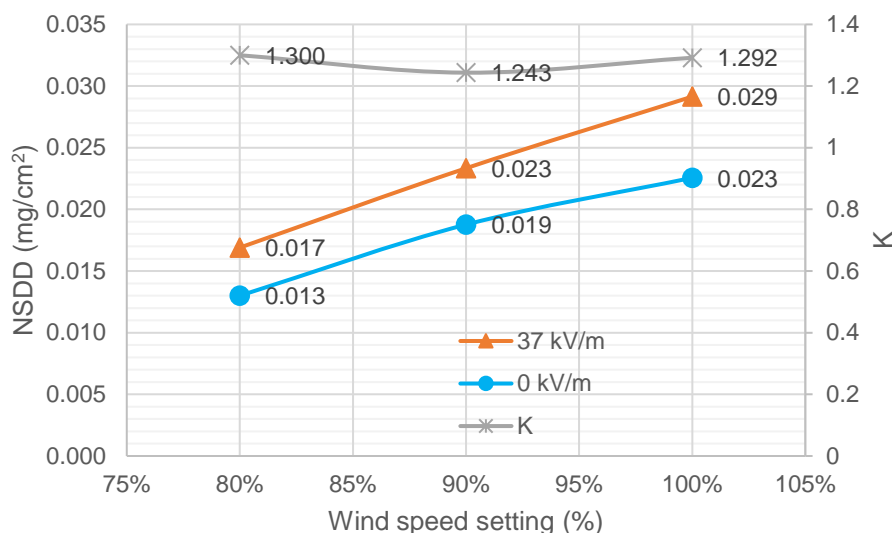


Fig. 6.9. NSDD under DC energised and non-energised conditions at three wind speed settings, and calculation of their ratio  $K_p$ .  $USCD_{DC}=80.5$  mm/kV.

Per each case, the contamination has been obtained in about ten minutes.

## 6.7. Discussion of results and possible improvements

Two important confirmations of the reviewed literature are provided by the results of this chapter. The first is that the DC energisation causes a larger NSDD compared to the non-energised condition. The second is that as the wind speed increases, the NSDD increases too in both the non-energised and energised cases.

The values found for  $K_p$  between 1.243 and 1.300 are low with respect to those reviewed in [113], in section 2.17.3, which are as high as 24 at low wind speeds, but these refer to relatively lower USCDs. However, in [114], reviewed in section 2.17.4, values between 1 and 1.5 are found for the largest value of  $USCD_{DC}=66.7$  mm/kV, which is relatively similar to 80.5 mm/kV, used in this work.

An evident increase of  $K_p$  cannot be observed as the wind speed decreases, as it would be expected from past research. This may be due to the non-sufficiently low wind speed given by the 70% setting. However, as mentioned in the methodology, this setting was the minimum to obtain a reliably measurable deposit.

### 6.7.1. Challenges and possible improvements

- a) **Contamination injection rate.** Only an average of about 45 mg of Kaolin deposited on the insulator, with respect to the injected 30 g. This may be due to two factors. The first is that the Kaolin particles fall in the tunnel at an excessive pace which does not allow the wind force to be uniformly exerted on all the particles. The injection rate is positively correlated with the intensity of the vibration exerted by the DC motor and the diameter of the opening. To reduce the injection rate, the reduction of the vibration intensity or the opening diameter were attempted. However, neither of the two solutions allowed any Kaolin to be injected in the tunnel. Therefore, a different system needs to be implemented to reduce the amount of injected contaminant per second and to be able to regulate it smoothly. One option could be to realise a narrow slide on which the contaminant would be distributed and later carried towards the opening. The slide inclination would then allow to regulate the injection rate or a vibration could be incorporated to facilitate the pollution descent. Another option would be to place the contaminant in a cone inside which a long screw with a large thread would rotate. The thread would carry the contaminant at the entrance of the enclosure at a pace determined by the screw's angular speed.
- b) **Air flow uniformity across section.** To measure the wind speed at various wind generator settings, two different anemometers have been used to double check the measurements. In both cases, the anemometer was inserted in the tunnel from the insulator opening and the opening has then been closed to avoid air flow leakages. Attempts to measure the wind speed were made at various section heights, but low speeds of about 1 m/s were occasionally measured only at the section bottom. Elsewhere, the anemometer could not spin for long enough to perform a measurement. NSDD measurements confirm that there exists a flow from the opening to the insulator, but not large enough to be measured by the anemometers even at the maximum speed setting. To tackle the issue of flow uniformity across the section, it is proposed to realise a wind tunnel with a constant square section of about 500 mm per side. The horizontal sides can be realised by cutting flat polycarbonate sheets in the desired shape. The vertical sides can be realised

by cutting sheets of flat polycarbonate and by bending them at the desired radius, which would be larger for the outer side and smaller for the inner one. The use of insulating honeycomb structures is also proposed, especially before the air reaches the insulator.

## 6.8. Conclusions and future work

The main contribution is given by the introduction of an enclosure consisting of an insulating material in the vicinity of the insulator, to allow the electric field not to be too large, or possibly to be modified as desired with additional electrodes outside the enclosure.

The NSDD positive correlation with wind speed and DC energisation has been confirmed.  $K_p$  ratio of energised over non-energised conditions is found in the range of 1.24 to 1.30, but its increase as the wind speed decreases is not observed. However, similar values of  $K_p$  were found in [114], reviewed in section 2.17.4, for the largest value of  $USCD_{DC}=66.7$  mm/kV, which is relatively similar to 80.5 mm/kV, used in this work.

Two main issues exist. These are the contamination injection rate which is too high to allow all the particles to be airborne, and the non-uniformity of air flow across the wind tunnel section at the insulator location.

Some solutions are proposed as future work for the regulation of the injection rate, such as a slide with variable inclination or a large-threaded screw whose rotation allows the pollution to be carried towards the enclosure opening. For the uniformity of the air flow across the section, the construction of a constant square section wind tunnel is proposed, as well as the use of insulating honeycomb structures.

This chapter does not provide an investigation on which enclosure insulating material would minimise the pollution accumulation on the enclosure and, thus, the interference with the insulator pollution accumulation. Therefore, it is suggested as future work. The investigation on the material would also have to account for practicality of enclosure construction and wind tunnel assembly.

Alongside the enclosure material investigation, the wind tunnel section height could be increased to create a larger separation between the charged enclosure and the charged insulator. This way, the pollution directed towards the insulator would not be attracted by the enclosure in any meaningful way.



## Chapter 7. Conclusions and future work

This research work has investigated aspects of HVDC composite insulators by considering laboratory testing and modelling. The following are the main outcomes of this work.

It is clear that, under **heavy pollution** and as a result of modelling based on the test measurements, the electrode influence on the electric field tangent to the insulator surface is negligible. In fact, at the triple junction, the tangent electric field is at most 6.3 times larger when the electrode is modified. However, the notable difference is present only on less than 55 mm of creepage distance in the proximity of the triple junction. Elsewhere, along the insulator, the difference factor is reduced from 6.3 to 0.03

Under the same pollution conditions, the horizontal orientation performs better than the vertical, with an average USCD of 38.3 mm/kV for the horizontal orientation and 42.7 mm/kV for the vertical, in the flashover voltage range of 121 kV to 252 kV. This is attributed to the convection heat dissipating in upper air when the insulator is horizontal and heating the insulator when vertical. For the horizontal case, the lower insulator temperature, slower evaporation, and larger trunk pollution conductivities result in a slower formation of dry bands, and thus a slower flashover phenomenon.

Observations of the spatial arc propagation confirm the partial arcs move upwards in both orientations. As a consequence, in the vertical orientation, the arc tends to connect portions of the insulator more quickly, whereas in the horizontal orientation the arc tends to extinguish more easily. This is the second reason attributed to the better horizontal performance.

An orientation factor  $K_o$ , to account for the orientation-based performance, is proposed, and it estimated as 1 for the vertical and 0.896 for the horizontal. The introduction of  $K_o$  would allow a more accurate estimation of the flashover voltage for horizontally oriented insulators.

It is also confirmed, similarly to the referenced AC work, that the reason dry bands appear first on the trunks is that their pollution layer section is smaller

than the sheds'. Consequently, the current density on the trunks surface is larger and it causes more local evaporation, resulting in lower pollution conductivities, starting from an order of magnitude of  $10^{-2}$  S/m when wet and  $10^{-5}$  to  $10^{-4}$  S/m when dry, which facilitates the partial discharge activity.

With regards to the electric field tangent to the insulator surface, which is responsible for driving the leakage current from one electrode to the other, this varies in time as the phenomenon progresses from the initial current flow to the dry bands and, finally, to the partial arcs. Initially, the tangential electric field is uniform and relatively small, at about 0.02 kV/mm, then, it becomes substantially larger on the dry bands, between 0.16 and 0.28 kV/mm, due to a decreased layer conductivity, and, finally, when partial arcs appear, it decreases to about 0.01 kV/mm with relatively high peaks at the arc extremities where most of the current is being driven into.

Under ***clean and rain conditions***, the direct voltage pre-energisation was found to cause a negative impact on the flashover performance, under switching impulse stress, thus, confirming referenced work conducted at higher voltages. In particular, the three cases most affected by the direct voltage pre-energised state are the dry vertical, the dry horizontal, and the  $96.2 \mu\text{S}/\text{cm}$  rain horizontal cases, whose performance is affected respectively 45%, 68%, and 107% of the 16 kV direct voltage, at flashover voltages of 281.1 kV, 334.3 kV, and 264.5 kV, respectively.

As expected, the increase in rain conductivity leads to lower flashover values. However, the largest observed performance drop is observed between the dry and the least conductive rain conditions. Therefore, the study beyond  $100 \mu\text{S}/\text{cm}$  does not seem necessary.

The horizontal orientation outperforms the vertical. The reason for this in the dry case is that the vertical ground electrode has a sharper geometry than the horizontal ground electrode. In fact, A FEM model, run at 288 kV, found an electric field of 10.7 kV/mm at the triple junction of the ground electrode when the insulator is vertical, against 8.5 kV/mm for the horizontal. Whereas in the wet case, two factors facilitate flashover. The first is that the rain droplets are

oriented in the axial orientation when the insulator is vertical, and the second is the larger amount of deposited rain on the shed tops when the insulator is vertical.

The flashover voltages were all much larger than a typical DC operational switching surge voltage, which is 1.5 to 2 times the DC system voltage. Thus, in the case of pole to ground fault, the healthy pole failure risk appears small. However, further research is needed on higher direct voltages and polluted conditions, as well as on the positive superimposition.

It was confirmed that the time to flashover shortens as the flashover voltage increases. Whereas negligible role seems to be played by the direct voltage pre-energisation with regards to the time to flashover.

All the proposals for the ***HVDC conversion of existing towers***, under extreme and heavy pollution, suggest a potential increase in power transfer, with respect to the HVAC original lines. As measured by the  $k_{AC-DC}$  ratio, the converted DC lines would carry from 1.6 to 2.9 times the original AC power, at direct voltages in the range between 170 and 500 kV. The simple suspension insulators solution averages a  $k_{AC-DC}$  ratio of 2.1.

The addition of inclined insulators to fix the position in space of the poles would allow a further increase to a  $k_{AC-DC}$  ratio of 2.3.

The non-necessity of corona rings under DC for outdoor insulators is confirmed in the analysed cases. In fact, the FEM models have shown that a small current in the nA range is sufficient to satisfy the electric field requirements, as a current at least in the  $\mu A$  range is to be expected in service.

Also, the potential decrease of outdoor insulation performance due to switching impulse (or overvoltages in general) superimposed on direct voltage under polluted conditions is to be investigated and considered for the HVDC tower insulation design.

With regards to the initial ***wind tunnel study***, the main contribution is given by the introduction of an enclosure consisting of an insulating material in the

vicinity of the insulator, to allow the electric field not to be too large, or possibly to be modified as desired with additional electrodes outside the enclosure.

The NSDD positive correlation with wind speed and DC energisation has been confirmed.  $K_p$  ratio of energised over non-energised conditions is found in the range of 1.24 to 1.30, but its increase as the wind speed decreases is not observed. However, similar values of  $K_p$  were found in [114], reviewed in section 2.17.4, for the largest value of  $USCD_{DC}=66.7$  mm/kV, which is relatively similar to 80.5 mm/kV, used in this work.

Two main issues exist. These are the contamination injection rate which is too high to allow all the particles to be airborne, and the non-uniformity of air flow across the wind tunnel section at the insulator location. Some solutions are proposed as future work to try to solve or improve these issues.

## 7.1. Future work

To obtain more information and ultimately more reliable  $K_0$  values for a vast range of field applications, it would be beneficial to undertake future tests under different conditions, such as different profiles and pollution severities.

Future work is needed on the investigation of the positive SI superimposed on positive direct voltage under dry and clean conditions. Superimpositions of this kind should also be investigated in heavily polluted conditions and a larger range of voltage levels, as there is a lack of data on the topic.

3D models of the insulation solutions for the conversion of existing towers to HVDC should be undertaken once specific fittings are identified. This should be done to determine the minimum current above which the electric field requirements are satisfied, and to confirm that a larger current is generally found in service under conservative conditions, namely clean and dry. Also, other engineering challenges associated with the conversion of an existing HVAC OHL to HVDC were not covered in the thesis and are recommended as future work. These challenges include the assessment of audible noise and radio interference. At the system level, the challenges to address include substation design, converter design, insulation coordination, control and protection, grid code

reactive power support requirements, grid studies, capital and operating expenditure (CAPEX and OPEX) estimations, environmental impact of larger substation footprint, land permission, and community engagement.

Improvements or re-building of the wind tunnel initial prototype are suggested as future work to obtain a regulable contamination injection rate and a more uniform air flow across the section. For the first objective, one option could be to realise a narrow slide, with a variable inclination angle, on which the contaminant would be distributed and later carried towards the opening. Another option would be to place the contaminant in a cone inside which a long screw with a large thread would rotate at the desired angular speed. For the second objective, to tackle the issue of flow uniformity across the section, it is proposed to realise a wind tunnel with a constant square section of about 500 mm per side. The use of insulating honeycomb structures is also proposed, especially before the air reaches the insulator. Also, investigations at lower and, thus, more critical  $USCD_{DC}$  could be performed and compared with existing literature data.

Also, Chapter 6 does not provide an investigation on which enclosure insulating material would minimise the pollution accumulation on the wind tunnel enclosure and, thus, the interference with the insulator pollution accumulation. Therefore, it is suggested as future work. The investigation on the material would also have to account for practicality of enclosure construction and wind tunnel assembly. Alongside the enclosure material investigation, the wind tunnel section height could be increased to create a larger separation between the charged enclosure and the charged insulator. This way, the pollution directed towards the insulator would not be attracted by the enclosure in any meaningful way.

Recommendations of future work on specific dimensioning factors are done for IEC 60815-4 [40] and CIGRE TB 518 [4]. For example, to have a more specific representation of the effect of different types of salt, a salt type dependent differentiation of  $K_c$  would be appropriate. Also, at present, the contamination uniformity ratio factor  $K_{CUR}$  is not available for HTM coated insulators, thus, future investigations would be beneficial to make the methodology more

comprehensive. Lastly, it is clear that the pollution accumulation also depends on the insulator orientation, thus, it could be worth carrying out investigations on the applicability of  $K_D$  to horizontal arrangements.

## 7.2. Comprehensive remarks

The research results which seem most meaningful from a practical industrial perspective are the following. The horizontally oriented insulator generally performs better than the vertically oriented insulator under polluted and rain conditions, which is a confirmation of past findings accompanied by new and detailed scientific justifications.

The HVDC conversion of the L6, L2, and L7 towers would allow a power transfer increase factor of 1.6 to 2.9 under conservative contamination assumptions. The use of corona rings is not necessary as far as revealed by the voltage distribution study of the axisymmetric models.

The importance of the HVDC overhead line conversion should be stressed because an increasing number of policy targets are being set to electrify transportation and household heating. At the same time, in the UK, the electrical power industry is working to achieve offshore wind power plants with a capacity of 80 GW by 2050, with large penetration of HVDC power electronics. This would be an opportunity to extend the HVDC offshore network to onshore, by placing the conversion stations more onshore, rather than on the coast.



## References

- [1] K. Sun, S. Yuan, and Y. Qiu, "Chapter 2: Development of UHV Power Transmission in China," in *Ultra-high Voltage AC/DC Power Transmission*, Springer, 2018, pp. 23–37.
- [2] CIGRE Task Force 33.04.01, "Polluted insulators: a review of current knowledge." CIGRE, Jun. 2000. Accessed: Jun. 05, 2018. [Online]. Available: <https://e-cigre.org/publication/158-polluted-insulators--a-review-of-current-knowledge>
- [3] "BS EN 3288-1,2:2014. Insulator and conductor fittings for overhead lines." BSI Standards PEL/11, 2014.
- [4] CIGRE Working Group C4.303, "Outdoor insulation in polluted conditions: Guidelines for selection and dimensioning - PART 2: THE DC CASE." CIGRE, Dec. 2012. Accessed: Jul. 24, 2018. [Online]. Available: <https://e-cigre.org/publication/518-outdoor-insulation-in-polluted-conditionsguidelines-for-selection-and-dimensioning---part-2-the-dc-case>
- [5] "Failure of cap-and-pin insulators subjected to HVDC," *e-cigré*. [https://e-cigre.org/publication/ELT\\_153\\_1-failure-of-cap-and-pin-insulators-subjected-to-hvdc](https://e-cigre.org/publication/ELT_153_1-failure-of-cap-and-pin-insulators-subjected-to-hvdc) (accessed Jun. 06, 2018).
- [6] "DD IEC TS 60815:1986, Selection and dimensioning of high-voltage insulators intended for use in polluted conditions. Ceramic and glass insulators for a.c. systems." BSI Standards PEL/36, 1986.
- [7] A. Küchler, *High Voltage Engineering. Fundamentals - Technology - Applications*. Springer, 2018.
- [8] A. Pigni, R. Brambilla, and G. Pirovano, "Are Shielding Electrodes Necessary for HVDC Line Insulators?," presented at the 20th International Symposium on High Voltage Engineering, Buenos Aires, Argentina, Sep. 2017. [Online]. Available: <https://www.inmr.com/shielding-electrodes-for-ac-dc-insulators/>
- [9] INMR, "Optimal Dimensioning of Grading Rings for Composite Insulators," *Insulators*, Aug. 2020.
- [10] A. J. Phillips, A. J. Maxwell, C. S. Engelbrecht, and I. Gutman, "Electric-Field Limits for the Design of Grading Rings for Composite Line Insulators," *IEEE*

- Transactions on Power Delivery*, vol. 30, no. 3, pp. 1110–1118, Jun. 2015, doi: 10.1109/TPWRD.2014.2362074.
- [11] M. Dai *et al.*, “Corona onset characteristics of grading rings on  $\pm 800$ kV UHVDC transmission line,” in *2014 International Conference on Information Science, Electronics and Electrical Engineering*, Apr. 2014, vol. 2, pp. 800–804. doi: 10.1109/InfoSEEE.2014.6947777.
- [12] W. Sima, K. Wu, Q. Yang, and C. Sun, “Corona Ring Design of  $\pm 800$ kV DC Composite Insulator Based on Computer Analysis,” in *2006 IEEE Conference on Electrical Insulation and Dielectric Phenomena*, Oct. 2006, pp. 457–460. doi: 10.1109/CEIDP.2006.311968.
- [13] J. Cheng, Z. Peng, H. Cai, Y. Zhao, and Y. Xiang, “Research on the Grading Ring Configuration of  $\pm 800$ kV Ultra-High Voltage DC Switchyard Post Insulators,” in *2012 Asia-Pacific Power and Energy Engineering Conference*, Mar. 2012, pp. 1–4. doi: 10.1109/APPEEC.2012.6307265.
- [14] D. Tao, L. Qingfeng, Z. Xuejun, and S. Zhiyi, “The Optimization of Grading Ring Design of  $\pm 800$ kV UHV DC Lines,” presented at the Second International Symposium on Standards for Ultra High Voltage Transmission, Beijing, 2009.
- [15] L. Yongwei, Z. Kang, L. Li, and H. Jiang, “Design of  $\pm 800$ kV DC Transmission Line,” presented at the Second International Symposium on Standards for Ultra High Voltage Transmission, Beijing, 2009.
- [16] CIGRE Working Group 33-04, “The measurement of site pollution severity and its application to insulator dimensioning for AC systems,” *Electra*, vol. No. 64, pp. 101–116, 1979.
- [17] “Mathematical models for pollution flashover,” *e-cigré*. [https://e-cigre.org/publication/ELT\\_078\\_1-mathematical-models-for-pollution-flashover](https://e-cigre.org/publication/ELT_078_1-mathematical-models-for-pollution-flashover) (accessed Jun. 05, 2018).
- [18] F. Obenaus, “Fremdschichtueberschlag und kriechweglaenge,” *Deutsche Elektrotechnik*, vol. 4, pp. 135–136, 1958.
- [19] B. F. Hampton, “Flashover mechanism of polluted insulation,” *Proceedings of the Institution of Electrical Engineers*, vol. 111, no. 5, pp. 985–990, May 1964, doi: 10.1049/piee.1964.0155.

- [20] H. Boehme and F. Obenaus, "Pollution flashover tests on insulators in the laboratory and in systems and the model concept of creepage path flashover," *CIGRE paper*, no. 7, pp. 1–15, 1969.
- [21] H. H. Woodson and A. J. Mcelroy, "Insulators with contaminated surfaces, part II: Modeling of discharge mechanisms," *IEEE Transactions on Power Apparatus and Systems*, no. 8, pp. 1858–1867, 1970.
- [22] H. Nacke, "Stabilität der Fremdschichtentladungen und Theorie des Fremdschichtüberschlags," *Elektrotechnische Zeitschrift-A*, vol. 87, pp. 577–585, 1966.
- [23] R. Wilkins, "Flashover voltage of high-voltage insulators with uniform surface-pollution films," in *Proceedings of the Institution of Electrical Engineers*, 1969, vol. 116, pp. 457–465.
- [24] F. Erler, "Zum Kriechüberschlag dicker Isolatoren bei Wechselspannung," *Elektrie*, vol. 3, pp. 100–102, 1969.
- [25] J. Mackevich and M. Shah, "Polymer outdoor insulating materials. Part I: Comparison of porcelain and polymer electrical insulation," *IEEE Electrical Insulation Magazine*, vol. 13, no. 3, pp. 5–12, May 1997, doi: 10.1109/57.591510.
- [26] L. Xidong, W. Shaowu, F. Ju, and G. Zhicheng, "Development of composite insulators in China," *IEEE Transactions on Dielectrics and Electrical Insulation*, vol. 6, no. 5, pp. 586–594, Dec. 1999, doi: 10.1109/TDEI.1999.9286760.
- [27] G. G. Karady, M. Shah, and R. L. Brown, "Flashover mechanism of silicone rubber insulators used for outdoor insulation-I," *IEEE transactions on power delivery*, vol. 10, no. 4, pp. 1965–1971, 1995.
- [28] X. Yu, X. Yang, Q. Zhang, J. Zhou, B. Liu, and Y. Xu, "Influence of Non-Soluble Contamination Microscopic Properties on Hydrophobicity Transfer on Silicone Rubber Surface of Composite Insulator," in *2019 2nd International Conference on Electrical Materials and Power Equipment (ICEMPE)*, Apr. 2019, pp. 417–420. doi: 10.1109/ICEMPE.2019.8727236.
- [29] "PD IEC/TS 62073:2016, Guidance on the measurement of hydrophobicity of insulator surfaces." BSI Standards PEL/36, 2016.

- [30] Z. Yang *et al.*, "Hydrophobicity distribution analysis of DC composite insulators," in *2014 IEEE Electrical Insulation Conference (EIC)*, Jun. 2014, pp. 465–468. doi: 10.1109/EIC.2014.6869431.
- [31] Y. Tu, H. Zhang, Z. Xu, J. Chen, and C. Chen, "Influences of Electric-Field Distribution Along the String on the Aging of Composite Insulators," *IEEE Transactions on Power Delivery*, vol. 28, no. 3, pp. 1865–1871, Jul. 2013, doi: 10.1109/TPWRD.2013.2244103.
- [32] X. Yu, Q. Zhang, X. Yang, H. Yang, J. Zhou, and B. Liu, "Influence of non-uniform hydrophobicity distribution on pollution flashover characteristics of composite insulators," *IET Science, Measurement & Technology*, vol. 12, no. 8, pp. 1009–1014, Aug. 2018, doi: 10.1049/iet-smt.2018.5266.
- [33] F. Zhang, L. Wang, Z. Guan, and M. Macalpine, "Influence of composite insulator shed design on contamination flashover performance at high altitudes," *IEEE Transactions on Dielectrics and Electrical Insulation*, vol. 18, no. 3, pp. 739–744, Jun. 2011, doi: 10.1109/TDEI.2011.5931060.
- [34] R. Znaidi, A. Eklund, and R. Hartings, "Simulation of marine and desert conditions in the laboratory using a new pollution test method," Amman, Jordan, Jun. 1996.
- [35] NGK, *Technical Guide, Cat. No. 91 R, First Revision*. 1989.
- [36] "BS EN 60507:2014. Artificial pollution tests on high-voltage ceramic and glass insulators to be used on a.c. systems." BSI Standards PEL/36, 2014.
- [37] S. Zhiyi, Y. Yu, Z. Jun, G. Haifeng, D. Tao, and L. Xidong, "Reliability of Composite Insulators Used For UHV AC/DC Transmission Lines," presented at the International Conference on UHV Transmission, Beijing, 2009.
- [38] J. Seifert, "Private communication."
- [39] CIGRE WG 22.03, "Service performance of composite insulators used on HVDC lines," *Electra*, no. 161, 1995.
- [40] "BS EN 60815-4:2016. Selection and dimensioning of high-voltage insulators intended for use in polluted conditions. Part 4: Insulators for d.c. systems." BSI Standards PEL/36, 2016.
- [41] Rizk FAM, "A systematical approach to high voltage insulator selection for polluted environment," presented at the Second regional conference of CIGRE in Arab countries, Amman, Jordan, May 1997.

- [42] "IEC/TS 60815-2:2008." BSI Standards, 2008.
- [43] R. Matsuoka, S. Ito, K. Sakanishi, and K. Naito, "Flashover on contaminated insulators with different diameters," *IEEE Transactions on Electrical Insulation*, vol. 26, no. 6, pp. 1140–1146, Dec. 1991, doi: 10.1109/14.108151.
- [44] IEEE Working Group on Insulator Contamination, Lightning and Insulator Subcommittee, "Application of insulators in a contaminated environment," *IEEE Trans. on Power Apparatus and Systems*, vol. Vol. PAS-98, No. 5, pp. 1676–1695, Oct. 1979.
- [45] G. Kaiser, "The mouse buzzard as a cause of breakdowns on 110 kV single pole high-tension lines," *Elektrotechnische Zeitschrift*, 1970.
- [46] H. J. West, J. E. Brown, and A. L. Kinyon, "Simulation of EHV transmission line flashovers initiated by, bird excretion," *IEEE Transactions on Power Apparatus and Systems*, no. 4, pp. 1627–1630, 1971.
- [47] J. T. Burnham, "Bird streamer flashovers on FPL transmission lines," *IEEE Transactions on Power Delivery*, vol. 10, no. 2, pp. 970–977, 1995.
- [48] R. Matsuoka, K. Kondo, K. Naito, and M. Ishii, "Influence of nonsoluble contaminants on the flashover voltages of artificially contaminated insulators," *IEEE Transactions on Power Delivery*, vol. 11, no. 1, pp. 420–430, Jan. 1996, doi: 10.1109/61.484042.
- [49] R. Matsuoka, H. Shinokubo, K. Kondo, T. Fujimura, and T. Terada, "Artificial contamination withstand voltage characteristics of polymer insulators," in *Electrical Insulating Materials, 1995. International Symposium on*, 1995, pp. 487–490.
- [50] CIGRE Task Force 33.04.04, "Artificial pollution testing of HVDC insulators analysis of factors influencing performance," *Electra*, vol. No 140, pp. 99–113, Feb. 1992.
- [51] Z.Y. Su, X.D. Liang, Y. Yin, J.Zhou, W.F.Li, P. Li, "Important correction factors in HVDC line insulation selection," Beijing, Aug. 2005.
- [52] Kondo, K., Ito, S., Kondo, S., Imakoma, T., "Investigation results of suspension insulators removed from DC 500 kV Gezhouba-Shanghai Line in China."
- [53] L. J. Williams, J. H. Kim, Y. B. Kim, N. Arai, O. Shimoda, and K. C. Holte, "Contaminated insulators-chemical dependence of flashover voltages and

- salt migration," *IEEE Transactions on Power Apparatus and Systems*, no. 5, pp. 1572–1580, 1974.
- [54] Y. Hasegawa, K. Naito, K. Arakawa, H. M. Schneider, and L. E. Zaffanella, "A comparative program on HVDC contamination tests," *IEEE transactions on power delivery*, vol. 3, no. 4, pp. 1986–1995, 1988.
- [55] K. Chrzan, Z. Pohl, and T. Kowalak, "Hygroscopic properties of pollutants on HV insulators," *IEEE Transactions on Electrical Insulation*, vol. 24, no. 1, pp. 107–112, Feb. 1989, doi: 10.1109/14.19874.
- [56] M. Farzaneh and W. A. Chisholm, *Insulators for Icing and Polluted Environments*. John Wiley & Sons, 2009.
- [57] K. Naito, K. Izumi, K. Takasu, and R. Matsuoka, "Performance of Composite Insulators under Polluted Conditions," *CIGRE Session Paper No. 33-301*, 1996.
- [58] "BS EN 62217:2013. Polymeric HV insulators for indoor and outdoor use — General definitions, test methods and acceptance criteria." BSI Standards PEL/36, 2013.
- [59] "PD IEC TS 61245:2015 Artificial pollution tests on high-voltage ceramic and glass insulators to be used on d.c. systems." BSI Standards IEC/TC36, Apr. 2015.
- [60] J. S. T. Looms, *Insulators for high voltages*. IET, 1988.
- [61] A. K. Gertsik, A. V. Korsuntser, and N. K. Nikol'Skii, "The effect of fouling on insulators for HVDC overhead lines," *Direct current*, vol. 3, pp. 219–226, 1957.
- [62] A. Annestrand and A. Schei, "A test procedure for artificial pollution tests on direct voltage," *Direct Current*, vol. 12, no. 1, pp. 1–8, 1967.
- [63] J. F. Hall and T. Paul, "Wind tunnel studies of the insulator contamination process," *IEEE Transactions on Electrical Insulation*, no. 3, pp. 180–188, 1981.
- [64] Y. Taniguchi, N. Arai, and Y. Imano, "Natural contamination test of insulators at Noto testing station near Japan Sea," *IEEE Transactions on Power Apparatus and Systems*, no. 1, pp. 239–245, 1979.

- [65] I. Kimoto, K. Kito, and T. Takatori, "Anti-pollution design criteria for line and station insulators," *IEEE Transactions on Power Apparatus and Systems*, no. 1, pp. 317–327, 1972.
- [66] R. Znaidi, "Composite insulators: Results of outdoor and laboratory experiments in Tunisia," presented at the Société des Electriciens et des Electroniciens (SEE), Paris, Apr. 1993.
- [67] F. A. M. Rizk, A. A. El-Sarky, A. A. Assaad, and M. M. Awad, "Comparative tests on contaminated insulators with reference to desert conditions," *CIGRE, 1972 Session*, 1972.
- [68] W. Heise and H. K. Koethe, "Das Isoliervermogen verschmutzter Isolatoren gegen Überspannungen stossartigen Verlaufs," *ETZ (A)*, vol. 20, pp. 493–497, 1967.
- [69] K. Naito, R. Matsuoka, S. Ito, and S. Morikawa, "An investigation of the horizontally mounted insulators for HVDC stations," *IEEE Transactions on Power Delivery*, vol. 4, no. 1, pp. 653–666, 1989.
- [70] H. M. Schneider, "Measurements of contamination on post insulators in HVDC converter stations," *IEEE transactions on power delivery*, vol. 3, no. 1, pp. 398–404, 1988.
- [71] W. Lampe, T. K. E. Hoglund, C. L. Nellis, P. E. Renner, and R. D. Stearns, "Long-term tests of HVDC insulators under natural pollution conditions at the Big Eddy Test Center," *IEEE Transactions on Power Delivery*, vol. 4, no. 1, pp. 248–259, 1989.
- [72] Britannica, The Editors of Encyclopaedia, "Electric Polarization," *Encyclopedia Britannica*, <https://www.britannica.com/science/electric-polarization>. Feb. 14, 2020.
- [73] A. Pignini and P. Bertolotto, "Design of External Insulation for UHV DC in Contaminated Environment," Ljubljana, Slovenia, Aug. 2007, pp. T4-347.
- [74] S. Zhiyi, F. Jianbin, L. Qingfeng, L. Yansheng, and Z. Jun, "Natural Contamination Performances on Insulators under DC Stress and the Pollution Deposit Density Ratio of DC to AC," Ljubljana, Slovenia, Aug. 2007, pp. T4-324.

- [75] F. Rizk, A. El-Arabaty, and A. El-Sarky, "Laboratory and field experiences with EHV transmission line insulators in the desert," *IEEE Transactions on Power Apparatus and Systems*, vol. 94, no. 5, pp. 1770–1776, 1975.
- [76] G. Karady, "The effect of fog parameters on the testing of artificially contaminated insulators in a fog chamber," *IEEE Transactions on power apparatus and systems*, vol. 94, no. 2, pp. 378–387, 1975.
- [77] P. J. Robinson and A. Henderson-Sellers, *Contemporary Climatology*, 2 edition. Harlow: Routledge, 1999.
- [78] M. Leclerc, R.-P. Bouchard, Y. Gervais, and D. Mukhedkar, "Wetting processes on a contaminated insulator surface," *IEEE Transactions on Power Apparatus and Systems*, no. 5, pp. 1005–1011, 1982.
- [79] A. El-Morhedy and O. Gouda, "Laboratory simulation of natural pollution conditions of high voltage insulator," Braunschweig, Germany, Aug. 1987, p. Paper 52.17.
- [80] M. Elkoshairy and F. Rizk, "Performance of EHV transmission line insulators under desert pollution conditions," Paris, 1970, p. Paper no. 33-05.
- [81] Met Office, "Drizzle." <https://www.metoffice.gov.uk/weather/learn-about/weather/types-of-weather/rain/drizzle>
- [82] T. Fujimura and K. Naito, "Electrical Phenomena and High Voltage Insulators," presented at the Proc. International Symposium on Ceramics held at Bangalore, India, Nov. 1982.
- [83] T. V. Ferreira *et al.*, "Laboratory Tests of a Composite Insulator Instrumented with Optical Fiber Sensors," in *Proceedings of the 21st International Symposium on High Voltage Engineering*, Cham, 2020, pp. 483–491. doi: 10.1007/978-3-030-31680-8\_49.
- [84] T. Kawamura and K. Isaka, "Humidity dependence of moisture absorption, leakage current and flashover voltage on contaminated insulator surfaces," *Electrical Engineering in Japan*, vol. 93, no. 5, pp. 62–68, 1973.
- [85] M. Farzaneh, "Insulator flashover under icing conditions," *IEEE Transactions on Dielectrics and Electrical Insulation*, vol. 21, no. 5, pp. 1997–2011, Oct. 2014, doi: 10.1109/TDEI.2014.004598.
- [86] G. Ramos, M. Campillo, R. Diaz, P. Velazquez, and V. Gerez, "Regional patterns of pollution accumulation on insulators in Mexico: Its use as a design tool

- and for preventive maintenance,” in *9th International Symposium on High Voltage Engineering (ISH)*, Graz, Austria, Sep. 1995, p. Paper 3218.
- [87] R. Matsuoka, S. Ito, K. Sakanishi, and K. Naito, “Flashover on contaminated insulators with different diameters,” *IEEE transactions on Electrical Insulation*, vol. 26, no. 6, pp. 1140–1146, 1991.
- [88] R. Matsuoka, S. Ito, K. Tanaka, and K. Kondo, “Contamination withstand voltage characteristics of polymer insulators,” Montreal, Quebec Canada, 1997.
- [89] Imagawa, R. Matsuoka, K. Sakanishi, K. Kondo, N. Okada, and T. Yonezawa, “Comparative Contamination Degrees on porcelain and silicone rubber insulator in fields,” in *Cigré colloquium SC 33-97*, Toronto Ontario Canada, p. paper 33-4.5.
- [90] S. M. Rowland, Y. Xiong, J. Robertson, and S. Hoffmann, “Aging of silicone rubber composite insulators on 400 kV transmission lines,” *IEEE Transactions on Dielectrics and Electrical Insulation*, vol. 14, no. 1, pp. 130–136, Feb. 2007, doi: 10.1109/TDEI.2007.302881.
- [91] S. M. Gubanski, A. Dornfalk, S. Wallstrom, and S. Karlsson, “Performance and Diagnostics of Biologically Contaminated Insulators,” in *2006 IEEE 8th International Conference on Properties applications of Dielectric Materials*, Jun. 2006, pp. 23–30. doi: 10.1109/ICPADM.2006.284109.
- [92] Y. Shang, “Study of an Outdoor Composite Insulating Cross-Arm for Overhead Transmission Lines,” The University of Manchester, Manchester, UK, 2018.
- [93] G. E. Company, G. E. C. P. UHV, and E. P. R. Institute, *Transmission line reference book, 345 kV and above*, vol. 2500. Electric Power Research Institute, 1982.
- [94] A. C. Baker, L. E. Zaffanella, L. D. Anzivino, H. M. Schneider, and J. H. Moran, “Contamination performance of HVDC station post insulators,” *IEEE transactions on power delivery*, vol. 3, no. 4, pp. 1968–1975, 1988.
- [95] D. Wu, R. Hartings, U. Aström, B. Almgren, and S. Nord, “The performance of station post insulators for UHVDC applications,” in *10th International Symposium on High Voltage Engineering (ISH)*, Montreal, Canada, Aug. 1997, vol. 3, pp. 41–44.

- [96] M. Kawai, "Research at Project UHV on the performance of contaminated insulators Part I basic problems," *IEEE Transactions on Power Apparatus and Systems*, no. 3, pp. 1102–1110, 1973.
- [97] H. M. Schneider and C. W. Nicholls, "Contamination flashover performance of insulators for UHV," *IEEE Transactions on Power Apparatus and Systems*, no. 4, pp. 1411–1420, 1978.
- [98] A. Pigini, D. Perin, F. Zagliani, M. Ramamoorthy, C. Lakshminarasimha, and V. Rammohan, "Performance of insulators for EHVDC systems under polluted conditions," in *Cigré 32nd session*, Paris, Sep. 1988, p. Paper no. 33-11.
- [99] L. Qisheng *et al.*, "Natural contamination test results of various insulators under DC voltage in an inland area in China," in *Properties and Applications of Dielectric Materials, 1991., Proceedings of the 3rd International Conference on*, 1991, pp. 350–353.
- [100] T. C. Cheng, C. T. Wu, J. N. Rippey, and F. M. Zedan, "Pollution performance of DC insulators under operating conditions," *IEEE Transactions on Electrical Insulation*, no. 3, pp. 154–164, 1981.
- [101] L. Shuzi, "Pollution accumulation performance of insulators under negative DC voltage," Xian, China, Jun. 1985.
- [102] E. M. Sherif, *Performance and ageing of HVAC and HVDC overhead line insulators*. Chalmers tekn. hogsk. Goteborg, 1987.
- [103] S. Minemura, T. Iso, K. Naito, T. Irie, and Y. Suzuki, "Insulation design of Hokkaido-Hoshu interconnecting DC transmission line," USA, Mar. 1983.
- [104] F. Hirsch, H. V. Rheinbaben, and R. Sorms, "Flashovers of insulators under natural pollution and HVDC," *IEEE Transactions on Power Apparatus and Systems*, vol. 94, no. 1, pp. 45–50, 1975.
- [105] I. Kimoto, T. Fujimura, and K. Naito, "Performance of Insulators for Direct Current Transmission Line Under Polluted Condition," *IEEE Transactions on Power Apparatus and Systems*, vol. PAS-92, no. 3, pp. 943–949, May 1973, doi: 10.1109/TPAS.1973.293660.
- [106] D. Wu and S. Su Zhiyi, "The correlation factor between DC and AC pollution levels: Review and Proposal," in *10th International Symposium on High Voltage Engineering (ISH)*, Montreal, Canada, Aug. 1997, vol. 3, pp. 253–256.

- [107] EPRI, *HVDC Transmission line reference Book*, vol. TR 102764. Palo Alto, CA, 1993.
- [108] T. Imakoma, "DC Pollution performance of insulators."
- [109] Z. Y. Su, W. Ma, D. Wu, U. Åström, and G. Karlsson, "Measurement of Site Pollution Severity Under DC Voltage by Means of a Portable Test Station," Tsinghua University, Beijing China, Aug. 2005.
- [110] Z. Y. Su, X. D. Liang, Y. Yin, J. Zhou, W. F. Li, and P. Li, "Outdoor insulation selection method of HVDC lines," in *Proceedings of the 14th International Symposium on High Voltage Engineering*, Tsinghua University, Beijing China, Aug. 2005, p. Paper D-18.
- [111] A. Pignini, "Private communication."
- [112] Takaie Matsumoto, Toru Kawakami, and Masaaki Kurokawa, "Contamination Characteristics of Polymeric Insulators by the Wind Blow Method," presented at the 19th International Symposium on High Voltage Engineering, Pilsen, Czech Republic, Aug. 2015.
- [113] Yukun Lv, Weiping Zhao, Jingang Li, Yazhao Zhang 1, "Simulation of Contamination Deposition on Typical Shed Porcelain Insulators," *Energies*, 2017, doi: 10.3390/en10071045.
- [114] Xinhan Qiao, Zhijin Zhang, Xingliang Jiang and Tian Liang, "Influence of DC Electric Fields on Pollution of HVDC Composite Insulator Short Samples with Different Environmental Parameters," *Energies*, 2019, doi: 10.3390/en12122304.
- [115] W. Xiang, S. Yang, L. Xu, J. Zhang, W. Lin, and J. Wen, "A Transient Voltage-Based DC Fault Line Protection Scheme for MMC-Based DC Grid Embedding DC Breakers," *IEEE Transactions on Power Delivery*, vol. 34, no. 1, pp. 334–345, Feb. 2019, doi: 10.1109/TPWRD.2018.2874817.
- [116] M. K. Bucher and C. M. Franck, "Contribution of Fault Current Sources in Multiterminal HVDC Cable Networks," *IEEE Transactions on Power Delivery*, vol. 28, no. 3, pp. 1796–1803, Jul. 2013, doi: 10.1109/TPWRD.2013.2260359.
- [117] W. Mosch, E. Lemke, J. Pilling, M. Dietrich, W. Hauschild, and J. Wolf, "Model of the Creeping Flashover of Polluted Insulators and Direct Voltage

- Generators for Pollution Tests,” in *International Conference on Large High Voltage Electric Systems*, Paris, Aug. 1988, vol. 33–05, pp. 1–6.
- [118] F. A. M. Rizk and D. H. Nguyen, “Digital simulation of source-insulator interaction in HVDC pollution tests,” *IEEE Transactions on Power Delivery*, vol. 3, no. 1, pp. 405–410, Jan. 1988, doi: 10.1109/61.4271.
- [119] M. E.-A. Slama, A. Beroual, and H. Hadi, “Analytical computation of discharge characteristic constants and critical parameters of flashover of polluted insulators,” *IEEE Transactions on Dielectrics and Electrical Insulation*, vol. 17, no. 6, pp. 1764–1771, Dec. 2010, doi: 10.1109/TDEI.2010.5658227.
- [120] F. A. M. Rizk, “Mathematical models for pollution flashover,” *Electra*, vol. 78, no. 5, pp. 71–103, 1981.
- [121] “BS EN 61109:2008 Insulators for overhead lines — Composite suspension and tension insulators for a.c. systems with a nominal voltage greater than 1 000 V — Definitions, test methods and acceptance criteria.” BSI Standards PEL/36B, Mar. 2009.
- [122] D. Pinzan *et al.*, “Performance of Composite Outdoor Insulator under Superimposed Direct and Switching Impulse Voltages,” *IEEE Transactions on Power Delivery*, 2020, doi: 10.1109/TPWRD.2020.3003980.
- [123] M. Andriollo, G. Martinelli, and A. Morini, *I trasformatori. Teoria ed esercizi*. Cortina (Padova), 2010.
- [124] A. Paolucci, “Capitolo VI: Il Metodo ‘per Unità’ nello Studio delle Reti,” in *Lezioni di Trasmissione dell’Energia Elettrica*, 4th ed., 1998.
- [125] S. D. Pawar, P. Murugavel, and D. M. Lal, “Effect of relative humidity and sea level pressure on electrical conductivity of air over Indian Ocean,” *Journal of Geophysical Research: Atmospheres*, vol. 114, no. D2, 2009, doi: 10.1029/2007JD009716.
- [126] W. Zhou, S. Qi, C. Tu, H. Zhao, C. Wang, and J. Kou, “Effect of the particle size of Al<sub>2</sub>O<sub>3</sub> on the properties of filled heat-conductive silicone rubber,” *Journal of Applied Polymer Science - Wiley Online Library*, pp. 1312–1318, Nov. 2006, doi: 10.1002/app.25789.

- [127] "Chapter 15 - External Insulation Characteristics of UHVDC Lines," in *UHV Transmission Technology*, Oxford: Academic Press, 2018, pp. 559–590. doi: 10.1016/B978-0-12-805193-1.00015-X.
- [128] C. S. Ilomuanya, A. Nekahi, and S. Farokhi, "Acid Rain Pollution Effect on the Electric Field Distribution of a Glass Insulator," in *2018 IEEE International Conference on High Voltage Engineering and Application (ICHVE)*, Sep. 2018, pp. 1–4. doi: 10.1109/ICHVE.2018.8642231.
- [129] R. Wilkins, "Flashover voltage of high-voltage insulators with uniform surface-pollution films," *Proceedings of the Institution of Electrical Engineers*, vol. 116, no. 3, pp. 457–465, Mar. 1969, doi: 10.1049/piee.1969.0093.
- [130] C. A. Spellman, H. M. Young, A. Haddad, A. R. Rowlands, and R. T. Waters, "Survey of polymeric insulator ageing factors," in *1999 Eleventh International Symposium on High Voltage Engineering*, Aug. 1999, vol. 4, pp. 160–163 vol.4. doi: 10.1049/cp:19990817.
- [131] "BS EN 60060-1:2010, High Voltage test techniques. Part 1, Section 5.2.1.2: Tolerances." BSI Standards PEL/42, 2010.
- [132] WG 33.04, "The measurement of site pollution severity and its application to insulator dimensioning for a.c. systems," *Electra*, vol. No. 64, pp. 101–116, 1979.
- [133] M. Albano, R. T. Waters, P. Charalampidis, H. Griffiths, and A. Haddad, "Infrared analysis of dry-band flashover of silicone rubber insulators," *IEEE Transactions on Dielectrics and Electrical Insulation*, vol. 23, no. 1, pp. 304–310, Feb. 2016, doi: 10.1109/TDEI.2015.005026.
- [134] P. Charalampidis, M. Albano, H. Griffiths, A. Haddad, and R. T. Waters, "Silicone rubber insulators for polluted environments part 1: enhanced artificial pollution tests," *IEEE Transactions on Dielectrics and Electrical Insulation*, vol. 21, no. 2, pp. 740–748, Apr. 2014, doi: 10.1109/TDEI.2013.004015.
- [135] M. Albano, P. Charalampidis, R. T. Waters, H. Griffiths, and A. Haddad, "Silicone rubber insulators for polluted environments part 2: textured insulators," *IEEE Transactions on Dielectrics and Electrical Insulation*, vol. 21, no. 2, pp. 749–757, Apr. 2014, doi: 10.1109/TDEI.2013.004016.

- [136] N. G. Hingorani, "Transient Overvoltage on a Bipolar HVDC Overhead Line Caused by DC Line Faults," *IEEE Transactions on Power Apparatus and Systems*, vol. PAS-89, no. 4, pp. 592–610, Apr. 1970, doi: 10.1109/TPAS.1970.292606.
- [137] E. W. Kimbark, "Transient Overvoltages Caused by Monopolar Ground Fault on Bipolar DC Line: Theory and Simulation," *IEEE Transactions on Power Apparatus and Systems*, vol. PAS-89, no. 4, pp. 584–592, Apr. 1970, doi: 10.1109/TPAS.1970.292605.
- [138] D. J. Melvold, P. C. Odam, and J. J. Vithayathil, "Transient overvoltages on an HVDC bipolar line during monopolar line faults," *IEEE Transactions on Power Apparatus and Systems*, vol. 96, no. 2, pp. 591–601, Mar. 1977, doi: 10.1109/T-PAS.1977.32370.
- [139] G. T. Wrate *et al.*, "Transient overvoltages on a three terminal DC transmission system due to monopolar ground faults," *IEEE Transactions on Power Delivery*, vol. 5, no. 2, pp. 1047–1053, Apr. 1990, doi: 10.1109/61.53120.
- [140] CIGRE WG B2.41, "Guide to the conversion of existing AC lines to DC operation. Technical Brochure 583." CIGRE, May 2014.
- [141] Oak Ridge National Laboratory (ORNL), "HVDC Power Transmission Technology Assessment," Oak Ridge, Tennessee 37831, Apr. 1997.
- [142] Electric Power Research Institute, EPRI, "AC-to-DC Power Transmission Line Conversion," Nov. 2010.
- [143] National Electric Safety Code NESC, Part 1, Section 12, "C2-2017." IEEE, 2017.
- [144] S. K. Shifidi, H. J. Vermeulen, J. P. Holtzhausen, and P. Pieterse, "Impulse Testing of a Polluted Insulator with a DC Bias Voltage," Cape Town, South Africa, 2009.
- [145] R. Cortina, G. Marrone, A. Pigni, L. Thione, W. Petrusch, and M. P. Verma, "Study of the Dielectric Strength of External Insulation of HVDC Systems and Application to Design and Testing," presented at the International Conference on Large High Voltage Electric Systems, Paris, 1984.
- [146] Y. Watanabe, "Influence of Preexisting DC Voltage on Switching Surge Flashover Characteristics," *IEEE Transactions on Power Apparatus and*

- Systems*, vol. PAS-87, no. 4, pp. 964–969, Apr. 1968, doi: 10.1109/TPAS.1968.292071.
- [147] H. Rodhe, F. Dentener, and M. Schulz, “The Global Distribution of Acidifying Wet Deposition,” *Environmental Science & Technology*, vol. 36, no. 20, pp. 4382–4388, 2002, doi: 10.1021/es020057g.
- [148] T. Fujimura and K. Naito, “Electrical Phenomena and High Voltage Insulators,” presented at the International Symposium on Ceramics, Bangalore, India, 1982.
- [149] W. Liao, G. Cui, and Z. Sun, “Flashover test on air clearances of  $\pm 800$  kV DC transmission tower with switching surges superimposed on DC voltage,” *Power System Technology*, 2008.
- [150] “BS EN 60060-1 High Voltage test techniques. Part 1: General definitions and test requirements.” BSI Standards PEL/42, 2010.
- [151] G. E. Likens and T. J. Butler, “Acid Rain: Causes, Consequences, and Recovery in Terrestrial, Aquatic, and Human Systems,” in *Encyclopedia of the Anthropocene*, D. A. Dellasala and M. I. Goldstein, Eds. Oxford: Elsevier, 2018, pp. 23–31. doi: 10.1016/B978-0-12-809665-9.09977-8.
- [152] Lightning and Insulator Subcommittee, “Application of Insulators in a Contaminated Environment,” *IEEE Transactions on Power Apparatus and Systems*, vol. PAS-98, no. 5, pp. 1676–1695, Sep. 1979, doi: 10.1109/TPAS.1979.319486.
- [153] D. Pinzan, M. E. A. Slama, O. Cwikowski, and M. A. Haddad, “Insulation Solutions for HVAC to HVDC Conversion of a High Voltage Transmission Overhead Line: The L7 Tower Case Study,” in *Proceedings of the 21st International Symposium on High Voltage Engineering*, Budapest, Hungary, 2019, pp. 1359–1371.
- [154] S. I. Barannik, S. B. Vasserman, and A. N. Lukin, “Resistance and Inductance of a Gas Arc,” *Soviet Physics, Technical Physics*, vol. 9, no. 11, pp. 1449–1453, 1975.
- [155] G. M. Gomcharenko and I. N. Romanenko, “Discharge Channel in Helium at 100 atm and in Air,” *Soviet Physics, Technical Physics*, vol. 15, pp. 1990–1995, Jun. 1971.

- [156] I. V. Demenik, "Resistance of a Xenon Plasma in a Large Flash Lamp," *Soviet Physics, Technical Physics*, vol. 13, pp. 829–832, Dec. 1968.
- [157] M. J. Kushner, W. D. Kimura, and S. R. Byron, "Arc resistance of laser-triggered spark gaps," *Journal of Applied Physics*, vol. 58, no. 5, pp. 1744–1751, 1985, doi: 10.1063/1.336023.
- [158] M. M. Popovic, "Investigation of the Beginning of High Current Discharges in Pulsed Arcs," 1974, pp. 32–36.
- [159] R. Rompe and W. Weizel, "Über das Toeplersche Funkengesetz," *Zeitschrift für Physik*, vol. 122, no. 9–12, pp. 636–639, 1944, doi: 10.1007/BF01330625.
- [160] M. Toepler, "Zur Kenntnis der Gesetz der Gleitfunkenbildung," *Annals of Physics*, pp. 193–222, 1906.
- [161] A. E. Vlastos, "The Resistance of Sparks," *Journal of Applied Physics*, vol. 43, pp. 1987–1989, Apr. 1972.
- [162] J. Kuffel and P. Kuffel, "Operation, design and construction of impulse generators," in *High Voltage Engineering Fundamentals*, 2nd ed., Newnes, 2000.
- [163] "BS EN 60052:2002. Voltage measurement by means of standard air gaps." BSI Standards PEL/42, 2002.
- [164] J. Yu, K. Smith, M. Urizarbarrena, N. MacLeod, R. Bryans, and A. Moon, "Initial designs for the ANGLE DC project; converting existing AC cable and overhead line into DC operation," in *13th IET International Conference on AC and DC Power Transmission (ACDC 2017)*, Feb. 2017, pp. 1–6. doi: 10.1049/cp.2017.0002.
- [165] I. C. on N.-I. R. Protection, "GUIDELINES ON LIMITS OF EXPOSURE TO STATIC MAGNETIC FIELDS," *Health Physics*, vol. 96, no. 4, pp. 504–514, Apr. 2009, doi: 10.1097/01.HP.0000343164.27920.4a.
- [166] "BS EN 3288-2:2009, Insulator and Conductor Fittings for Overhead Lines. Part 2: Specification for a Range of Insulator Fittings." BSI Standards PEL/11, 2009.
- [167] "BS EN 60071-1:2019, Insulation co-ordination. Table A.2: Correlation between standard rated switching impulse withstand voltages and minimum phase-to-earth air clearances." BSI Standards PEL/99, 2019.

*References*

- [168] K. Papailiou, "Section 2: DC Transmission Lines, 4.13: Overvoltages and Insulation Coordination," in *Overhead Lines*, 1st ed., Springer International Publishing, 2017.



# Appendix A

## Current dependent arc resistance model

In Section 4.5.1, the Toepler arc resistance was used to model the breakdown of the sphere gap of the experimental circuit, needed for the superimposition of a switching impulse on direct voltage.

The resistance  $R(i(t))$  is expressed as:

$$R(i(t)) = \frac{k_t \cdot d}{\int_0^t i(t) dt} \quad (\Omega) \quad (4.4)$$

And it was modelled in EMTP/ATP with the following code. For the understanding of the basic principles of the EMTP/ATP language, the thesis author would like to thank Doctor Stephen Robson.

```

MODEL R_arc
DATA d1,d2
INPUT cur
OUTPUT curint2, curint
VAR curint2, curint;
INIT
  curint2:=1e11;
  curint:= 1.25e-15;
ENDINIT
EXEC
IF t>2.000038 THEN
  curint:=curint + ((abs(cur) + abs(prevval(cur)))/2)*timestep
  curint2:=(1.25e-4)/(curint)
ELSE
  curint2:=1e11
ENDIF
ENDEXEC
ENDMODEL

```

As shown in the above code, the model uses the current “cur” flowing through the resistance as an input, and it produces the outputs “curint2” and “curint”, which are respectively the current resistance and the integral of the current through the resistance.

Initially, the resistance is set at the very large value of  $10^{11} \Omega$ , and the current integral at  $1.25 \cdot 10^{-15}$ , which will be later discussed.

An IF and ELSE logic operator allows to distinguish the calculations the model performs before and after 2.000038 s. In fact, two second are left running to extinguish the initial transient due to the charging of the Marx generator, and at exactly 2 s the impulse is triggered. In the following 38  $\mu\text{s}$ , the voltage across the air gap reaches -70 kV, which is the breakdown voltage for the used 2.5 cm air gap [163].

Thus, up to 2.000038 s, the resistance is fixed to the initial value of  $10^{11} \Omega$ , which models the air resistance, and from this instant on, the Toepler law is used to model the arc resistance. The first step gives a resistance result of  $(1.25 \cdot 10^{-4}) / (1.25 \cdot 10^{-15}) = 10^{11} \Omega$ , which explains the current integral initial value of  $1.25 \cdot 10^{-15}$ . This number allows the resistance value to smoothly transition from the pre-breakdown phase to the arc phase. Please, note that  $1.25 \cdot 10^{-4}$  is the result of the Toepler constant  $0.5 \cdot 10^{-4} \text{ V}\cdot\text{s}/\text{cm}$  multiplied by the 2.5 cm air gap.

From this point on, the arc resistance quickly collapses to a negligible value, due to the progressive increase of the integral of the current flowing through the resistance itself.

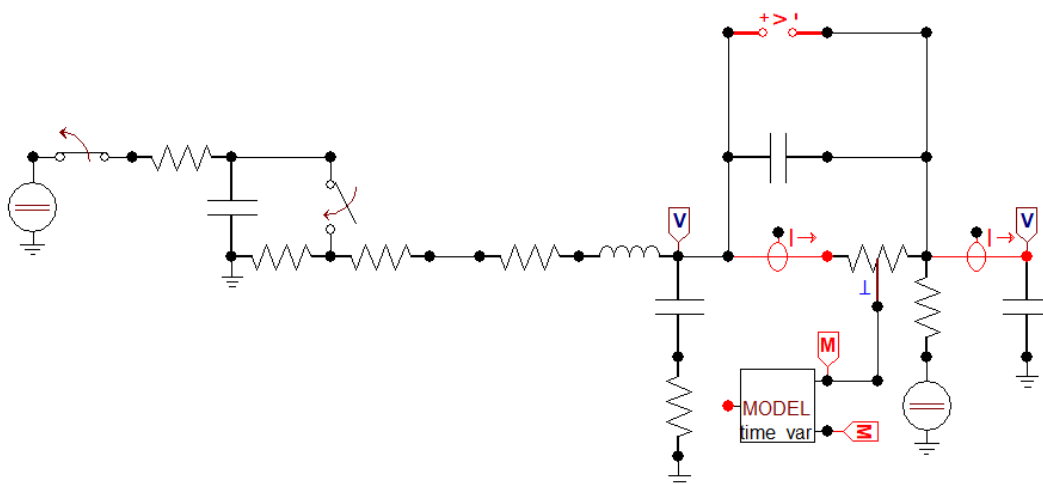


Fig. A. 1. Full circuit of Section 4.5.1, with model for sphere gap breakdown.